SENSITIVITY STUDY OF THE ASSEMBLY AVERAGED THERMAL-HYDRAULIC MODELS OF THE MEKIN COMPUTER CODE IN POWER TRANSIENTS

by

THOMAS RODACK

B.S.E. (MEAM), UNIVERSITY OF PENNSYLVANIA
(1975)

SUBMITTED IN PARTIAL FULFILLMENT
OF THE REQUIREMENTS FOR THE
DEGREES OF

NUCLEAR ENGINEER
and
MASTER OF SCIENCE IN MECHANICAL ENGINEERING

at the
MASSACHUSETTS INSTITUTE OF TECHNOLOGY
AUGUST 1977

Signature of Author.....
Department of Nuclear Engineering, August 10, 1977

Certified by..... .....
Thesis Supervisor

Accepted by.. .....
Chairman, Department Committee

ARCHIVES
JAN 27 1978

SENSITIVITY STUDY OF THE ASSEMBLY AVERAGED THERMAL-HYDRAULIC MODELS OF THE MEKIN COMPUTER CODE IN POWER TRANSIENTS

by

THOMAS RODACK

Submitted to the Department of Nuclear Engineering and the Department of Mechanical Engineering, August 1977, in partial fulfillment of the requirements for the Degrees of Nuclear Engineer and Master of Science in Mechanical Engineering.

ABSTRACT

The thermal-hydraulic (T-H) models and solution schemes employed by the MEKIN computer code have been examined. The effects of T-H input parameters on predicted fuel temperatures and coolant densities were determined in transient analyses. Consideration was limited primarily to a simulated PWR control rod ejection transient. Limitations to the use of MEKIN that arise because of simplifying assumptions in the T-H models are discussed. Computation time may be reduced without altering the results of a transient analysis if appropriate MEKIN options are selected. Guidelines are presented to facilitate the selection of these options. Suggestions for improvement of the code are also made.

Thesis Supervisor: Lothar Wolf, Associate Professor of Nuclear Engineering

ACKNOWLEDGEMENTS

The author wishes to express his gratitude to the people who assisted him in formulating and expressing the concepts that are presented in this thesis. Foremost among these is Professor Lothar Wolf who, as thesis advisor, was always available to offer advice, counsel, and criticism.

Sincere thanks are offerred to Rachel Morton who, with her limitless patience, helped to unravel the intricacies of the MIT-IPC computer system.

Portions of this thesis are the culmination of discussions with Kerry Basehore, Chong Chiu, and Michael Corradini; their criticism and suggestions are gratefully acknowledged.

Finally, the author wishes to thank his family and friends, especially his brother Richard and good friend Vincent Spunar. Without the continuous encouragement and moral support they so generously provided, this thesis could never have been completed.

The work embodied in this thesis was performed under the auspices of the Electric Power Research Institute.

TABLE OF CONTENTS

	Page
ABSTRACT	
ACKNOWLEDGEMENTS	3
TABLE OF CONTENTS	4
LIST OF FIGURES	9
LIST OF TABLES	14
NOMENCLATURE	16
Chapter 1: INTRODUCTION	20
1.1 Sensitivity	20
1.2 Background	22
1.3 Previous Work	23
1.4 Research Objectives	25
Chapter 2: OVERVIEW	27
2.1 The MEKIN Code	27
2.2 General MEKIN Sensitivity Study	31
2.3 T-H Sensitivity Study	31
2.3.1 Relevant Parameters	31
2.3.2 Problems Adressed	32
2.3.3 T-H Sensitivity Study Methodology	35
2.3.3.1 Class of Transients	35
2.3.3.2 Code Used (COBRA III-C/MIT)	37
2.3.3.3 Power Histories	38
Chapter 3: RADIAL T-H MESH SIZE SENSITIVITY	44
3.1 Introduction	44
3.2 Steady State Lumping Scheme Sensitivity	45
3.2.1 Methodology	45
3.2.2 Steady State Results	50
3.2.2.1 Discrete Average vs. Lumped Channel Behavior	50
3.2.2.2 Average vs Local Behavior	52
3.3 Adequacy of the T-H Lumping Scheme in Power Transients	55
3.3.1 Transient Studies Methodology	56
3.3.2 T-H Averaging Schemes	61
3.3.3 Applicability of Averaging Schemes for Neutronics Feedback Calculations	67

Page

3.3.4 Results of the Comparison 68

3.3.4.1 Discrete Average vs. Lumped Channel Behavior 68
3.3.4.2 Average vs Local Behavior 72

3.4 Sensitivity to Model Size 75

3.4.1 Objectives 75
3.4.2 Methodology 75
3.4.3 Results 78

3.5 Summary of Radial Mesh Results 84

Chapter 4: NUMERICAL SOLUTION SCHEME PARAMETER SENSITIVITY 87

4.1 Introduction 87

4.1.1 T-H Solution Technique (COBRA III-C/MIT) 87
4.1.2 General Methodology for Numerical Parameter Studies 91

4.2 Axial Mesh Sensitivities 93

4.2.1 Cases Studied 93
4.2.2 Sensitivities in the Fuel Temperature 93
4.2.3 Axial Mesh Sensitivity of Coolant 103

4.3 Time Step Sensitivity 108

4.3.1 Cases Studied 108
4.3.2 Sensitivity of Fuel Temperature to Time Step Size 108
4.3.3 Time Step Sensitivity of Coolant 118

4.4 Relationship between Axial Level Size and Time Step Size 124

4.4.1 The Courant Criterion 128
4.4.2 Discussion of Courant Criterion Applicability to COBRA 128

4.5 T-H Convergence Criterion 129

4.5.1 Transients Considered 129
4.5.2 Observed Sensitivities 130
4.5.3 Discussion of T-H C.C. Sensitivity 136

4.6 Summary of Numerical Parameter Results 141

Page

Chapter 5: SENSITIVITIES IN THE FUEL CONDUCTION MODEL 145

5.1 Introduction 145

5.1.1 Fuel Conduction Modeling in COBRA and MEKIN 145
5.1.2 Conduction Studies Objectives 147

5.2 Radial Fuel Mesh Sensitivity 149

5.2.1 Methodology 149
5.2.2 Hot Zero Power Studies 151

5.2.2.1 Fuel Temperature Sensitivity to Mesh Size 151
5.2.2.2 Coolant Sensitivity to Fuel Mesh Size 151

5.2.3 Hot Full Power Studies 161

5.2.3.1 Fuel Temperature Mesh Size Sensitivity 161
5.2.3.2 Coolant Sensitivity to Fuel Mesh Size 167

5.3 Fuel Temperature Averaging Scheme 167

5.3.1 Methodology 167
5.3.2 Numerical Averaging Schemes 171
5.3.3 Analytic Average Fuel Temperatures of Ideal Temperature Profiles 174

5.3.3.1 Flat-Linear Profile 174
5.3.3.2 Flat-Parabolic Profile 176

5.3.4 Comparison of Linear, Parabolic, and Analytic Results 178

5.4 Sensitivity to the Gap Heat Transfer Coefficent 181

5.4.1 Fuel Temperature Sensitivity to h_{gap} 181

5.4.1.1 Steady State 181
5.4.1.2 Transient 184

5.4.2 Coolant Parameter Sensitivity to the Gap Heat Transfer Coefficient 185

5.4.2.1 Methodology 187
5.4.2.2 Results 187

Page

5.5 Limitations of the Fuel Conduction Model 194

5.5.1 Introduction 194
5.5.2 Spatially Dependent Volumetric Heat Generation Rate 194
5.5.3 Axial Conduction Effects 199
5.5.4 Temperature Dependent Thermal Properties 200
5.5.5 Remarks on Limitations 201

5.6 Summary of Results 202

Chapter 6: SENSITIVITY TO THE COOLANT MODELS 204

6.1 Introduction 204

6.1.1 Models and Objectives 204
6.1.2 Methodology 204

6.2 Two-Phase Pressure Drop Correlation Sensitivity 205
6.3 Turbulent Mixing Factor Sensitivity 208
6.4 Slip Ratio and Subcooled Void Correlation Sensitivity 215
6.5 Summary 221

Chapter 7: LIMITATIONS TO THE MEKIN T-H SOLUTION SCHEME 223

7.1 Introduction and Objectives 223
7.2 Physical Limitations of the MEKIN T-H Scheme 224

7.2.1 Applicability of the Momentum Integral Equations 224
7.2.2 Limitations in Extreme Power Transients 227
7.2.3 Limitations of the Coolant Model 228

7.3 Calculational Limitations of the MEKIN T-H Scheme 228

7.3.1 Clad-Coolant Heat Transfer Correlation 228
7.3.2 Deficiencies of the Axial Iteration Scheme 229
7.3.3 Pressure Drop Instability at Small Time Steps 230

7.4 Experimental Verification of the T-H Solution Scheme 232

7.5 Summary 233

Chapter 8: CONCLUSIONS AND RECOMMENDATIONS 235

8.1 Conclusions 235
8.2 Recommended Modifications to the Current Version of MEKIN 237

Page

8.3 Recommended Features of a New Version of MEKIN 238

8.4 Recommendations for Future Study 239

REFERENCES 242

APPENDICES

APPENDIX A: INPUT DATA USED THROUGHOUT SENSITIVITY STUDY 248

APPENDIX B: POWER HISTORIES USED IN THE SENSITIVITY STUDY 251

B.1 Data Used to Generate Power Histories 251

B.2 Method Used to Generate Power Histories 258

B.3 Prompt Jump Power History 258

APPENDIX C: FUEL TEMPERATURE ERRORS RESULTING FROM LARGE AXIAL MESHES AND TIME STEPS 263

C.1 Fuel Centerline Temperature Error with Coarse Axial Mesh 263

C.2 Average Fuel Temperature Error with Large Time Steps 267

C.3 Examples 271

APPENDIX D: LIMITING CRITERION FOR NEGLECTING AXIAL CONDUCTION IN FUEL PINS 280

LIST OF FIGURES

Number		Page
2.1	MEKIN Calculational Mesh (2 channels, 3 axial levels, 2 x 2 neutronic fine mesh)	28
2.2	MEKIN Calculational Strategy	30
2.3	Ideal Power History for Power Profile Class 2	42
3.1	Steady State Discrete and Lumped Channel Models	46
3.2	Radial Power Profiles of Power Profile Class 1	47
3.3	Power Profile Class 1 Axial Profiles	48
3.4	Isolated Hot Assembly Models for Transient Studies	57
3.5	Models of Hot Assembly in Quarter Core for Transient Studies	59
3.6	Alternate Assembly Configurations Modeled	77
3.7	Effect of Radial Mesh Size on Crossflow (single phase coolant flow, t = 0.5 seconds)	82
3.8	Effect of Radial Mesh Size on Crossflow (two-phase coolant flow, t = 1.0 seconds)	83
4.1	COBRA Transient Solution Strategy	90
4.2	T-H Models Used in Numerical Parameter Sensitivity Studies	94
4.3	Fuel Centerline Temperature Sensitivity to Axial Mesh Size (Power Profile Class 5, t=0.2 seconds)	95
4.4	Fuel Centerline Temperature Sensitivity to Axial Mesh Size (Power Profile Class 2A, t=1.0 seconds)	96
4.5	Fuel Surface Temperature Sensitivity to Axial Mesh Size (Power Profile Class 5)	98
4.6	Fuel Surface Temperature Sensitivity to Axial Mesh Size (Power Profile Class 2A)	99
4.7	Determination of Correct Axial Mesh Size	101
4.8	Heat Flux Sensitivity to Axial Mesh Size	105
4.9	Coolant Enthalpy Sensitivity to Axial Mesh Size (Power Profile Class 2A, t=1.0 seconds)	106

Number		Page
4.10	Coolant Enthalpy Sensitivity to Axial Mesh Size (Power Profile Class 2A, t=3.0 seconds)	107
4.11	Coolant Density Sensitivity to Axial Mesh Size (Power Profile Class 2A, t=1.0 seconds)	109
4.12	Coolant Density Sensitivity to Axial Mesh Size (Power Profile Class 2A, t=3.0 seconds)	110
4.13	Fuel Centerline Temperature Sensitivity to Time Step Size (Power Profile Class 2A)	111
4.14	Fuel Temperature Sensitivity to Time Step Size (Power Profile Class 2A)	112
4.15	Qualitative Representation of Energy Deposition Error for Large Time Steps	115
4.16	Comparison of Observed and Predicted Average Fuel Temperature Sensitivity to Time Step Size	117
4.17	Coolant Enthalpy Sensitivity to Time Step Size (Power Profile Class 2A)	119
4.18	Coolant Enthalpy Sensitivity to Time Step Size (Power Profile Class 2A)	121
4.19	Coolant Enthalpy Sensitivity to Time Step Size (Power Profile Class 2B)	122
4.20	Effects of Time Step Size on Crossflow	123
4.21	Coolant Void Fraction Sensitivity to Time Step Size	125
4.22	Coolant Void Fraction Sensitivity to Time Step Size	126
4.23	Execution Time Sensitivity to Time Step Size	127
4.24	T-H C.C. Sensitivity Study Transients	131
4.25	Coolant Density Sensitivity to T-H C.C.	137
4.26	Effect of T-H C.C. on Diversion Crossflow	140
5.1	Fuel Pin Heat Conduction Model	146
5.2	Electric Circuit Analog of Fuel Conduction Model	148
5.3	Hot Full Power Transient Power History (Power Profile Class 3)	150

Number		Page
5.4	Fuel Temperature Sensitivity to Radial Fuel Mesh Size (Hot Zero Power Transient, t=0.5 seconds)	152
5.5	Fuel Temperature Sensitivity to Radial Fuel Mesh Size (Hot Zero Power Transient, t=1.0 seconds)	153
5.6	Fuel Temperature Sensitivity to Radial Fuel Mesh Size (Hot Zero Power Transient, t=2.0 seconds)	154
5.7	Average Fuel Temperature Sensitivity to Radial Fuel Mesh Size (Hot Zero Power)	155
5.8	Fuel Centerline Temperature Sensitivity to Radial Fuel Mesh Size (Hot Zero Power Transient)	157
5.9	Fuel Surface Temperature Sensitivity to Radial Fuel Mesh Size (Hot Zero Power Transient)	158
5.10	Fuel Surface Heat Flux Sensitivity to Radial Fuel Mesh Size (Hot Zero Power Transient)	159
5.11	Fuel Temperature Sensitivity to Radial Fuel Mesh Size (Hot Full Power Transient, t=1.0 seconds)	164
5.12	Average Fuel Temperature Sensitivity to Radial Fuel Mesh Size (Hot Full Power Transient)	165
5.13	Fuel Surface Heat Flux Sensitivity to Radial Fuel Mesh Size (Hot Full Power Transient)	166
5.14	Centerline Temperature Error vs. Time (Hot Full Power)	168
5.15	Fuel Surface Temperature Sensitivity to Radial Fuel Mesh Size (Hot Full Power Transient)	169
5.16	Development of Fuel Temperature Profile in Hot Zero Power Transient	172
5.17	Flat-Linear Profile	175
5.18	Flat-Parabolic Profile	177
5.19	Fuel Surface Temperature Sensitivity to h_{gap}	183
5.20	Fuel and Coolant Time Constant Sensitivity to h_{gap}	186
5.21	Exit Enthalpy vs. Gap Conductance (3.0 second transient)	188
5.22	Coolant Enthalpy Sensitivity to h_{gap} (power profile class 4)	189

Number		Page
5.23	Coolant Density Sensitivity to h_{gap} (power profile class 2A)	190
5.24	Coolant Density Sensitivity to Gap Conductance (12 second transient)	191
5.25	Coolant Density Sensitivity to Gap Conductance (12 second transient)	192
5.26	Temperature Dependence of UO_2 Thermal Diffusivity	195
5.27	Temperature Dependence of UO_2 Density	196
5.28	Temperature Dependence of UO_2 Thermal Conductivity	197
5.29	Temperature Dependence of UO_2 Heat Capacity	198
6.1	Single Phase Coolant Sensitivity to β (t=0.5 seconds)	210
6.2	Coolant Density Sensitivity to β (t=1 second, jsut after onset of nucleate boiling)	211
6.3	Two-Phase Coolant Density Sensitivity to β (t=2 seconds, boiling well established)	212
6.4	Sensitivity of Minimum Coolant Density History to β	213
6.5	Dependence of β on Coolant Quality and Mass Flow Rates (from reference [48])	214
6.6	Dependence of β on Coolant Quality (from reference [49])	214
6.7	Void Fraction Sensitivity to Slip Ratio and Subcooled Void Correlations (t=1 second, just after onset of nucleate boiling)	216
6.8	Void Fraction Sensitivity to Slip Ratio and Subcooled Void Correlations (t=2 seconds, boiling well established)	217
6.9	Void Fraction Sensitivity to Slip Ratio and Subcooled Void Correlations (t=3 seconds, zero power generation)	218
6.10	Coolant Density Sensitivity to Slip Ratio and Subcooled Void Correlations	219
7.1	Channel Composed of Nine Subchannels	226

Number		Page
B.1	Assembly Average Radial Peaking Factors (maximum worth control gang fully inserted)	252
B.2	Local Radial Peaking Factors in Ejecting Fuel Assembly (maximum worth control gang fully inserted)	253
B.3	Assembly Average Radial Peaking Factors (maximum worth control rod gang fully withdrawn)	254
B.4	Local Radial Peaking Factors in Ejecting Fuel Assembly (maximum worth control rod gang fully withdrawn)	255
B.5	Axial Power Profile Used to Generate Power Profile Classes 2, 3, and 4	256
B.6	Axial Power Profile for Prompt Jump Transient (power profile class 5)	259
B.7	Prompt Jump Power History (power profile class 5)	260
C.1	COBRA Step Approximation to Axial Power Profile	264
D.1	Equivalent Thermal Resistances between Axial and Radial Fuel Nodes	281

LIST OF TABLES

Number		Page
1.1	Previous Studies	24
2.1	Power Profiles Used	40
2.2	Studies Where Power Profiles Were Used	41
3.1	Discrete and Lumped Channel Results (Steady State)	51
3.2	Local vs. Assembly Average Behavior (Steady State)	53
3.3	Discrete Average and Lumped Channel Results (Transient)	69
3.4	Local vs Average Transient Behavior in Hot Assembly	73
3.5	Hot Channel Parameters with Various Models	79
4.1	Comparison of Observed and Predicted Values of $[(T_{\mathfrak{c}} - T_f)_{4\Delta z} / (T_{\mathfrak{c}} - T_f)^*_{\Delta z}]$	100
4.2	Fuel Centerline Temperature Sensitivity to Time Step Size	114
4.3	Coolant Density Sensitivity to T-H C.C.	134
5.1	Sensitivity of Average Fuel Temperature to Radial Mesh Size (Hot Zero Power Transient)	160
5.2	Sensitivity of Coolant Parameters to Radial Fuel Mesh Size (Hot Zero Power Transient)	162
5.3	Sensitivity of Coolant Parameters to Radial Fuel Mesh Size (Hot Full Power Transient)	170
5.4	Comparison of Average Temperature Weighting Factors Found Numerically and Analytically	179
6.1	Sensitivity to the Choice of Pressure Drop Correlations	206
8.1	Summary of Observed Sensitivities in the Simulated Rod Ejection Transient	236
B.1	Axial Power Peaking Factors	257
C.1	Power Generation Rates for Example 1	274
C.2	Power Generation Rates for Examples and 3	274

Number		Page
C.3	Powers for use in Example 4	276
C.4	Powers for use in Example 5	278

NOMENCLATURE

a	fraction used to define ideal temperature profile in Sec. 5.3 $[0 \leq a \leq 1]$
A	channel flow area
c	clad thickness (Eq. C.5)
c_p	specific heat of fuel if no additional subscripts
C	equivalent thermal capacitance
$[C]$	thermal conduction coefficient matrix (Eq. 4.5)
D_h	hydraulic diameter of T-H channel
D_I	inner diameter of clad
D_o	outer diameter of clad
f	fraction of fission energy deposited in fuel
G	mass velocity
h	coolant enthalpy
h_c	clad-coolant heat transfer coefficient
h_{gap}	heat transfer coefficient between fuel surface and clad
h^*	enthalpy transported by diversion crossflow
H_e	extrapolation height of "chopped cosine" axial power profile (Eq. C.10)
k	thermal conductivity
L	length of T-H channel
$\dot{m}$	mass flow rate
M	number of coarse time steps from beginning of transient to time of interest (Eq. 4.3)
n	number of fine mesh axial levels contained in one coarse mesh level
N	number of small time steps contained in one coarse time step (Eq. 4.3)

P_h	channel heated perimeter
q	total fission energy generation rate in discrete channels (Eq. 3.16); equivalent thermal "current" in Fig. 5.2
Δq	volumetric energy deposition difference between coarse and fine time step representation of power vs. time curve over a single coarse time step
q'	fine mesh linear heat generation rate
q''	clad heat flux
q'''	volumetric heat generation rate
Q	total fission energy generation rate of entire fuel assembly (Eq. 3.17)
ΔQ	volumetric energy deposition difference between coarse and fine time step representation of power vs. time curve after M coarse time steps (Eq. C.14)
Δr	radial fuel mesh size
R	radius of fuel pin
R_n	equivalent thermal resistance between the nth and $(n+1)^{th}$ radial fuel nodes (Fig. 5.2)
Re	Reynold's number
$S_{i,j}$	gap spacing between channels i and j (Eq. 6.1)
[s]	matrix transformation defining adjacent channels (Eq.4.5)
t	elapsed time from beginning of transient
[t]	coolant temperature matrix [Eq. 4.5]
Δt	time step
T	temperature
T'	temperature at previous time step
T_o	fuel centerline temperature (eq. 5.15)
T_s	fuel surface temperature (eq. 5.15)

T_f	coolant temperature
u"	effective velocity for enthalpy transport (Eq. 4.5)
v	coolant axial velocity
V	volume
w	diversion crossflow between channels
w'	turbulent (fluctuating) crossflow
Δx	axial mesh size (Eq.4.5)
Δz	axial mesh size
α	void fraction
β	turbulent mixing factor
η_f	feedback correction coefficient
ρ	density (coolant density if no subscript)
Σ	macroscopic neutronic cross section
T	time constant

Subscripts

av	average value
b	bulk coolant property
c	coolant property; denotes clad properties in Ch. 5
f	fuel property (except T_f)
i	discrete channel index
j	axial level index
l	linear temperature profile assumed between radial fuel nodes to calculate value
min	minimum value
p	parabolic temperature profile assumed between radial fuel nodes to claculate value
r	radial direction

v	coolant vapor phase
z	axial direction
℄	fuel centerline

Superscripts

*	denotes reference fine mesh axial level in Eq. 4.1
-	average value; previous time step value in Eq. 4.5

CHAPTER 1

INTRODUCTION

1.1 Sensitivity

Sensitivity is defined as "the response of a system to external stimuli" [1]. In a mathematical sense, given the functional dependence of some parameter $P = P(x_1, x_2, \ldots x_n)$, the sensitivity of the parameter P to the variable x, is $\frac{dP}{dx_i}$. P is said to be more sensitive to x_i than x_j if [2] $\left|\frac{dP}{dx_i}\right| > \left|\frac{dP}{dx_j}\right|$.

A set of parameters is used to specify the state of an LWR core. Among these parameters are the power level, system pressure, coolant enthalpy, fuel temperatures, etc. When such a system is modeled by a set of equations, each of these state parameters exhibits a functional dependence on physical variables used to define the system. The state parameters are sensitive to these variables.

For example, the fuel temperature is a function of the power generation in the fuel, the fuel density, thermal conductivity, diameter, and other variables. Hence, the fuel temperature is sensitive to the fuel density, the thermal conductivity, etc.

The governing equations for LWR state parameters are a set of coupled nonlinear differential equations. No

general, closed form, analytic solution to this set of equations has been found. Approximate numerical solution schemes such as MEKIN have been formulated in lieu of the analytic solution.

Use of a numerical model introduces additional terms that influence the predicted state parameters. The spatial and temporal mesh sizes and convergence criteria will affect the predicted values. For example, the temperature calculated by a numerical method is sensitive to the axial and radial fuel mesh sizes and the time step size, as well as the physical variables used to describe the fuel.

Analytic prediction of the sensitivity of numerical solution schemes is impossible in many cases because of the complexity of the scheme. In these cases, approximate snesitivities may be determined "empirically" by varying input parameters and observing the effect on the predicted state parameters.

Tests may be made in which a single input value is varied or in which a set of input values is changed. Variation of a single input parameter provides estimates of the sensitivity and is useful in determining general trends in the sensitivity of a solution scheme. Simultaneous variation of several input parameters is used for accurate determination of sensitivity. Unfortunately initial estimates of the sensitivity are needed to determine the range over which sets of parameters will be varied in the

latter scheme.

The sensitivities of MEKIN-predicted fuel temperature and coolant density discussed in this thesis, were determined by varying input parameters individually.

1.2 Background

The MEKIN computer program, developed at MIT for the Electric Power Research Institute is currently the only non-proprietary code for 3-D LWR transient analysis that takes into account coupling between neutronic and thermal hydraulic (T-H) parameters.

MEKIN is considered to be a benchmark code, hence transient MEKIN analyses are, in general, quite expensive. Simplifying assumptions may be justified in many classes of transients. Currently, these assumptions are made and point kinetics codes such as CHIC-KIN are used in coupled transient analyses.

Both the cost of running MEKIN and the lack of user experience with the code are considered detrimental to the acceptance and use of MEKIN. One problem aggravates the other: little experience may be gained without considerable expense and few are willing to incur such expense if they are unfamiliar with the code. MEKIN is expensive to use because of the large amounts of computer storage and lengthy execution time it requires for typical LWR coupled transient analysis.

1.3 Previous Work

Information is exchanged between individual neutronic and T-H solution schemes. T-H behavior is determined with a version of COBRA III-C/MIT. Descriptions of the MEKIN and COBRA solution schemes are presented in Sec. 2.3.3 and Sec. 4.1.1. Studies have already been made with COBRA III-C/MIT. Much of this work has involved the development of techniques for modeling large areas in the radial plane as single calculational channels with equivalent T-H parameters. For example, an entire fuel assembly, containing 176 fuel pins and 5 control rods might be modeled as a single T-H channel for COBRA calculations. Studies that seek to model the core with such large channels are referred to as radial lumping scheme studies.

Previous work with COBRA III-C/MIT and MEKIN is summarized in Table 1.1. Moreno [5] investigated the effects of radial lumping schemes in COBRA III-C/MIT calculations, while Chiu [6] developed two dimensional transport coefficients for use with such schemes to improve the momentum and energy transfer models. Both Moreno and Chiu considered only PWR steady state models.

Steady state PWR sensitivity studies using COBRA III-C were made by Ladieu [7]. Similar studies with COBRA III-C/MIT were made by Emami [8] for BRW's. PWR steady state and flow transient sensitivity in COBRA III-C/MIT was examined by

TABLE 1.1

PREVIOUS STUDIES

Principal Investigator	Code Used	Conditions Modeled	Information Presented
Moreno [5]	COBRA III-C/MIT	PWR Steady State	Method for modeling many sub-channels with few equivalent calculational channels (lumped channel approach)
Chiu [6]	COBRA III-C/MIT	PWR Steady State	Transport coefficients to improve results found with lumped channel approach
Ladieu [7]	COBRA III-C	PWR Steady State	Sensitivity of COBRA solution to user input parameters
Emami [8]	COBRA III-C/MIT	BWR Steady State	Sensitivity of COBRA solution to user input parameters and user selected correlations
Liu [9]	COBRA III-C/MIT	PWR Steady State and Flow Transients	Sensitivity of COBRA solution to user input parameters, discussion of experimental verification of COBRA
Valente [10]	MEKIN	BWR Rod Drop Accident	Coupled transient analysis
SAI [11]	MEKIN	BWR Transients	MEKIN sensitivty studies and rod worth calculations (ongoing study)

Liu [9]. All of the preceding studies were concerned with T-H behavior from a design point of view; thus DNBR, coolant enthalpy and fuel clad temperature were the chief figures of merit.

Comparatively little overall work has been done with MEKIN. Valente [10] attempted to model a BWR rod drop accident with the code. Science Applications, Inc. [11] is currently using the code in BWR rod worth calculations; some coupled steady state and transient sensitivities are being examined before actual rod worth calculations will be made.

1.4 Research Objectives

This thesis attempts to provide guidelines for potential MEKIN users. Many aspects of the T-H solution schemes and models were examined. The sensitivity of these schemes was observed and quantified when possible. Three main objectives were pursued in these studies:

i) assessment of T-H sensitivity of parameters important in coupled calculations;

ii) reduction in the detail of the models used for transient analysis;

iii) evaluation of the range of applicability of T-H models used in MEKIN.

As a result of the first objective, fuel temperature and coolant density were the figures of merit in this study, rather than more accepted T-H design parameters such as peak clad temperature and MDNBR.

In pursuing the second objective, an attempt was made to determine the minimum degree of detail that could be used in the models withou appreciably changing the results of an analysis.

The third objective alerts the user to potential cases where the results of MEKIN analysis must be regarded with skepticism.

CHAPTER 2

OVERVIEW

2.1 The MEKIN Code

A detailed description of MEKIN models and calculational strategies is provided in the code manual [12]. A brief review of these areas is included here so that this study may be seen in the proper perspective.

The MEKIN computer code is capable of three-dimensional transient analysis of LWR cores that takes into account the interaction between the neutronic and thermal hydraulic (T-H) parameters. This is achieved through the use of neutron diffusion theory and state-of-the-art T-H calculational methods.

In the MEKIN analysis, a Cartesian geometry is imposed upon the core, which is divided into a series of rectangular parallelapipeds; neutronics parameters are effectively homogenized and stored for each of these regions. A fine mesh grid for neutronics calculations is then superimposed upon each of these regions in order to provide a more accurate representation of the neutron flux. A sample MEKIN calculational grid is presented in Fig. 2.1.

If T-H parameters are expected to vary in these regions inthe course of a transient (e.g. if the regions correspond to axial segments of a fuel assembly), each region is a T-H

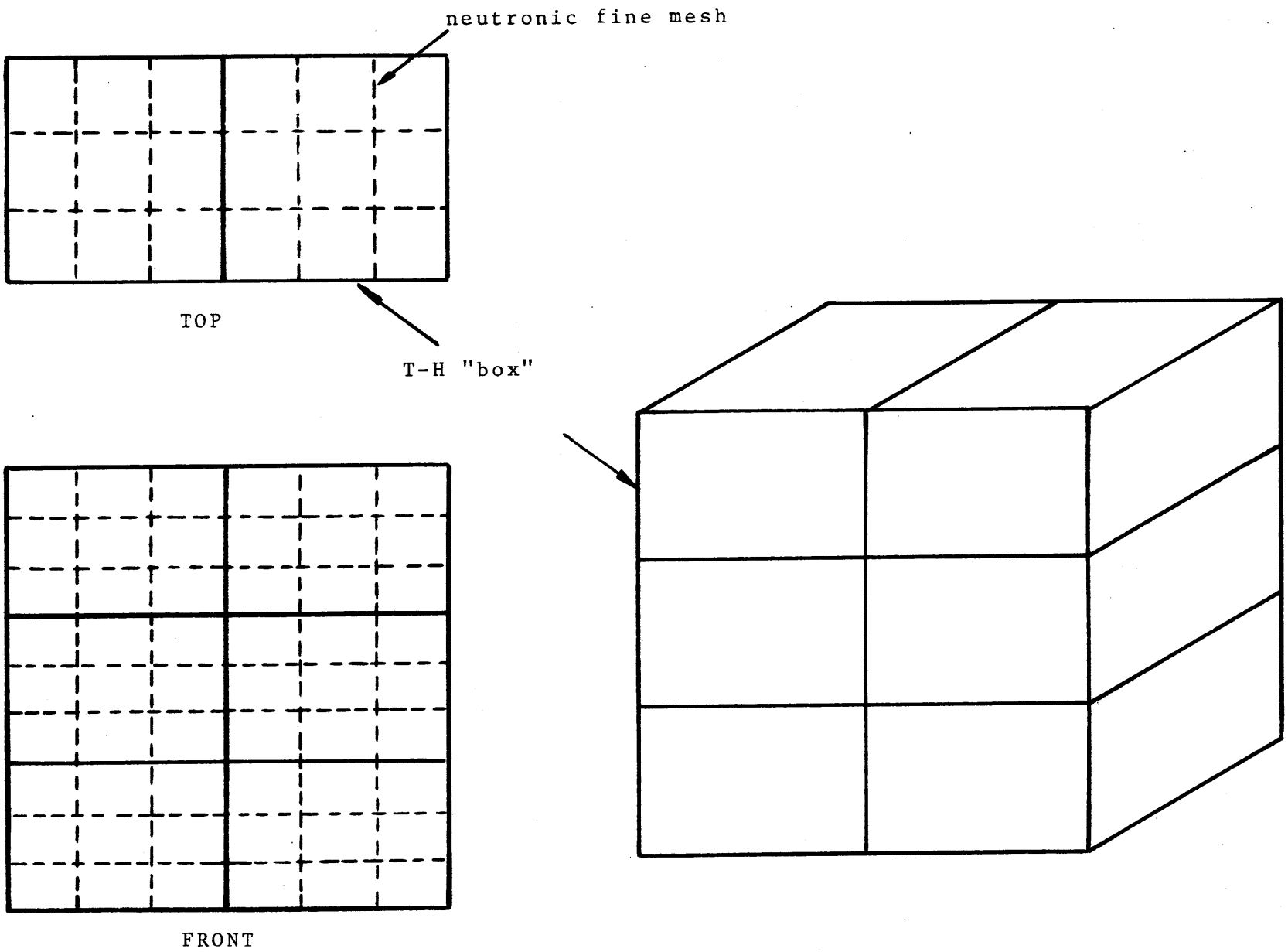

FIG. 2.1: MEKIN CALCULATIONAL MESH (2 channels, 3 axial levels, 2x2 neutronic fine mesh)

calculational volume. Conservation of mass, momentum, and energy is required in each of these volumes.

Different solution schemes are used in steady state and transient MEKIN calculations. However, the overall calculational strategy for coupling neutronic and T-H behavior, shown in Fig. 2.2, is essentially the same. Neutronic cross sections are calculated for a chosen set of T-H conditions and neutronic calculations are performed, taking into account any external neutronic perturbations. Heat generation rates are determined from these results and T-H parameters are updated based on the energy deposition and any external T-H perturbations. An updated set of cross sections for the new T-H conditions is then generated, and the cycle is repeated. In the steady state this process continues until selected convergence criteria are satisfied; in a transient, only one such cycle is used at each time step.

Much data is required to specify neutronic and T-H behavior in a MEKIN analysis. A significant fraction of the cost of a MEKIN analysis results from the vast amount of data that must be stored and managed. In addition, the neutronic and T-H solution techniques are iterative procedures that require many calculations at each iteration. When these techniques are coupled in the overall MEKIN calculation strategy, the resulting execution time and cost are considerable.

Although faster neutronic [13] [14] and T-H [15] solution schemes have been devised since the development of MEKIN , no

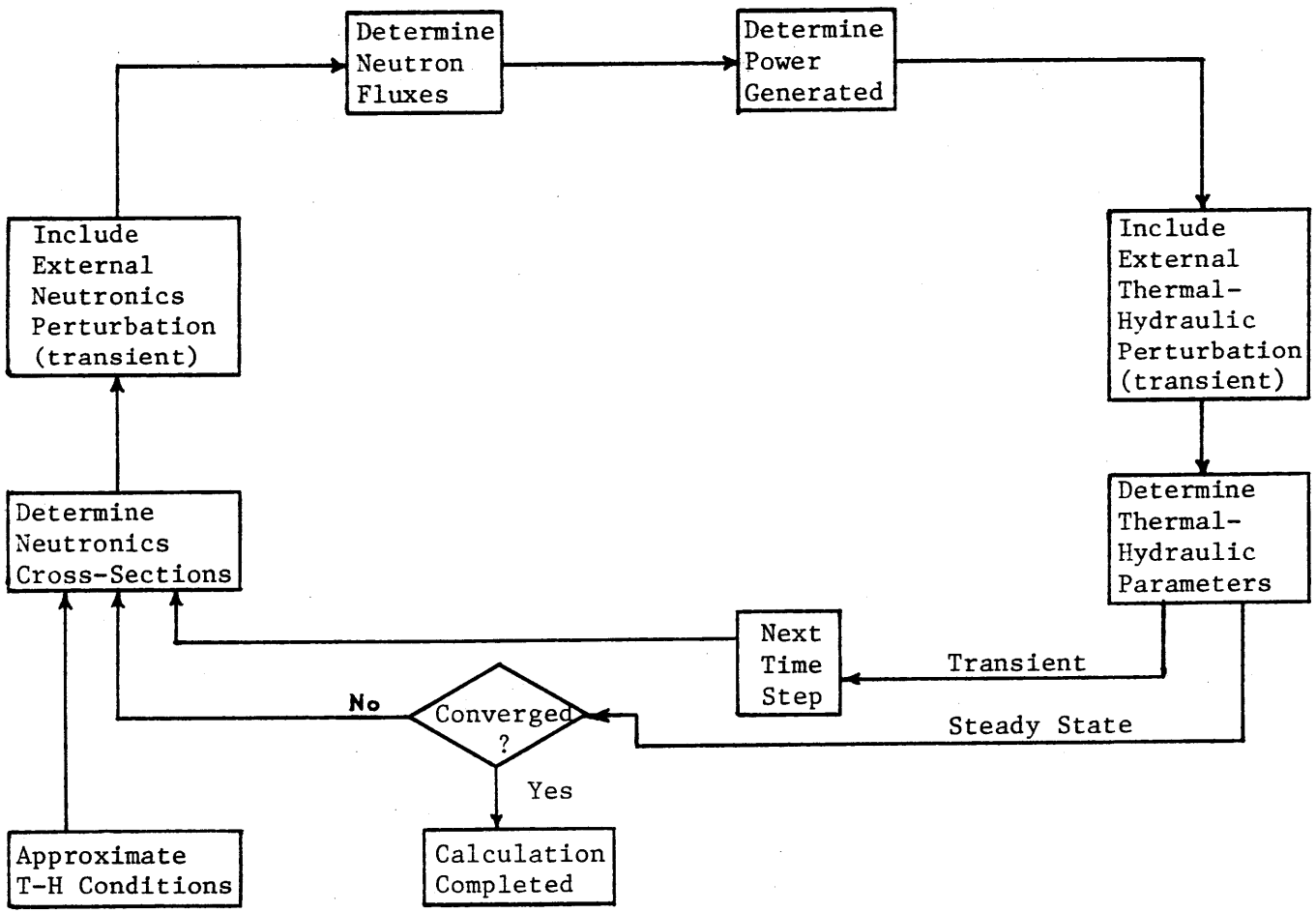

FIGURE 2.2: MEKIN CALCULATIONAL STRATEGY

effort has yet been made to implement these techniques in MEKIN. Preliminary studies have just begun in this area, hence a new, faster, running version of MEKIN will not be available for several years.

2.2 General MEKIN Sensitivity Study

A MEKIN sensitivity study has been undertaken by members of the MIT Nuclear Engineering Department. Little work was done with MEKIN prior to the MIT study, although the code had been used with some success to model a BWR rod drop accident [10]. A similar sensitivity study was performed at Science Applications, Inc. [11] concurrent with the MIT work.

The MIT study was divided into three sections: i) neutronic sensitivity, ii) T-H sensitivity, and iii) coupled neutronic/T-H sensitivity. The work described in this thesis comprises a major part of the second section of the study, namely, the T-H sensitivity.

2.3 T-H Sensitivity Study

2.3.1 Relevant Parameters

Since this effort was intended to establish the effect of T-H models and calculational schemes in a coupled neutronic/T-H computer code, the parameters of interest were those with the most direct impact on the neutronic solution. Coolant density and fuel temperature are most important in this respect, for these parameters are used to update neutronic cross-sections according to equations of the form:

$$\Sigma_f(T) = \Sigma_f(T_{ref}) + \frac{\partial \Sigma_f}{\partial T}(T - T_{ref}) \qquad (2.1)$$

$$\Sigma_c(\rho) = \Sigma_c(\rho_{ref}) = \frac{\partial \Sigma_c}{\partial \rho}(\rho - \rho_{ref}) \qquad (2.2)$$

From a reactor design viewpoint, other T-H parameters may be of greater interest than the fuel temperature and coolant density, but the effect of the design parameters on the neutronic solution is less significant. For example, MDNBR is an accepted design criterion; yet this parameter has no impact whatsoever on the MEKIN solution. MDNBR values are not even computed in a MEKIN analysis.

Although observed sensitivities in the fuel temperature and coolant density are presented in this thesis the significance of these sensitivites in coupled neutronic/T-H analyses is not established. This problem was investigated in the third general study area, coupled neutronic/T-H sensitivity, and will be discussed in a forthcoming thesis [16].

2.3.2 Problems Addressed

A number of interrelated models are used in the T-H section of MEKIN. It was necessary to divide the T-H sensitivity study into four major areas to facilitate determination and discussion of the sensitivities. No single area is completely independent of effects observed in other areas, however the divisions were made to minimize overlap between study areas. The major divisions of this study are:

i) adequacy of the radial lumping scheme

ii) sensitivity to numerical parameters

iii) sensitivity to the fuel pin conduction model

iv) transient sensitivity to two phase flow models and correlations

Detailed descriptions of each study area are given in the following chapters; only a brief explanation is included here.

MEKIN is based on the assumption that the average values of T-H parameters in a region may be determined in both the steady state and transients from a lumped parameter analysis of the region. In a typical MEKIN analysis, an entire fuel assembly is represented as a single T-H channel with several axial levels. The validity of this modeling scheme is examined in the first study area, presented in Chapter Three. The effects of the radial model size on T-H parameters are also discussed in the third chapter.

The second study area, discussed in Chapter Four, is devoted to those parameters that specify the degree of detail desired in the model. Axial mesh size, time step size, and the T-H convergence criterion (T-H C.C.) sensitivities are examined. Values of the numerical parameters are sought to minimize the number of calculations needed for "relatively accurate" results. Relative accuracy is established by comparing coarse mesh solutions with limiting fine mesh results; coarse mesh values are said to be "relatively accurate" if they are within an arbitrarily assigned 2% range of the fine mesh results.

Average fuel temperature is the most significant neutronic feedback parameter in many transients. The model used to determine fuel temperatures is examined in the third study area, which is presented in Chapter Five. The sensitivity of the fuel temperatures to both numerical and physical parameters as well as the effects of the fuel model on the coolant are discussed in Chapter Five.

The significance of the models and correlations used to describe two phase coolant flow is examined in the fourth and final study area which is discussed in Chapter 6. Several different two phase flow options are available in MEKIN. Different options were used to analyze the same transient; the results are presented and compared in Chapter Six. Data bases for the correlations included in MEKIN are also discussed in this chapter.

For optimal use of the code, the parameters and models in the four study areas must be compatible with one another. Little is gained if, for example, a very fine axial mesh and small time step are used along with correlations having a high degree of uncertainty. Sets of parameters and models that complement one another and yield results with the same degree of accuracy should be used to model T-H behavior. The alternative is to set parameters to arbitrarily "tight" values in a haphazard manner. Although this point is not specifically addressed in this thesis, it must be considered when any analysis is performed.

2.3.3 T-H Sensitivity Study Methodology

2.3.3.1 Class of Transients

An infinite number of transients may be analyzed with MEKIN. In order to perform a meaningful study, attention was focused on a specific class of transients. Ideally, this class should have been narrow enough to allow detailed MEKIN sensitivity studies for those transients most often analyzed with the code, yet broad enough to allow extrapolation of observed sensitivities to other transients.

This study has been limited primarily to short (i.e. less than 5 seconds) PWR power transients. Since MEKIN analyses are expensive, and the cost increases with the length of the transient, it is unlikely that many long transients will be analyzed with this code. These long transients might be analyzed with less expensive, quasi-steady state solution schemes.

The use of short transients made detailed sensitivity studies possible in several areas. If longer transients were used, the number of possible studies would have been severely limited by economic constraints.

Consideration was limited to PWR's because a similar study was underway elsewhere for BWR's [17].

Power excursion transients are likely candidates for MEKIN analysis. In the course of these transients, T-H parameters change as energy is deposited, bringing about a corresponding change in neutronic parameters which alters the power generation

and energy deposition. This coupling is strong in extreme power transients, such as the hot zero power rod ejection transient.

Hot zero power initial conditions were used in most sensitivity studies, since these conditions resulted in the most extreme rod ejection transient for the reactor that was modeled. At hot zero power, the reactor is critical and operational, but only a negligible amount of power is generated. The coolant and internal reactor components are all at the same initial temperature.

This initially isothermal condition eliminated most steady state sensitivities that might have propagated into the transient. Although steady state calculations were performed, they served only to initialize temperatures to the same value throughout the core. Few steady state sensitivities could exist, since most values were the same in the steady state, regardless of the modeling scheme employed. For example, there could be no sensitivity to axial mesh size since the coolant enthalpy was the same at each axial level.

Propagation of steady state sensitivity was a concern because studies had been limited to short transients. Had alternate initial conditions been imposed, it is quite possible, given the sluggish response of fuel temperature, that steady state sensitivity would predominate throughout the transient.

Steady state sensitivities are not examined in this thesis, since much work has already been done in this area [5] [7] [8] [17].

Accurate, detailed modeling of an actual PWR core is not

required in a sensitivity study, which seeks to determine the effects of changes in input parameters. A consistent set of input parameters is perfectly adequate. Typical PWR parameters were used throughout this study; a list of these parameters is presented in Appendix A. The results of this study should be applicable to the entire class of current PWR's.

2.3.3.2 Code Used (COBRA III-C/MIT)

T-H calculations in MEKIN are performed by a modified more efficient version of COBRA III-C. This T-H package was developed at MIT and is available in COBRA III-C/MIT as an independent T-H code that may be used for transient T-H calculations if power histories are supplied.

Since COBRA III-C/MIT is used for T-H calculations in MEKIN, the T-H solution schemes of the two codes are identical. The basic T-H models used in these codes are the same as those used in COBRA III-C and described in detail in the COBRA III-C manual [18]. When applied to the same problem, both COBRA III-C and COBRA III-C/MIT yield identical results [19].

Although it is possible to perform transient T-H calculations alone with MEKIN if a power history is provided, the process is both cumbersome and expensive. In order to minimize effort and cost, COBRA III-C/MIT was used in the majority of the T-H sensitivity studies. COBRA III-C/MIT has been modified slightly since its incorporation into MEKIN, making it a more versatile T-H code.

The expanded capability of the current version of COBRA III-C/MIT allows the user to select a non-uniform radial channel grid. In this manner, channel size may be varied and a fine grid may be used in the area of interest while a coarse grid is used in other areas. This feature allows computations to be kept to a minimum when large regions of the reactor core are modeled [5].

The MIT Information Processing Center IBM 370/168 computer was used in all studies.

2.3.3.3 Power Histories

No transient 3-D power history of a rod ejection transient was available for use in the T-H sensitivity study. Such a history might have been obtained, at considerable cost, from a MEKIN analysis of some appropriate base case. However, an accurate power history was not necessary for the sensitivity study.

In this study, the primary concern was not to model an actual transient, but to determine the sensitivity of the code in a typical transient analysis. A power history that resembled actual transient behavior was perfectly adequate for this purpose.

An artificial set of power histories was used throughout this study. These power histories were based on data that was available at the beginning of the sensitivity study. This data included a steady state axial power profile, radial power

peaking factors from steady state neutronic calculations with one control rod fully withdrawn, and also, histories of the total reactor power in a rod ejection transient. This data is included in Appendix B, along with a description of the computer program that was used to generate the artifical power histories.

Different power profiles were created from the above data to study various T-H sensitivities. In certain cases MEKIN was used to generate power profile input for use in COBRA III-C/MIT. A brief description and general classification of the power profiles used in the T-H sensitivity study is presented in Table 2.1; a matrix indicating the studies in which each power profile was used is provided in Table 2.2

The hot zero power coastdown transient, power profile class 2A, was used in the greatest number of studies. This transient will be described here; other transients are described where they are used. An index of these descriptions is included in Table 2.1.

The hot zero power coastdown transient profile class 2A, is a simulation of the transient behavior in a rod ejection accident. The artificial power vs. time curve, presented in Fig. 2.3, was adjusted so that the total energy generated during the artificial transient was approximately equal to that of the actual transient. A steady state power peaking factor was found for each T-H region modeled by multiplying the steady state axial peaking factor by the radial peaking

TABLE 2.1

POWER PROFILES USED

Power Profile Class	Description	Detailed Explanation	
		Section	Figures
1	Steady State MEKIN powers	3.2.1	3.2, 3.3
1 A	Neutronics only		
1 B	Coupled Neutronic/T-H		
2	3 second hot zero power coast down transient		
2A	4% coolant heating	2.3.3.3	2.3
2B	No coolant heating	4.3.3	
2C	Two channels unheated	4.5.1	4.22
2D	Subdivided hot assembly	3.3.1	3.4, 3.5
2E	Different radial configurations	3.4.2	3.6
3	3 second hot full power transient	5.2.1	5.3
4	12 second hot zero power coastdown transient	4.5.1	4.22
5	Prompt jump transient from MEKIN "neutronics	4.1.2	Appendix B

TABLE 2.2

STUDIES WHERE POWER PROFILES WERE USED

power profile class	SENSITIVITY STUDIES								
	Adequacy of single channel per assembly		radial size of model	axial mesh	time step	T-HC.C.	fuel mesh size	h_{gap}	2 ϕ flow models
	steady state	transient							
1A	✓								
1B	✓								
2A				✓	✓	✓	✓	✓	✓
2B					✓				
2C						✓			
2D		✓							
2E			✓						
3							✓		
4						✓		✓	
5				✓	✓				

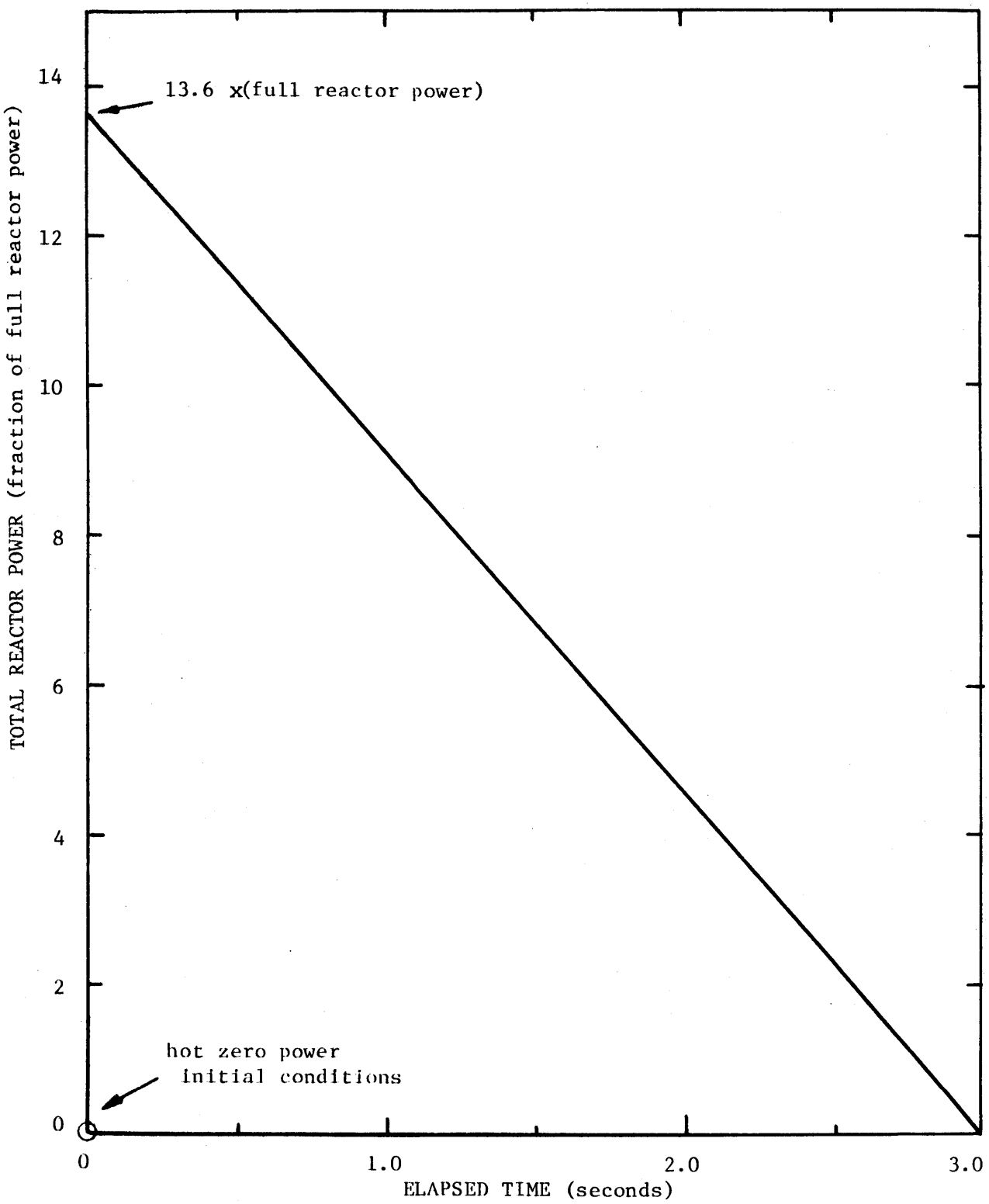

FIG. 2.3: IDEAL POWER HISTORY FOR POWER PROFILE CLASS 2

factor that had been determined from steady state calculations with the control rod withdrawn. This product was then multiplied by a scaling factor to determine the steady state region power. These steady state powers were multiplied by the appropriate value from the total reactor power vs. time curve in Fig. 2.3 to determine region powers throughout the transient.

Gamma and neutron heating of the coolant was simulated in all power profiles, except class 2B, by assuming that 4% of the region power was generated in the coolant.

The power histories that were generated by this method are admittedly approximate and should not be viewed as an attempt to reproduce the power behavior that might be seen in an actual rod ejection accident. These histories are only intended to approximate the actual behavior for the purpose of this T-H sensitivity study.

CHAPTER 3

RADIAL T-H MESH SIZE SENSITIVITY

3.1 Introduction

Coupled neutronic/T-H analyses typically require large amounts of computer storage and may demand excessive execution times. It is to the user's advantage to minimize the number of coupled calculations, especially in transient studies. This may be achieved by limiting the number of T-H regions in the model. Such a reduction in problem size would be found with a model having few T-H channels and a coarse axial mesh. The implications of using models with few T-H channels are discussed here, while T-H axial mesh sensitivity is examined in the next chapter.

The number of T-H channels may be minimized in two ways. First, large regions of the core may be lumped into a single channel (e.g. typical PWR analyses model an entire fuel assembly as a single T-H channel). Second, T-H analyses may be limited to a small portion of the reactor core, with adiabatic, impervious boundary conditions imposed on the exterior channel walls, as in the CHIC-KIN code [20]. A third alternative, namely the use of varying size channels, small in hot, active regions of the core and large in more benign regions [9],

is precluded by the MEKIN requirement of a uniform square grid in the horizontal plane.

3.2 Steady State Lumping Scheme Sensitivity

The adequacy of the lumped "single T-H channel per fuel assembly" modeling scheme for representation of steady state T-H behavior was investigated using both COBRA III-C/MIT and MEKIN.

3.2.1 Methodology

The upper half of two fuel assemblies was modeled specifically for use in this study. A fine neutronic mesh was imposed on this model and a steady state MEKIN analysis was performed to determine the artificial "neutronics only" powers that would result if no T-H feedback were present.

Each of the fuel assemblies was then subdivided into sixty four T-H channels as indicated in Fig. 3.1, and a steady state MEKIN analysis with T-H feedback was performed. Hence two sets of steady state power profiles were generated for the model. One set was based upon an artificial "neutronics only" calculation, the other took into account feedback effects.

Selected radial and axial power profiles for the discrete, fine mesh model are presented in Fig. 3.2 and Fig. 3.3. A radial power tilt may be seen between the hottest and coldest channels, channels 1 and 128. Channel 1 power generation was approximately 2.5 times greater than that of Channel 128. The location of these channels may be seen in Fig. 3.1 and

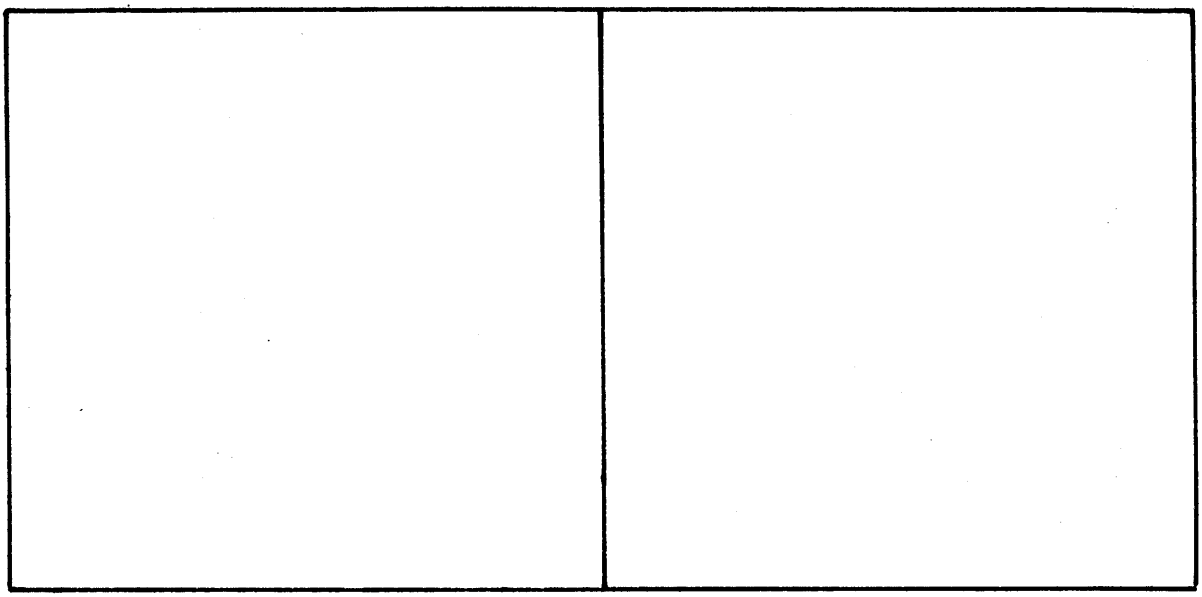

LUMPED CHANNEL MODEL

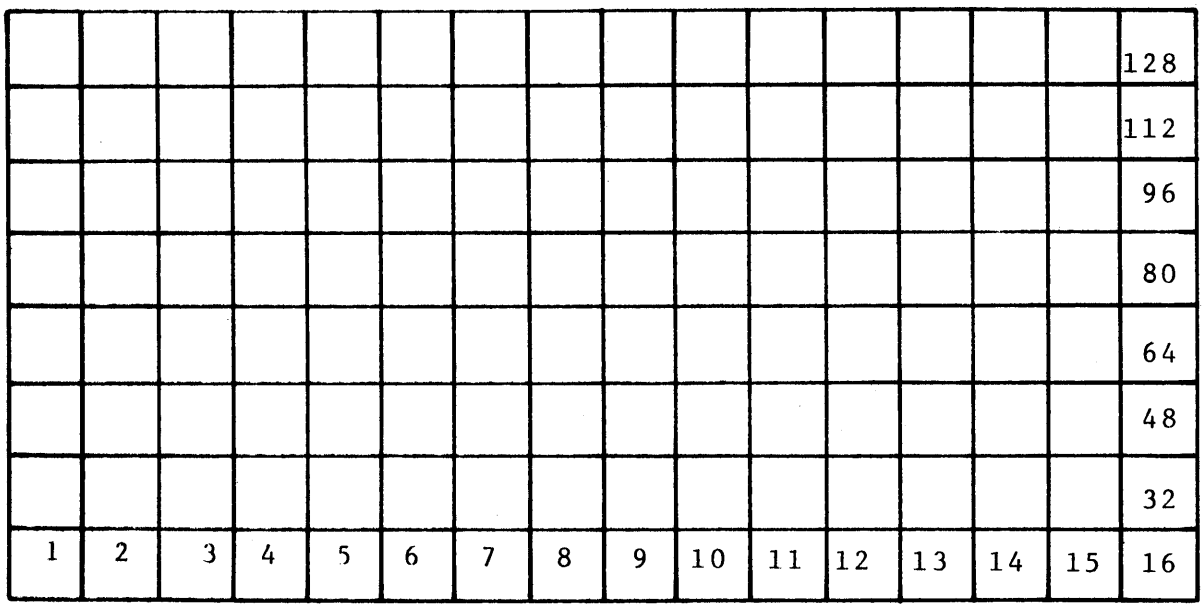

DISCRETE, FINE MESH MODEL AND NUMBERING SCHEME

FIG. 3.1: STEADY STATE DISCRETE AND LUMPED CHANNEL MODELS

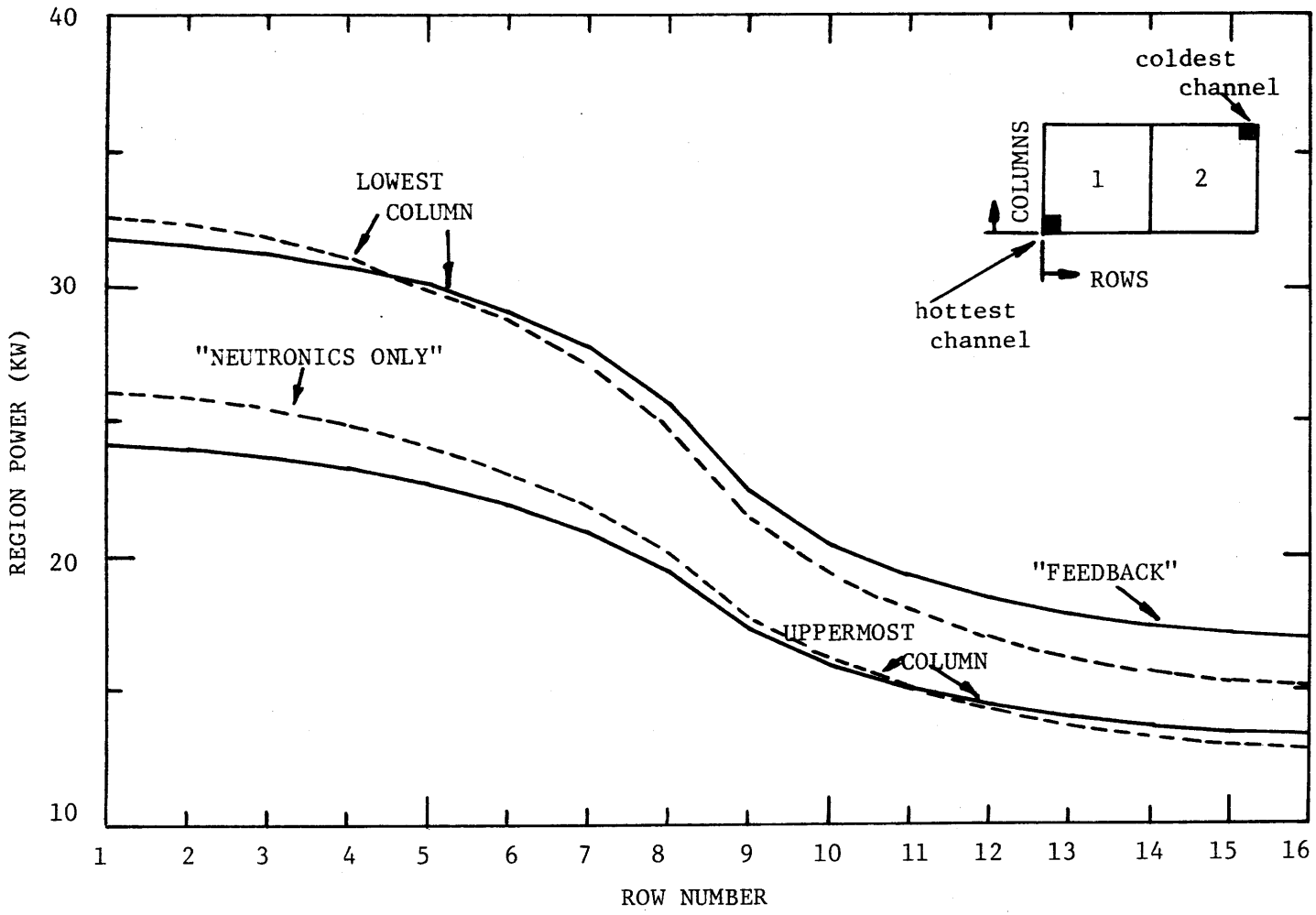

FIG. 3.2: RADIAL POWER PROFILES OF POWER PROFILE CLASS 1

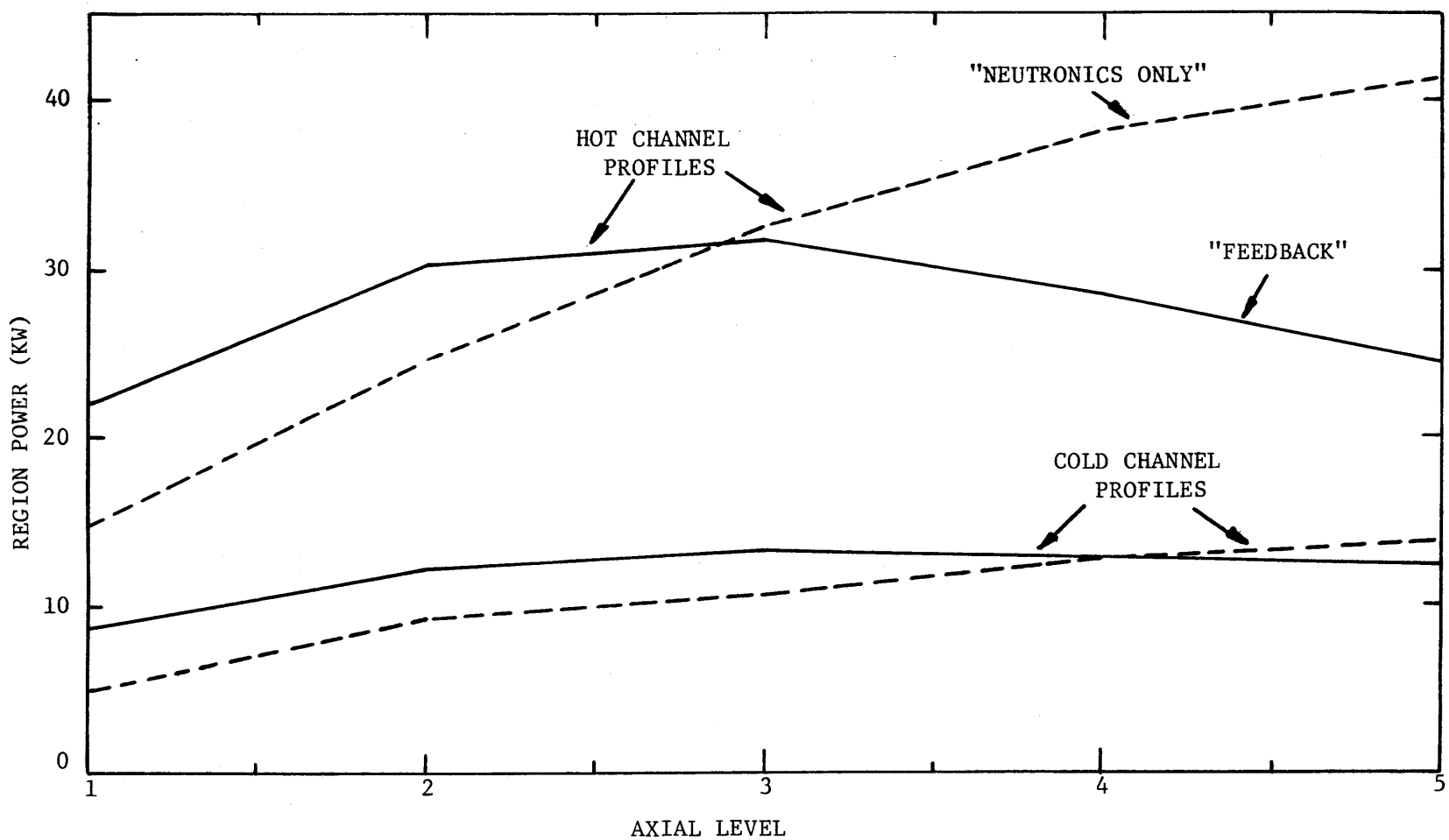

FIG.3.3: POWER PROFILE CLASS1 AXIAL POWER PROFILES

in the insert of Fig. 3.2

Comparison of the "neutronics only" and "feedback" powers shows that the power tilt is increased when feedback effects are ignored. This is seen in both the axial and radial profiles where the neglect of feedback effects increases the difference in power generation between the hottest and coldest channels.

These profiles were used as input to COBRA III-C/MIT analyses in which the fuel assemblies were modeled first as two lumped T-H channels and then as 128 discrete T-H channels. A total of four COBRA analyses were made: lumped and discrete model analyses using "neutronics only" powers, then using the feedback powers.

Two sets of powers were used since neither set alone was completely acceptable. The "neutronics only" profile was jagged, since no T-H feedback was present to smooth the neutron flux shape. Yet the feedback powers were found by assuming a fine mesh (128 channel) T-H representation and presupposing discrete model feedback.

Coolant inlet enthalpy was raised to near the saturated liquid value to encourage boiling. This test was thought to be more extreme than the use of a highly subcooled liquid, since heat transfer and crossflow change drastically at the onset of boiling and increase the importance of local effects.

A simple area weighted averaging scheme was used to

determine average parameters for the discrete models. As will be seen later, when a detailed derivation of these schemes is presented in Sec. 3.3.1, a question arises as to the propriety of this scheme in transients. However, in the steady state, flows differ only slightly from one discrete channel to the next, hence area weighted, mass flow weighted, and volumetric flow weighted averages are virtually identical.

3.2.2 Steady State Results

3.2.2.1 Discrete Average vs. Lumped Channel Behavior

Selected area weighted average parameters from the discrete channel analyses are compared to those found with the lumped, two channel model in Table 3.1.

Excellent agreement is seen between the average discrete coolant parameters and lumped channel coolant values with both power profiles. Good agreement is also seen in the assembly averaged fuel temperatures found with the feedback power profile. Poorer, but by no means unsatisfactory agreement, is seen between the assembly averaged fuel temperatures from the analyses in which "neutronics only" power profiles were used. This weaker agreement with the "neutronics only" powers results from the jagged axial and radial power profiles that result from "neutronics only" calculation, rather than from a deficiency in the T-H model.

As was anticipated, good agreement between average exit parameters of the discrete model and lumped channel exit

TABLE 3.1

DISCRETE AND LUMPED CHANNEL RESULTS (STEADY STATE)

		exit coolant parameters			exit fuel temperature		
		enthalpy	void fraction	quality	center-line	surface	power profile
Assembly	Case	(Btu/lbm)	(-)	(-)	(°F)	(°F)	
1	Lumped	703.34	0.232	0.044	3764.3	1449.4	"neutronics only"
	Discrete Average	703.91	0.232	0.045	3776.2	1457.2	
2	Lumped	683.19	0.0	0.0	2513.9	1148.9	
	Discrete average	683.01	0.020	0.003	2497.0	1144.3	
1	Lumped	701.41	0.213	0.039	2698.6	1174.5	"feedback"
	Discrete Average	701.94	0.215	0.040	2702.8	1176.3	
2	Lumped	685.15	0.016	0.002	2119.8	1042.9	
	Discrete Average	684.93	0.027	0.004	2120.1	1041.4	

parameters was found in the steady state. Little more than a heat balance is performed to arrive at these values in the T-H solution. If the power generated is the same in each case, average discrete and lumped channel results will agree well in the steady state.

3.2.2.2 Average vs. Local Behavior

Parameters from the hottest and coolest discrete channels, along with the average discrete model values from each assembly are listed in Table 3.2. Significant differences between local and average behavior are apparent. The differences are most evident for the fuel temperature, where local centerline values are 700°F greater than the hot assembly average centerline temperature.

The differences between local and average T-H behavior are a direct result of the difference between the discrete fine mesh and assembly average power profiles. Hot channel power is about 15% greater than the assembly 1 average power while the cold channel power is 15% less than the assembly 2 average power.

The single channel per assembly model has been found to yield excellent predictions of average steady state T-H behavior. However, 15% differences between local and assembly average powers have been found to cause large local deviations from assembly averaged T-H behavior. These two findings indicate the desirability of a variable radial mesh option in the MEKIN T-H package.

TABLE 3.2

LOCAL VS. ASSEMBLY AVERAGE BEHAVIOR (STEADY STATE)

	exit coolant parameters		exit fuel temperature		
	enthalpy	void fraction	centerline	surface	power profile
Case	(Btu/lbm)	(-)	(°F)	(°F)	
Channel 1	715.61	0.337	4486.2	1635.2	"neutronics only"
Assembly 1 average	703.91	0.232	3776.2	1457.5	
Channel 128	674.48	0.0	1944.4	991.1	
Assembly 2 average	683.01	0.020	2497.1	1144.3	
Channel 1	709.55	0.288	3657.2	1461.3	"feedback"
Assembly 1 average	701.87	0.215	2702.8	1176.2	
Channel 128	677.96	0.0	1820.1	958.8	
Assembly 2 average	686.07	0.036	2120.1	1041.1	

With such an option, regions of the core with relatively flat power profiles could be represented by a few large T-H channels. Small channels could be used in the same analysis in regions where local peaks in the power profile would be anticipated. In this way, the number of channels and the resulting computation time could be reduced without an appreciable effect on the T-H results.

Until such an option becomes available to the MEKIN user, a cascade-type analysis may be used for coupled steady state calculations. This type of analysis would require at least two individual MEKIN analyses. In the first analysis, a coarse mesh, single T-H channel per assembly model would be used to locate the hot assembly.

The hot assembly would be subdivided into many channels and considered apart from the remainder of the reactor core in the second analysis to determine local hot channel behavior. Implicit in such an analysis is the assumption that the hot channel is located in the hot assembly. If it is thought possible that one of several fuel assemblies might contain the hot channel, fine mesh analyses must be performed for each of these "suspect" assemblies.

Albedo boundary conditions to be used in the fine mesh analyses of these assemblies could be determined from the results of the coarse mesh analysis. Unfortunately, MEKIN will not accept crosseflow boundary conditions; the exterior

"walls" of the subdivided assembly must be modeled as adiabatic and impervious. However, unless flow blockages or very severe power tilts exist in the subdivided assembly, this T-H boundary condition will have little effect on the solution, since crossflow is negligible under normal PWR operating conditions.

3.3 Adequacy of the T-H Lumping Scheme in Power Transients

Insight gained from steady state tests made possible approximations that reduced the cost of similar transient studies and made them economically feasible. The general study method used in the transient remained identical to that of the steady state. The hot assembly was represented as a single T-H channel then subdivided into many T-H channels in a discrete model. Average results from the latter model were compared to those found using the former "single channel per assembly" model.

However, fewer subdivisions were used in the transient discrete models. Also, subtle points became significant when averaging schemes were devised to determine the assembly averaged parameters for the discrete model.

Preliminary transient studies were made in the course of MEKIN development to establish the adequacy of the "single channel per assembly" modeling scheme [20] [21] [22]. These earlier studies were limited to small "canned" BWR bundles which were subjected to mild transients. Extrapolation of these results to drastic PWR transients, such as the rod

ejection accident, is not appropriate since crossflow effects were minimized in the small bundles and mild transients.

3.3.1 Transient Studies Methodology

In a transient COBRA analysis, a complete set of computations is made for every channel at each time step. Computation time increases dramatically as more channels are added to a transient model. This fact necessitated a reduction in the number of channels used in the discrete model of the hot assembly for the transient studies.

Two sets of transient tests were made. In the first set, a single assembly, isolated from the remainder of the core, was modeled first as a single T-H assembly, then divided into 49 channels, as shown in Fig. 3.4.

If an attempt is made to use COBRA to analyze the T-H behavior of a single channel there is no crowwflow and the coefficient matrix in the crossflow equations is singular. The solution scheme breaks down when it attempts to invert this matrix. Because of this, it is essential that a COBRA model consist of at least two channels.

An approximate representation of the isolated hot assembly was used to satisfy this requirement. The model contained an unheated channel adjacent to the hot assembly. The gap width for interchannel momentum and energy transport was reduced to 10^{-4} inches; this effectively eliminated diversion crossflow and turbulent mixing between the two

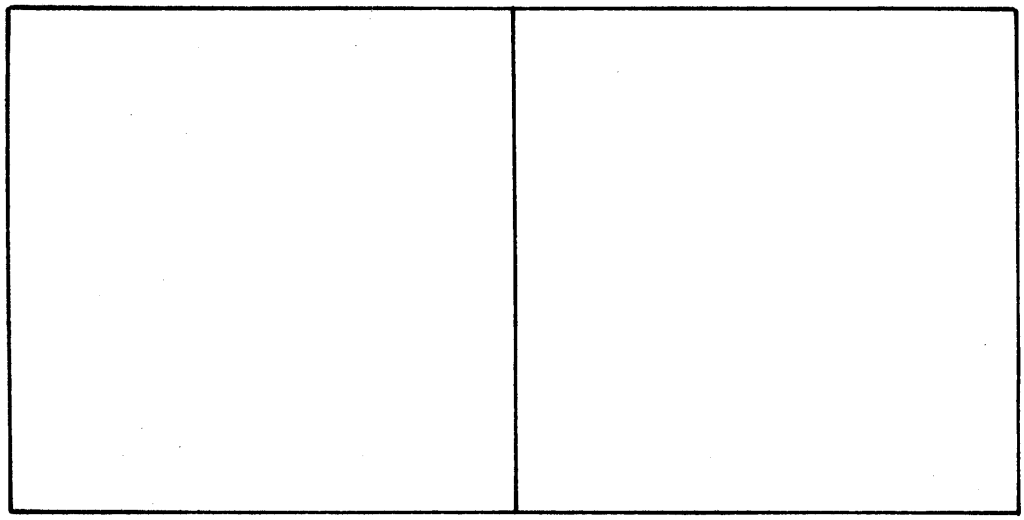

LUMPED CHANNEL MODEL

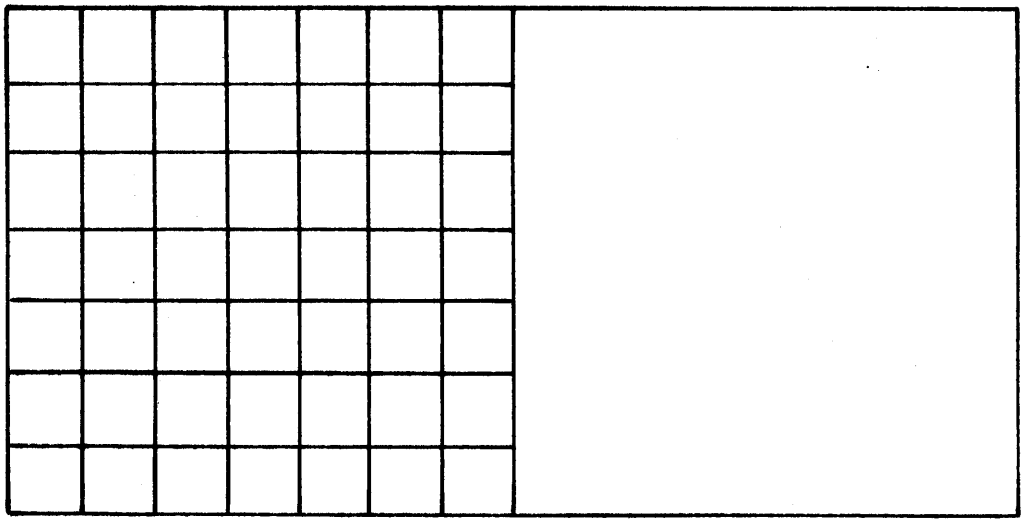

DISCRETE, FINE MESH MODEL

FIG. 3.4: ISOLATED HOT ASSEMBLY MODELS FOR TRANSIENT STUDIES

assemblies yet maintained a non-singular coefficient matrix in the crossflow equations.

In the second series of tests, a hot assembly was located in a model of the reactor quarter core. This assembly was first represented as a single channel, then subdivided into 49 channels, shown in Fig. 3.5.

It would have been possible to modify the model used in the first series of tests to allow a MEKIN analysis The model for the second set of tests, although unsuitable for a MEKIN analysis, was thought to provide a better approximation of the actual transient T-H behavior.

Crossflow and turbulent mixing between adjacent channels are important transport mechanisms. However, MEKIN requires a uniform square grid in the horizontal plane, and simply cannot accommodate a quarter core model using a fine mesh in the hot assembly. To accomplish this would require a fine mesh throughout the quarter core. With the present model, such a mesh would contain 2818 channels. Such an analysis is clearly beyond the ability of even the most advanced computers because of storage limitations and the computation time involved.

In the steady state, the T-H behavior seen with "neutronics only" powers was found to be at least parallel to, if not more extreme than the behavior observed when feedback powers were used. Generation of feedback powers

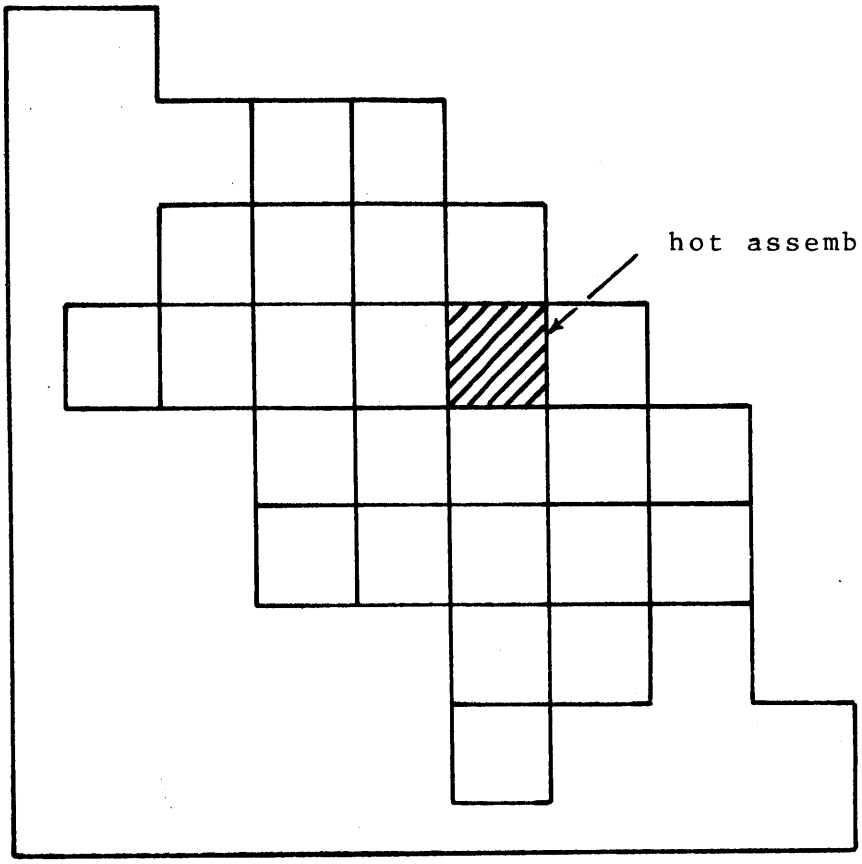

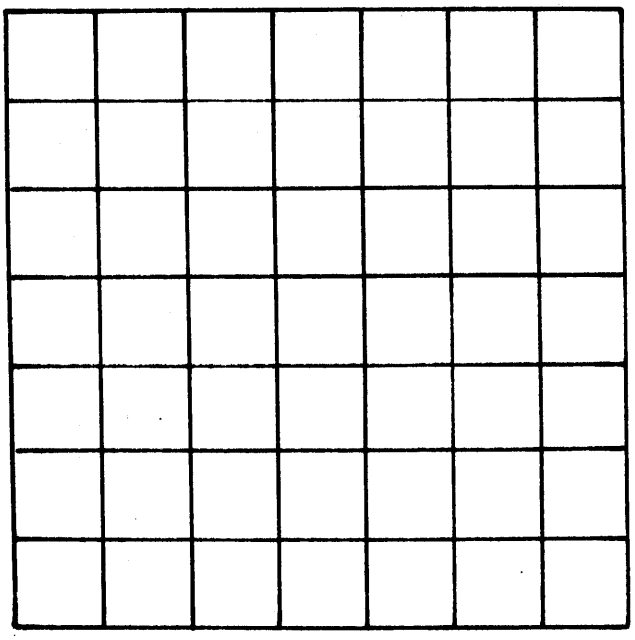

FIG. 3.5: MODELS OF HOT ASSEMBLY IN QUARTER CORE FOR TRANSIENT STUDIES

from the transient studies with a MEKIN analysis was immediately ruled out, because of economic constraints. Even generation of a set of transient "neutronics only" powers would have been too expensive. The steady state "neutronics only" power profile cost $400 to generate on the MIT IPC system using an IBM 370/168 computer.

Steady state runs indicated that a reasonable set of powers (i.e. the "neutronics only" profile) was adequate for radial mesh studies. This finding justified the use of a modified form of the "artifical power history," described earlier in subsection 2.3.3.3, for the transient radial mesh studies. The same total reactor power history was used in this modified history, but radial pin peaking factors were used to determine powers for each of the discrete hot assembly channels. These peaking factors were available from a previous steady state, "neutronics only" analysis with the control rod withdrawn.

Economic constraints also prohibited representation of each assembly as an individual channel in the quarter core configuration. Such a model would have contained 107 channels, 33 more than necessary. Separate transient studies had shown that results found with the 26 channel model in Fig. 3.3, compared well with those from more exact, single channel per assembly models of the quarter core. As it was, 20 CPU minutes of execution time were required to determine the T-H behavior using COBRA III-C/MIT for the first 1.5

seconds of the simulated rod ejection transient with the 74 channel model in Fig. 3.3

Thirteen axial levels (ΔZ = 11.2 inches) were used throughout this study. The first twelve levels were heated since they made up the active fuel length. The uppermost axial level was beyond the active fuel length and was unheated. A time of 0.05 seconds and T-H convergence criterion of 0.1 were used throughout this study, along with the MEKIN default T-H models. A justification of the time step chosen for this study is presented in Sec. 4.3.2 and Sec. 4.3.3; a similar discussion of the T-H convergence criterion appears in Sec. 4.5.2.

3.3.2 T-H Averaging Schemes

An appropriate set of averaging schemes was formulated before the attempt was made to compare average results from the coarse mesh models with their coarse meal counterparts. A set of schemes was selected that would most accurately represent the T-H behavior sought in the coarse mesh analyses. These averaging techniques yield average results at a horizontal plane in the T-H channel. It was required that the weighted averages satisfy the conservation equations.

After the averaging schemes were derived, temporary changes were made in COBRA III C/MIT to print out average results and selected local results when the fine mesh representation of the hot assembly was used. The amount of

computer printout generated for the fine mesh analyses as well as the cost of the analysis were significantly reduced with these modifications.

To satisfy the continuity equation, the sum of the mass flows in the discrete model must equal the total mass flow, that is,

$$\mathring{m}_j = \sum_{i=1}^{49} \mathring{m}_{i,j} \tag{3.1}$$

A quasi 1-D axial flow is assumed in COBRA. Assuming the flow area of a channel is the same at all axial levels,

$$\mathring{m}_{i,j} = \rho_{i,j}\, v_{i,j} A_j \tag{3.2}$$

Substitution of Eq. 3.2 into Eq. 3.1 yields

$$\mathring{m}_j = \sum_{1=1}^{49} \rho_{i,j} v_{i,j} A_j \tag{3.3}$$

The assembly average parameters (denoted by $^{-}$) must satisfy the continuity equation, thus

$$\mathring{m} = \overline{\rho_j}\ \overline{V_j}\ A \tag{3.4}$$

where

$$A = \sum_{i=1}^{49} A_i = \text{total cross sectional area of the hot assembly}$$

An expression for the average coolant density is found upon rearrangement of Eq. 3.4:

$$\bar{\rho}_j = \frac{\mathring{m}_j}{\bar{v}_j A} \tag{3.5}$$

A volumetric flow eighted average density and area weighted average velocity are indicated; that is

$$\bar{\rho} = \frac{\sum_{i=1}^{49} \mathring{m}_{i,j}}{\sum_{i=1}^{49} \frac{\mathring{m}_{i,j}}{\rho i,j}} \tag{3.6}$$

and

$$\bar{v} = \frac{\sum_{i=1}^{49} v_{i,j} A_i}{\sum_{i=1}^{49} A_i} \tag{3.7}$$

It is to be noted that the assembly averaged values defined in Eqs. 3.4 and 3.7 do not rigorously conserve momentum; if this were the case,

$$[\mathring{m}_j \bar{v}_j]_{IDEAL} = \sum_{i=1}^{49} \mathring{m}_{i,j} \, v_{i,j} \tag{3.8}$$

however, the average momentum calculated using Eqs. 3.4 and 3.7 is

$$\mathring{m}_j \bar{v}_j = \sum_{i=1}^{49} \mathring{m}_{i,j} \, \frac{\sum_{i=1}^{49} v_{i,j} Ai}{\sum_{i=1}^{49} A_i} \tag{3.9}$$

It is clear that the right hand sides of Eqs 3.8 and 3.9 differ and are equal only in the trivial case when the mass flow and velocity are the same for all channels in the assembly.

The discrepancy between the average and discrete momentum will affect the interassembly crossflow, which is determined from the momentum equations. Different crossflow behavior was found with fine and coarse radial meshes by other workers, and transport parameters have been proposed to alleviate this problem [6]. Fortunately, as explained in Sec. 4.5.3, minor changes in the diversion crossflow are unimportant in extreme power transients and inaccuracies in the diversion crossflow will have little effect in the present study.

Coolant enthalpies from the discrete analysis were weighted by the mass flow through each discrete channel, that is

$$\bar{h}_j = \frac{\sum_{i=1}^{49} h_{i,j} \, \mathring{m}_{i,j}}{\sum_{i=1}^{49} \mathring{m}_{i,j}} \tag{3.15}$$

Weighting of the enthalpy by the mass flow rate guarantees that energy is conserved when the product of the average enthalpy and total mass flow rate is examined.

For energy to be conserved, the total energy deposition

in the coolant as it passes from the $(j - 1)^{th}$ to the jth level must be detected as an increase in the coolant enthalpy,

$$q_{i,j-1/2} = [\dot{m}_{i,j} h_{i,j} - m_{i,j-1} h_{i,j-1}] / [1-f] \tag{3.16}$$

summing over the entire assembly requires

$$[1-f]\, Q_{j-1/2} = \sum_{i=1}^{49} \dot{m}_{i,j}\, h_{i,j} - \sum_{i=1}^{49} \dot{m}_{i,j-1}\, h_{i,j-1} \tag{3.17}$$

Since the coolant temperature and thermodynamic equilibrium quality are functions of the coolant enthalpy, mass weighting was also used to determine the assembly averaged values of these parameters.

The final coolant parameter of interest is the void fraction. This is defined as the instantaneous ratio of the vapor phase cross sectional area to the total coolant cross sectional area.

$$\alpha \equiv \frac{A_v}{A} \tag{3.18}$$

In keeping with this definition, the average void fraction at a horizontal phase in the hot assembly is

$$\bar{\alpha}_j = \frac{\sum_{i=1}^{49} A_{v_{i,j}}}{\sum_{i=1}^{49} A_i} \tag{3.19}$$

or, employing the definition in e.g. (3.18),

$$\bar{\alpha}_j = \frac{\sum_{i=1}^{49} \alpha_{i,j} A_i}{A} \tag{3.20}$$

The conservation of energy is invoked once again in the determination of an averaging scheme for fuel temperatures. The energy deposited in the fuel must raise the fuel enthalpy. Since the density and specific heat of the fuel are constant throughout T-H calculations, enthalpy increases are directly proportional to temperature increases,

$$^{f}q_{i,j}\Delta t = \rho_f C_{p_f} (T_{i,j} - T'_{i,j}) A_{if} \Delta z \tag{3.21}$$

Thus, for the entire assembly,

$$^{f}Q_j \Delta t = \sum_{i=1}^{49} {}^{f}q_{i,j}\Delta t = \rho_f C_{p_f} \Delta z \sum_{i=1}^{49} (T_{i,j} - T'_{i,j}) A_i \tag{3.22}$$

or

$$^{f}Q_j \Delta t = \rho_f C_{p_f} (\bar{T}_j - \bar{T}'_j) \tag{3.23}$$

where

$$\bar{T}_j \equiv \frac{\sum_{i=1}^{49} T_{i,j} A_i}{\sum_{i=1}^{49} A_i} \tag{3.24}$$

An an area weighted fuel temperature averaging scheme is seen to be appropriate.

3.3.3 Applicability of Averaging Schemes for Neutronics Feedback Calculations

The time scale for neutronics behavior is several orders of magnitude less than that of T-H phenomena. For all intents and purposes, the coolant is stationary insofar as neutronic behavior is concerned. In this case, a volume or area weighted averaging scheme would be more appropriate for determining the average coolant density instead of the volumetric flow weighted scheme described earlier.

To expect agreement between the results of a transient lumped channel analysis and area weighted averages from a discrete channel analysis is, in the case of coolant density, simply asking too much of the T-H solution scheme. Unless a density weighted average velocity is chosen, the product of the area weighted average density, average velocity, and total cross sectional area of the hot assembly will not be equal to the sum of the mass flow rates of individual channels; the total average mass flow will not equal the sum of the discrete mass flows.

A flow average density is implied by the COBRA solution scheme, which calculates the coolant density from the coolant enthalpy. Enthalpy changes result from heat addition per unit mass of coolant, as explained later in section 4.5.3. The change in enthalpy during a power transient is the ratio of the coolant heat deposition rate

to the mass flow rate. The density calculated from the new coolant enthalpy is thus flow weighted.

Tests were made using both area weighted and volumetric flow weighted schemes to calculate the average coolant density from the discrete analyses so that the effect of the averaging scheme could be determined.

3.3.4 Results of the Comparison

3.3.4.1 Discrete Average vs. Lumped Channel Behavior

Average discrete and lumped channel analysis results at selected transient times are listed in Table 3.3. As might be anticipated, given the sluggish response of the fuel (i.e. fuel response time = 5 seconds), excellent agreement is seen between fine and coarse model fuel temperatures. Deviations of no more than 0.5 degrees Fahrenheit are seen in the worst cases.

Since a relatively small portion of the fuel (i.e. the region near the fuel surface) feels the effect of changes in coolant behavior during this brief transient, the fuel temperature is essentially independent of the radial lumping scheme chosen. So long as the same amount of fuel is present and energy deposition is equal, average discrete fuel temperatures will be identical to the lumped values.

Good agreement (i.e. less than 1% difference) is also seen between average and lumped channel enthalpies throughout the transient. Similarly, the volumetric flow averaged

TABLE 3.3

DISCRETE AVERAGE AND LUMPED CHANNEL RESULTS (TRANSIENT)

		Exit enthalpy	Minimum density		Maximum void fraction	Max. fuel centerline temperature	Max. fuel surface temperature
	units	(Btu/lbm)	(lbm/ft^3)		-	(°F)	(°F)
	weighting scheme	mass flow	volumetric flow	area	area	area	area
elapsed time (secs)	total no. of channels						
0.5	74	597.69	42.63	42.44	-	1880.8	1518.5
	26	597.29	42.69		-	1880.7	1518.1
	50	600.27	42.54	42.29	-	1880.8	1518.4
	2	599.36	42.62		-	1880.7	1518.0
1.0	74	708.74	25.52	22.45	0.383	2982.5	1998.7
	26	705.13	26.62		0.366	2982.2	1997.8
	50	714.22	25.72	22.66	0.376	2982.5	1998.4
	2	708.51	26.92		0.345	2982.2	1997.5
1.5	74	791.75	15.43	13.79	0.697	3841.2	2224.4
	26	786.03	16.05		0.681	3840.9	2223.1
	50	781.53	16.76	14.79	0.656	3841.2	2223.9
	2	774.24	17.50		0.636	3840.9	2222.6
2.0	26	813.94	14.05		0.743	4449.3	2281.6
	50	802.83	15.09	13.49	0.708	4449.7	2282.6
	2	795.43	15.62		0.694	4449.3	2281.6

density compares well with the coarse model values. Just after the onset of nucleate boiling (i.e. one second into the transient), when the coolant density is most sensitive to slight variations in enthalpy, differences of less than five percent are seen between the volumetric average density of the discrete model and the density found with the single channel per assembly model. Void fraction also compares well in all cases.

As explained in the preceding section, neutronic phenomena would not detect a volumetric flow weighted average coolant density, but an area weighted average; these are also listed in Table 3.3 and will now be examined.

Only fair agreement is found between area weighted average and coarse model coolant density. After the onset of nucleate boiling, one second into the transient, the area weighted average density is almost 4 $^{lbm}/ft^3$ less than the lumped channel density, corresponding to a 15% difference in values.

Results indicate that the choice of weighting schemes has little effect on single phase average coolant density (e.g. 0.5 seconds into the transient). In two phase flow however, the differences mentioned above exist between the information provided for updating neutronics parameters (volumetric flow averaged density) and the information that is expected by the neutronic models (area weighted average

density). This is a subtle point that must be taken into account when the results of coupled neutronic/T-H analyses are examined.

This problem might be eliminated through the use of parameters similar to the transport coefficients calculated by Chiu [6], but which would be used to modify the results of T-H calculations rather than the T-H solution scheme. The proposed "feedback correction coefficients,"(η_f) would multiply the volumetric flow weighted density; the resulting product would be equal to the area weighted density. That is

$$\rho^a_{k,j}(t) = \eta_{k,j}(t)\ \rho^v_{k,j}(t)$$

when the superscripts "a" and "v" indicate area weighted and volumetric flow weighted averages, respectively.

For example, with the transient used in this study it was found that the minimum volumetric flow average density in the hot assembly was 1.125 times greater than the minimum area average density. The feedback correction coefficient is thus $\eta_{k,j}$ (1sec) = 1.125.

Determination of the feedback correction coefficients will be no easy task. The need for these coefficients arises when local subchannel coolant velocities and densities differ significantly from one subchannel to the next. Coupled, fine mesh MEKIN calculations will be required to determine the local transient behavior. In some cases it

may be necessary to use one T-H channel for each fuel pin to accurately determine local behavior. The feedback correction coefficients found in this manner would be dependent on both the transient and the model used in the analysis.

Not only would these coefficients vary from one class of transients to the next, but different coefficients would be needed at each axial level in each fuel assembly modeled. If axial mesh size were changed, the feedback correction coefficients would also change.

Unless it can be demonstrated the the volumetric flow weighted average density has the same effect as the area weighted average density in coupled neutronic/T-H transient calculations, terms like the proposed feedback correction coefficients must be used to adjust for the discrepancy. Otherwise, coupled MEKIN analyses will be of little value.

3.3.4.2 Average vs. Local Behavior

As in steady state studies, significant differences are found between the behavior of the hottest and coldest channels when compared to the assembly average in Table 3.4. Local fuel temperatures are seen to vary by more than 500°F from the average value, a differences of 18%.

Similarly, local coolant behavior also shows a marked deviation from the assembly average. Just after the onset of nucleate boiling, local minimum coolant densities of the

TABLE 3.

LOCAL VS. AVERAGE TRANSIENT BEHAVIOR IN HOT ASSEMBLY

Elapsed time (sec)	Model	Channel	Exit enthalpy (Btu/lbm)	Minimum density (lbm/ft^3)	Max. fuel centerline temperature (°F)	Max fuel surface temp. (°F)	Max fuel clad temperature (°F)
0.5	74 chan.	hot	602.07	42.14	2178.5	1735.4	677.9
		average	597.69	42.63	1880.7	1518.1	-
		cool	592.70	42.96	1720.1	1401.3	644.6
	50 chan.	hot	603.71	42.12	2178.8	1735.5	675.3
		average	599.36	42.62	1880.7	1518.0	-
		cool	596.71	42.96	1720.1	1401.2	644.2
1.0	74 chan.	hot	735.59	20.33	3524.9	2322.2	751.6
		average	708.74	25.52	2982.2	1977.8	-
		cool	689.22	30.13	2689.7	1824.2	729.9
	50 chan	hot	733.38	21.38	3525.4	2322.1	745.6
		average	714.22	25.72	2982.5	1998.4	-
		cool	700.66	29.93	2689.7	1824.0	718.1
1.5	74 chan.	hot	834.01	12.40	4574.4	2598.0	770.3
		average	791.75	15.43	3841.2	2224.4	-
		cool	767.63	17.43	3445.4	2023.1	727.4
	50 chan.	hot	804.33	14.37	4575.1	2597.7	764.6
		average	791.53	16.76	3841.2	2223.9	-
		cool	764.01	18.72	3445.4	2022.8	722.0

hottest and coldest channels show a deviation of $\sim 5\ ^{lbm}/ft^3$ or 20% from the minimum average density.

The large local deviations from assembly average parameters that have been observed in both steady state and transient T-H studies indicate the desirability of fine mesh analyses in selected regions of the model. A fine radial mesh is needed in the hot assembly and other regions where local power profiles deviate significantly from the assembly average power. If such a mesh is to be used, a variable radial T-H mesh size option must be included in MEKIN. This option, as described in subsection 3.2.2.2, would eliminate the requirement of a uniform square radial mesh for T-H analysis and would allow channels of varying sizes to be used in the same analysis.

The temporary cascade-type analysis proposed for use in steady state calculations until a variable radial mesh option becomes available in MEKIN cannot be used in transient analyses. Such a method would require both time varying albedo and crossflow boundary conditions in the second stage of the analysis. Neither is currently available in MEKIN. As will be seen in Sec. 3.4, crossflow is non-negligible in power transients. Even if time varying boundary conditions could be imposed, it is likely that they would be inadequate. Local effects would cause different crossflow patterns in fine and coarse mesh transient analyses. At present, MEKIN cannot accurately

model local effects in a transient analysis.

3.4 Sensitivity to Model Size

3.4.1 Objectives

The computations required for transient analyses may be reduced by limiting the model size to include the minimum required portion of the reactor core. Differences between results found with "in core" and "out of core" (isolated) models of the hot assembly have already been seen in the previous section. The effect of the number of assemblies included in the model is examined in this section.

A plausible model imposes adiabatic, impervious boundary conditions on the exterior walls of a few channels. The argument is then made that the resulting analysis will be conservative, since the energy excess in these channels may not be relieved by transport to contiguous channels. However, complex mechanisms are involved in T-H transients and this argument may not be valid.

3.4.2 Methodology

One quarter of the reactor core modeled in these studies contained 57.5 fuel assemblies. The noninteger number of assemblies comes about because the core centerlines fell in the middle, rather than on the edge of the central fuel assemblies. Consideration was limited to the quarter core based on symmetry arguments (i.e. a symmetric

rod ejection transient was postulated). Hot assembly behavior was then modeled using various configurations of the neighboring assemblies. A single T-H channel per fuel assembly was used throughout most of this study.

A twenty-six channel representation of the quarter core was the largest used in this study. Results found with this model in other studies compared well with those of larger, more exact models of the quarter core. The single channel per assembly scheme was retained near the hot assembly in this model, however the farthest assemblies were all lumped into a single T-H channel, as in Fig. 3.4.

The other radial schemes tested are shown in Fig. 3.6. As explained earlier in section 3.2.1, it was necessary to model an isolated channel as two channels with a very small effective gap width to prevent diversion crossflow and turbulent mixing between the channels.

Radial power peaking factors for each of the assemblies in the quarter core were obtained from a steady state neutronics analysis with the control rod withdrawn. These were used to generate power histories for new configurations. These power histories comprise the 2E class of power profiles, referred to in Table 2.1. Behavior of the hot assembly was noted throughout the simulated rod ejection transient for each configuration.

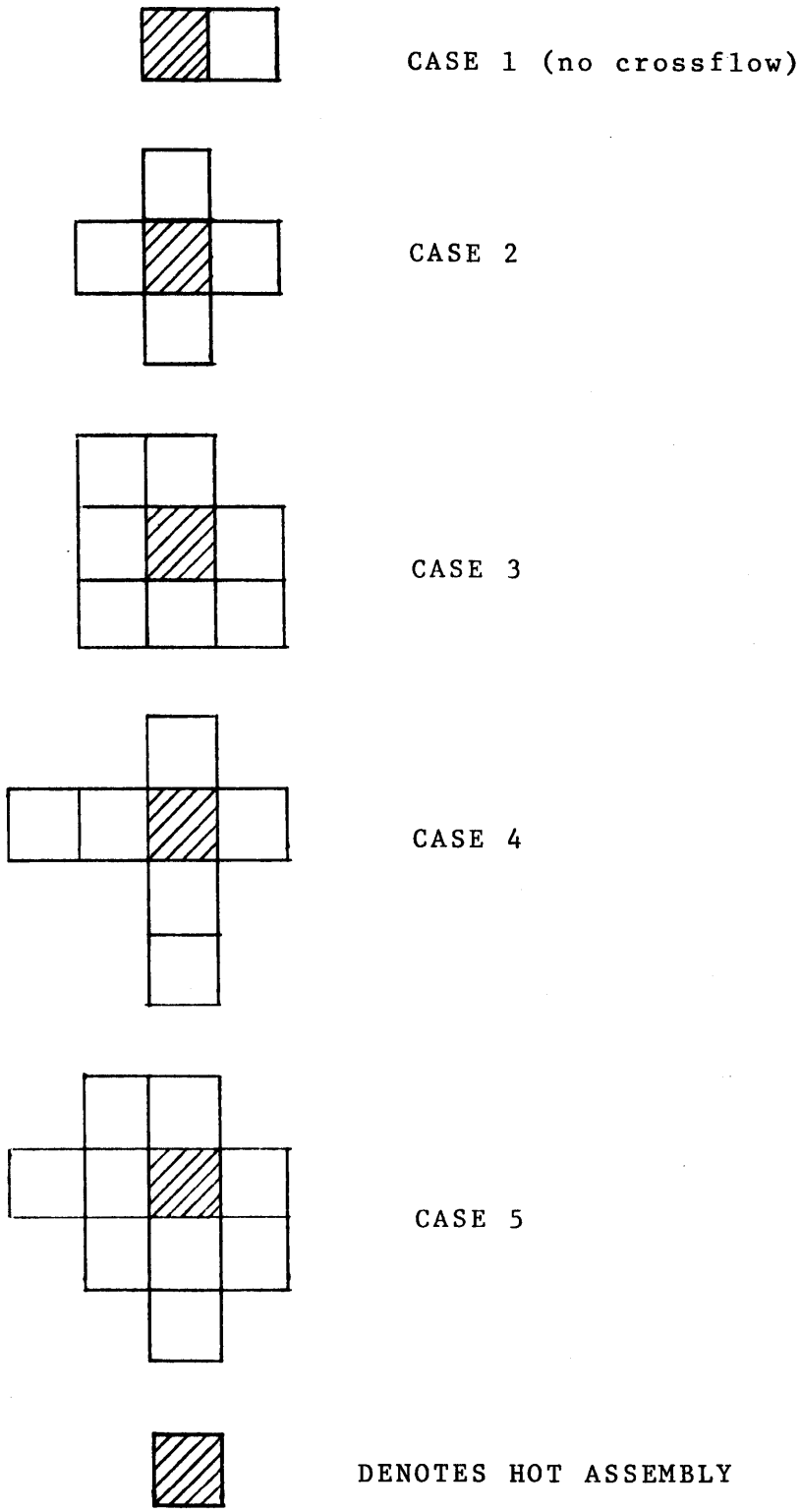

FIG. 3.6: ALTERNATE ASSEMBLY CONFIGURATIONS MODELED

3.4.3 Results

Selected hot channel parameter values at different times in the transient are presented in Table 3.5. Inspection of these values indicates that the outlet mass flow rate of the hot assembly is highly sensitive to the radial representation of the model. This sensitivity is apparent in single phase flow (0.5 seconds elapsed time), but is most pronounced for two phase flow (elapsed times greater than 0.75 seconds). The highest sensitivity is seen just after the onset of nucleate boiling, one second into the transient.

Higher mass flow rates result in higher clad-coolant heat transfer coefficients and correspondingly lower clad and fuel surface temperatures. A slight sensitivity to the model configuration is seen in these parameters.

Greater mass flow rates decrease the coolant enthalpy for constant heat flux. If however, the mass flow rate increase is large enough to cause substantial changes in the clad-coolant heat transfer coefficient, the heat flux may increase and a net enthalpy increase may occur. In these tests, the heat flux increase was dominant, resulting in higher coolant enthalpy at higher flow rates for the smaller models.

Coolant density is calculated from the coolant enthalpy, so the sensitivity of the density parallels that of the

TABLE 3.5

HOT CHANNEL PARAMETERS WITH VARIOUS MODELS

Case	Exit enthalpy (Btu/lbm)	Minimum density (lbm/ft^3)	Outlet flow (lbm/sec)	Maximum fuel surface temperature (°F)	Maximum clad temperature (°F)	Elapsed time (sec)
1	609.38	41.94	172.65	1654.2	670.4	
2	605.98	42.11	167.58	1679.8	671.8	
3	605.89	42.11	166.00	1679.8	672.1	0.5
4	606.01	42.11	167.73	1679.8	671.8	
5	605.94	42.11	166.59	1679.8	672.0	
26 channel	607.03	41.98	156.47	1679.9	674.6	
1	744.38	20.70	207.09	2200.5	730.5	
2	730.08	21.06	157.59	2238.8	741.7	
3	733.80	20.62	144.50	2238.8	742.4	1.0
4	734.37	20.93	158.25	2238.7	741.7	
5	736.17	20.74	149.12	2238.7	742.2	
26 channel	748.36	18.49	120.63	2239.1	737.6	
1	816.18	14.07	164.34	2457.0	755.9	
2	808.16	14.24	145.02	2501.1	758.7	
3	808.73	14.09	137.42	2501.2	759.4	1.5
4	810.05	14.12	144.29	2501.1	758.7	
5	811.07	14.00	138.54	2501.1	759.2	
26 channel	847.91	11.93	100.02	2501.8	765.1	
1	840.96	12.67	153.98	2523.7	756.0	
2	832.35	12.87	136.16	2569.3	769.5	
3	835.85	12.67	126.85	2569.4	770.4	2.0
4	832.82	12.85	136.40	2569.3	769.4	
5	835.75	12.69	129.54	2569.3	770.1	
26 channel	882.26	10.59	92.49	2570.1	764.5	

1	829.73	13.34	149.62	2444.6	750.7	
2	826.78	13.27	130.93	2488.3	763.8	
3	830.42	13.05	122.34	2488.4	764.5	2.5
4	827.62	13.22	130.96	2488.3	763.8	
5	830.45	13.08	124.81	2488.4	764.3	
26 channel	867.61	11.24	93.50	2489.2	757.9	
1	805.63	15.01	143.39	2243.9	740.9	
2	800.17	15.18	124.47	2283.0	744.3	
3	802.24	14.93	117.22	2283.1	744.8	3.0
4	801.29	15.08	125.27	2283.0	744.2	
5	802.45	14.97	119.61	2283.1	744.6	
26 channel	825.69	13.46	98.67	2283.9	746.4	

*Cases refer to Fig. 3.6.

TABLE 3.5 (continued)

enthalpy, although this is not obvious from the data presented in Table 3.5. Exit enthalpy, rather than maximum enthalpy is listed in this table. The two values differ because of the unheated length that has been included as the uppermost axial level of the models, as described earlier in Sec. 3.3.1.

The explanation for the sensitivity of the mass flow rate to the radial lumping scheme lies in the effect of this scheme on the interchannel crossflow, shown in Fig. 3.7 and Fig. 3.8. As the number of assemblies in the model is increased, pressure increases in the hot assemblies may be relieved by increased crossflow rather than accelerated axial flow. These pressure increases result from the expansion of the coolant as it is heated.

It is obvious from these studies that an increase in the number of assemblies represented will result in a more accurate approximation of the hot assembly behavior. However, the size of the model must be greatly increased to bring about significant changes. Given MEKIN's uniform channel size requirement this suggests the use of many T-H channels. Increasing the model size from 5 to 10 assemblies has little effect on hot channel parameters. This is seen when case 2 and case 5 results from Table 3.6 are compared.

It would appear that radial modeling should be restrictive (e.g. 5 assemblies) or all-inclusive (e.g.

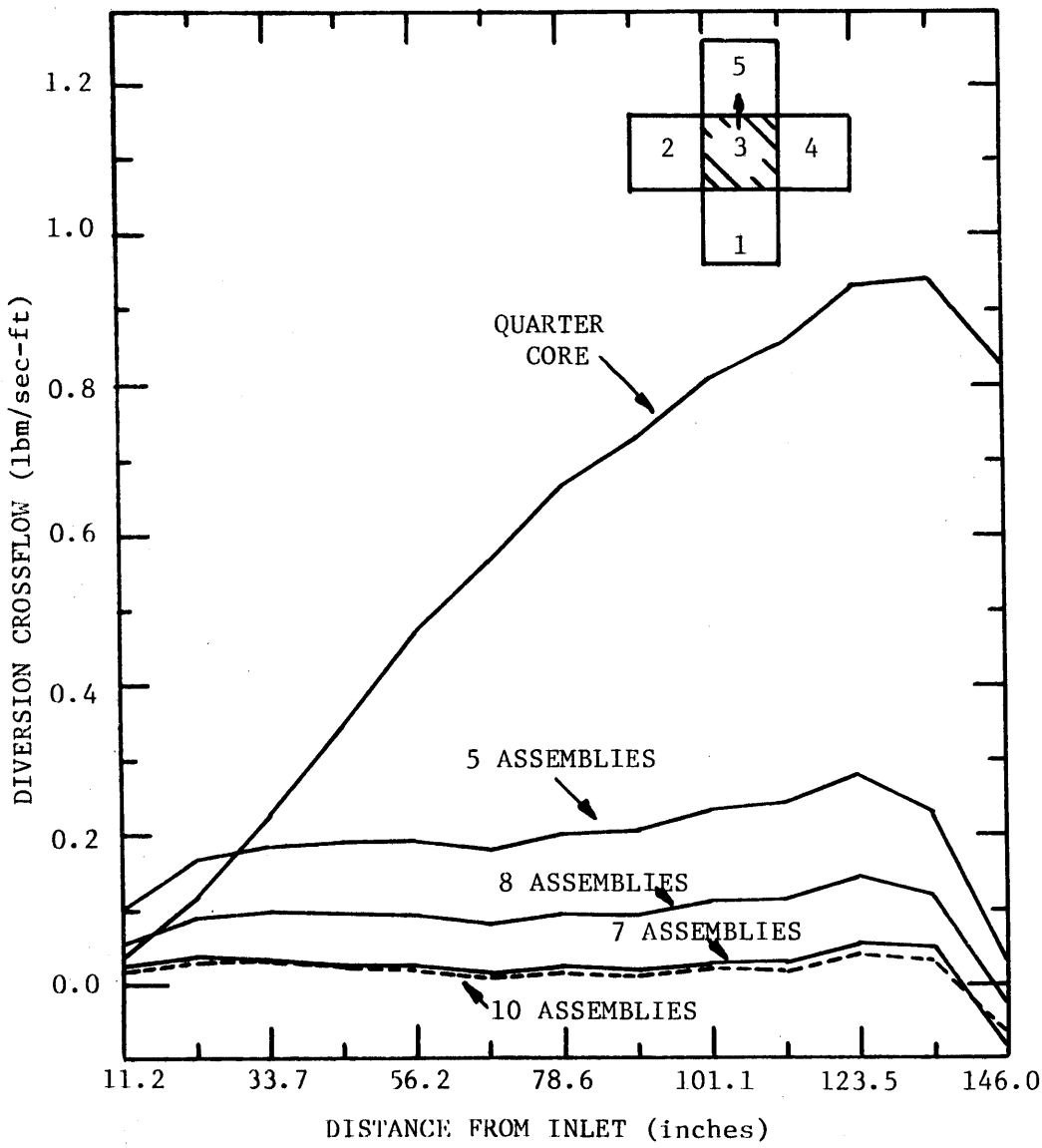

FIG. 3.7: EFFECT OF RADIAL MODEL SIZE ON CROSSFLOW
(single phase coolant flow, t = 0.5 seconds)

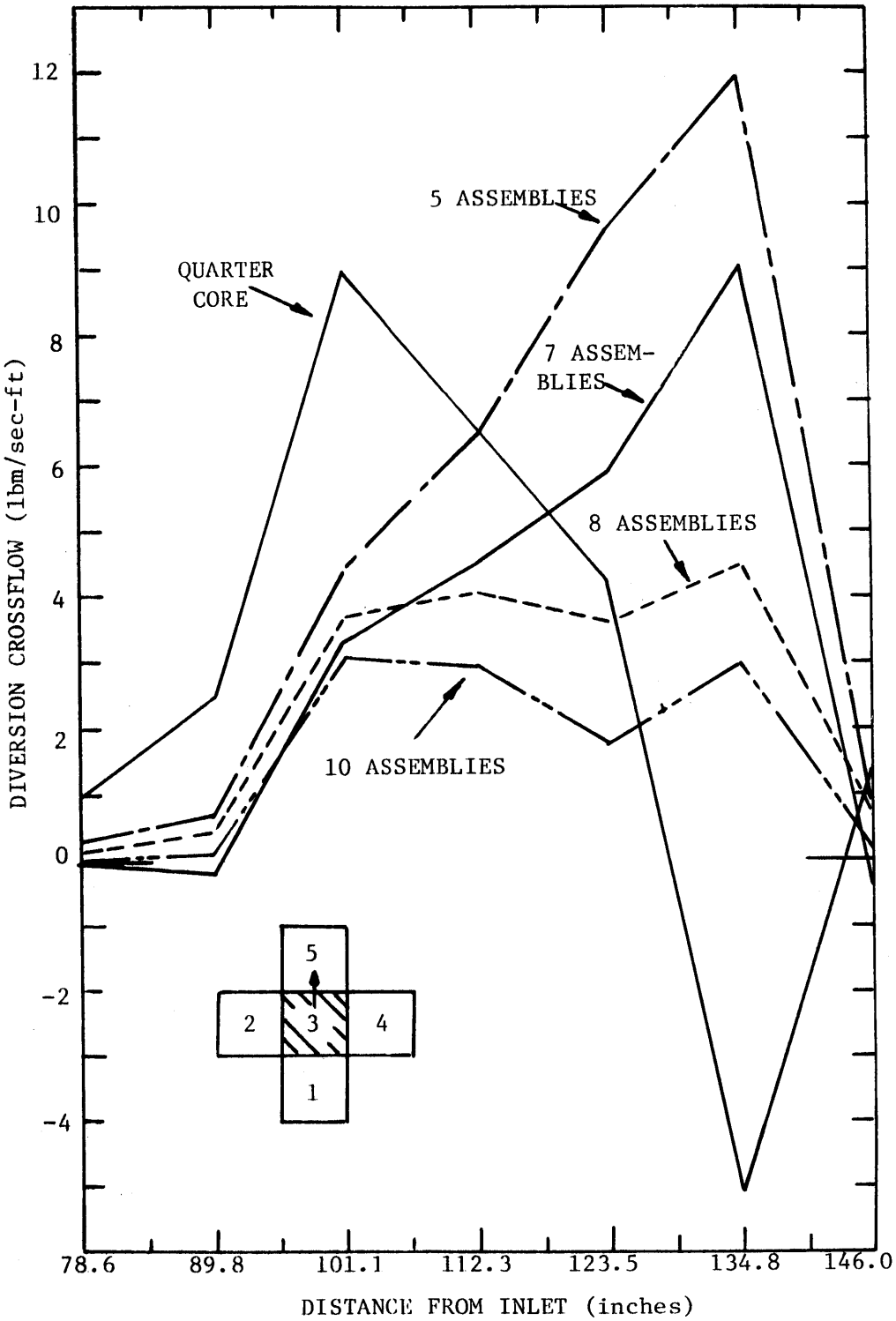

FIG. 3.8: EFFECT OF RADIAL MESH SIZE ON CROSSFLOW
(two phase coolant flow, t = 1.0 seconds)

quarter core modeling, 57.5 assemblies). Intermediate size models increase the computation time without substantially altering the T-H behavior of the hot assembly.

It is also apparent that limiting the analysis to a few assemblies and imposing adiabatic, impervious boundary conditions on the exterior walls is not, in all cases, a conservative approximation from the T-H viewpoint.

Although the energy generated is indeed "trapped" within these channels, the artificial flow acceleration that occurs when the energy is deposited in the coolant has significant effects. Higher clad-coolant heat transfer coefficients are calculated, resulting in lower clad and fuel temperatures than found with quarter core models. These differences are not great, hence the small model still yields a very good, inexpensive approximation, if not a conservative one.

3.5 Summary of Radial Mesh Results

Hot assembly T-H parameters from a single channel per assembly, coarse mesh analysis agreed well with the assembly average values from fine mesh models. Results were in good agreement only when the correct T-H averaging schemes were used. These averaging schemes were appropriate for neutronic feedback calculations in most cases. However, a volumetric flow weighted average coolant density is calculated by the MEKIN T-H package while an area weighted average is expected

by the neutronic package.

Significant differences between the volumetric flow weighted and area weighted average densities were found in two phase flow (e.g. 15% just after the onset of boiling). Feedback correction coefficients have been proposed to adjust the density found with the T-H solution scheme for use in neutronic feedback calculations. Determination of these coefficients will be both difficult and expensive. Feedback correction coefficients will not only be transient dependent, but also model dependent.

Local parameters deviated significantly from assembly average results in both steady state and transient studies. These deviations were found when the local power profile differed from the assembly average power.

Changes in the number of assemblies included in small models were found to have little effect on the predicted hot assembly behavior. However, hot assembly results were quite different when the entire quarter core was modeled.

Both the local deviations from assembly average values and the desirability of modeling very large regions of the reactor indicate that a variable size radial T-H mesh option should be included in MEKIN. The option should be similar to the "simplified method" option currently available in COBRA III-C/MIT. With such an option, quarter core or full core models could be used that would be capable of representing local behavior in selected regions. These

models would represent cooler, less important regions of the core with a few large T-H channels composed of several assemblies each. Hot regions of the core would be represented by several channels, each containing only a few fuel pins. With a model of this nature, the hot assembly cross-flow would be accurately represented and local behavior could be determined.

A variable size radial T-H mesh optionis essential if meaningful studies are to be made at a reasonable cost with the MEKIN code.

CHAPTER 4

NUMERICAL SOLUTION SCHEME PARAMETER SENSITIVITY

4.1 Introduction

When a continuous system, such as the core of a nuclear reactor, is modeled as a series of discrete regions and an analysis is performed which uses numerical approximations to the governing equations, the end result may exhibit a dependence on parameters that are not needed to describe the phenomena, yet which are essential to the analysis. These parameters describe the model and degree of accuracy chosen by the analyst.

In the T-H portion of MEKIN, there are three such parameters: axial mesh size, time step size, and the thermal hydraulic convergence criterion (T-H C.C.). The radial lumping scheme will also effect the results. However, many factors are involved in the selection of such a scheme; consequently this topic was addressed separately in Chapter Three.

4.1.1. T-H Solution Technique (COBRA III-C/MIT)

As explained in the second chapter, MEKIN models the reactor core as a series of contiguous channels, square in the horizontal plane, which are divided into a uniform series of axial levels. One axial level of such a channel

is a rectangular parallelepiped and may simply be described as a T-H "box" as illustrated earlier in Fig. 2.1. The T-H solution technique used in MEKIN requires that mass, axial and transverse momentum and energy are conserved for each of these "boxes" throughout both steady state and transient analyses.

Several assumptions are made in applying these requirements in order to arrive at the set of equations comprising the T-H solution scheme. Briefly, these assumptions model coolant behavior as one dimensional, two phase, homogeneous flow with slip, and neglect sonic velocity propagation. Both turbulent mixing and diversion crossflow serve as transport mechanisms between adjacent channels.

Energy is deposited in the coolant both directly, to model, neutron and gamma heating, and indirectly by the heat flux from the fuel, as determined by the fuel pin conduction model.

A detailed presentation of the models and assumptions just outlined, along with the resulting equations, is provided in the COBRA III-C manual [18]. The range of applicability of these models is discussed in Chapter Seven.

A set of coupled equations is generated in satisfying the conservation requirements imposed on a T-H "box." None of the resulting equations may be solved independently of the others. This difficulty is overcome through the use of an

iterative method in which an initial set of values is updated by substitution into the equations until the desired degree of precision is obtained.

A flowchart of the COBRA III-C iteration scheme for transient analysis appears in Fig. 4.1. The method begins by setting powers and boundary conditions according to the prescribed forcing functions. The inlet condition for mass flow are then used in the energy equations to solve for the enthalpy of the coolant at the first axial level. Coolant parameters are calculated based on the enthalpy and are used to determine the interchannel crossflow from the pressure gradients at the previous level. Axial mass flow is determined from the crossflow solution. This process is repeated at each axial level, using values from the previous levels, until the exit is reached. The entire procedure used to advance across the core and solve for coolant parameters is referred to as a single T-H iteration.

Iterations are made until the mass flow rate at each of the axial levels in every channel satisfies the thermal-hydraulic convergence criterion (T-H C.C.). This is defined as

$$\text{T-H C.C.} \equiv \left| \frac{\overset{\circ}{m}_j - \overset{\circ}{m}_j{}'}{\overset{\circ}{m}_j} \right|$$

where ' denotes the previous iterate value. Calculations moves to the next time step after the T-H C.C. has been

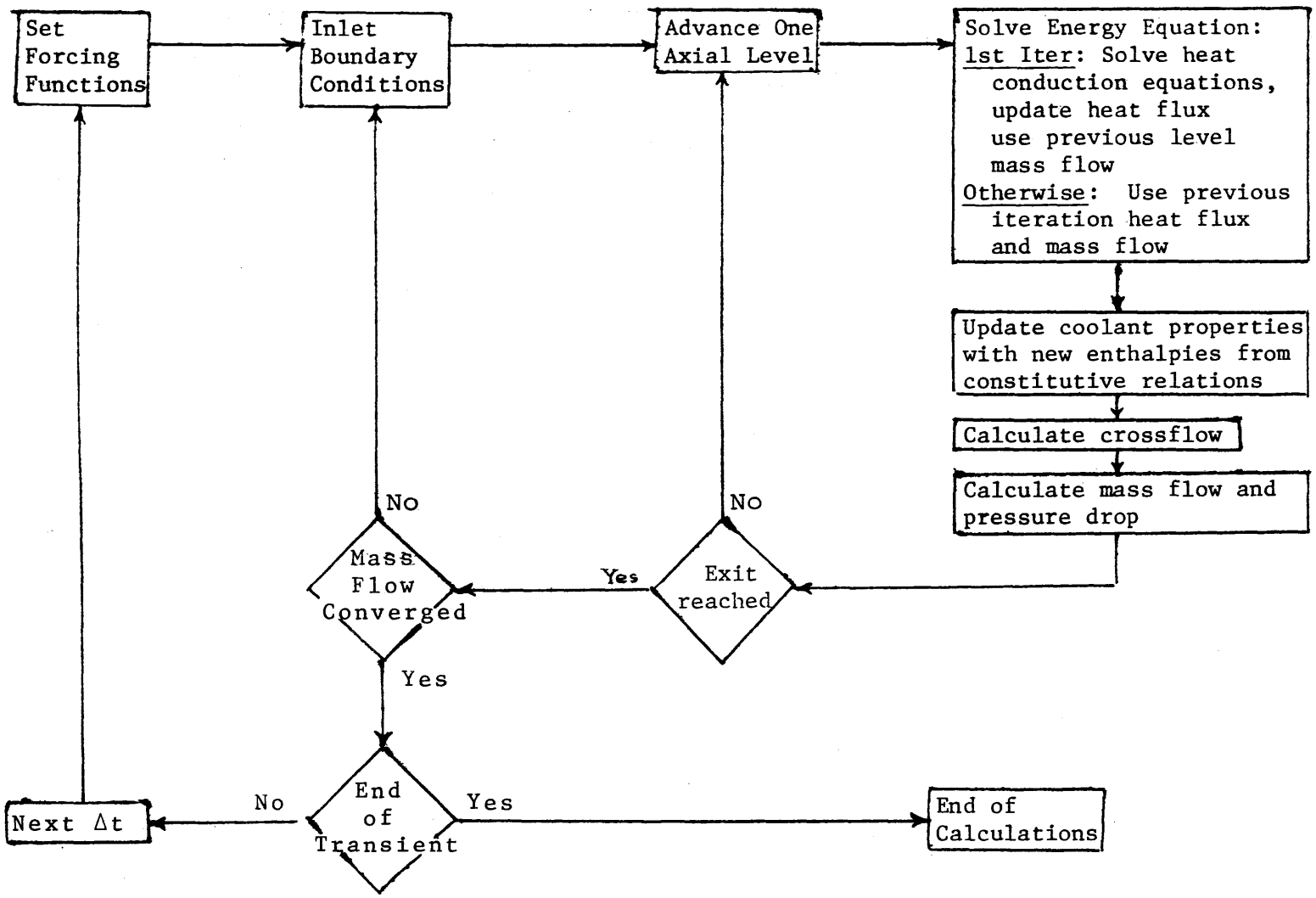

FIGURE 4.1: COBRA TRANSIENT SOLUTION STRATEGY

satisfied in a transient analysis.

4.1.2 General Methodology for Numerical Parameter Studies

In order to perform a meaningful evaluation of a solution technique's sensitivity to a specific parameter, one must be certain that the observed sensitivity is caused by that parameter. A number of options for T-H modeling are available to the MEKIN user. To ensure that an observed sensitivity was attributable to a specific parameter, the default set of T-H models was used throughout all studies described in this chapter. In addition, all other user selected parameters were held constant while a single parameter was varied.

Since the resulting sensitivities are not known to be linear functions, superposition of sensitivities is not, in general, valid. Hence, the sensitivity that will be observed when two or more parameters are varied simultaneously may not be equal to the sum of the sensitivities found when each of the parameters was varied independently of the others.

However, a linear approximation to the sensitivity will be valid for small changes in the input parameters. Thus, for small changes in the input parameters superposition of individual sensitivities may be used to predict sensitivities for simultaneous variation of the parameters. This linear approximation becomes less accurate as the changes in the

input parameters deviate from the test values. In these cases, superposition of individual sensitivities may be misleading.

A basic dichotomy exists between the models used for T-H calculations. Although emphasis has often been placed on the flow models, the transient fuel conduction model is of at least equal, if not greater importance, for power excursion analysis. This model is used to calculate the amount of energy that is transferred to the coolant during the transient. An essential parameter in this calculation is the best transfer coefficient between clad and coolant, which is largely dependent on coolant properties. Hence, a coupling exist between the fuel conduction and coolant models.

The rod ejection transient was divided into two parts, the prompt jump and a power coastdown. Both parts were used independently in the axial and time step sensitivity studies. Since coolant parameters remained essentially unchanged during the prompt jump phase, an unobstructed investigation of the fuel conduction model sensitivity was possible. On the other hand, in the power coastdown, the overall sensitivity of the coupled fuel conduction and coolant models could be observed as the coolant enthalpy and fuel temperatures changed during this transient.

Small models were formulated to test the numerical parameter sensitivities to reduce the cost of the studies. Two models were used. A 2 channel, 3 axial level model was

used with the prompt jump, power profile class 5, discussed in Appendix B. While a 5 channel, 13 axial level model shown in Fig. 4.2, was used with power profile class 2A described in subsection 2.3.3.3.

The smaller model was deemed adequate for the prompt jump studies since coolant properties were constant. The larger models, used in the power coastdown, allowed better representation of coolant behavior, which was significant in the longer transient.

4.2 Axial Mesh Sensitivities

4.2.1 Cases Studied

A range of values were used to assess the significance of the axial mesh size. Mesh sizes of 1.4, 2.8, 5.6, and 11.2 inches were used in the prompt jump studies while values of 6.1 12.3, and 24.4 inches were tested in the power coastdown. Time steps of 0.002 and 0.05 seconds, respectively, were used in the prompt jump and power coastdown transient analyses.

4.2.2 Sensitivities in the Fuel Temperature

The effects of axial mesh size became evident upon examination of the axial fuel centerline temperature profiles. These are presented in Fig. 4.3 for the prompt jump and Fig. 4.4 for the power coastdown. As the mesh size is increased, the axial power shape is less accurately represented. As a

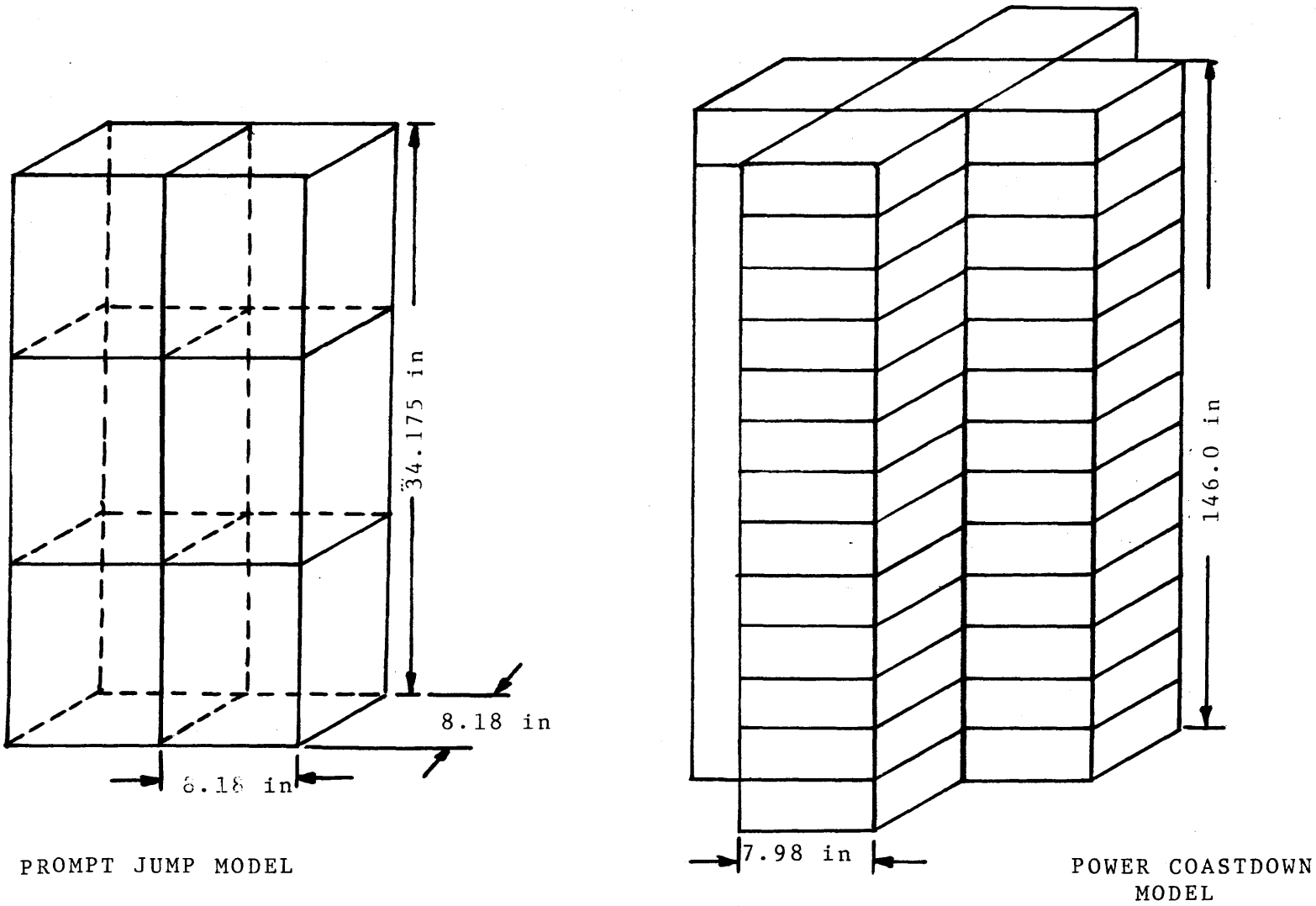

FIG. 4.2: T-H MODELS USED IN NUMERICAL PARAMETER SENSITIVITY STUDIES

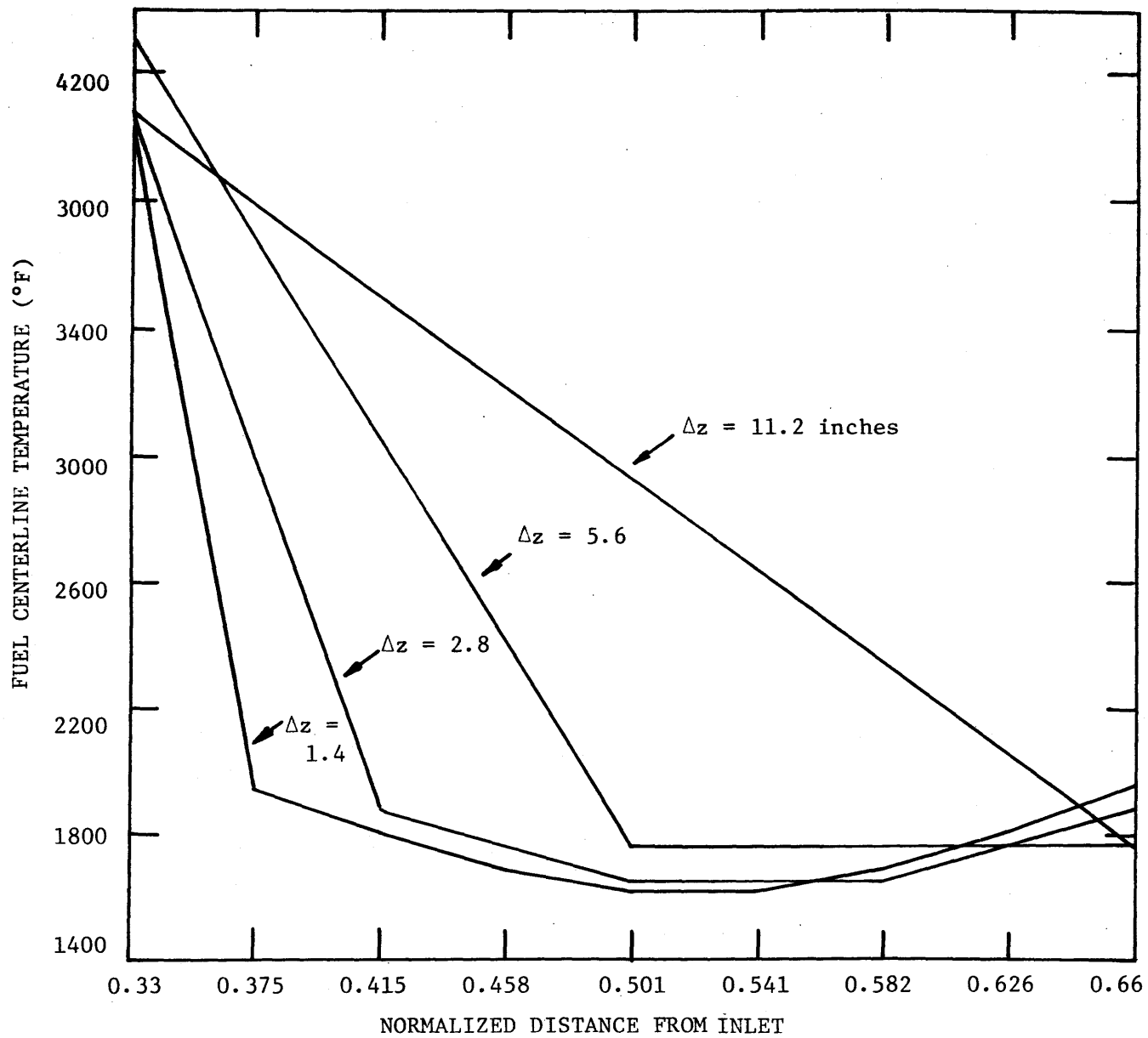

FIG. 4.3: FUEL CENTERLINE TEMPERATURE SENSITIVITY TO AXIAL MESH SIZE
(Power Profile Class 5, t = 0.02 seconds)

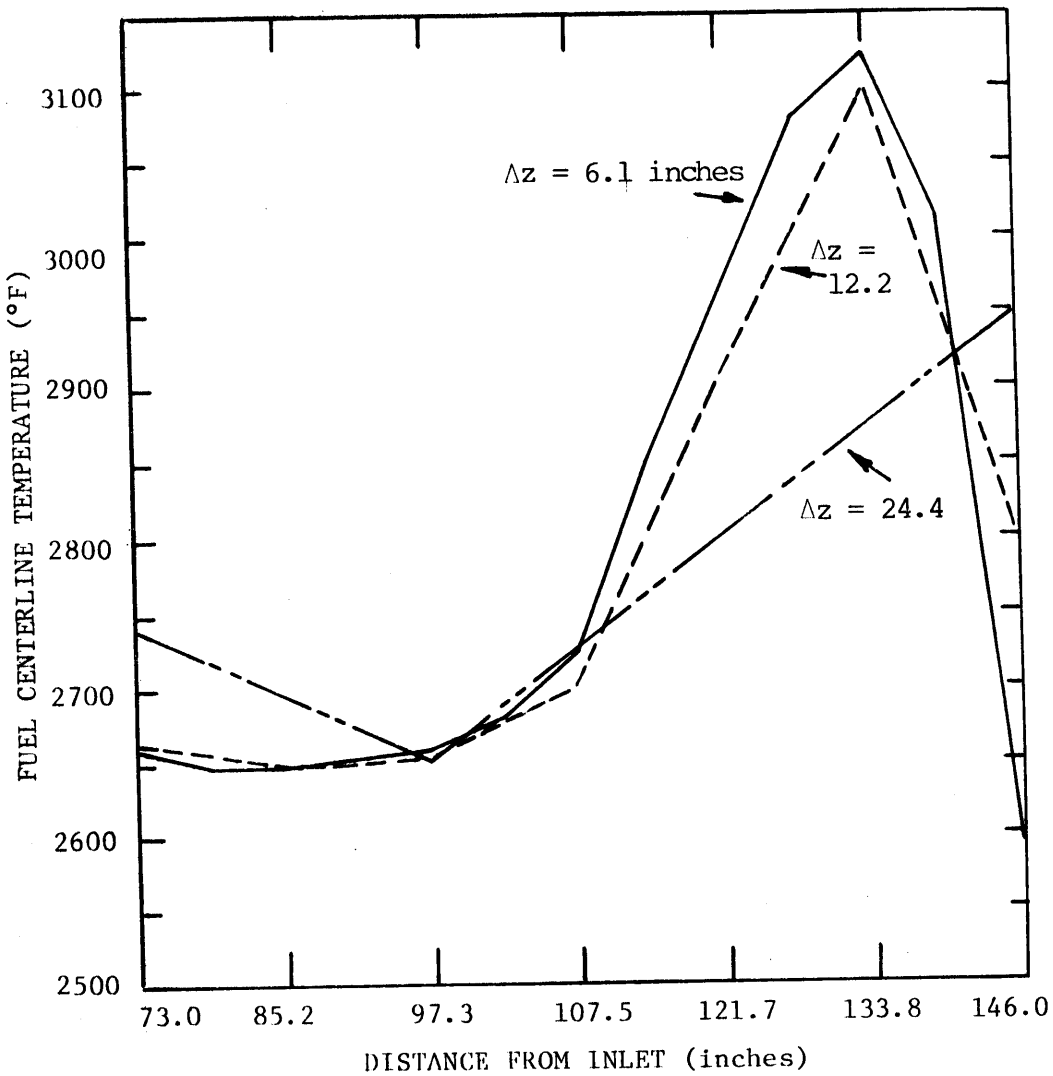

FIG. 4.4: FUEL CENTERLINE TEMPERATURE SENSITIVITY TO AXIAL MESH SIZE (Power Profile Class 2A, t = 1.0 seconds)

result, fine structure in the axial fuel temperature profile is obscured with a coarse axial mesh.

It is possible to derive a formula to describe the deterioration of the axial fuel centerline temperature profile that comes about as axial mesh size is increased from Δz to $n\Delta z$. Given the actual axial power profile over the level $n\Delta z$, the following equation will predict the ratio of coarse mesh to fine mesh temperatures (a derivation appears in Appendix C):

$$\frac{(T_{\mathfrak{C}} - T_f)_{n\Delta z}}{(T_{\mathfrak{C}} - T_f)^*_{\Delta z}} = \frac{1}{n}\left(1 + \frac{1}{q^*}\sum_{\substack{j=1\\ j\neq j^*}}^{n} q'_j\right) \qquad (4.1)$$

In most cases little error is introduced if the same value of bulk coolant temperature is used in both numerator and denominator of the left hand size of Eq. 4.1. Although this formula was derived based upon steady state assumptions, it has been used successfully to predict axial mesh sensitivities in relatively fast transients (i.e. transients of duration less than the fuel response time).

Relatively early in the transient (i.e. times less than one half the fuel response time), the fuel surface temperature exhibits the same axial mesh sensitivity as the fuel centerline temperature, although the sensitivity is decreased in magnitude, as can be seen in Fig. 4.5 and Fig. 4.6. Hence, if an axial mesh size is chosen that will ensure accurate representation of the fuel centerline temperature (e.g. by means of Eq. 4.1), the axial mesh

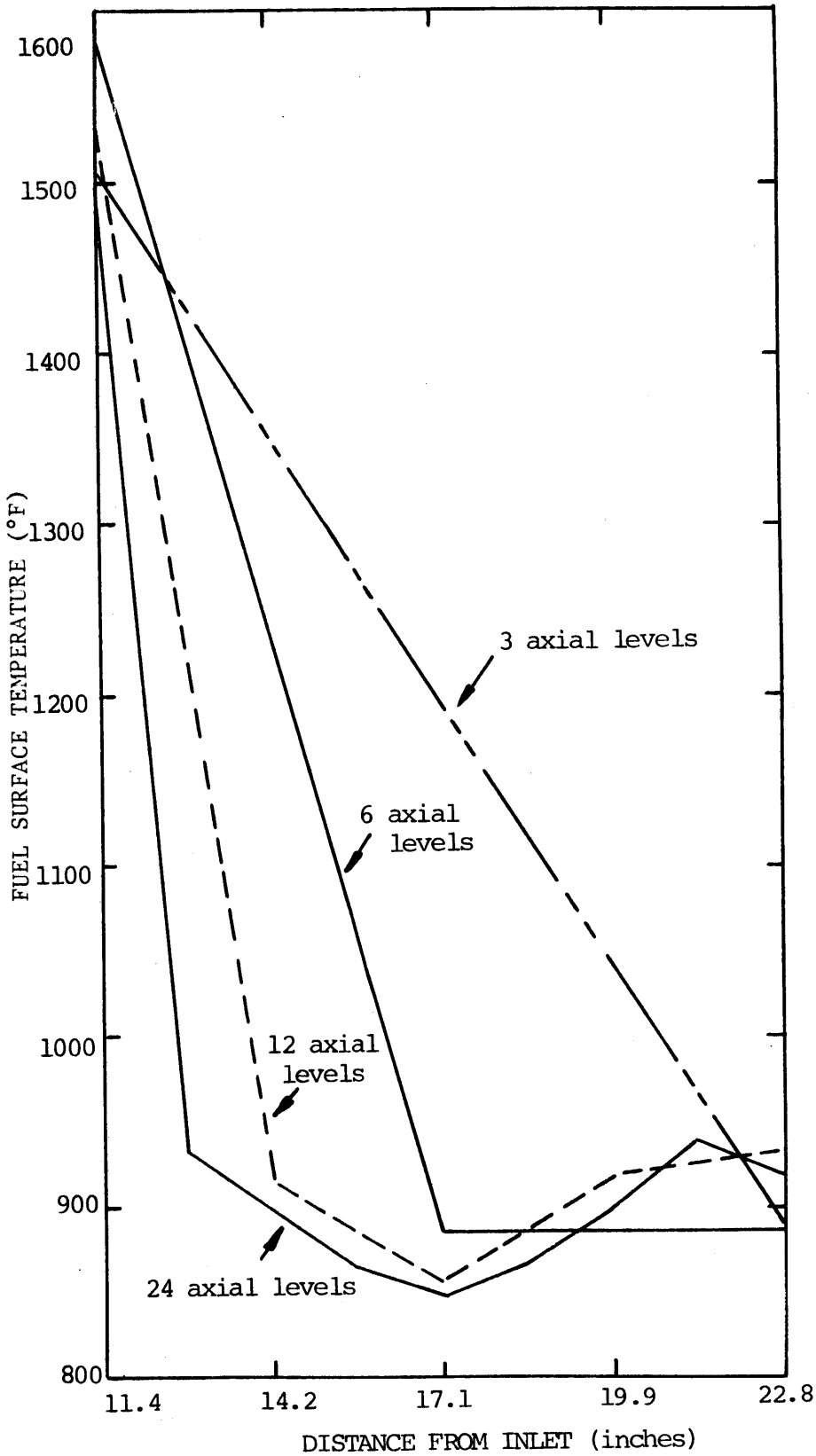

FIG. 4.5: FUEL SURFACE TEMPERATURE SENSITIVITY TO AXIAL MESH SIZE (POWER PROFILE CLASS 5)

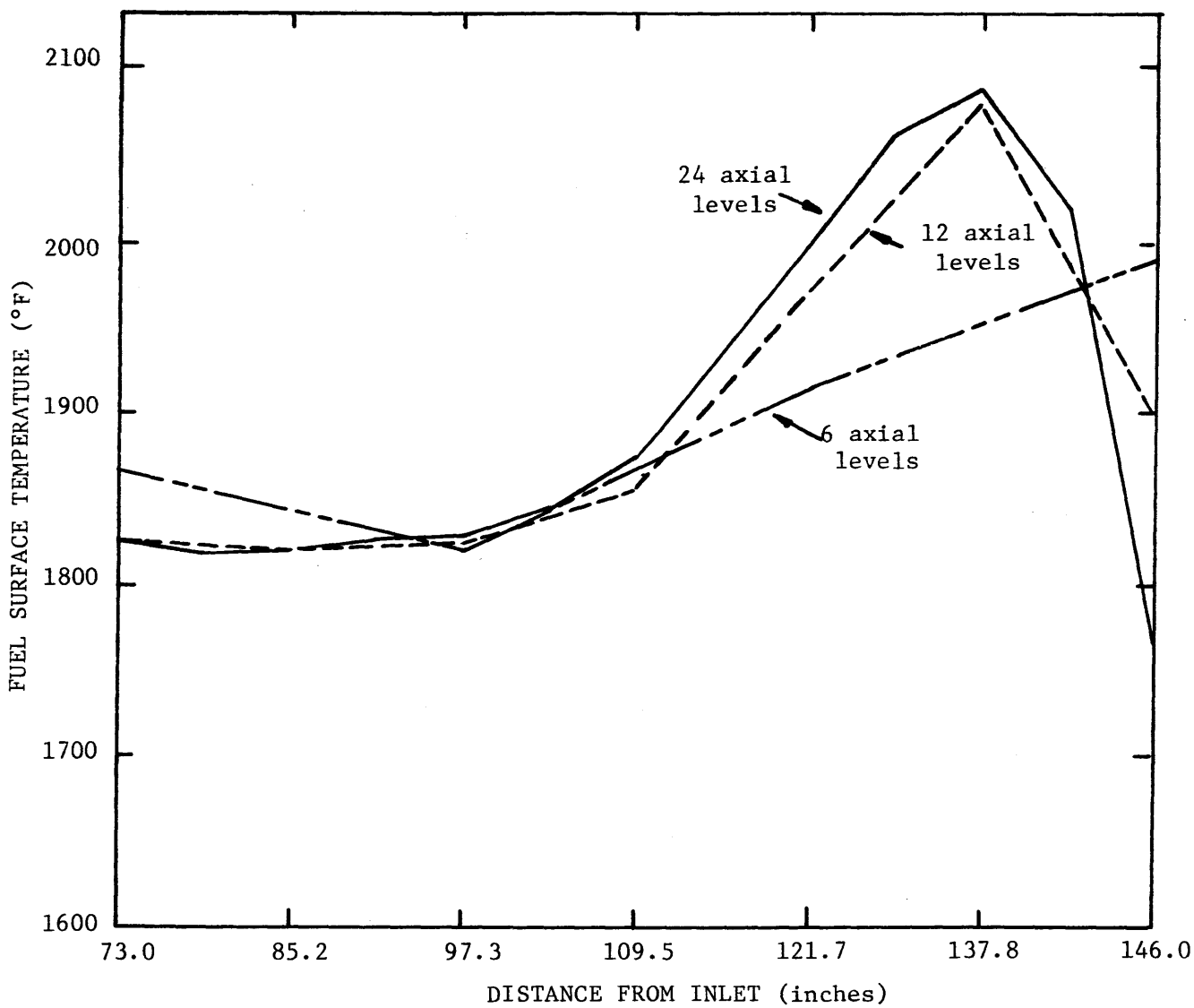

FIG. 4.6: FUEL SURFACE TEMPERATURE SENSITIVITY TO AXIAL MESH SIZE (POWER PROFILE CLASS 2A)

will be adequate for the remainder of the fuel temperature profile in fast transients.

Observed and calculated values of the coarse to fine axial mesh temperature ratio predicted in Eq. 4.1 are presented in Table 4.1. Observed values are included at 0.5 and 1.5 seconds into the power coastdown transient. Predicted values remain constant throughout the transient since the axial power profile shape does not change. Good agreement is found between observed and predicted values, with differences seen in the third decimal place.

The formula presented in Eq. 4.1 represents a tool for the COBRA and MEKIN users. If the axial power profile is known, the user may determine the appropriate axial mesh size with Eq. 4.1 in a simple iterative procedure.

This procedure is presented as a simple flow chart in Fig. 4.7. First, the user selects an arbitrarily fine axial mesh of size z and determines the discrete axial power profile shape. Attention is restricted to the most peaked section of this profile. The user then selects a coarse mesh size n z that he thinks will be appropriate for the particular transient. The ratio $\frac{(T_{\ell} - T_f)_{n\Delta z}}{(T_{\ell} - T_f)^*_{\Delta z}}$ is then determined for the most peaked portion of the fine mesh profile. If this ratio is not approximately equal to 1, a finer mesh must be used in the model. If the ratio is very nearly equal to 1, it may be possible to increase the axial mesh size.

TABLE 4.1

COMPARISON OF OBSERVED AND PREDICTED VALUES OF

$$\left(\frac{(T_{\mathfrak{C}} - T_f)_{4\Delta z}}{(T_{\mathfrak{C}} - T_f)^*_{\Delta z}} \right)$$

Normalized distance from inlet (z/L)	Observed Values Elapsed Time (Seconds)		Predicted Values From Eq. 4.1
	0.25	1.5	independent of time*
0.542	1.0035	1.0020	1.0019
0.583	1.0033	1.0020	1.0019
0.625	1.0008	0.9998	0.9997
0.667	0.9974	0.9965	0.9965
0.708	1.0596	1.0603	1.0582
0.750	1.0369	1.0376	1.0363
0.792	0.9796	0.9797	0.9804
0.833	0.9330	0.9325	0.9346
0.875	0.9466	0.9471	0.9487
0.917	0.9303	0.9300	0.9320
0.958	0.9747	0.9740	0.9748
1.000	1.1881	1.1874	1.1806

*Predicted values are time independent for this case because axial profile is constant for all times.

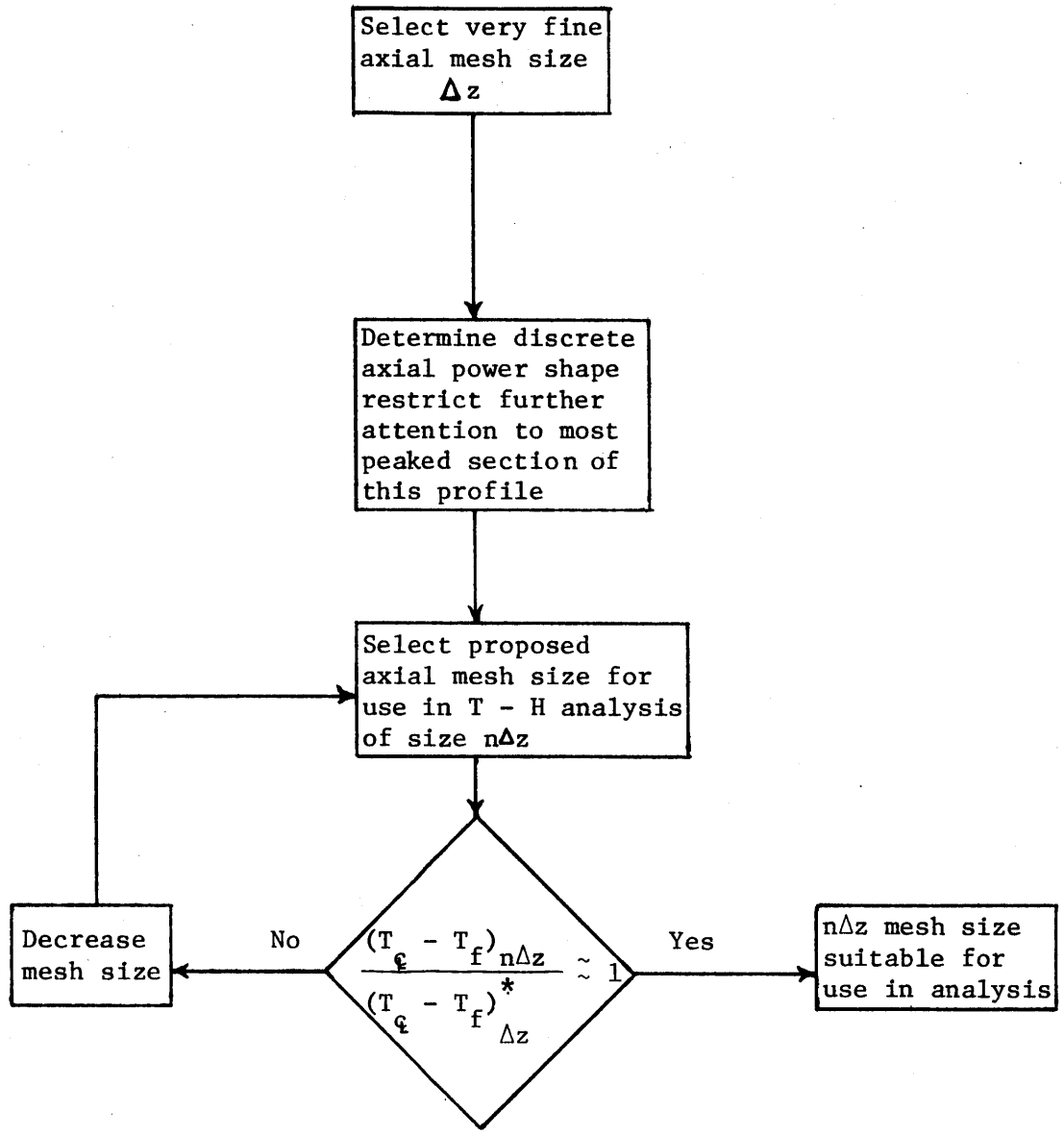

FIG. 4.7

DETERMINATION OF CORRECT AXIAL MESH SIZE

4.2.3 Axial Mesh Sensitivity of Coolant

As explained earlier, two energy transfer mechanisms for coolant heating are modeled in the T-H analysis, instantaneous and neutron heating and heat transfer from the fuel cladding to the coolant.

The axial mesh sensitivity of the coolant to the first mechanism is similar to that observed in the fuel. As axial mesh size is increased, the axial power profile is less accurately represented and the instantaneous energy deposition in the coolant becomes more approximate. This behavior has little effect on the state of the colant at the exit plane of the reactor, an integral parameter, but does result in different local effects as the coolant flows through a channel.

The coolant axial mesh sensitivity for the clad heat flux is more difficult to quantify. This heat flux, given by

$$q'' = h_c (T_{clad} - T_b) \qquad (4.2)$$

is seen to be dependent on the fuel surface temperature and will reflect, in part, the fuel temperature sensitivity. However, the heat transfer coefficient between the fuel clad and the cooalnt as well as the bulk coolant temperature also affect the clad heat flux.

Heat flux profiles obtained with different axial mesh sizes at 1 second into the power coastdown transient appear

in Fig. 4.8. The "spikes" seen in the fine mesh profiles of Fig. 4.8 occur at the onset of boiling. The heat transfer coefficient between clad and coolant increases dramatically upon incipient boiling and yields higher heat fluxes.

The differences in heat flux that are found when axial mesh size is changed affect coolant behavior both locally and in an integral sense. Not only are local phenomena, such as the onset of nucleate boiling, less accurately represented as the mesh size is increased, but the amount of energy deposited in the coolant as it passes through the channel is also changed. This alters the state of the coolant at the channel exit. This behavior may be seen in axial enthalpy profiles of the coolant presented in Fig. 4.9 and 4.10. As the mesh size is reduced, heat transfer phenomena are more accurately modeled, and the coolant enthalpy is increased.

Relatively little sensitivity to axial mesh size is seen late in the transient, as demonstrated in Fig. 4.10. At this time, boiling has long since been established throughout the upper regions of the channel and heat transfer coefficients have increased accordingly regardless of mesh size. Instantaneous coolant heating is virtually non-existent by this time, leaving the clad-coolant heat flux as the only energy deposition mechanism.

Axial mesh size sensitivity of the coolant density, a neutronics feedback parameter, closely parallels that

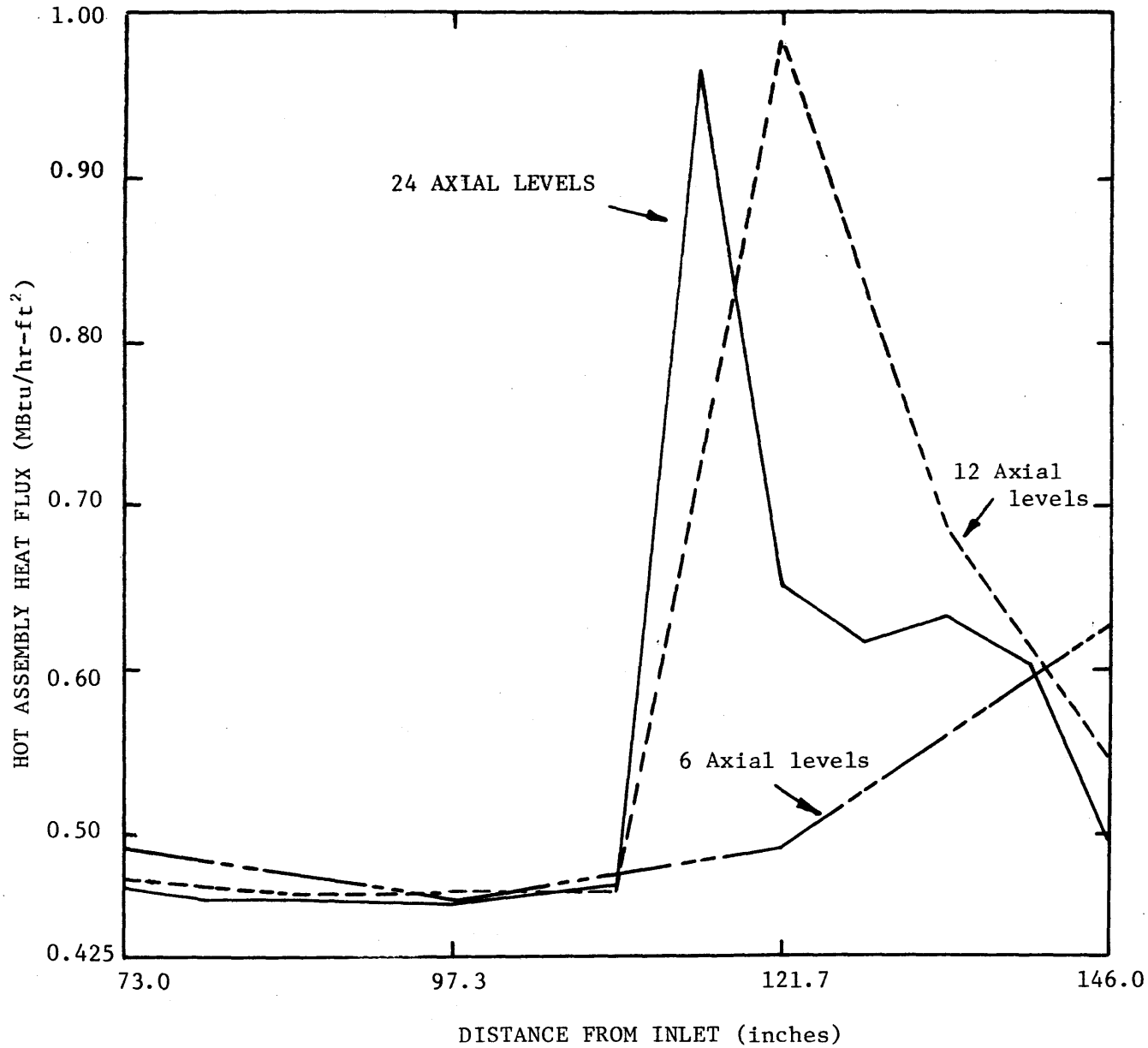

FIG. 4.8: HEAT FLUX SENSITIVITY TO AXIAL MESH SIZE

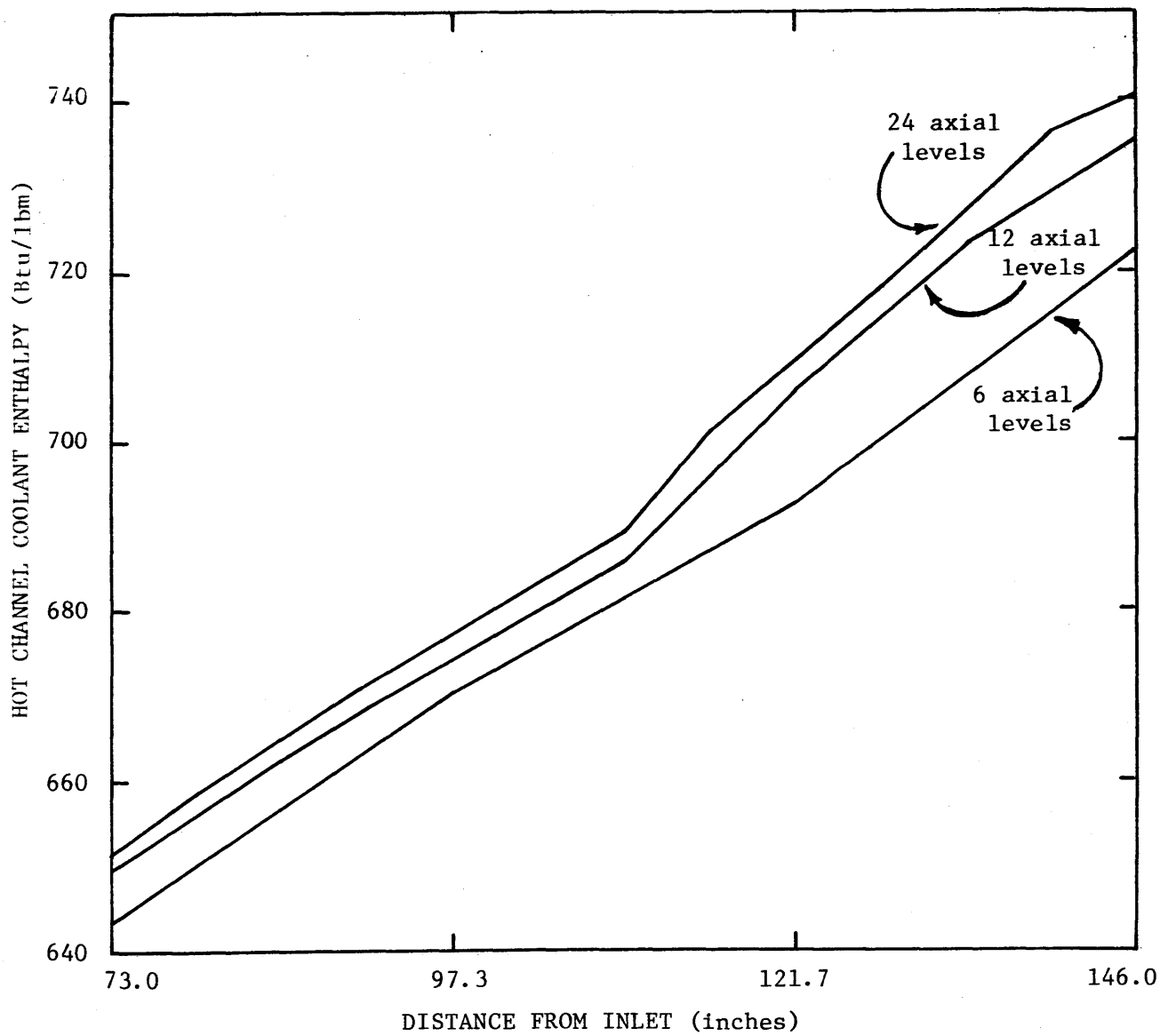

FIG. 4.9: COOLANT ENTHALPY SENSITIVITY TO AXIAL MESH SIZE

(power profile class 2A, t=1.0 seconds)

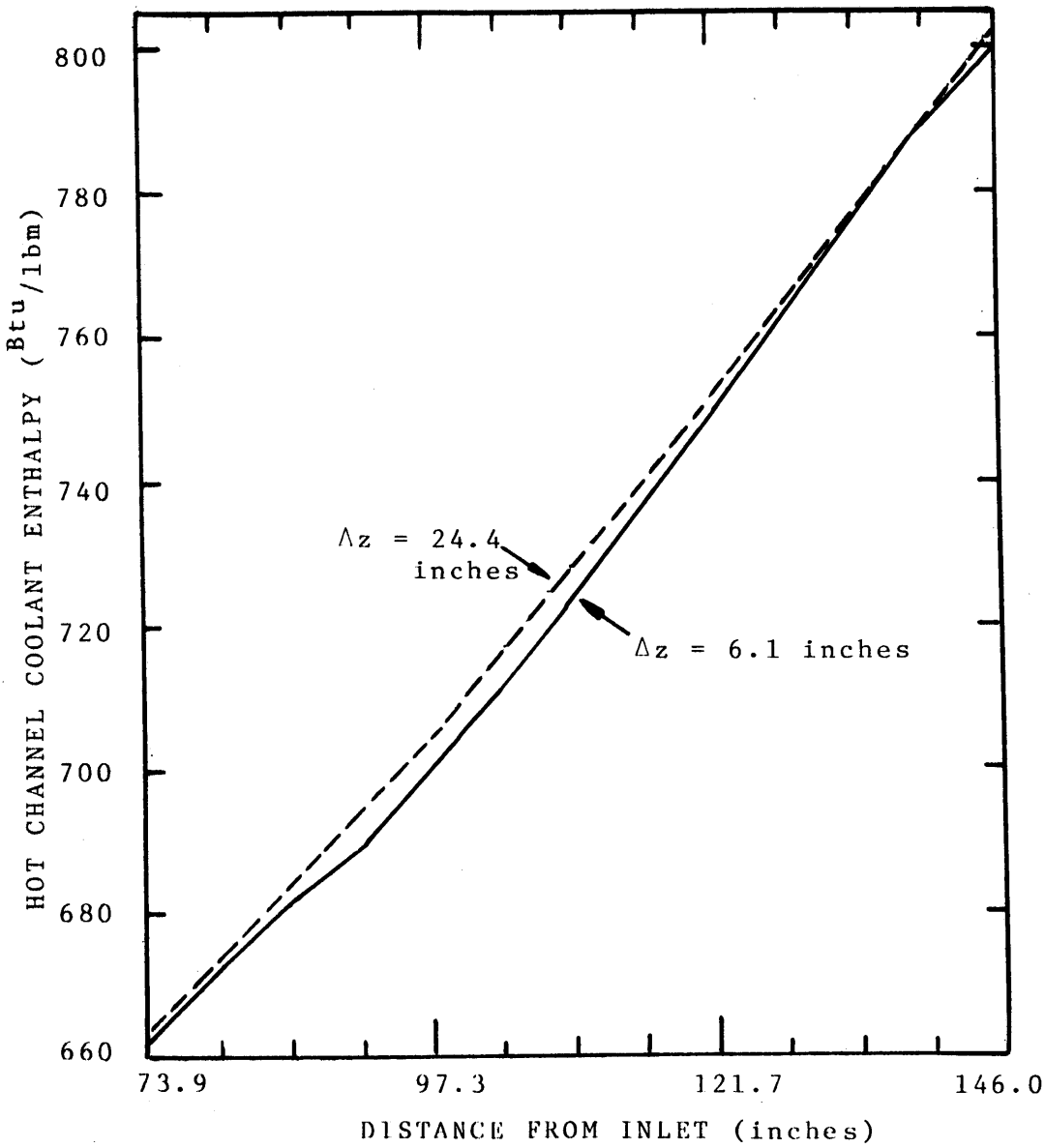

FIG. 4.10: COOLANT ENTHALPY SENSITIVITY TO AXIAL MESH SIZE

(Power Profile Class 2A, t = 3 seconds)

of the coolant enthalpy, since the former is calculated as a function of the latter. These effects may be seen in Fig. 4.11 and Fig. 4.12.

4.3 Time Step Sensitivity

4.3.1 Cases Studied

The same models were used in axial mesh and time step studies. Three axial levels (Δz = 11.4 inches) were used in prompt jump time step sensitivity studies while thirteen levels (Δz = 11.2 inches) were used in the power coastdown studies. No power was generated in the uppermost axial level of the power coastdown model, since this level was beyond the active length of the fuel rods.

Time steps were varied over different ranges in the two transients. Values of Δt = 1, 2, and 10 milliseconds were selected for the prompt jump while time steps of 2.5, 5, 10, 50, 100 and 250 milliseconds were used in the power coastdown studies.

4.3.2 Sensitivity of Fuel Temperature to Time Step Size

The behavior of fuel temperature for varying time steps is illustrated in Fig. 4.13 and Fig. 4.14. As expected, errors in fuel temperature increase as the time step is increased. In the COBRA and MEKIN fuel conduction models, the specific heat of the fuel is constant, so the observed temperature differences may be related directly to errors in the energy deposition.

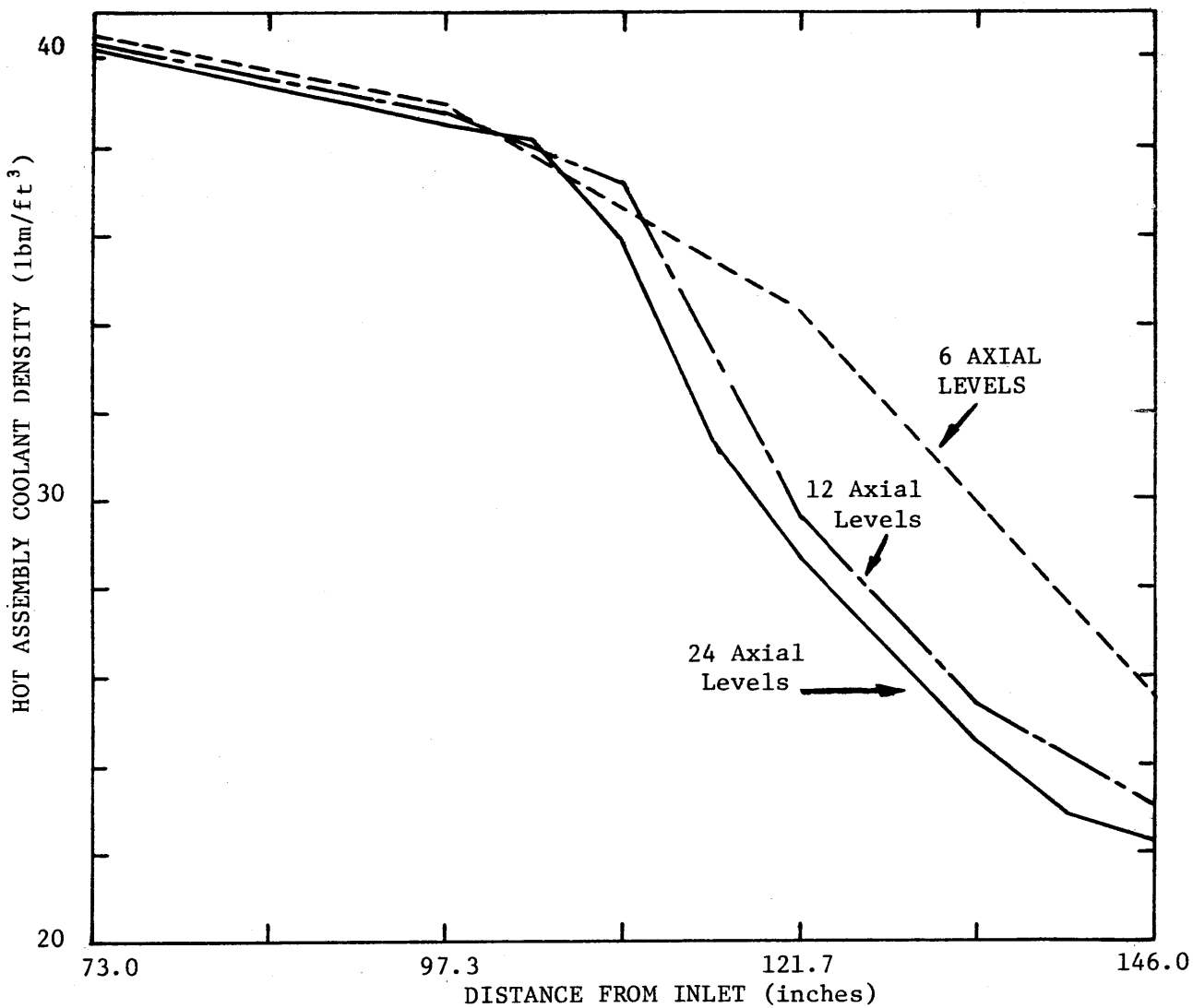

FIG. 4.11: COOLANT DENSITY SENSITIVITY TO AXIAL MESH SIZE

(power profile class 2A, t=1.0 seconds)

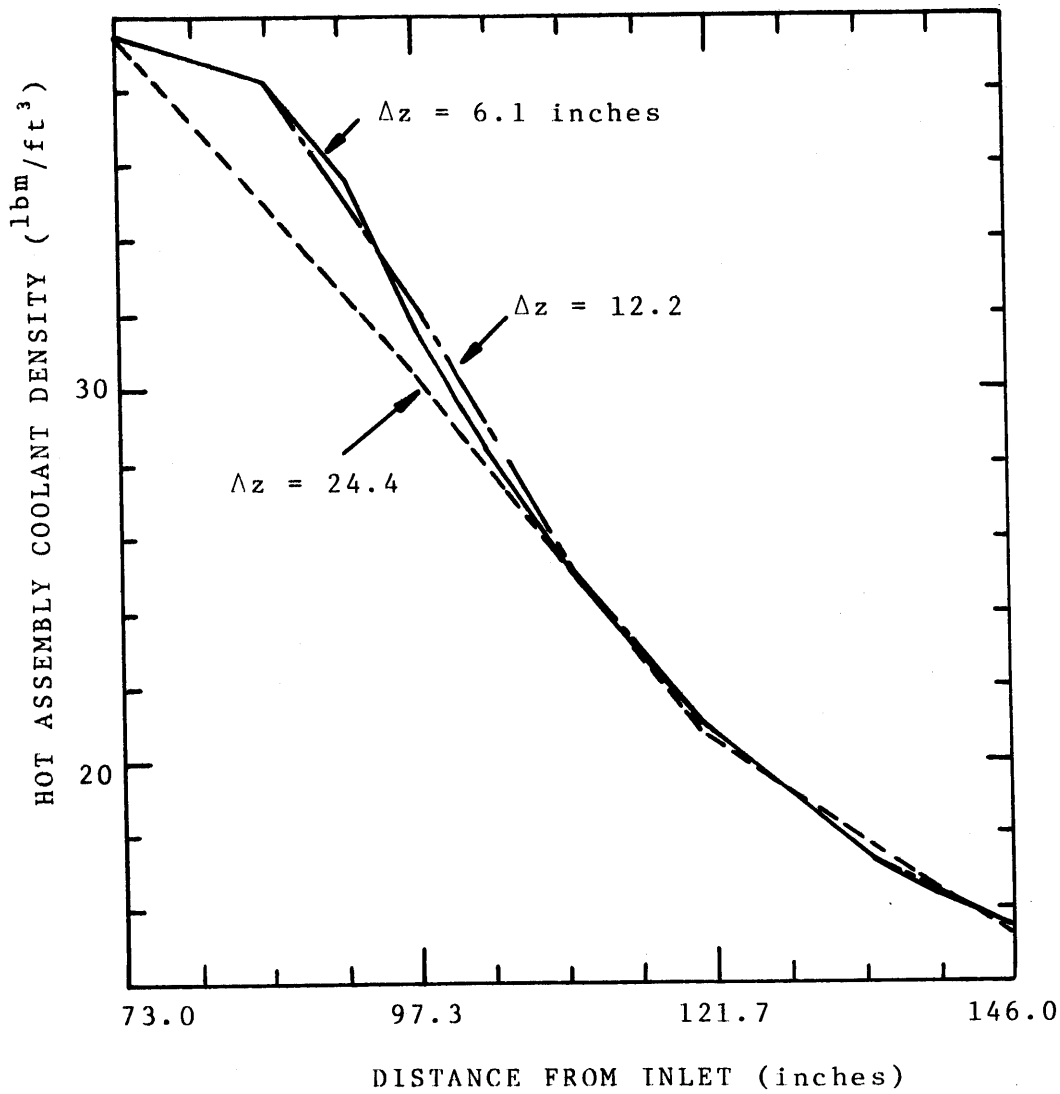

FIG. 4.12: COOLANT DENSITY SENSITIVITY TO AXIAL MESH SIZE
(Power Profile Class 2A, t = 3 seconds)

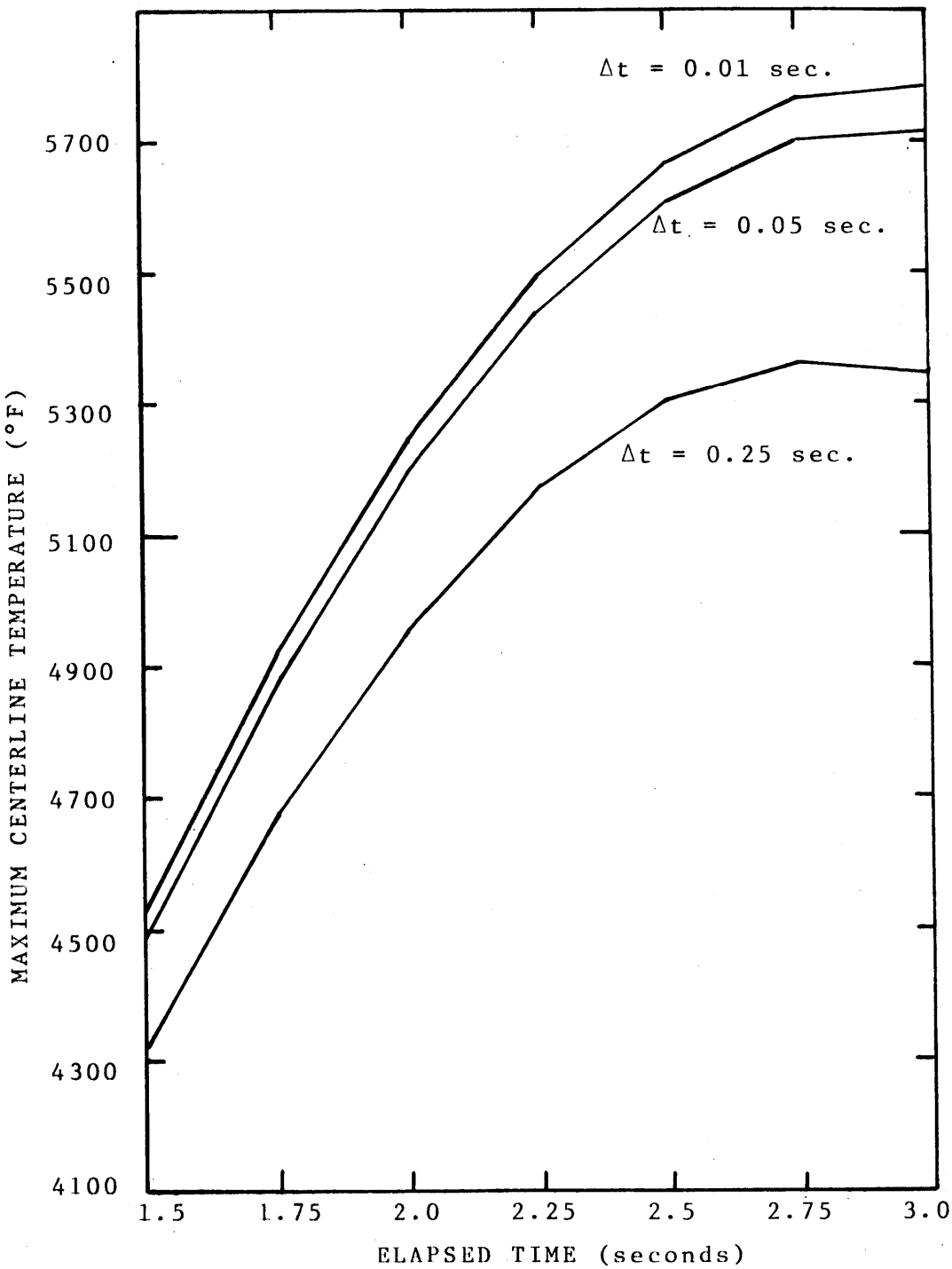

FIG. 4.13: FUEL CENTERLINE TEMPERATURE SENSITIVITY TO TIME STEP SIZE
(Power Profile Class 2A)

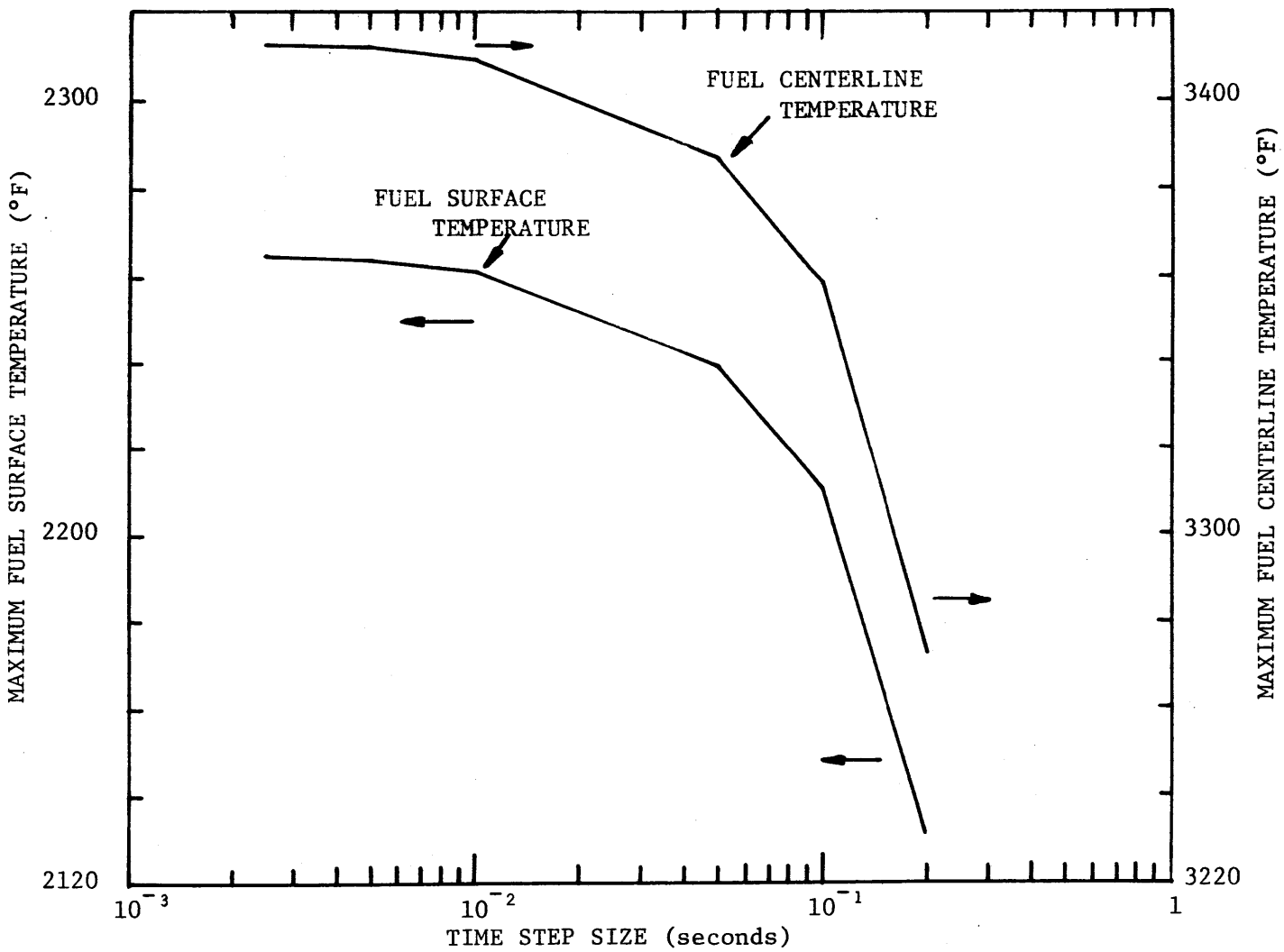

FIG. 4.14: FUEL TEMPERATURE SENSITIVITY TO TIME STEP SIZE
(power profile class 2A)

An important difference appears in the behavior of the fuel centerline temperature for the two transients studied; this is shown in Table 4.2. In the prompt jump, where power increases with time, the fuel centerline temperature increases with increases in time step size. However, in the power coastdown transient, power decreases with time, and the fuel centerline temperature decreases as larger time steps are chosen, as shown in Fig. 4.14.

The key to the fuel temperature sensitivity lies in the method that COBRA and MEKIN use to represent the power history. The codes model power, a continuous function in time, as a series of steps. The power, $P(t + \Delta t)$ that is supplied at time $(t + \Delta t)$ is assumed to have been constant over the time interval Δt. Unless this was in fact the case, a net energy deposition error is made at each time step. A qualitative illustration of this error may be seen in Fig. 4.15.

If the power increases with time, the resultant energy deposition error is positive. This brings about a higher fuel temperature as the time step size is increased. On the other hand, in the power coastdown, the energy deposition error is negative, resulting in lower fuel temperatures as the length of a time step is increased.

An analytic expression may be derived for the full temperature error resulting from the use of the large time step $n\Delta t$. The derivation assumes that the power

TABLE 4.2

FUEL CENTERLINE TEMPERATURE SENSITIVITY

TO TIME STEP SIZE

time step (sec)	centerline fuel temperature (°F)	case
0.001	4061.2	prompt jump
0.002	4061.3	t = 0.02 sec
0.01	4062.4	
0.0025	3413.0	
0.005	3411.8	
0.01	3409.3	power coastdown
0.05	3386.7	t = 1 sec
0.10	3358.3	
0.25	3272.4	

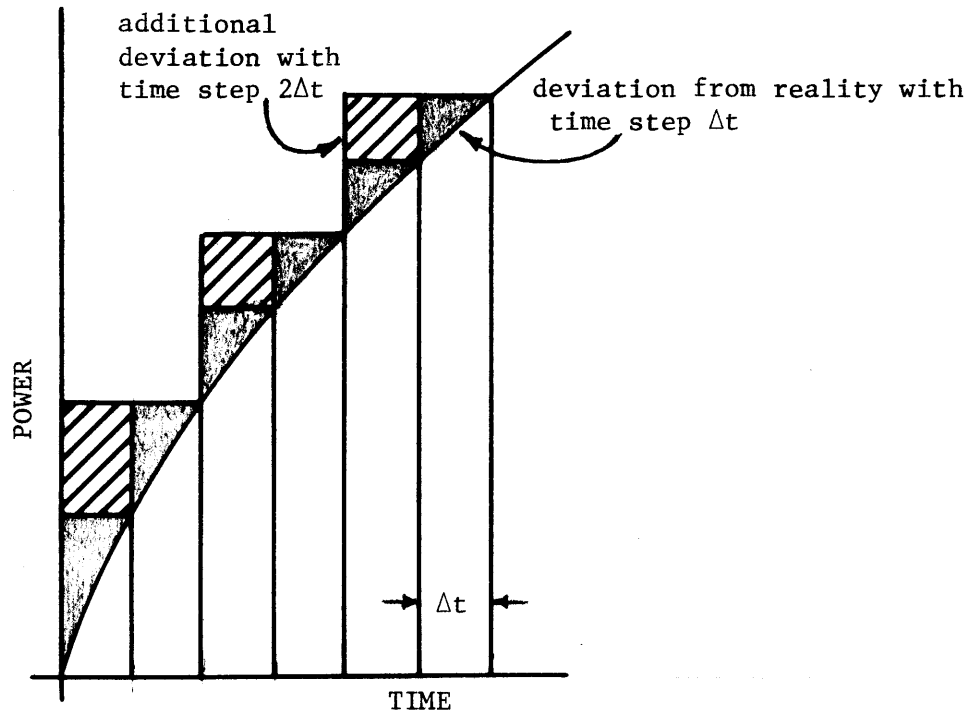

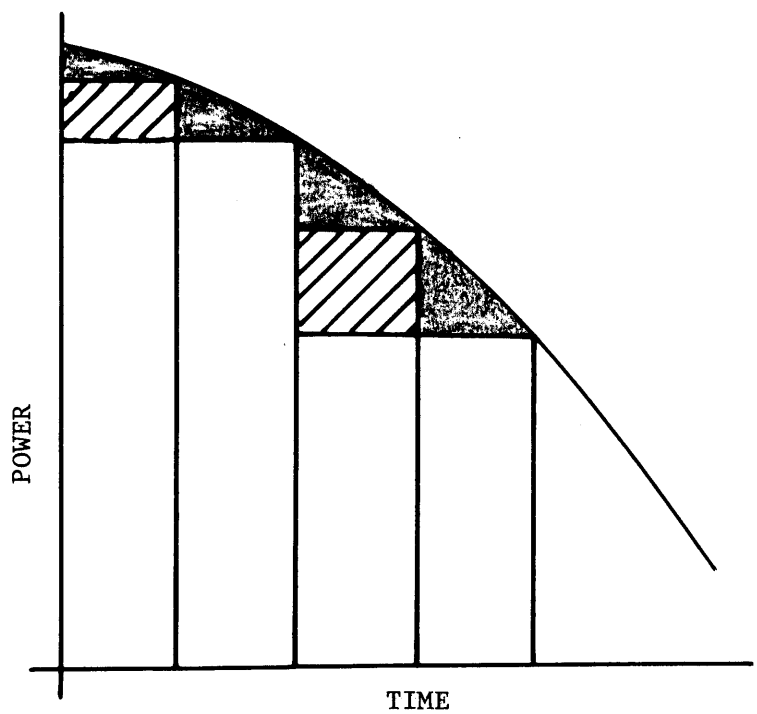

FIG. 4.15: QUALITATIVE REPRESENTATION OF ENERGY DEPOSITION ERROR FOR LARGE TIME STEPS

history is known, as it must be for a COBRA analysis to be performed. The derivation is presented in Appendix C. The following expression was found for the difference in average fuel temperature that results when a time step size $n\Delta t$ is used rather than the smaller time step Δt:

$$\Delta T_{av} = \frac{\Delta t}{\rho_f C_p} \sum_{k=1}^{M/N} \sum_{n=1}^{N-1} n \left(q'''_{n+1+N(k-1)} - q'''_{n+N(k-1)}\right) \tag{4.3}$$

A comparison between predicted and observed differences in average fuel temperature is presented in Fig. 4.16. The comparison is made between the differences in the maximum average hot assembly fuel temperature found with time steps of 0.01 and 0.05 seconds. The changes in heat transfer to the coolant that are caused by slight changes in the average fuel temperature were neglected in the derivation of Eq. 4.3. Because of this, discrepancies of up to 20% are seen between the observed and predicted results.

Late in the transient, energy deposition in the fuel drops to near zero, as seen earlier in Fig. 2.3, and heat transfer effects become the dominant energy transfer mechanism. Eq. 4.3 cannot take these effects into account and predicted differences diverge from the observed results late in the transient.

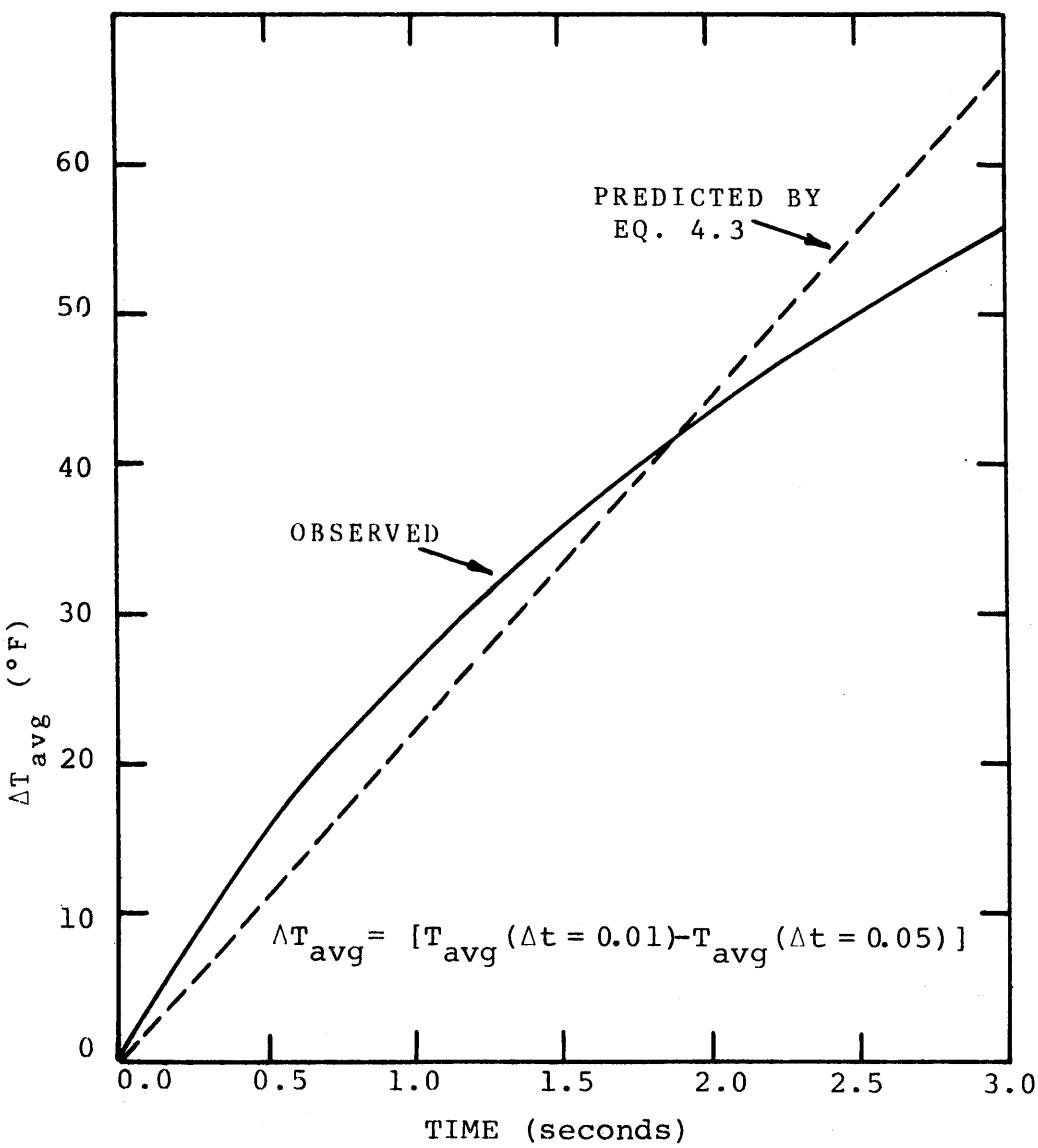

FIG. 4.16: COMPARISON OF OBSERVED AND PREDICTED AVERAGE FUEL TEMPERATURE SENSITIVITY TO TIME STEP SIZE

Another tool for the user is provided by Eq. 4.3. If the power history is known, this formula may be used to compare the differences in average fuel temperature that will be found when the time step is changed. An iterative process similar to that described in Sec. 4.2.2 for the axial mesh may be used to find the appropriate time step size for use in a transient analysis.

The T-H solution scheme should be modified to reduce the time step dependence. This could be accomplished by using linear interpolation between points in the power history rather than the current "step change" approach. That is, the energy deposited over the time interval Δt should be represented as $0.5\ [P\ (t + \Delta t) + P\ (t)]\Delta t$ rather than $[P\ (t + \Delta t)]\ \Delta t$. Such a change will increase the number of computations performed at a time step, but will ultimately reduce the cost of T-H analyses since larger time steps may then be used with little error.

4.3.3 Time Step Sensitivity of Coolant

The error in coolant energy deposition that increases as larger time steps are used is thought to be responsible for the observed coolant parameter sensitivty to time step size. The changes seen in coolant enthalpy when the time step size is changed indicate that this is the case.

Higher enthalpies are seen in Fig. 4.17 when the time step size is reduced in the power coastdown transient.

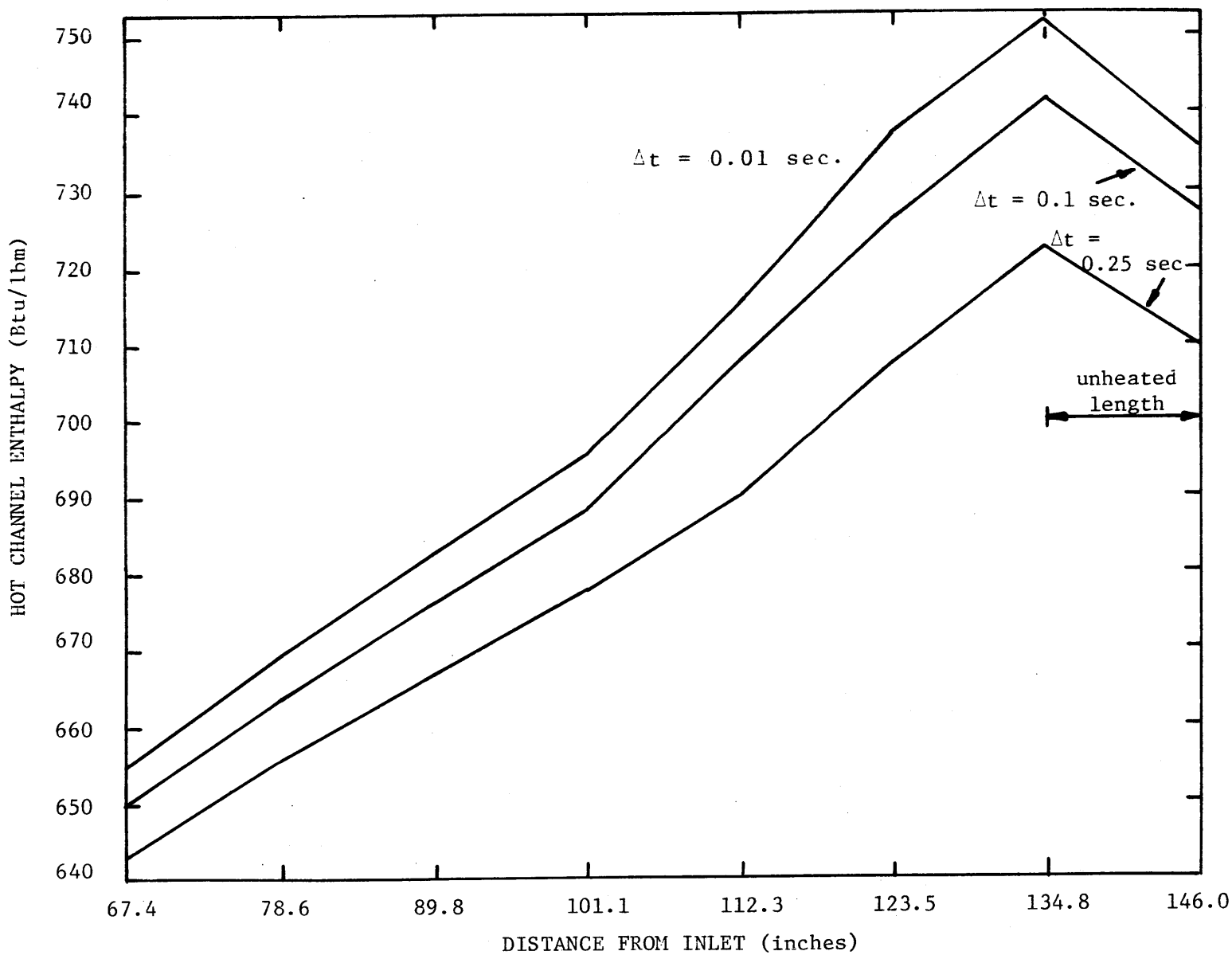

FIG. 4.17: COOLANT ENTHALPY SENSITIVITY TO TIME STEP SIZE
(power profile class 2A)

A plot of channel exit enthalpy vs. time for the same transient, presented in Fig. 4.18, shows curves having essentially the same shape but which increase in magnitude as the time step size is decreased. Since the coolant enthalpy is directly proportional to the energy added to the coolant, this change in magnitude of exit enthalpy may be explained in terms of differences in the energy deposited.

When instantaneous coolant heating, simulating γ and neutron heating, was eliminated in a series of tests using power profile class 2B, the coolant enthalpy was found to exhibit a decreased sensitivity to the time step size, seen in Fig. 4.19. In these cases, the only differences in heat transfer to the coolant for different time steps were those brought about in the heat flux as a result of the fuel temperature time step sensitivity. Changes in the fuel surface temperature cause changes in the clad temperature, which is related to the heat flux by Eq. 4.2.

Unfortunately, the coolant sensitivity to time step size is more complex than the fuel temperature sensitivity. Not only do changes in the time step size cause changes in the instantaneous coolant heating and in the clad heat flux, but the interchannel crossflow, shown in Fig. 4.20, is also sensitive to the time step size. Hence, interchannel energy transport is also sensitive to the time step size.

No simple formula has been derived to predict the

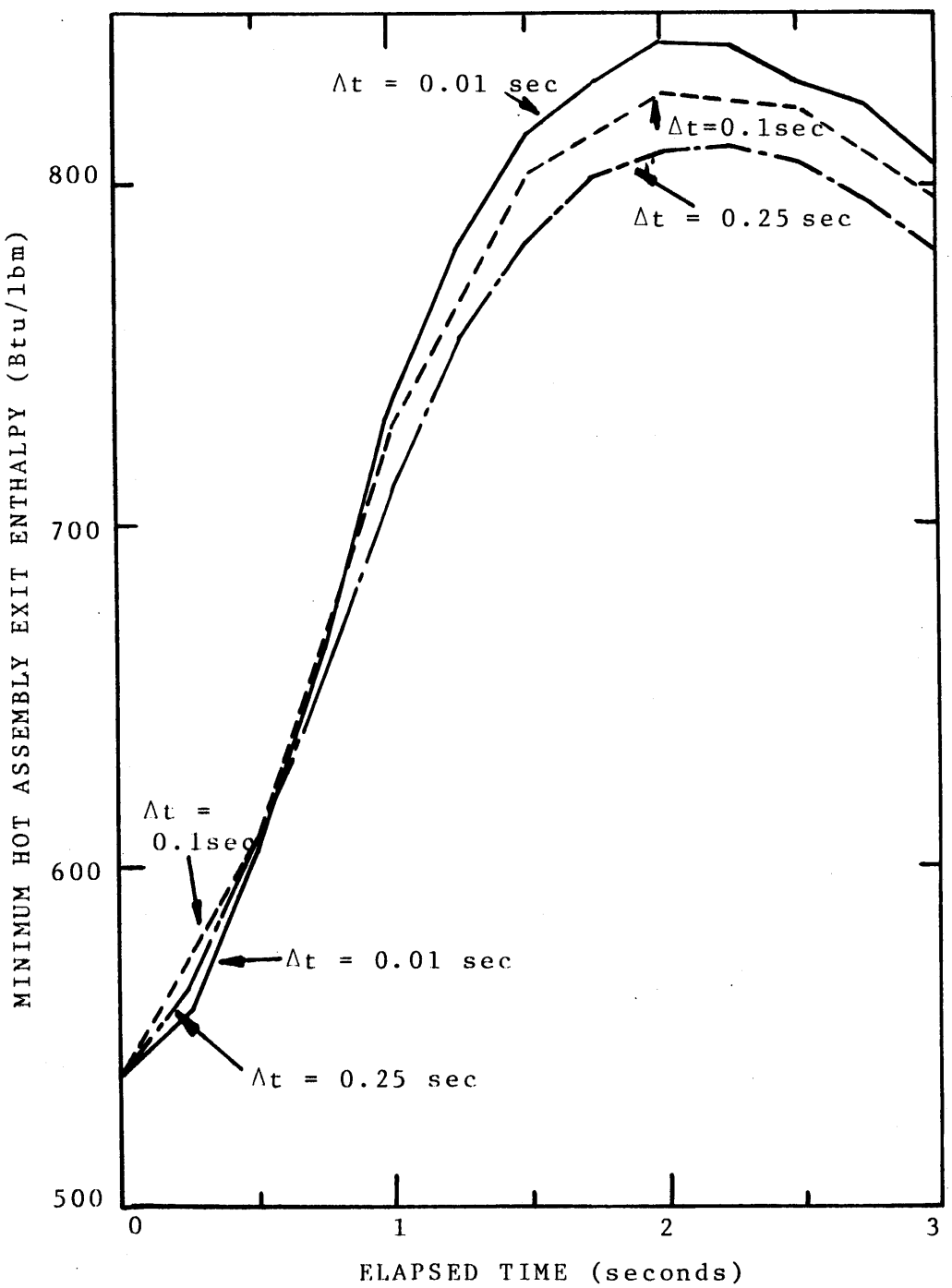

FIG. 4.18: COOLANT ENTHALPY SENSITIVITY TO TIME STEP SIZE

(Power Profile Class 2A)

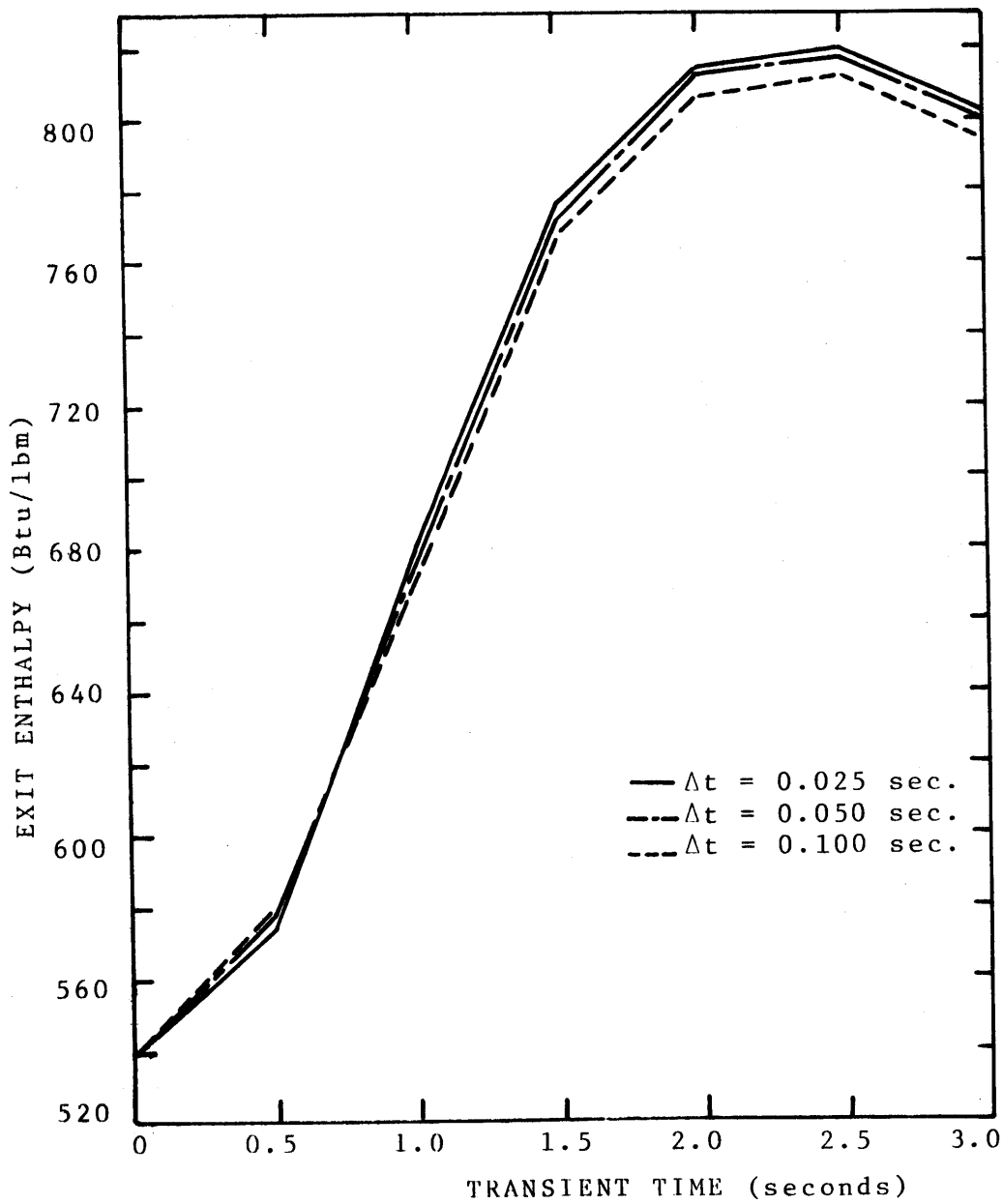

FIG. 4.19: COOLANT ENTHALPY SENSITIVITY TO TIME STEP SIZE
(Power Profile Class 2B)

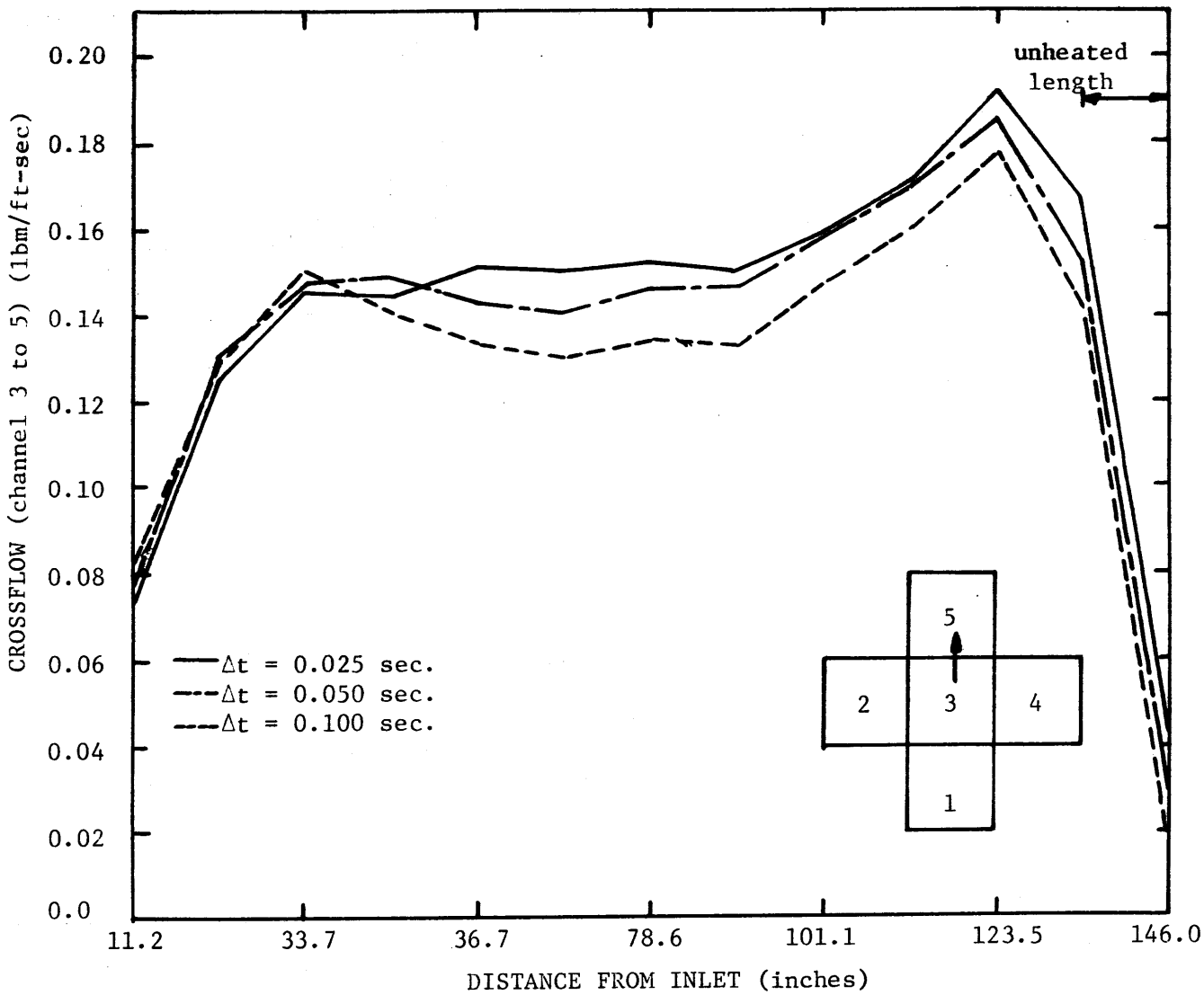

FIG. 4.20: EFFECTS OF TIME STEP SIZE ON CROSSFLOW

coolant time step sensitivity. However, void fraction and coolant density are functions of the coolant enthalpy and exhibit a similar sensitivity to the time step size, as seen in Fig. 4.21 and Fig. 4.22. Since energy deposition error is responsible for the time step sensitivity of both the fuel and the coolant, it is to be expected that if the sensitivity is reduced in one area, a similar reduction will be brought about in the remaining area.

The fuel temperature has been found to display the greatest sensitivity to time step size. This was anticipated, since energy deposition error causes the sensitivity and 96 percent of the energy is deposited in the fuel. Hence, a time step chosen to minimize fuel temperature error will also result in small errors in coolant parameters. Errors in instantaneous coolant heating and in the clad heat flux will be reduced when the fuel temperature error is minimized.

However, care must be taken to reduce this error without resorting to an arbitrarily small time step. As Fig. 4.23 shows, execution times for T-H calculations increase quickly as the number of time steps is increased.

4.4 Relationship between Axial Level Size and Time Step Size

The solution scheme used in COBRA III-C, COBRA III-C/MIT, and for T-H calculations in MEKIN is based upon a semi-implicit finite difference technique. No analytic proof of convergence for this numerical method has yet been demonstrated [15]. As a result, no stability criterion

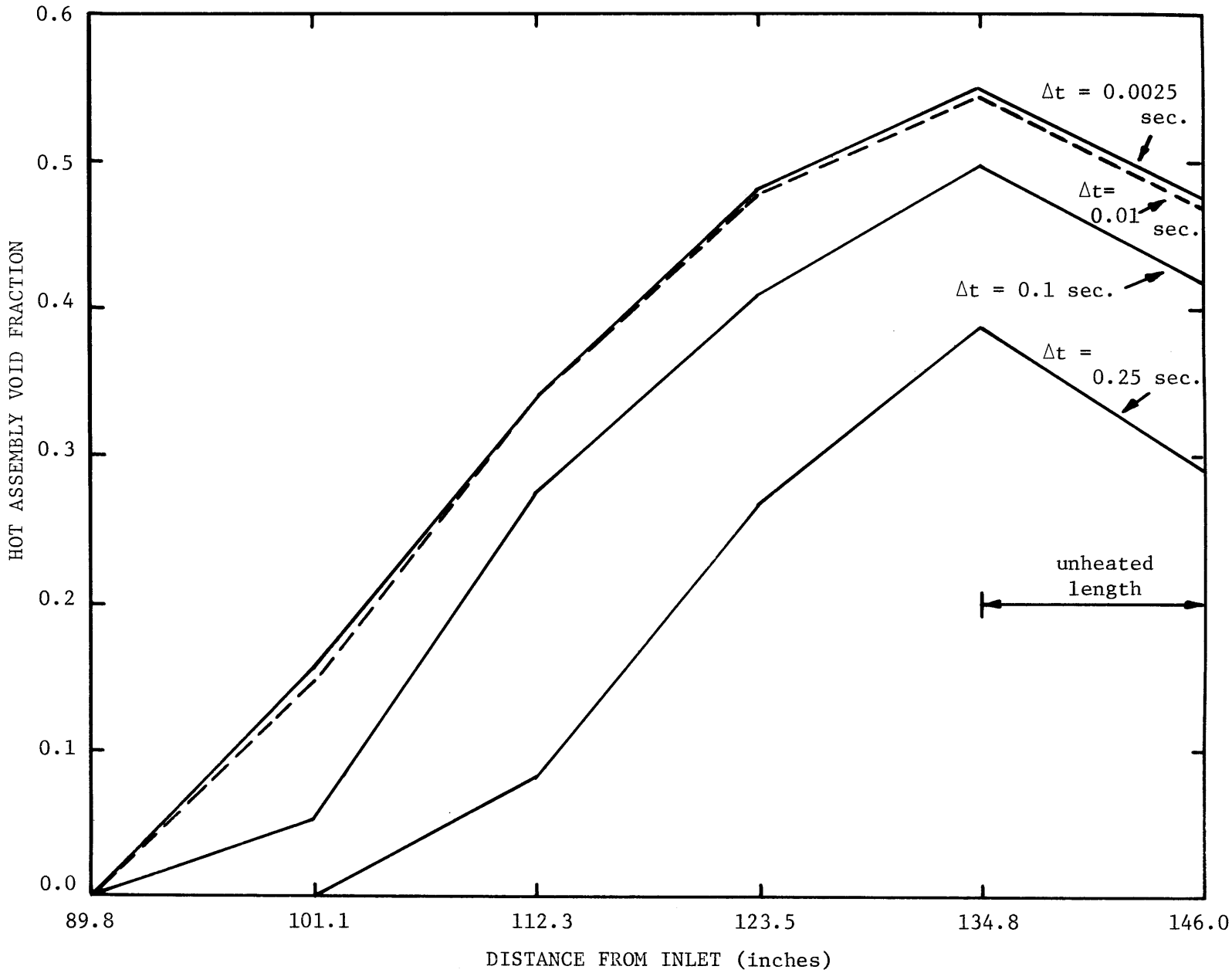

FIG. 4.21: COOLANT VOID FRACTION SENSITIVITY TO TIME STEP SIZE

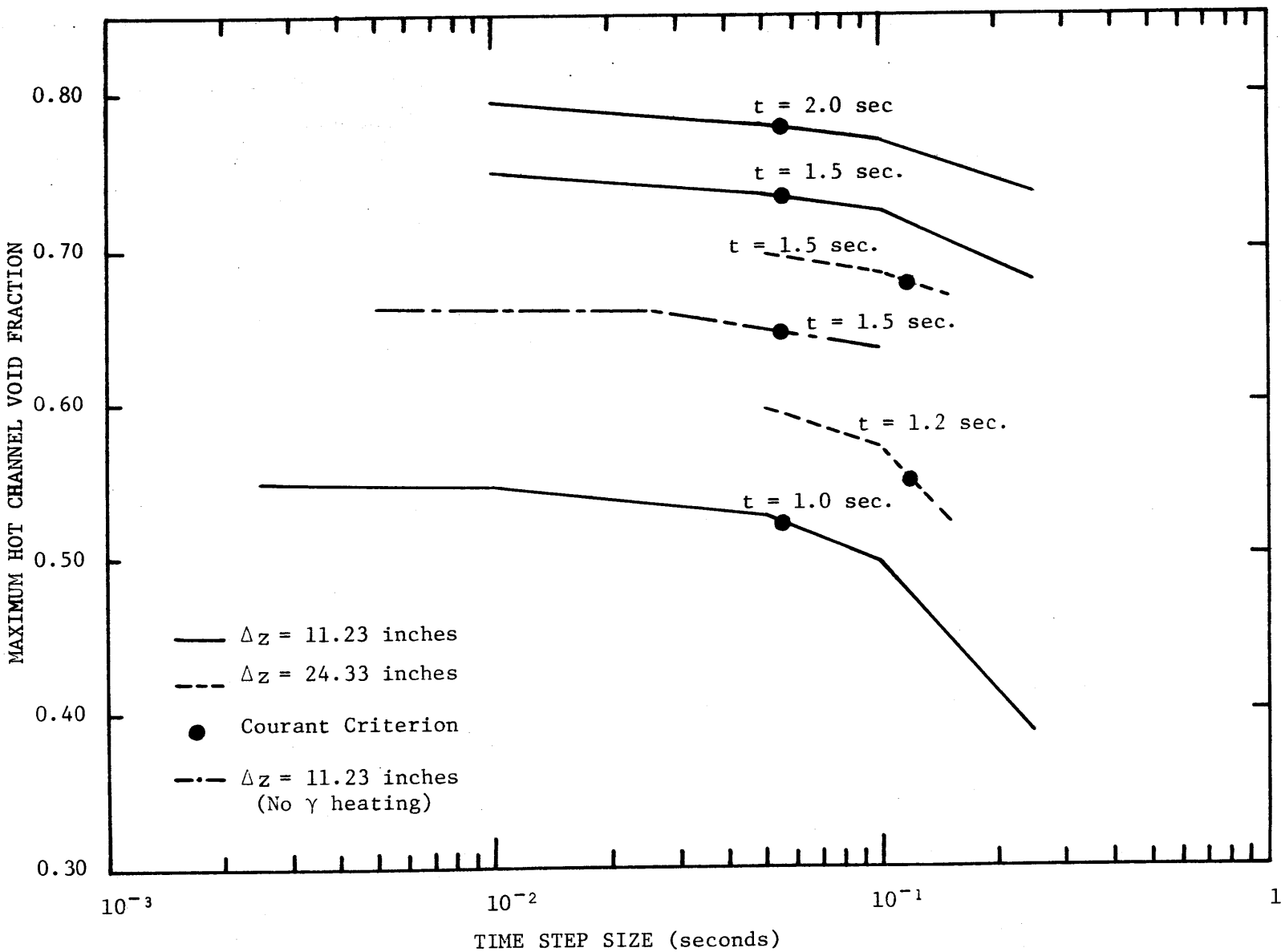

FIG. 4.22: COOLANT VOID FRACTION SENSITIVITY TO TIME STEP SIZE

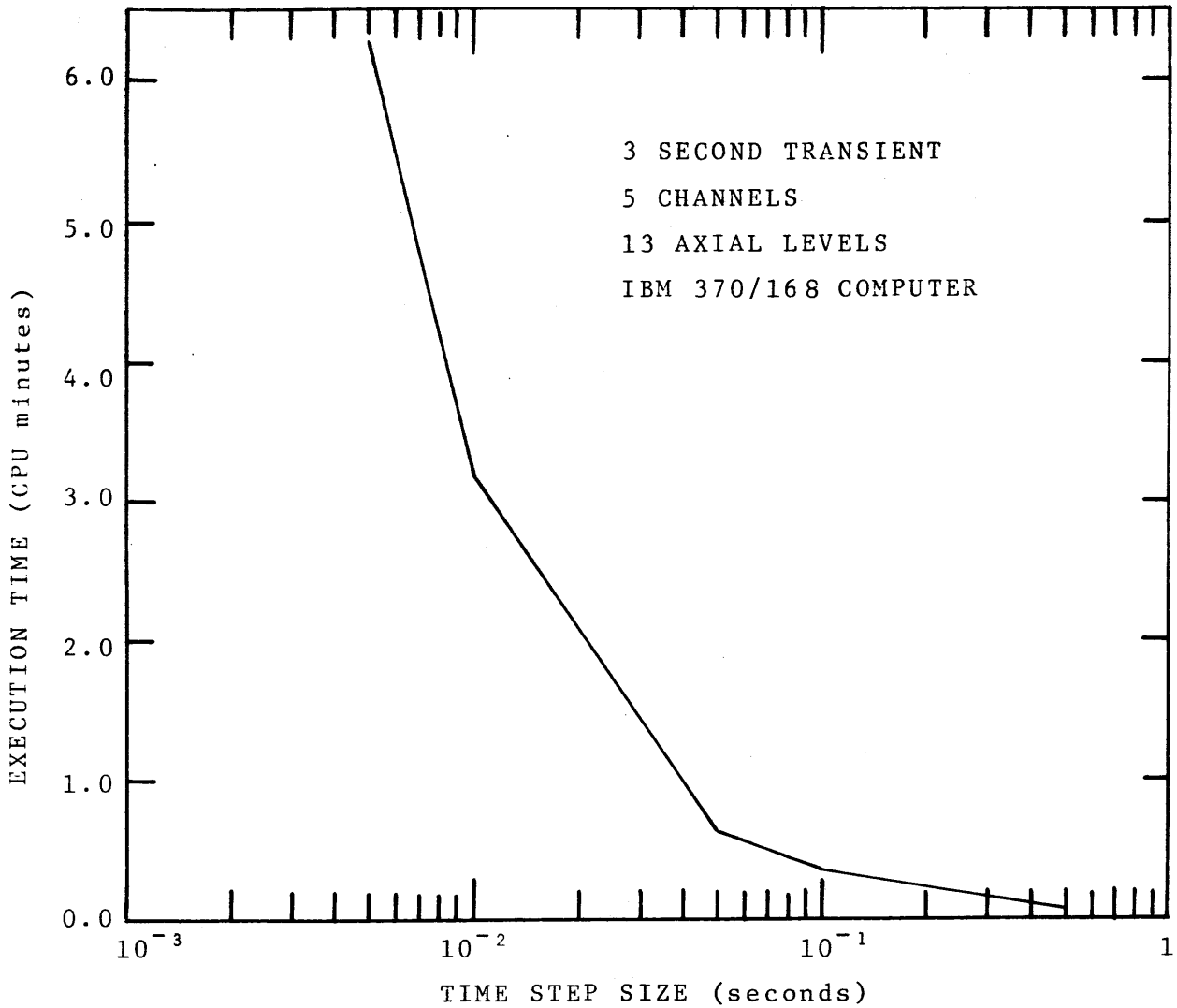

FIG. 4.23: EXECUTION TIME SENSITIVITY TO TIME STEP SIZE

has been offered. Indeed, such a criterion may not even exist, since the method is semi-implicit and may converge in all cases.

4.4.1 The Courant Criterion

The Courant criterion is a stability criterion for explicit T-H solution techniques. This criterion limits the ratio of the axial step to the time step ($\Delta z/\Delta t$), such that the coolant may not pass through more than one axial level during a time step, that is

$$\frac{\Delta z}{\Delta t} \geq v \tag{4.4}$$

4.4.2 Discussion of Courant Criterion Applicability to COBRA

The Courant criterion was found to be a useful parameter when it was applied to the time step sensitivities of the coolant, discussed earlier in Sec. 4.3.3. When this criterion was satisfied, results were found to be on the "knee" of the approach to the asymptotic value. Values of the Courant criterion are indicated in Fig. 4.22. Axial mesh size was changed and instantaneous coolant heating was eliminated to determine whether the significance of the Courant criterion was a mere coincidence. Yet the Courant criterion was found to be equally useful in these cases.

The reason for the apparent applicability of this criterion to the COBRA solution technique is not completely

understood; indeed, in a strict sense it cannot apply; since the solution technique is semi implicit. But the criterion has been found to ensure relatively good results. The Courant criterion provides a rough "rule of thumb" useful in establishing a compatibility between the axial mesh and time step sizes for T-H models. If this criterion is to be used for sizing COBRA input parameters, it should be applied as an empirically proven "rule of thumb" rather than a mathematically demonstrated stability criterion.

4.5 T-H Convergence Criterion

As mentioned earlier in Sec. 4.1.1, the T-H convergence criterion (T-H C.C.) serves to limit the number of axial iterations performed in determining the mass flow ratio. The significance of this parameter in power transient analyses is discussed in this section.

4.5.1 Transients Considered

Three transients were used to determine the effect of the T-H C.C. In each transient, the 5 channel, 13 axial level model described in Sec. 4.1.2 was used, while only the power history was changed.

The first series of tests was made using the 3.0 second hot zero power transient of subsection 2.3.3.3. In the second series of tests, the same power history was used, but two of the four channels adjacent to the hot assembly

were unheated, resulting in strong crossflow. A 12 second transient was used in the third series of tests. The energy produced in the course of this transient was approximately equal to that generated in the 3.0 second transient used in the first tests. The three transients are described in Fig. 4.24. The longer transient was used to determine whether T-H C.C. sensitivities would propagate if given sufficient time. Since very large crossflows occur when cold assemblies are located next to the hot assembly, the second transient described in Fig 4.24 violates the assumptions that the COBRA solution scheme is based upon. This transient was used here to test the sensitivity of the T-H C.C. hence true, physical results were not required. It is recommended that more advanced T-H codes such as COBRA IV be used to analyze transients of this nature if true physical results are needed.

In each series of tests, T-H C.C. values of 0.005, 0.005, and 0.05 were used, resulting in, at most, seven, four, and two axial iterations respectively per time step.

4.5.2 Observed Sensitivities

Behavior of the minimum hot channel density was noted in each series of tests described above; results at several times in the transient appear in Table 4.3. Only a barely discernible sensitivity to the T-H C.C. is found in each case.

FIGURE 4.24

T-H C.C. SENSITIVITY STUDY TRANSIENTS

<u>3 Transients Used in T-H C.C. Studies</u>

5 channel, 13 axial level model

used in all cases

1) 3 second hot zero power rod ejection(power profile class 2A) (discussed in subsection 2.3.3.3)

2) Drastic 3 second hot zero power rod ejection(Δt = 0.05 channels 2 & 4 unheated (strong crossflow) (power profile class 2C)

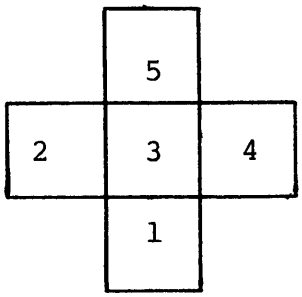

3) Mild 12 second hot zero power transient (Δt=0.1 sec) total energy generated approximately equal to that of 3 second transient)

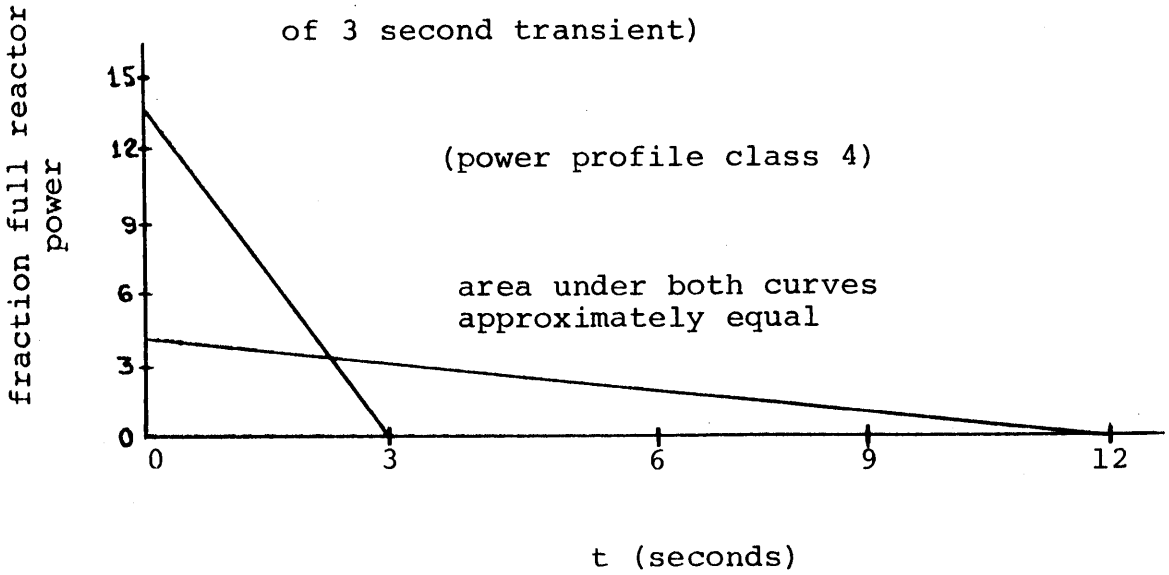

MITLibraries
Document Services

Room 14-0551
77 Massachusetts Avenue
Cambridge, MA 02139
Ph: 617.253.2800
Email: docs@mit.edu
http://libraries.mit.edu/docs

DISCLAIMER

Page has been ommitted due to a pagination error by the author.

Page 132

MIT Libraries
Document Services

Room 14-0551
77 Massachusetts Avenue
Cambridge, MA 02139
Ph: 617.253.2800
Email: docs@mit.edu
http://libraries.mit.edu/docs

DISCLAIMER

Page has been ommitted due to a pagination error by the author.

Page 133

TABLE 4.3:

COOLANT DENSITY SENSITIVITY TO T-H C.C.

	Minimum Hot Channel Density ($^{lbm}/ft^3$)				
T-H C.C.	Elapsed Time (sec)	1	2	3	Case
0.0005		21.03	12.83	15.05	3 sec.trans.
0.05		21.06	12.87	15.18	(series 1)
T-H C.C.	Elapsed Time (sec)	1	2	3	
0.0005		24.48	14.66	17.47	drastic 3 sec. (series 2)
0.05		24.51	14.77	17.70	
T-H C.C.	Elapsed Time (sec)	4	8	12	
0.0005		38.63	38.08	40.96	12 sec.
0.05		38.63	38.09	40.97	(series 3)

	axial interations performed	
T-H C.C.	single phase flow	two phase flow
0.0005	6	7
0.05	1	2

Although not included here, the behavior of other coolant parameters was also observed. Only minute differences in coolant enthalpy, equilibrium, quality, and void fraction were seen between the results of calculations performed using tight and loose T-H C.C. Fuel temperatures remained completely unaffected. Indeed the only parameters that were appreciably affected by changes in the T-H C.C. were the coolant mass flow rate and the mass flux. This sensitivity was, of course, anticipated since the T-H C.C. is defined in terms of the mass flow rate.

A plot of the percentage error in the minimum hot channel density vs. time for each transient considered appears in Fig. 4.25. This error was defined as

$$\% \text{ density error} = \frac{\rho_{min}(\text{T-H C.C.}=0.005) - \rho_{min}\ (\text{T-HC.C.}=0.05)}{\rho\ min\ (\text{T-H C.C.}=0.005)} \times 100$$

Upon examination of these curves, one finds that T-H C.C. sensitivity is most noticeable after the onset of boiling when the coolant is a low quality two-phase mixture. However, even in these cases, the sensitivity is slight (i.e. less than 2%).

It would appear from the curves for the two short (i.e. 3 second) transients that the potential exists for marked T-H C.C. sensitivity in long transients with two-phase flow. Although this potential may exist, the transient demonstrating such a sensitivity would be extremely drastic.

Since generation of void in the coolant results in a large negative reactivity insertion, it is unlikely that the conditions of sustained two-phase flow needed to bring about a T-H C.C. sensitivity would be encountered in PWR transients.

The 3.0 second transients represent extreme power excursions and, as argued above, it is unlikely that the T-H package in MEKIN will ever be called upon to analyze more drastic transients. It is significant that in the 12 second transient behavior seen in Fig. 4.25, a noticeable, but slight, sensitivity is observed during the time the coolant is a two phase mixture. Later in the transient, the sensitivity is barely perceptible, even on the fine scale used in Fig. 4.25. It may be concluded then that errors resulting from a loose convergence criterion will propagate in time and possibly eventually become significant only if the coolant remains a two phase mixture. Should the coolant return to a saturated liquid state, any cumulative errors would disappear.

4.5.3 Discussion of T-H C.C. Sensitivity

It is clear from the studies just discussed that loose T-H C.C. will produce satisfactory results in most power transients. The explanation of the insensitivity of the results to the T-H C.C. may be found in the equations comprising the T-H solution scheme.

The energy equation used in this scheme is [18]

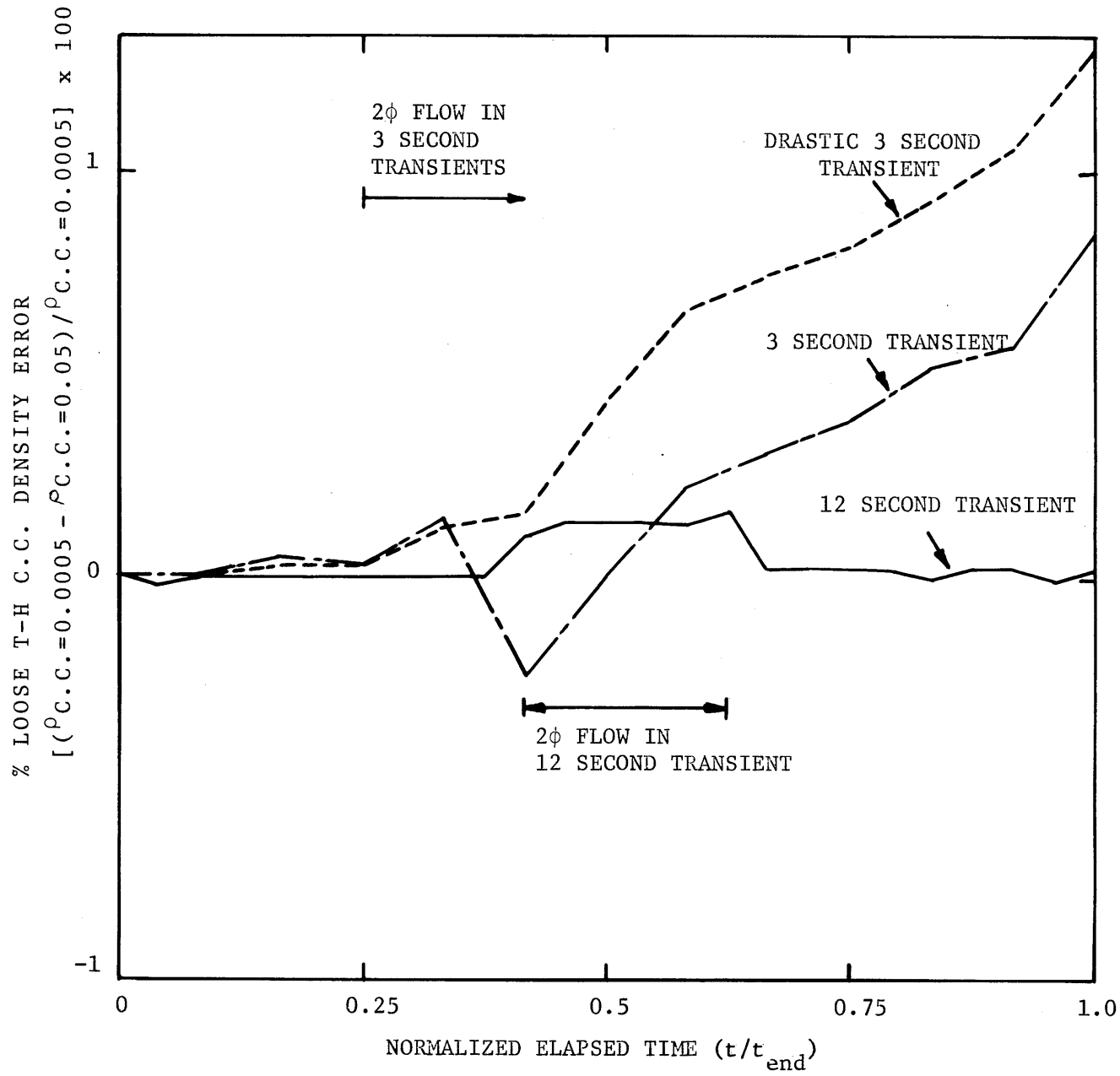

FIG. 4.25: COOLANT DENSITY SENSITIVITY TO T-HC.C.

$$\left(\frac{1}{u''_j} \quad \frac{h_j-\overline{h}_j}{\Delta t}\right)+\left(\frac{h_j-h_{j-1}}{\Delta x}\right) = [m_j-1]^{-1} \left(q_{j-\frac{1}{2}} - [S]^T[\Delta h_{j-1}]\left(w'_{J-1}\right)\right.$$

$$\left.-[S]^T\ [t_{j-1}]\left(C_{j-1}\right) + [[h_{J-1}][S]^T - [S]^T\ [h^*_{j-1}]]\left(w_{j-1}\right)\right)$$

(4.5)

The enthalpy at the Jth level is found from the equation:

$$h_j=\left(\frac{1}{u''_j\Delta t} + \frac{1}{x}\right)^{-1}\left(\frac{\overline{h}_j}{u''_j\Delta t} + \frac{h_{j-1}}{\Delta x} + [m_{j-1}]^{-1}\left(q_{j-\frac{1}{2}} - [S]^T\ [\Delta h_{j-1}]\left(w'_{j-1}\right)\right.\right.$$

$$\left.\left.- [S]^T\ [t_{j-1}]\left(C_{j-1}\right) + [[h_{j-1}]\ [S]^T - [S]^T\ [h^*_{j-1}]]\left(w_{j-1}\right)\right)\right)$$

(4.6)

This equation may be divided into three parts,

$h_j \sim$ (j^{th} level enthalpy at previous time)

+ ($j-1^{th}$ level enthalpy) + (energy transported to and generated in j^{th} level). (4.7)

The enthalpy at the previous time step as well as the current enthalpy are indirectly affected by the changes in the mass flow rate that occur when the T-H C.C. is altered. Although these terms become important when considering th cumulative effect of a loose T.H C.C., the mass flow rate and hence T-H C.C. do not appear in these terms. That is, if the previous time step and previous axial level enthalpies are assumed to be correct, the mass flow rate has no effect on

these terms when they are used to determine the current j^{th} level enthalpy.

The inverse of the mass flow rate matrix does however multiply the transport and generation terms in the third part of Eq. 4.7; this may be expanded as

(energy transported and generated) = (coolant energy deposited in passing from j-1 to j^{th} level) + (conducted energy from adjacent channels) + (turbulent mixing energy transport) + (diversion crossflow energy transport) (4.8)

Only minor changes in heat flux result when the mass flow deviates slightly, and this term far outweighs the others in Eq. 4.8 in a power transient analysis. However, the remaining terms are themselves only moderately sensitive to small changes in the mass flow rate. For example, the T-H C.C. is seen to have little effect on the crossflow in Fig. 4.26. Hence the significance of deviations in the mass flow rate lies not in their effect on individual terms but rather in that the sum of these terms is divided by the mass flow rate to determine the enthalpy increase of the coolant.

However, the magnitude of this increase is slight. If reasonable time steps and axial mesh sizes are used (e.g. 0.1 sec. and 1 ft.), the resulting coolant enthalpy increase

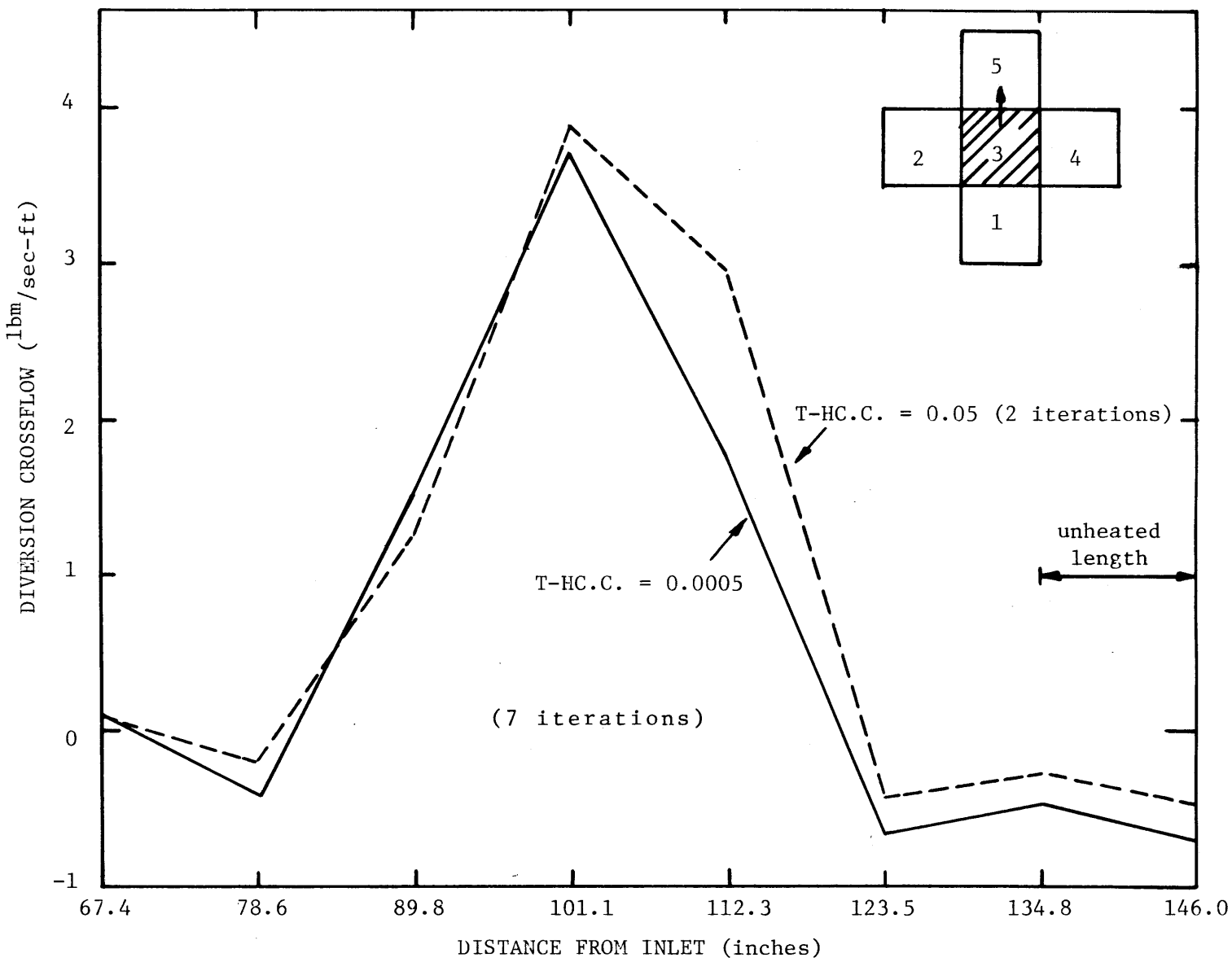

FIG. 4.26: EFFECT OF T-HC.C. ON DIVERSION CROSSFLOW

seen even in the drastic power transients studied here will never exceed 50 $^{Btu}/lbm$.

In this case, a 10 percent change in mass flow rate might cause the coolant enthalpy increase to change by 5 $^{Btu}/lbm$. Yet in Eq. 4.7, this increase is added to the enthalpy at the previous axial level and at the previous time step. These latter enthalpies would typically be between 500 and 700 $^{Btu}/lbm$. A simple order of magnitude analysis then indicates that small deviations (e.g. 10%) in the mass flow rate have only a minor impact upon the calculated coolant enthalpy. This impact would be increased if a flow reduction accompanied the power excursion.

The calculated enthalpy is used to determine the physical properties of the coolant. These properties are most sensitive to enthalpy changes when the coolant is a low quality two phase mixture, which explains why a slight T-H C.C. sensitivity is seen in these cases while virtually none is detected for single phase coolant parameters.

The insensitivity of coolant parameters to the T-H C.C. is due to the minor effect of small mass flow deviations in the COBRA energy equation.

4.6 Summary of Numerical Parameter Results

A formula has been presented in Eq. 4.1 that can be used to determine the difference in fuel temperature that will be found when the axial mesh size is changed. This

formula may be used in an iterative process to determine an adequate axial mesh size if the axial power profile is known. Good agreement was found between predictions from this formula and observed behavior in the axial mesh studies.

Time step sensitivity was found to result from an energy deposition error that arises from the "step" representation of the power history currently used in COBRA III-C/MIT and MEKIN. A formula was presented in Eq. 4.3 for the difference in average fuel temperature that will be found when the time step size is changed. The derivation of this formula was based solely on the energy deposition error; changes in the heat flux to the coolant were ignored. Consequently, this formula was found to be in good agreement with observed time step sensitivity when energy deposition dominated in the early part of the power coastdown transient (power profile class 2A). Predictions from this formula diverged from observed behavior late in the transient when heat transfer effects dominated.

A modification to the T-H solution scheme was proposed to model the power history more accurately and decrease time step sensitivity. With the current "step" model, the energy deposited in the time interval from (t) to $(t + \Delta t)$ is $[P\ (t + \Delta t)]\Delta t$. The proposed change would use linear interpolation and model the energy deposition as $0.5[P(t + \Delta t) + P\ (t)\ \Delta t$. Time step sensitivity could

be reduced considerably with this modification.

The axial mesh size and time step size were found to be related. A "rule-of-thumb" was proposed to limit the ratio of the axial mesh size to time step size to values greater than the average coolant velocity. This requirement is identical to that which is imposed by the Courant stability criterion; however, justification for the use of this requirement in COBRA analyses is based on empirical rather than mathematical grounds.

The COBRA and MEKIN users may employ Eqs. 4.1 and 4.3, along with the Courant criterion, to determine appropriate axial and time step sizes below the T-H analysis is made. The use of these relations will minimize the number of costly T-H "scoring" runs needed to determine a reasonable modeling scheme for a specific transient analysis and hence reduce the overall cost of such a study. Unfortunately, the applicability of these relationships has thus far only been demonstrated in power transients.

Neutronic feedback parameters, the fuel temperature and coolant density, were found to be insensitive to the T-H convergence criterion (T-H C.C.) in power transients. The insensitivity results from the small effect that mass flow changes have in the energy equation during power transits. A T-H C.C. of 0.05, corresponding to one axial iteration with single phase coolant flow and two

iterations with two phase flow, was found to yield satisfactory results. Significant reductions in execution time may be achieved with this value of the T-H C.C. without changing neutronic feedback parameters.

CHAPTER 5

SENSITIVITIES IN THE FUEL CONDUCTION MODEL

5.1 Introduction

The heat flux used in the energy equation that was described in Sec. 4.1.1 and Sec. 4.5.3 is calculated once at each time step from the fuel conduction model. This model takes on increased significance in the present studies which are restricted to power transients. The sensitivities of fuel temperature and coolant density to input parameters for the fuel conduction model are examined in this chapter.

5.1.1 Fuel Conduction Modeling in COBRA and MEKIN

The average fuel pin in a channel is divided into a series of equispaced concentric rings at each axial level, as shown in Fig. 5.1. Axial and circumferential conduction are ignored and, over a given time step, the heat generation is assumed to be constant throughout the fuel at an axial level.

Radial conduction is modeled by assigning a node to each concentric ring in the fuel and using finite difference approximations in the heat conduction equation. The resulting set of finite difference equations derived in the COBRA III-C

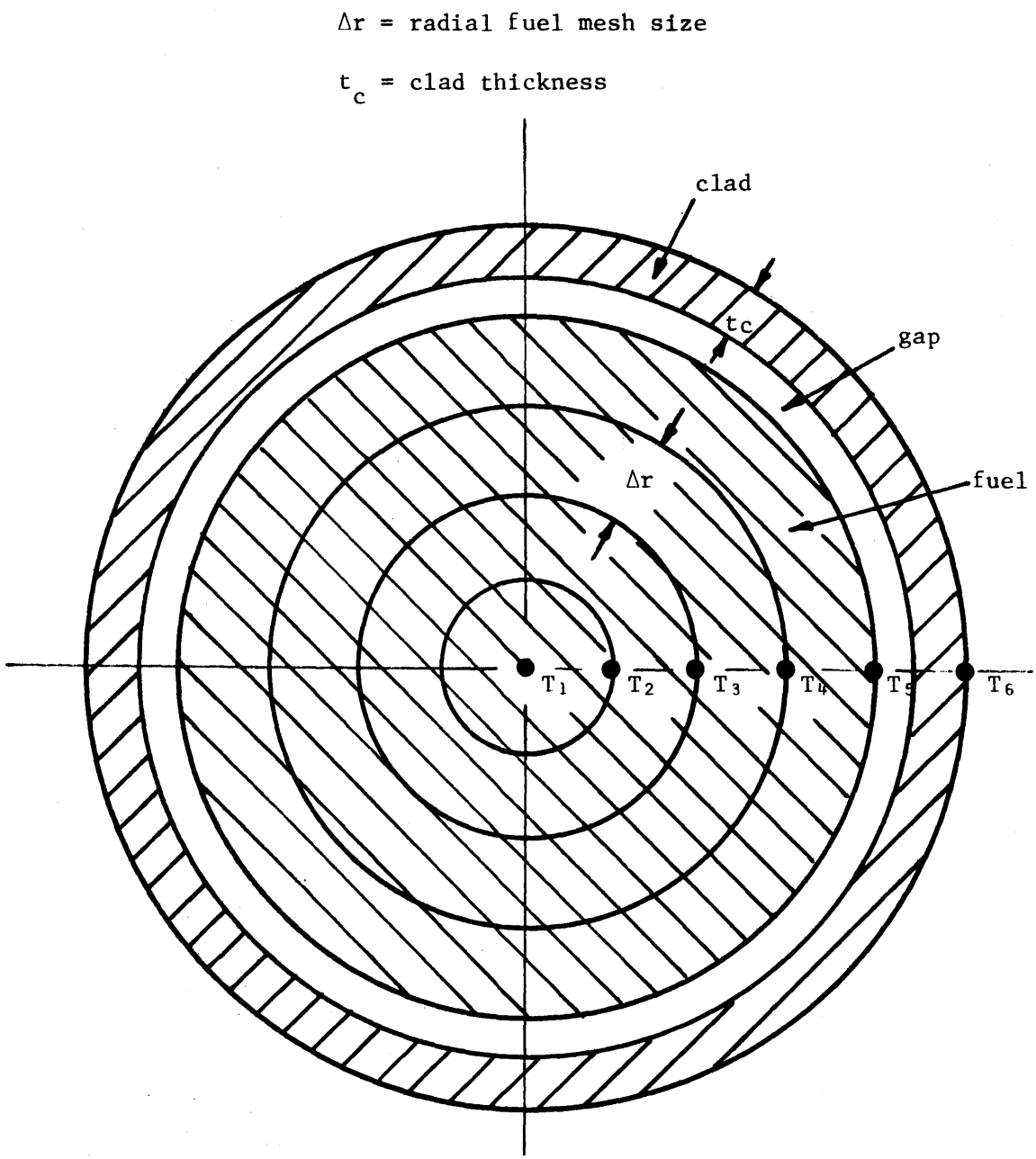

FIG. 5.1: FUEL PIN HEAT CONDUCTION MODEL

manual [18], are solved by an implicit method using Gaussian elimination. An electric circuit analog [23] [24] of the radial conduction model is presented in Fig. 5.2 to facilitate understanding of the model.

The fuel clad conductivity and gap heat transfer coefficient are lumped together into an equivalent thermal resistance between the fuel surface and exterior clad surface. This equivalent resistance approach ignores the temperature distribution in the gap and clad. A single gap heat transfer coefficient is input by the user for all fuel pins. The node at the clad exterior is coupled to the coolant by a clad-coolant heat transfer coefficient. This coefficient is determined from the Thom correlation [25], based on the clad heat flux and coolant parameters.

5.1.2 Conduction Studies Objectives

The user determines both the fuel mesh size and gap heat transfer coefficient. The sensitivity of fuel temperature and coolant density to the radial fuel mesh size and the gap heat transfer coefficient was examined in power transients. The optimum mesh size was sought which would ensure good results, even in drastic transients, while minimizing calculations. Similar studies were made in the early stages of MEKIN development for moderate transients. In these studies, a linear scheme was used to determine the average fuel temperature [20]. The current version of MEKIN employs a parabolic averaging scheme [26]; this will be discussed further in Sec. 5.3.

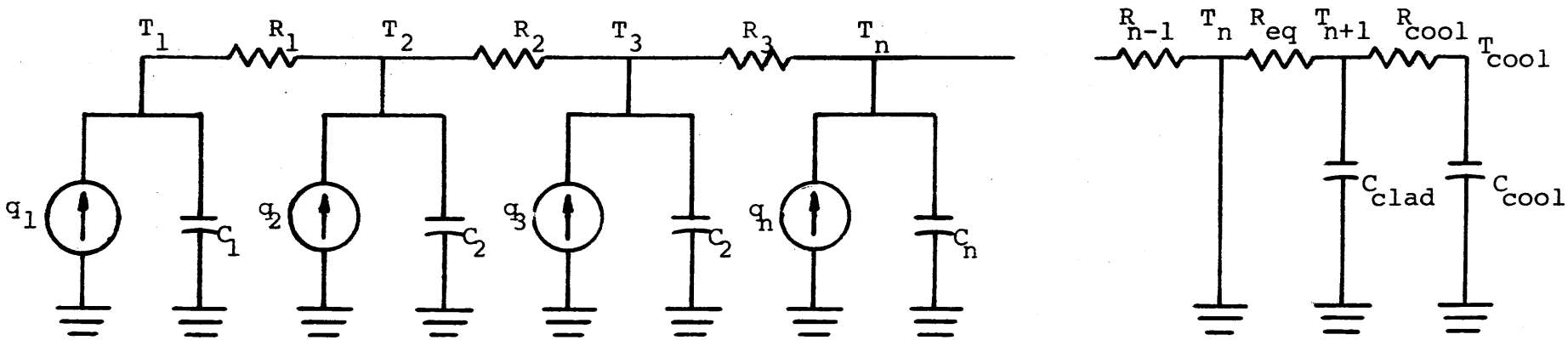

$$q_n = \pi q''' \Delta r^2([n+1]^2 - [n]^2)$$

$$R_n = \frac{1}{\pi k(2n-1)}$$

$$R_{eq} = \frac{4}{\pi U_{eq} D_o} \quad (U_{eq} \text{ from Eq.5.1})$$

$$R_{cool} = \frac{4}{\pi h_{cool} D_o}$$

$$C_n = \pi C_{p_f} \rho_f \Delta r^2([n+1]^2 - [n]^2)$$

$$C_{clad} = \pi C_{p_c} \rho_c t_c D_o$$

$$C_{cool} = C_{p_w} \rho_w A$$

$$q = C\frac{dT}{dt} \quad \text{and} \quad q = \frac{\Delta T}{R}$$

FIG. 5.2: ELECTRIC CIRCUIT ANALOG OF FUEL CONDUCTION MODEL

The fuel pin conduction model is idealized. Axial conduction, temperature dependent thermal properties, and non-uniform heat generation rates are observed in actual LWR cores. The limitations placed on the fuel model because it neglects these effects are also discussed in this chapter.

5.2 Radial Fuel Mesh Sensitivity

5.2.1 Methodology

Studies were made to determine the sensitivity of fuel temperatures and coolant density to the radial fuel mesh size. COBRA III-C/MIT was used in these studies and all other input parameters were held constant while the radial mesh size was varied. Results were compared to determine when decreasing the radial mesh size had negligible effects.

Two sets of comparisons were made, one with hot zero power initial conditions, the other with hot fuel power initial conditions. In this way, the effects of radial fuel mesh size were determined for both possible classes of initial conditions.

The hot full power transient, power profile class 3, was simulated in the same manner as the hot-zero power transient. The same peaking factors were used in both cases, however the power histories differed. The power vs. time curve used in the hot full power transient appears in Fig. 5.3.

Since the effects of the fuel conduction model were the primary concern in these studies, accurate modeling of the coolant behavior was unnecessary. Consequently, a two channel, three axial level model of the hot assembly and an

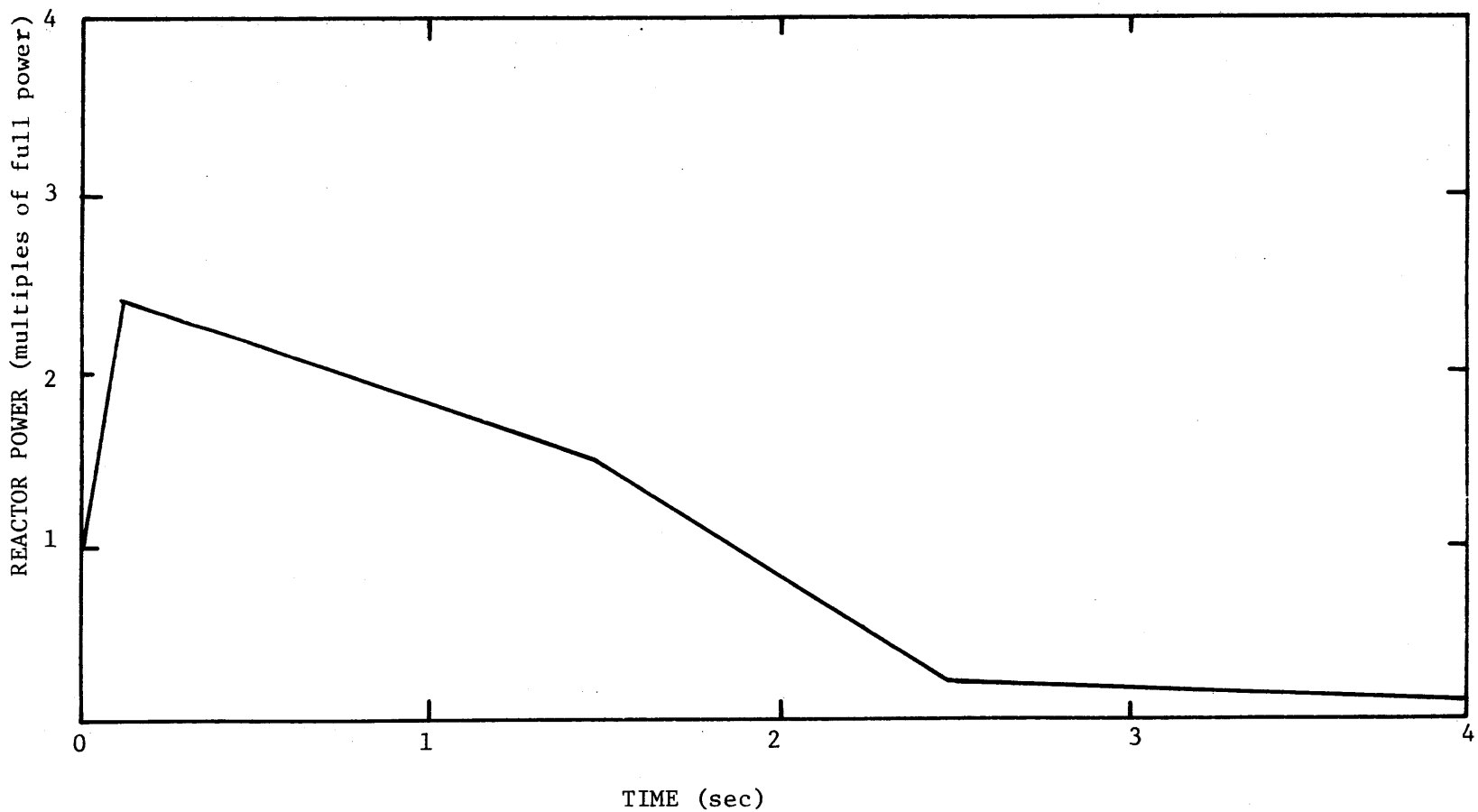

FIG. 5.3: HOT FULL POWER TRANSIENT POWER HISTORY (power profile class 3)

adjacent assembly was used with axial peaking factors of 0.5, 1.0 and 1.5.

5.2.2 Hot Zero Power Studies

5.2.2.1 Fuel Temperature Sensitivity to Mesh Size

Plots of the radial fuel temperature profile for the same axial level at 0.5, 1.0, and 2.0 seconds into the hot zero power transient are presented in Figs. 5.4, 5.5 and 5.6 respectively. Upon inspection of these curves, it becomes apparent that even in a drastic hot zero power transient four fuel nodes provide an adequate representation of the radial temperature profile. Nine fuel mesh points yield an almost perfect representation of the fine mesh, 24 node profiles.

Average fuel temperature is plotted vs. the number of nodes in the fuel in Fig. 5.7. As one would expect, the predicted average fuel temperature improves as the radial temperature profile is more accurately represented by increasing the number of fuel mesh points. Acceptable (i.e. 1% error) values are calculated with only 5 nodes in the fuel mesh. Virtual convergence to the fine mesh limit is found when 9 fuel mesh points are used. The average fuel temperature found with 9 fuel nodes differs from the 24 node result by only 0.2%.

Although good representation of the fuel temperatures was found with a relatively coarse mesh, coarse and fine mesh results diverged as the transient progressed. These differences are small and not readily apparent from the temperature profile plots. The percent difference between coarse and fine mesh fuel centerline and surface temperatures seen

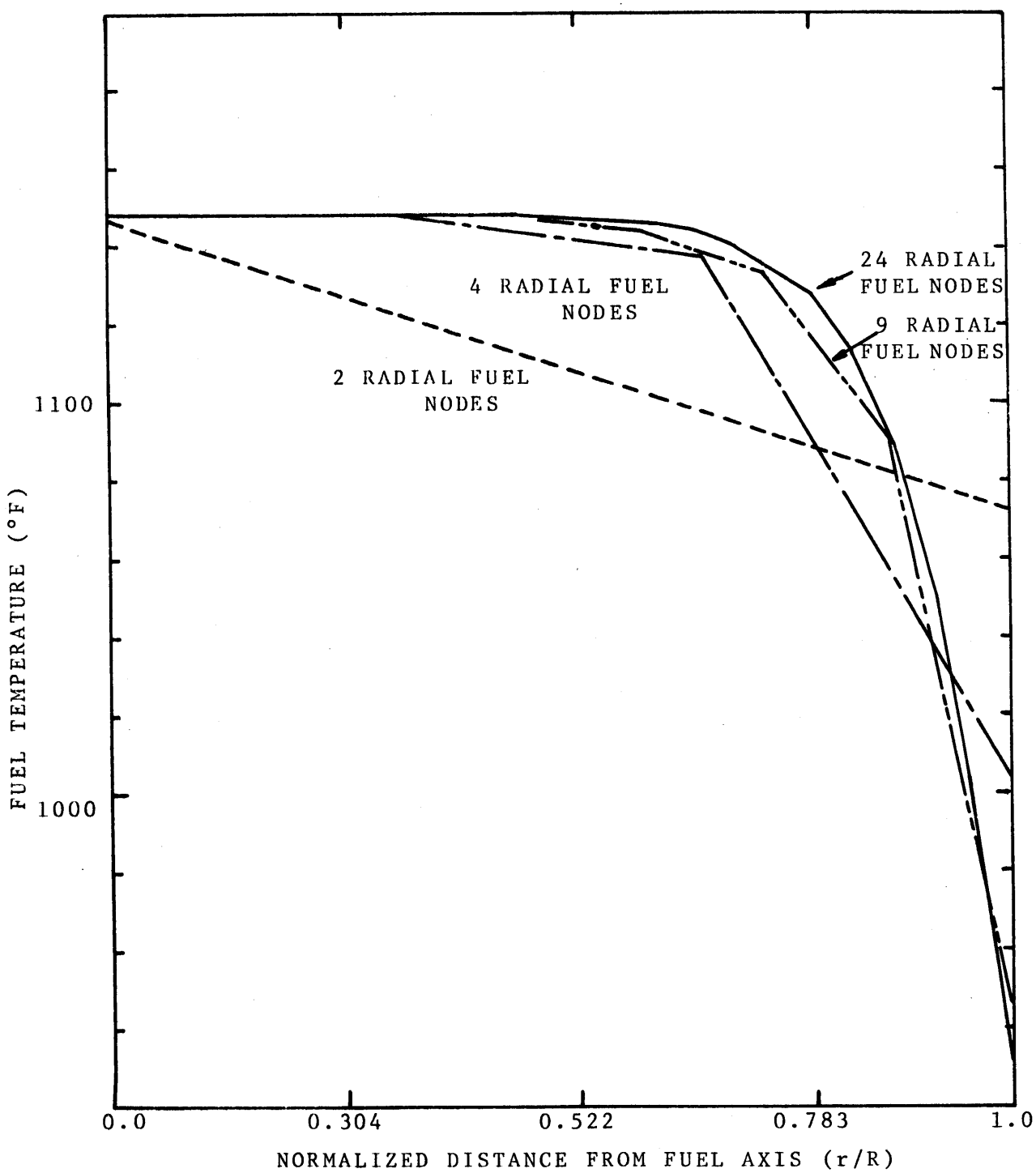

FIG. 5.4: FUEL TEMPERATURE SENSITIVITY TO RADIAL FUEL MESH SIZE (Hot Zero Power Transient, t = 0.5 seconds)

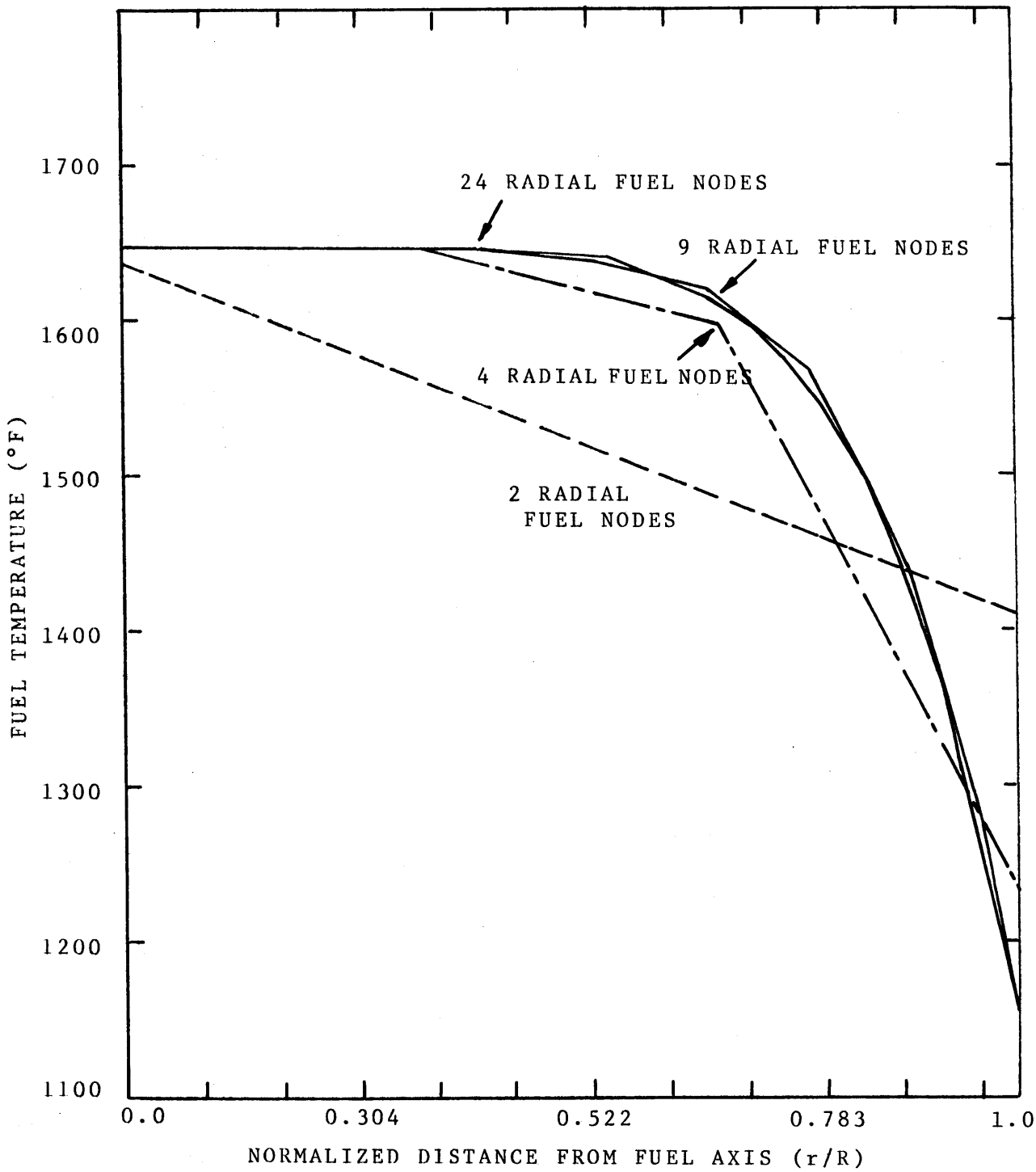

FIG. 5.5: FUEL TEMPERATURE SENSITIVITY TO RADIAL FUEL MESH SIZE (Hot Zero Power Transient, t = 1.0 seconds)

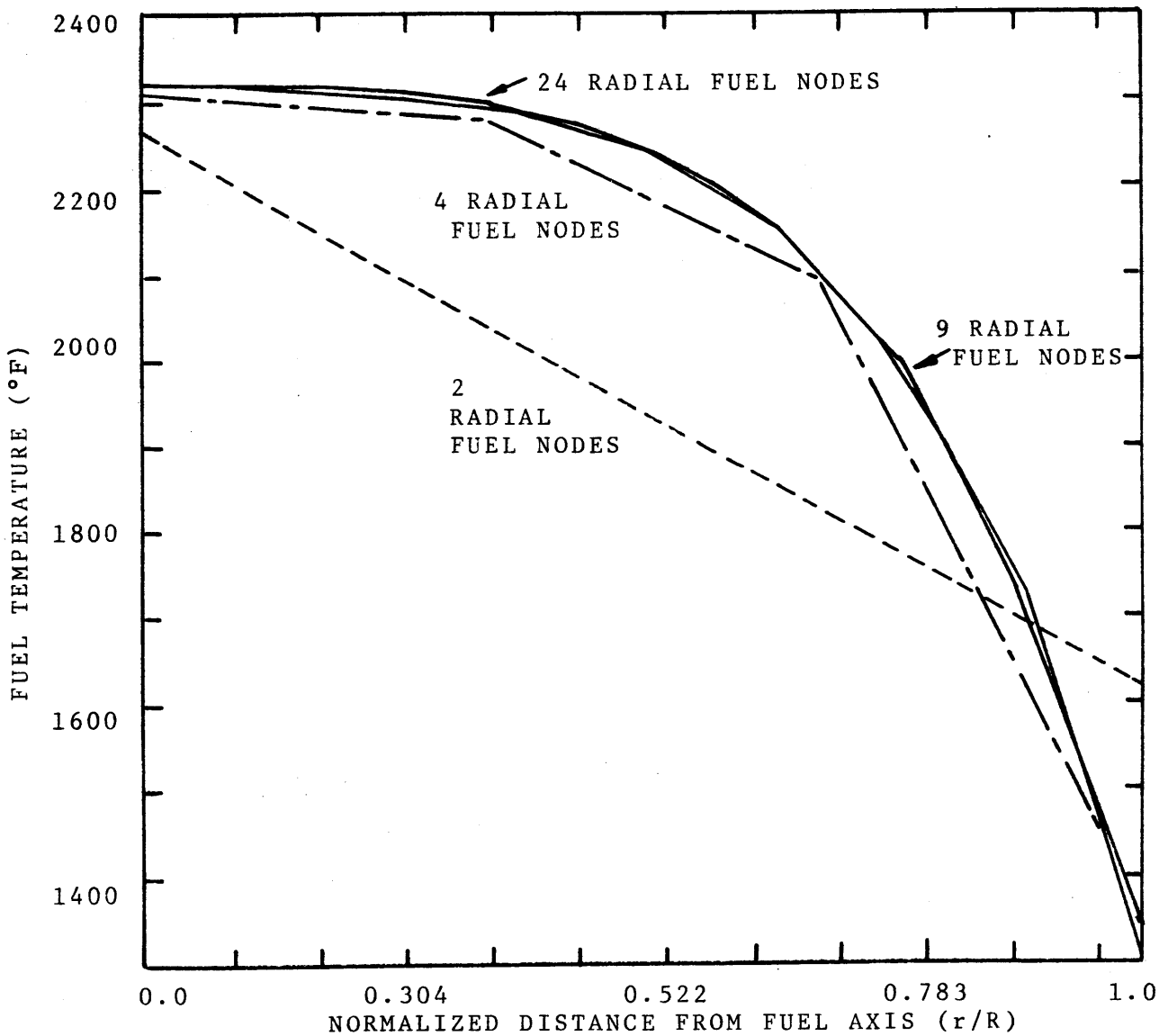

FIG. 5.6: FUEL TEMPERATURE SENSITIVITY TO RADIAL FUEL MESH SIZE
(Hot Zero Power Transient, t = 2.0 seconds)

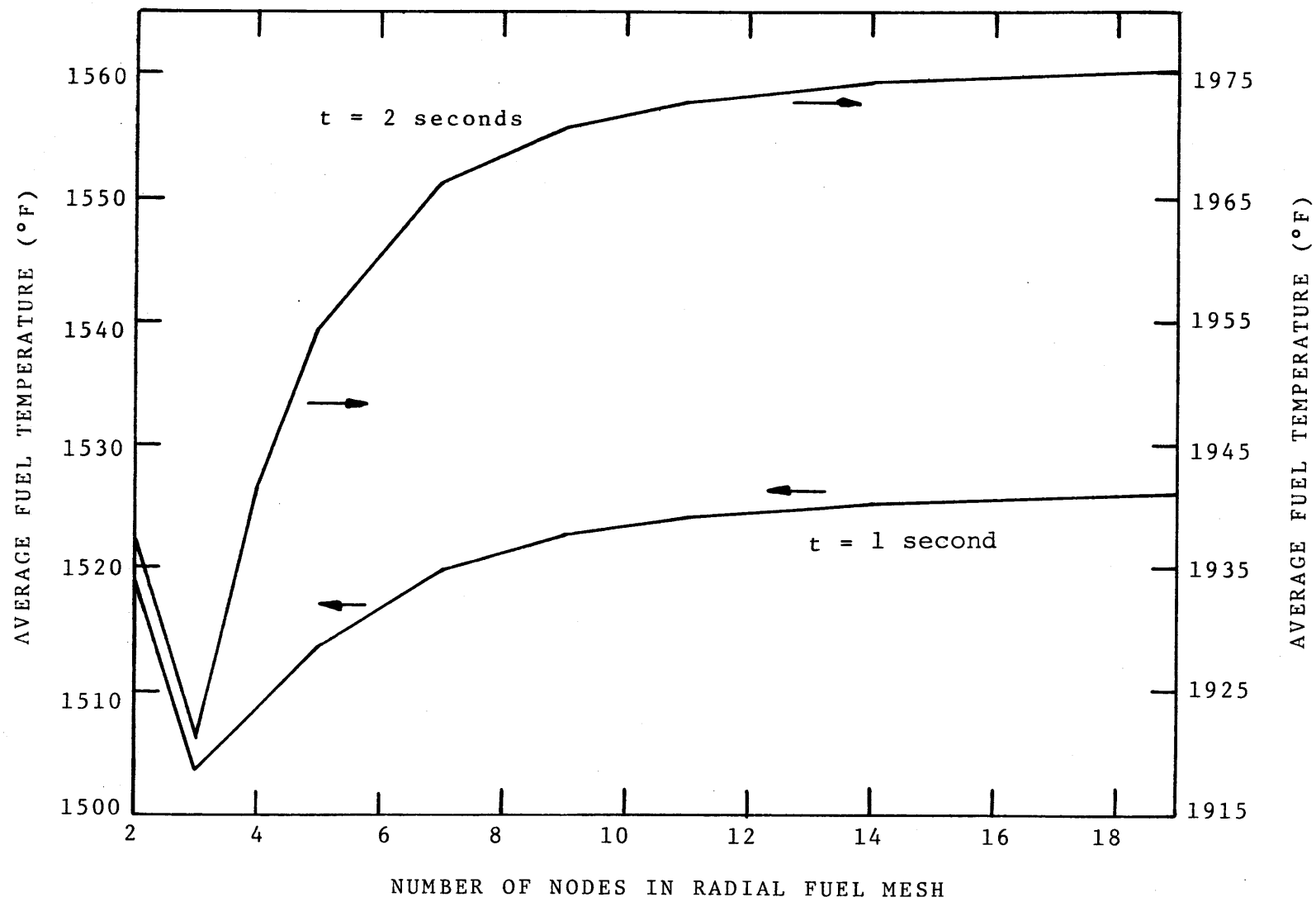

FIG. 5.7: AVERAGE FUEL TEMPERATURE SENSITIVITY TO RADIAL FUEL MESH SIZE (HOT ZERO POWER)

during the transient are presented in Fig. 5.8 and Fig. 5.9. After an initial rise, coarse mesh results fall progressively farther below fine mesh values as the transient proceeds.

A coarse mesh in incapable of accurately representing the fuel surface heat flux in the hot zero power transient. As seen in the radial temperature profiles of Secs. 5.4, 5.5 and 5.6, the central region fuel temperature profile is relatively flat and drops off sharply to a low fuel surface temperature in the outer region of the fuel. In the early stages of the transient, when the shape of the fuel temperature profile changes rapidly with time, use of a coarse mesh causes the flat central temperature profile to dominate and "pull" the exterior fuel region along. This results in higher heat fluxes and higher fuel surface temperatures. This behavior may be seen in Fig. 5.10. More energy is conducted from the fuel at high heat fluxes. Consequently, later in the transient, less energy remains stored in the fuel and coarse mesh temperatures are lower than fine mesh values. This explains the behavior noted in Fig. 5.8 and Fig. 5.9.

Average fuel temperature was found to be far less sensitive to the number of nodes in the fuel mesh than local temperatures. The percent difference between coarse mesh and fine mesh average fuel temperatures is presented in Table 5.1 for selected times during the transient. Even with the coarsest mesh possible, two nodes in the fuel, the worst deviation from the fine mesh results is 3.5% When fewer than 14 nodes were used in the fuel, local temperatures diverged from fine mesh results as the transient progressed. No di-

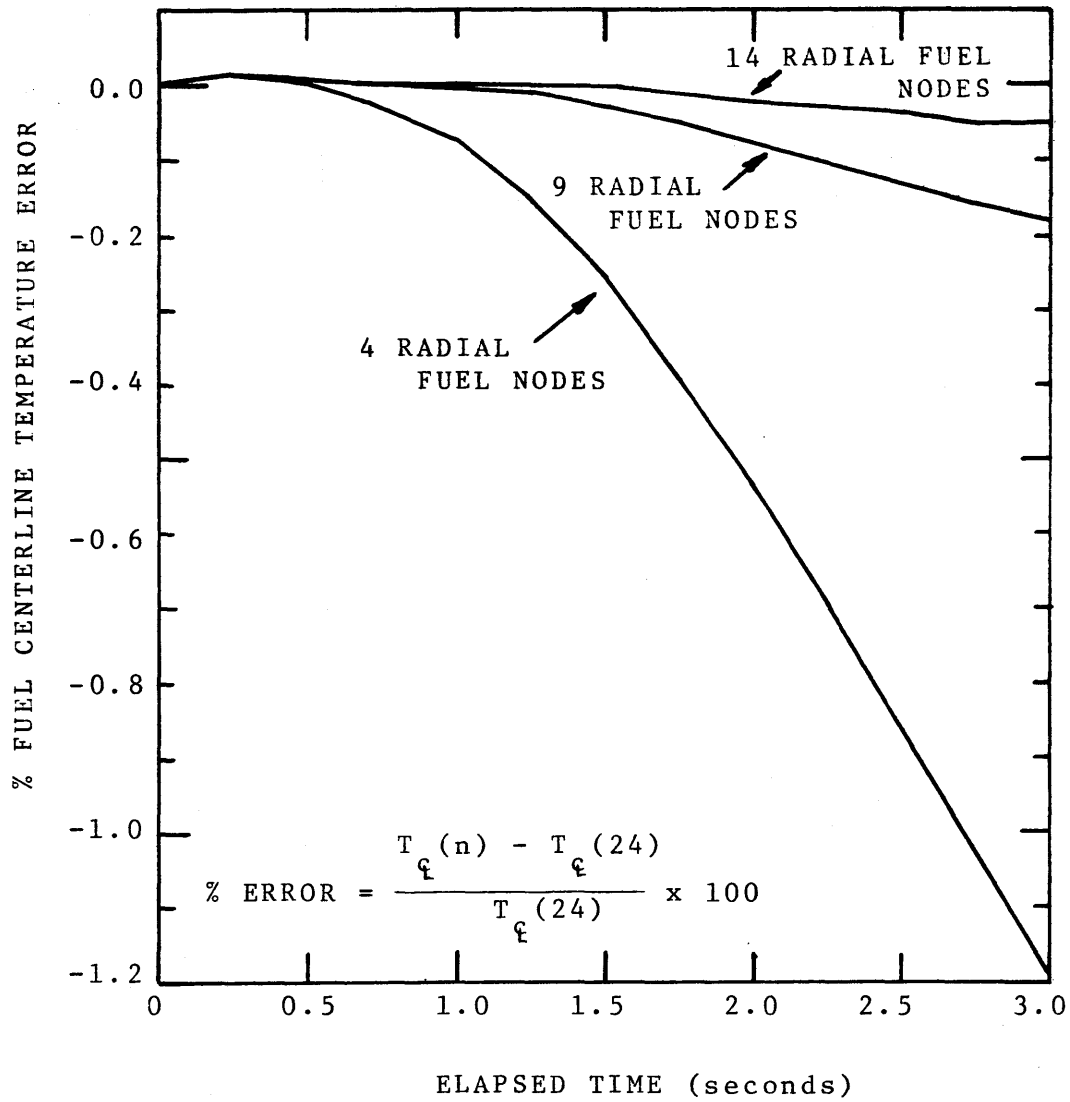

FIG. 5.8: FUEL CENTERLINE TEMPERATURE SENSITIVITY TO RADIAL FUEL MESH SIZE
(Hot Zero Power Transient)

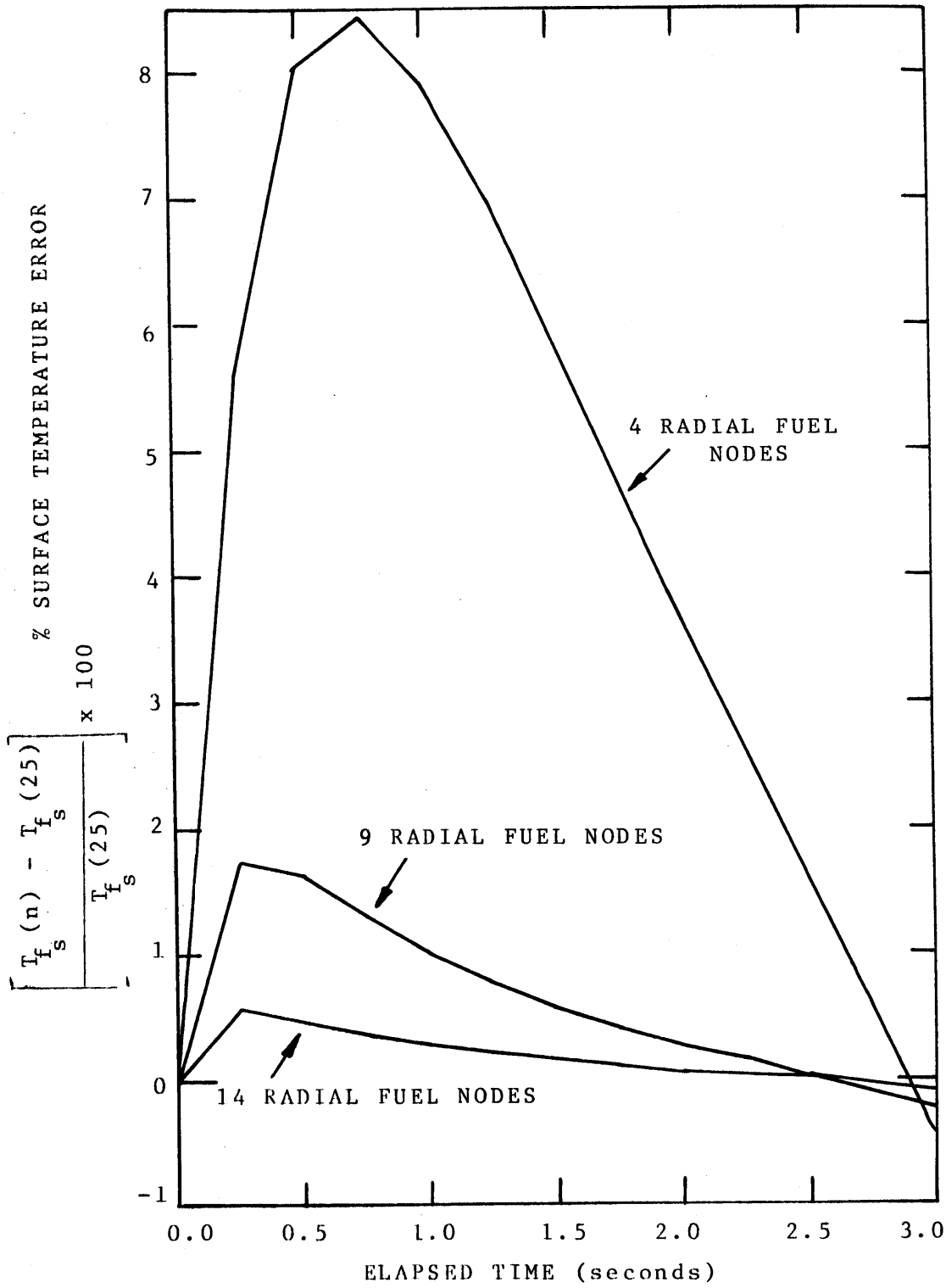

FIG. 5.9: FUEL SURFACE TEMPERATURE SENSITIVITY TO RADIAL FUEL MESH SIZE
(Hot Zero Power Transient)

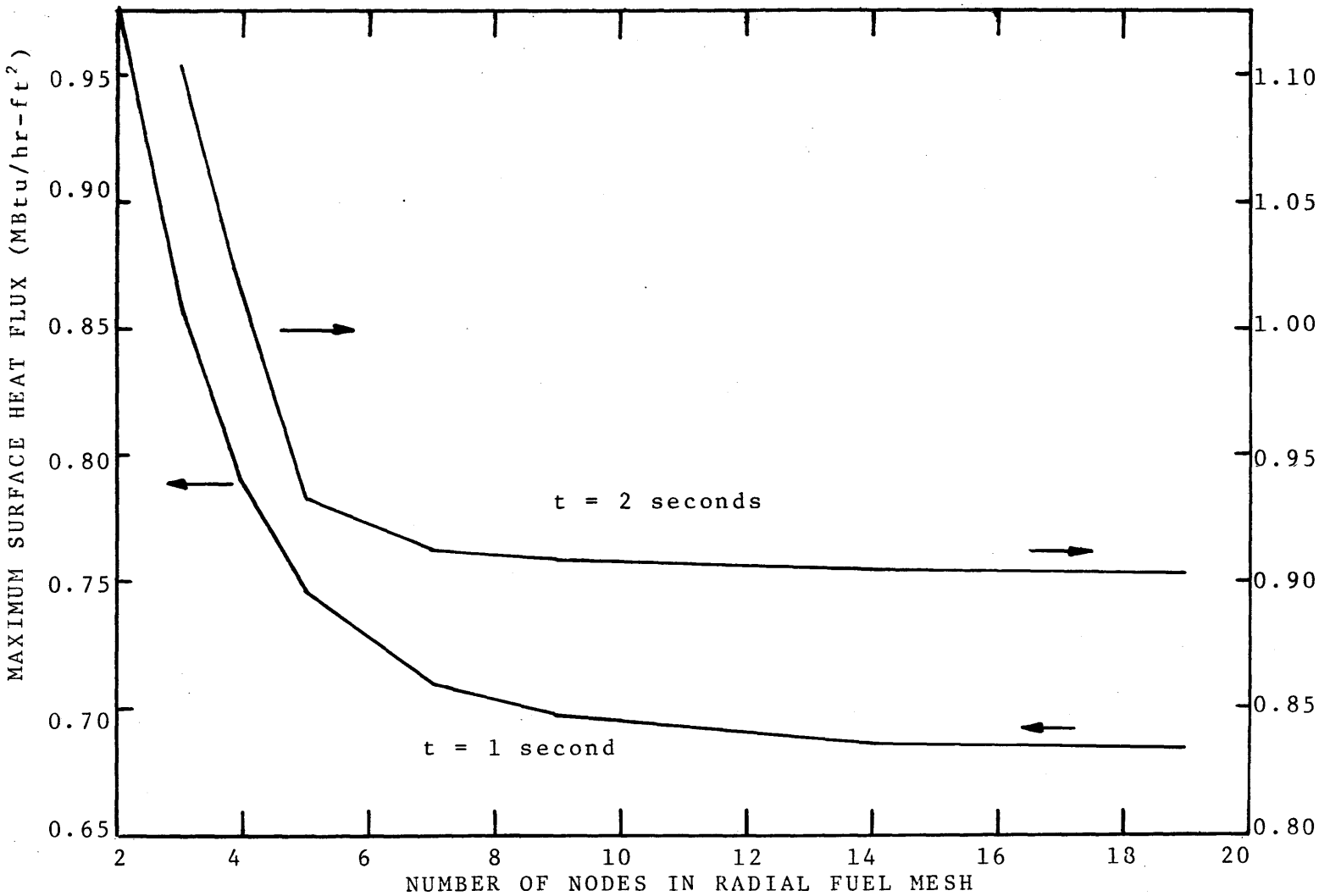

FIG. 5.10: FUEL SURFACE HEAT FLUX SENSITIVITY TO RADIAL FUEL MESH SIZE
(Hot Zero Power Transient)

nodes in fuel mesh	HOT ZERO POWER % difference in average fuel temperature (Δ) Elapsed Time (seconds) 1	2	3
2	0.48	1.94	3.49
4	1.14	1.73	1.77
9	0.24	0.25	0.22
14	0.06	0.07	0.06
19	0.02	0.02	0.02

$$\Delta(n) \equiv \frac{[\,T_{avg}\ (24\ \text{nodes}) - T_{avg}\ (n\ \text{nodes})\,]}{T_{avg}\ (24\ \text{nodes})} \times 100$$

TABLE 5.1 Sensitivity of Average Fuel Temperature to Radial Mesh Size (Hot Zero Power Transient)

vergence was found for the average fuel temperature when more than 9 nodes were used in the fuel mesh.

5.2.2.2 Coolant Sensitivity to Fuel Mesh Size

The higher heat fluxes calculated with a coarse fuel mesh increase the coolant energy deposition, raising the coolant enthalpy. Increased enthalpy results in lower coolant density. The difference between coolant parameters that was found when the fuel mesh size was varied is presented in Table 5.2. Marked differences are seen when fewer than nine nodes are used in the fuel mesh.

Since the coolant density is quite sensitive to the heat flux from the fuel, this heat flux must be accurately represented. Although the average fuel temperature was almost converged to its fine mesh value when five nodes were used in the fuel, at least nine nodes are needed to accurately model the heat flux and the resulting coolant density.

5.2.3 Hot Full Power Studies

5.2.3.1 Fuel Temperature Mesh Size Sensitivity

In the course of the hot zero power transient, the radial temperature profile changes shape from flat to parabolic. The hot zero power transient is thus a severe test of the fuel conduction model. A less extreme test of the fuel conduction model will now be discussed, the hot full power transient.

As the name suggests, the reactor is intitially operating at full power in this transient and a parabolic radial temperature profile is already established in the fuel. This profile

	% Difference			
	1 sec		2 sec	
nodes in fuel	enthalpy	density	enthalpy	density
2	-7.5	33.3	-14.5	36.3
3	-4.4	22.7	-6.3	19.7
4	-3.3	17.9	-4.4	14.6
5	-1.7	10.3	-0.9	3.3
9	-0.6	3.6	-0.3	1.2
14	-0.2	1.1	-0.09	0.3
19	-0.05	0.3	-0.02	0.1

$$\% \text{ Difference} = \frac{\text{fine mesh} - \text{coarse mesh}}{\text{fine mesh}} \times 100$$

fine mesh → 24 nodes in fuel

TABLE 5.2 Sensitivity of Coolant Parameters to Radial Fuel Mesh Size (Hot Zero Power Transient)

is shifted in magnitude throughout the transient but retains essentially the same shape. Since the shape of the temperature profile does not change with time, fewer demands are placed on the fuel conduction model in this transient and results are less sensitive to the fuel mesh size.

Good prediction of local fuel temperatures is found with only four fuel nodes, as seen in Fig. 5.11. Coarse mesh average fuel temperatures are found to agree very well with fine mesh results. Average fuel temperatures found as the number of nodes in the fuel was varied are presented in Fig. 5.12. Average temperatures calculated with only two nodes in the fuel differ from fine mesh values by less than 5°F, a difference of less than 0.4 percent. The average fuel temperature is thus seen to be insensitive to the number of fuel nodes in hot full power transients.

This insensitivity was observed for two reasons. First, local fuel temperatures found with a coarse mesh were found to agree well with fine mesh values because the shape of the radial temperature profile was unchanged throughout the transient. Second, the fuel temperature averaging scheme, discussed further in Sec. 5.3, assumes that a parabolic temperature profile exists between the fuel nodes; this is certainly true in the hot full power transient.

Excellent representation of the heat flux, presented in Fig. 5.13, is also achieved with relatively few fuel nodes. The heat flux predicted with four fuel nodes differes by only 2.5% from fine mesh values. Since the fuel surface heat flux

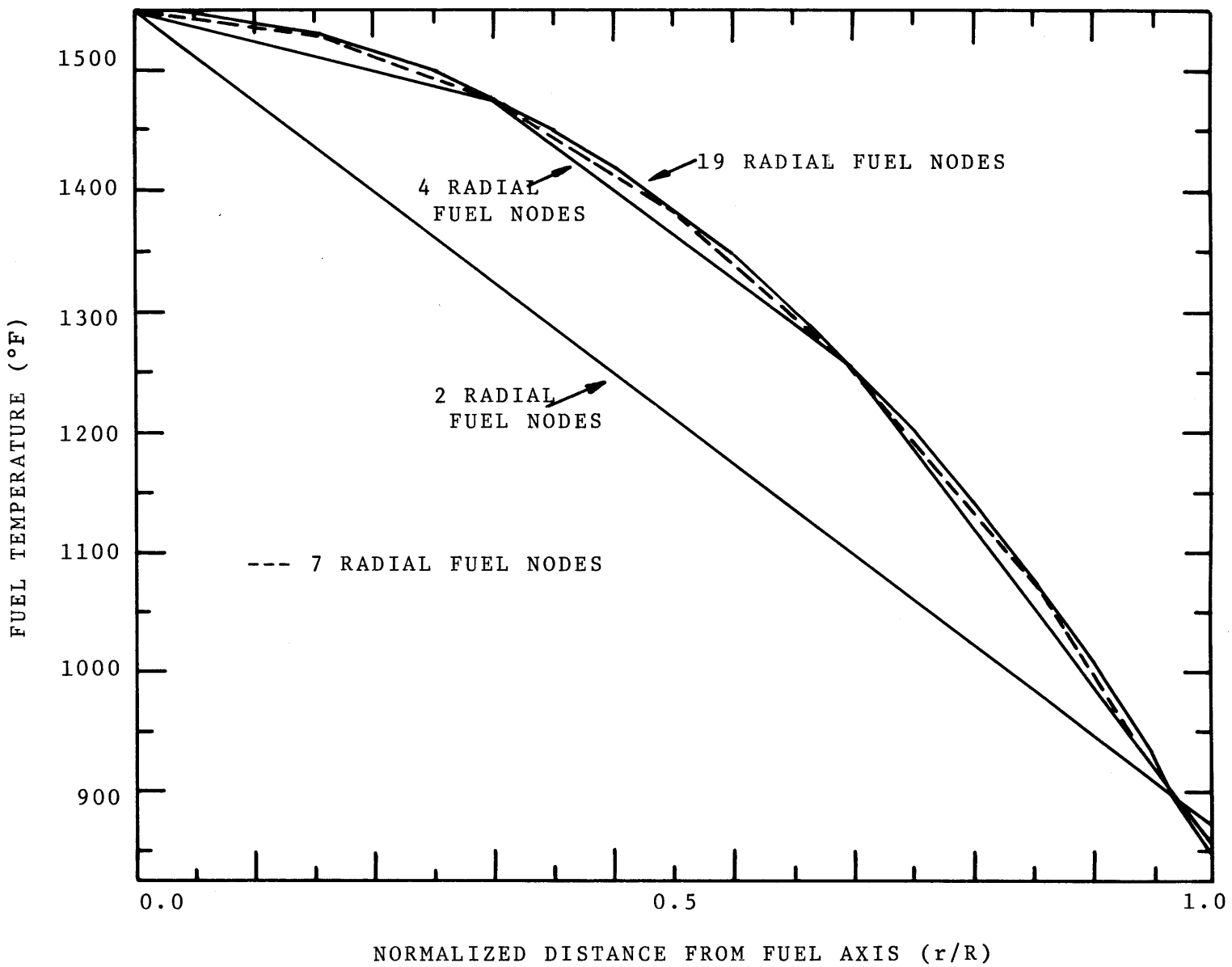

FIG. 5.11: FUEL TEMPERATURE SENSITIVITY TO RADIAL FUEL MESH SIZE
(HOT FULL POWER TRANSIENT, t = 1.0 seconds)

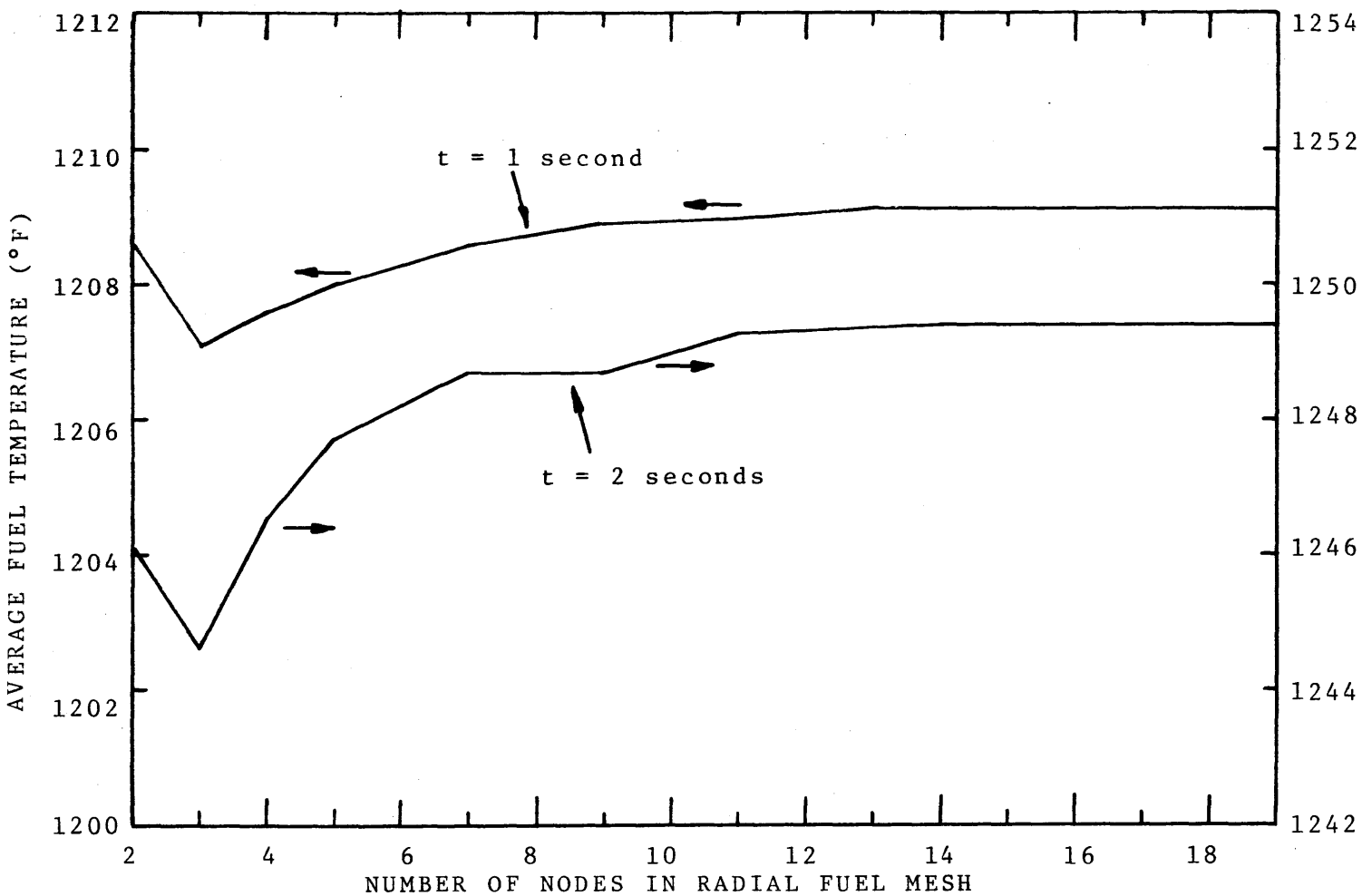

FIG. 5.12: AVERAGE FUEL TEMPERATURE SENSITIVITY TO RADIAL FUEL MESH SIZE
(Hot Full Power Transient)

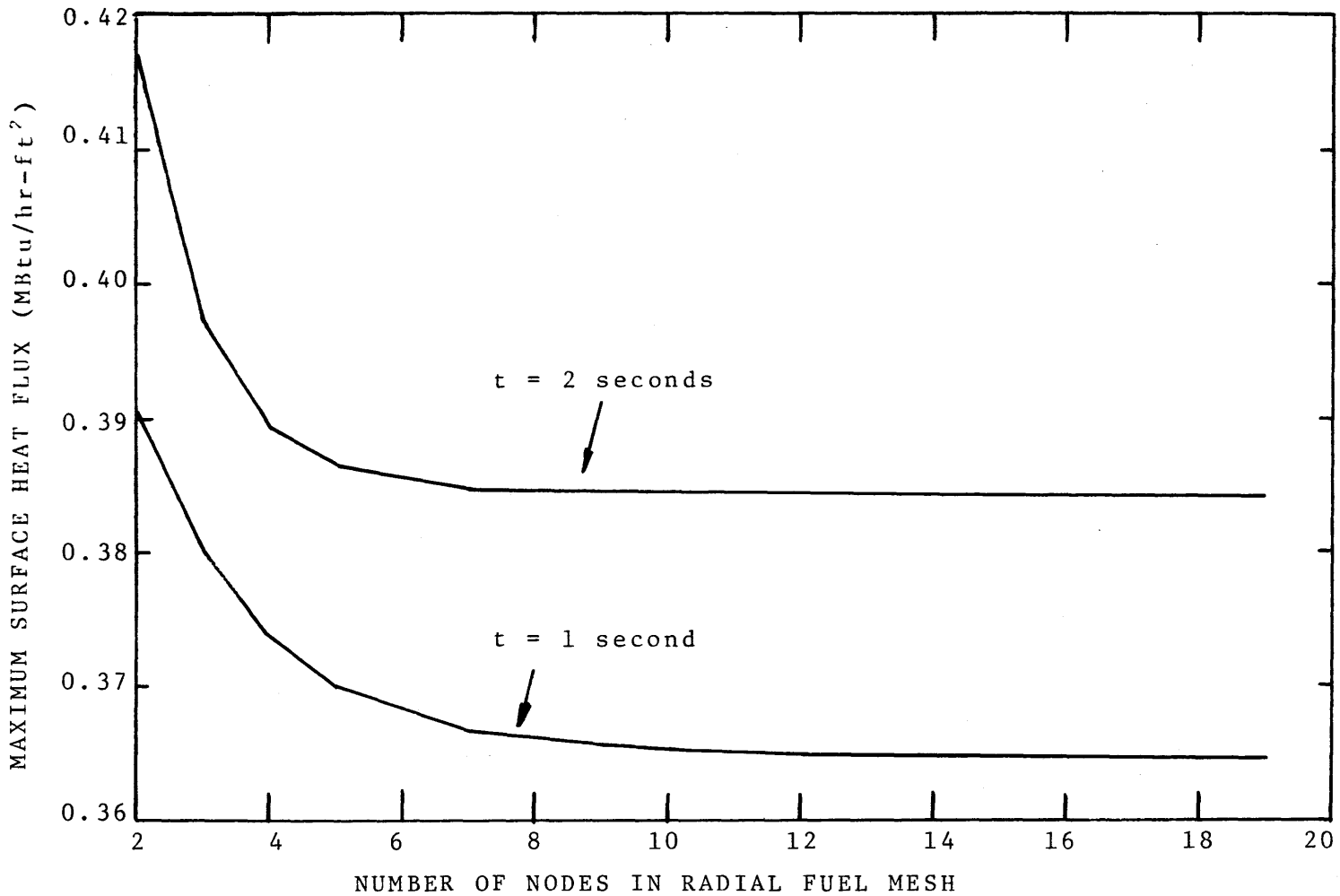

FIG. 5.13: FUEL SURFACE HEAT FLUX SENSITIVITY TO RADIAL FUEL MESH SIZE

(Hot Full Power Transient)

is represented well with few nodes, the divergence with time of the coarse and fine mesh temperatures is almost an order of magnitude below that which was seen in the hot zero power transient. The percent error of coarse mesh centerline and surface fuel temperatures is plotted against time in Fig. 5.14 and Fig. 5.15.

5.2.3.2 Coolant Sensitivity to Fuel Mesh Size

The decreased sensitivity of the surface heat flux to fuel mesh size in the hot full power transient brings about a corresponding decrease in the sensitivity of coolant parameters. The percent difference between coarse mesh and fine mesh predictions of the coolant enthalpy and density is presented in Table 5.3.

When the data in Table 5.3 is compared with similar data for the hot zero power transient in Table 5.2, the sensitivity of coolant parameters to fuel mesh size is seen to be an order of magnitude less in the hot full power transient.

5.3 Fuel Temperature Averaging Scheme

5.3.1 Methodology

The MEKIN fuel temperature averaging scheme assumes that a parabolic temperature profile exists between radial fuel nodes. This parabolic averaging scheme was thought to be superior to a linear, area weighted averaging scheme [26], but the superiority was never demonstrated.

A parabolic temperature profile exists in the fuel through-

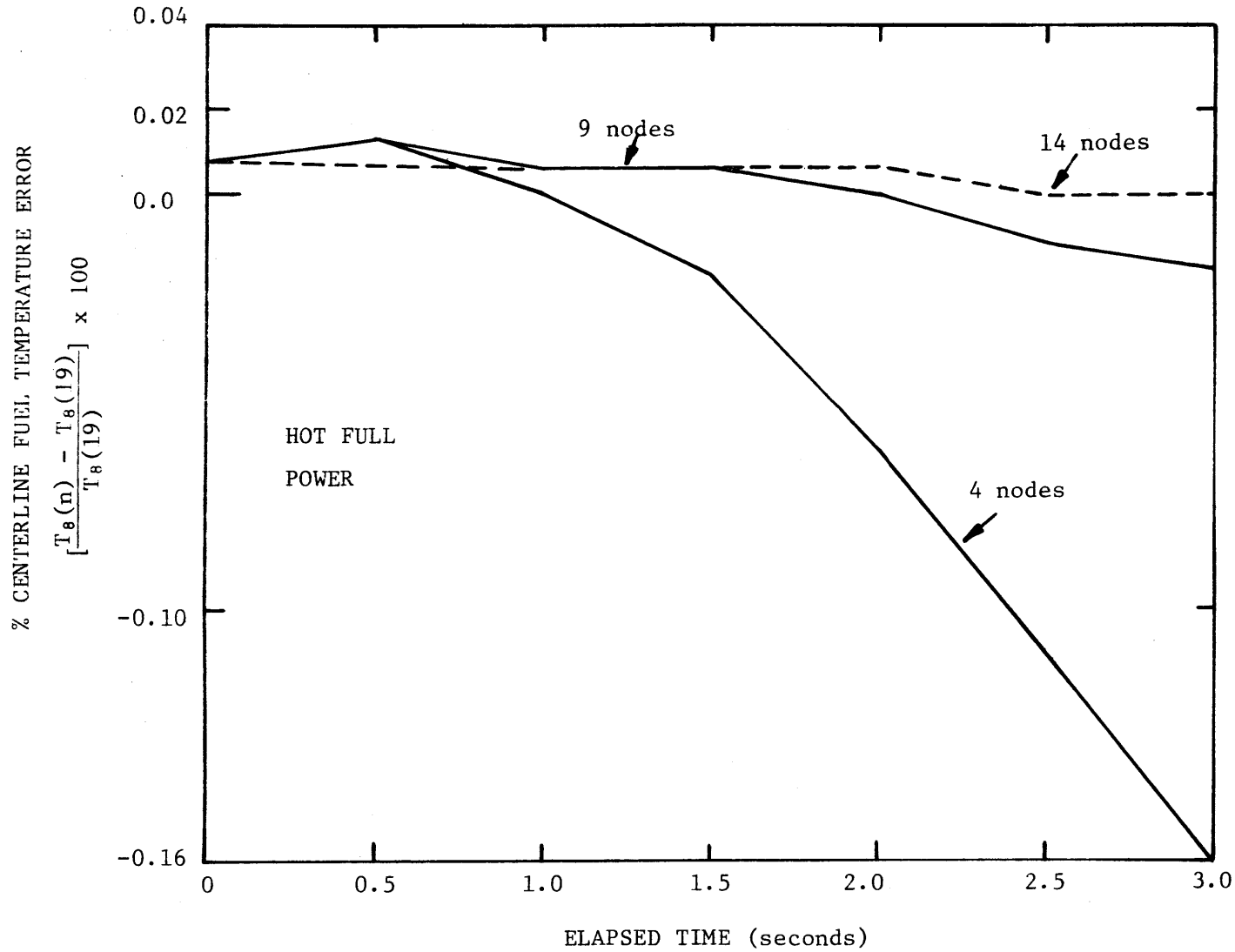

FIG. 5.14: CENTERLINE TEMPERATURE ERROR VS. TIME (HOT FULL POWER)

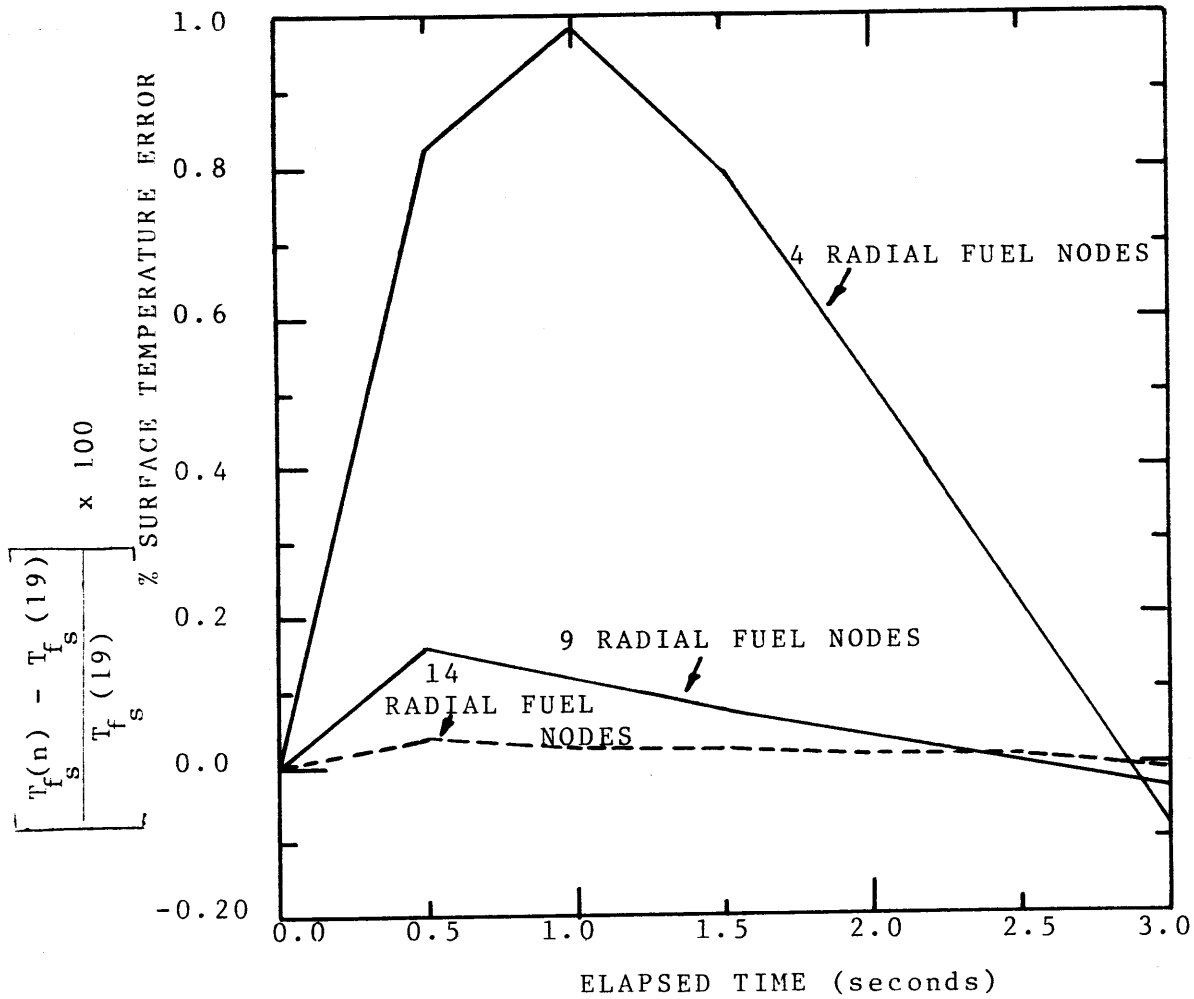

FIG. 5.15: FUEL SURFACE TEMPERATURE SENSITIVITY TO RADIAL FUEL MESH SIZE
(Hot Full Power Transient)

	% Difference			
	1 sec		2 sec	
nodes in fuel	enthalpy	density	enthalpy	density
2	-0.72	0.69	-1.39	1.47
3	-0.47	0.47	-0.67	0.70
4	-0.31	0.30	-0.32	0.35
5	-0.21	0.20	-0.17	0.17
7	-0.10	0.07	-0.06	0.07
9	-0.05	0.05	-0.03	0.05
14	-0.01	0.0	-0.01	0.02

$$\% \text{ Difference} = \frac{\text{fine mesh} - \text{coarse mesh}}{\text{fine mesh}} \times 100$$

fine mesh → 19 nodes in fuel

TABLE 5.3 Sensitivity of Coolant Parameters to Radial Fuel Mesh Size (Hot Full Power Transient)

out the hot full power transient, and the parabolic averaging scheme yields excellent predictions of the average fuel temperature with a very coarse mesh. However, as may be seen in Fig. 5.16, the fuel temperature profile is relatively flat in the early stages of a hot zero power transient and assumes a parabolic shape only in the final stages of the transient. The assumption of a parabolic profile between fuel nodes is questionable in the early stages of the hot zero power transient and may result in an overprediction of the average fuel temperature.

An alternate fuel temperature averaging scheme which assumes a linear temperature profile between fuel nodes is derived in this section. Average fuel temperatures are determined analytically for ideal temperature profiles and compared with predictions based on the linear and parabolic averaging schemes. The ideal profiles model the fuel temperature profiles that might be encountered in a hot zero power transient. Ideal profiles are used to facilitate analytic determination of the average fuel temperature and to decouple the mesh sensitivity of the averaging schemes from that of the fuel conduction model.

5.3.2 Numerical Averaging Schemes

Assume that the fuel is divided into N nodes and the temperature profile between nodes n and (n+1) is linear, that is

$$T(r) = a_2 - a_1 r \qquad (5.1)$$

where

$$a_1 = \frac{T_n - T_{n+1}}{\Delta r} \qquad (5.2)$$

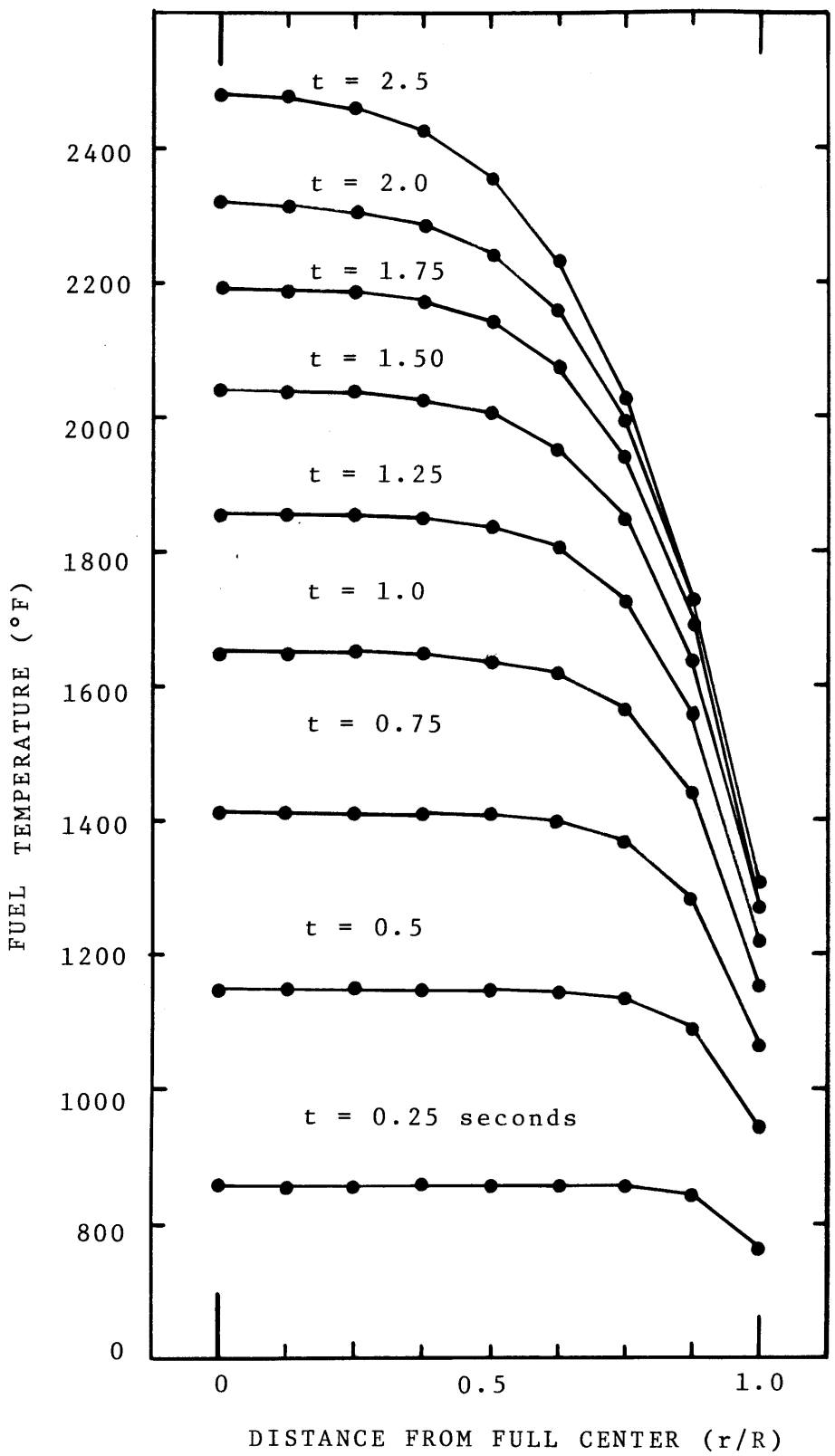

FIG. 5.16: DEVELOPMENT OF FUEL TEMPERATURE PROFILE IN HOT SERO POWER TRANSIENT

↑
Z

$$a_2 = T_n + [n-1]\Delta r a_1 \tag{5.3}$$

Following the method outlined by Bowring [26], the energy stored per unit length of the fuel pin is $\pi R^2 \rho C_p \overline{T}$. With the pin divided into N nodes, the energy stored per unit length between nodes n and (n+1) is $\int_{(n-1)\Delta r}^{n\Delta r} 2\pi r \rho C_p T(r)\,dr$.

If the fuel temperature averaging scheme is to be consistent, the total stored energy must be equal to the sum of the stored energy between nodes, that is

$$\pi R^2 \rho C_p \overline{T} = 2\pi \rho C_p \sum_{n=1}^{N-1} \int_{(n-1)\Delta r}^{n\Delta r} rT(r)\,dr \tag{5.4}$$

After rearranging terms and substituting for T(r) from Eq. 5.1, the average temperature is

$$\overline{T} = \frac{2}{R^2} \sum_{n=1}^{N-1} \int_{(n-1)\Delta r}^{n\Delta r} [a_2 - a_1 r]\,dr \tag{5.5}$$

Integration and simplification result in

$$\overline{T} = \left[\frac{\Delta r}{R}\right]^2 \sum_{n=1}^{N-1} \{n[T_n + T_{n+1}] - \frac{1}{3}[2T_n + T_{n+1}]\} \tag{5.6}$$

But the fuel, of radius R, was divided into N nodes, thus

$$\Delta r = \frac{R}{N-1} \tag{5.7}$$

Substitution of Eq. 5.7 into Eq. 5.6 yields the linear averaging formula:

$$\overline{T} = \frac{1}{[N-1]^2} \sum_{n=1}^{N-1} \{n[T_n + T_{n+1}] - \frac{1}{3}[2T_n + T_{n+1}]\} \tag{5.8}$$

The parabolic averaging scheme used in MEKIN is slightly easier to evaluate:

$$\bar{T}_p = \frac{1}{[N-1]^2} \sum_{n=1}^{N-1} [n-0.5] \; [T_n + T_{n+1}] \tag{5.9}$$

These formulas will be used to determine the average fuel temperature with ideal temperature profiles in Sec. 5.3.4. The results will be compared with the "true" average fuel temperature, which is determined analytically in Sec. 5.3.3.

5.3.3 Analytic Average Fuel Temperatures of Ideal Temperature Profiles

5.3.3.1 Flat-Linear Profile

The temperature profile considered in case 1 is presented in Fig. 5.17. The temperature at any radial section in the pin is given by

$$T(r) = \begin{cases} T_o & 0 \leq \frac{r}{R} \leq a \\ b_2 - b_1 r & a \leq \frac{r}{R} \leq 1 \end{cases} \tag{5.10}$$

where

$$b_1 = \frac{T_o - T_s}{(1-a)R}$$

$$b_2 = T_s + b_1 R$$

$$0 \leq a \leq 1$$

The average fuel temperature is defined as

$$\bar{T} = \frac{\iiint T(r,\theta,z)\, dV}{\iiint dV} \tag{5.11}$$

For a 1-D radial temperature profile in cylindrical coordinates,

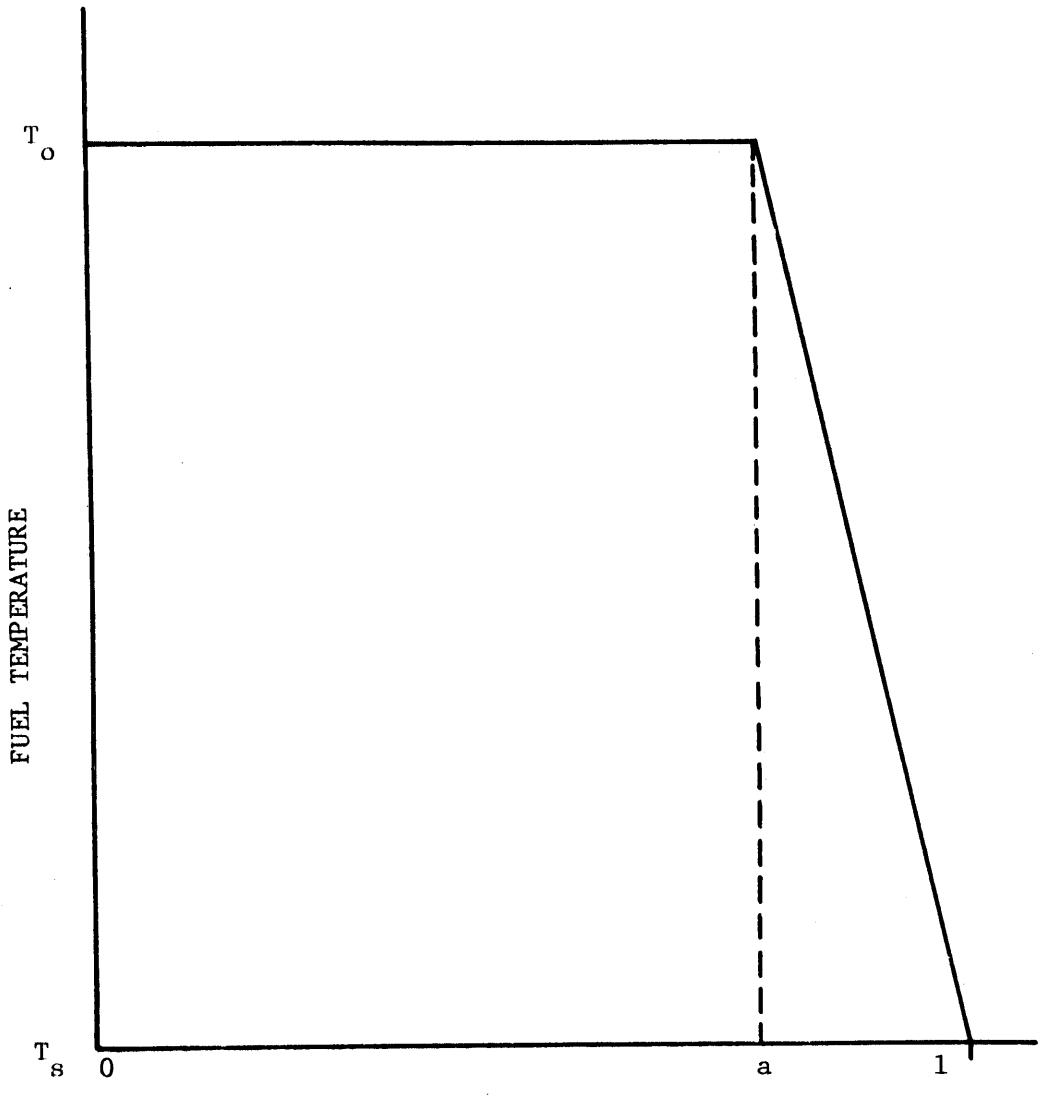

$$T(r) = \begin{cases} T_o & 0 \leq \frac{r}{R} \leq a \\ \left[\frac{T_o - T_s}{1-a}\right](1 - \frac{r}{R}) + T_s & a \leq \frac{r}{R} \leq 1 \end{cases}$$

FIG. 5.17: FLAT-LINEAR PROFILE

this reduces to

$$\bar{T} = \frac{2}{R^2} \int_0^R T(r)\,r\,dr \tag{5.12}$$

Upon substitution of Eq. 5.10 into Eq. 5.12, the expression for the average temperature of the "flat-linear" temperature profile is found to be

$$T = \frac{2}{R^2} \left\{ \int_0^{aR} rT_o\,dr + \int_{aR}^{R} \{b_2 - b_1 r\}\,r\,dr \right\} \tag{5.13}$$

After integration and simplification, the average fuel temperature for the "flat-linear" temperature profile may be expressed as

$$\bar{T} = \frac{T_o}{3} \left\{1+a+a^2 + \left[\frac{T_s}{T_o}\right][1-a]\ [2+a]\right\} \tag{5.14}$$

5.3.3.2 Flat-Parabolic Profile

The temperature profile considered in case 2 is presented in Fig. 5.18. The temperature at any radial section in the pin is given by

$$\bar{T}(r) = \begin{cases} T_o & 0 \le \frac{r}{R} \le a \\ b_4 - b_3 r^2 & a \le \frac{r}{R} \le 1 \end{cases} \tag{5.15}$$

where

$$b_3 = \left[\frac{T_o - T_s}{1-a^2}\right] \left[\frac{1}{R^2}\right]$$

$$b_4 = T_s + b_3 R^2$$

$$0 \le a \le 1$$

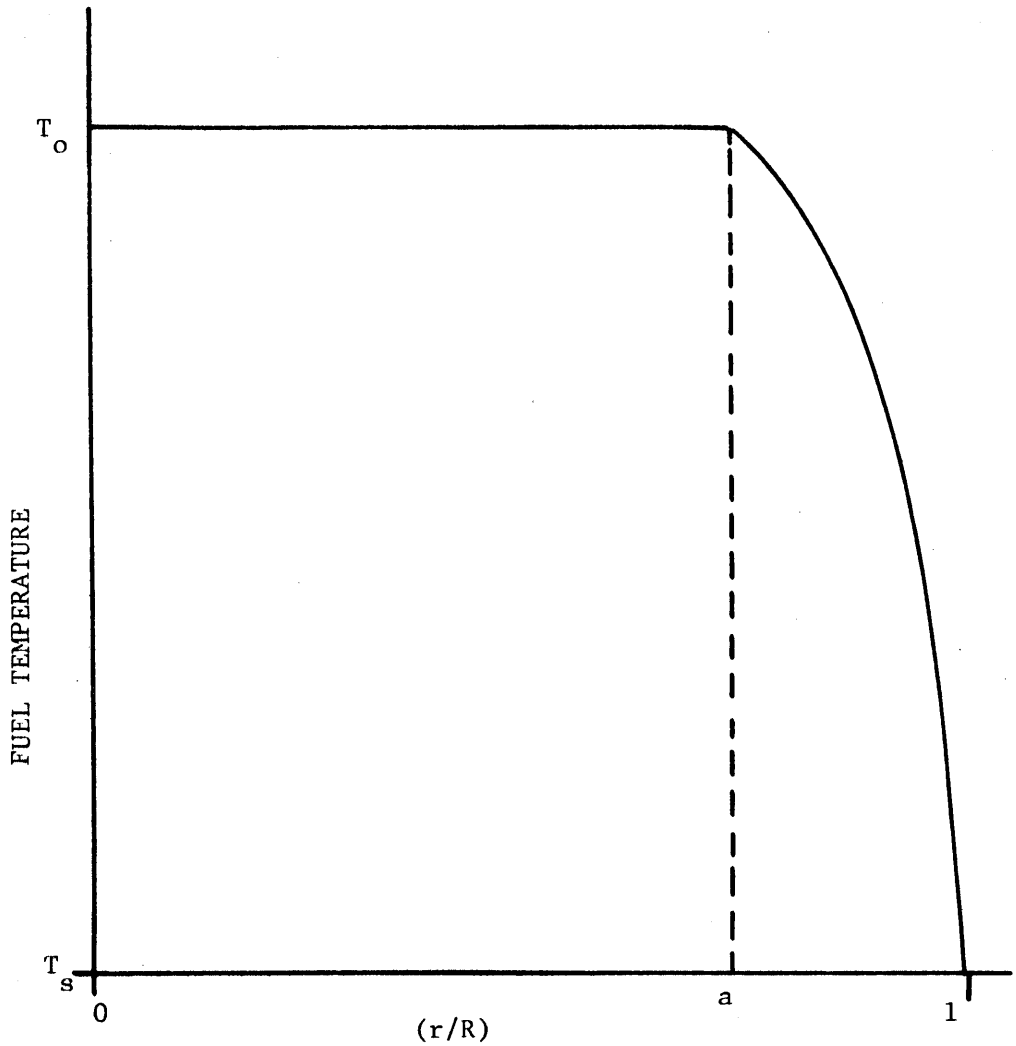

$$T(r) = \begin{cases} T_o & 0 \le \frac{r}{R} \le a \\ T_s + \left[\frac{T_o - T_s}{1-a^2}\right]\left[1 - \left(\frac{r}{R}\right)^2\right] & a \le \frac{r}{R} \le 1 \end{cases}$$

FIG. 5.18: FLAT PARABOLIC PROFILE

An expression for the average fuel temperature for this case is found upon substitution of Eq. 5.15 into Eq. 5.12; the result is:

$$\bar{T} = \frac{2}{R^2}\left\{\int_0^{aR} rT_o dr + \int_{aR}^{R} \{b_4 - b_3 r^2\} r dr\right\} \tag{5.16}$$

After integration and simplification, the average fuel temperature for the "flat-parabolic" temperature profile is

$$\bar{T} = \frac{T_o}{2}\left[1+a^2 + \left[\frac{T_s}{T_o}\right]\left[1-a^2\right]\right] \tag{5.17}$$

5.3.4 Comparison of Linear, Parabolic and Analytic Results

Average fuel temperatures for the profiles described earlier may be determined from Table 5.4. This table contains values of the weighting factor "b" in the expression

$$\bar{T} = bT_o + [1-b]T_s. \tag{5.18}$$

Since the fuel centerline temperature is weighted by b, higher values of b will result in higher average temperatures.

Results found with the linear and parabolic averaging schemes were found to be in perfect agreement with analytic results when these schemes were matched with the appropriate temperature profiles (e.g. parabolic averaging scheme used with "flat-parabolic" temperature profile). As expected, when a mismatch existed between the averaging scheme and the temperature profile, the results found with the averaging scheme differred from those found analytically. For example, when the linear averaging scheme was used with a completely parabolic profile

		Case 1*			Case 2*		
a	nodes in fuel	linear scheme	parabolic scheme	analytic	linear scheme	parabolic scheme	analytic
0.0	2	0.3333	0.5000	0.3333	0.3333	0.5000	0.5000
	3	0.3333	0.3750		0.4583	0.5000	
	4	0.3333	0.3518		0.4815	0.5000	
0.50	5	0.5833	0.5938	0.5833	0.6224	0.6250	0.6250
	9	0.5833	0.5859		0.6224	0.6250	
0.75	5	0.7708	0.7813	0.7708	0.7708	0.7813	0.7813
	9	0.7708	0.7734		0.7786	0.7813	

* note: to determine the actual value of the average temperature from data in this table, the tabulated value of "b" must be substituted into the expression

$$\overline{T} = bT_o + [1-b]T_s$$

TABLE 5.4 Comparison of Average Temperature Weighting Factors found Numerically and Analytically

(i.e. the flat-parabolic profile with a = 0), a 4% difference was observed.

However, improper matching of averaging scheme and temperature profile does not necessarily guarantee that the average temperature will be incorrect. This is the case only when very few values from the temperature profile are used to compute the average temperature. As the number of points used in average fuel temperature calculations is increased, results approach the analytic values.

This study has shown that both the linear and parabolic averaging schemes accurately take into account the flat portion of the fuel temperature profile. The parabolic scheme has been found to overpredict the average fuel temperature when the temperature decreases linearly with distance from the fuel centerline. Similarly, the linear averaging scheme has been found to underpredict the average fuel temperature when portions of the temperature are parabolic. Both schemes will yield accurate values if several fuel nodes are used (e.g. with 9 nodes, the deviation from analytic results drops to 0.3%).

The parabolic averaging scheme appears to be the best choice for use in MEKIN, since parabolic profiles are most often encountered in PWR analysis. Use of this scheme will provide accurate average fuel temperatures with relatively few fuel nodes if the temperature profile is parabolic. Linear temperature profiles may be encountered in some transients. However, in these cases, the fuel conduction model will require several nodes to determine the fuel temperature profile; with several

nodes, the parabolic scheme will provide accurate results regardless of the temperature profile.

5.4 Sensitivity to the Gap Heat Transfer Coefficient

A single value of the gap heat transfer coefficient, input by the user, is used in all fuel assemblies in a MEKIN or COBRA III-C/MIT analysis. Experiments have shown that the heat transfer coefficient is a crucial parameter in coupled neutronic/T-H transient analysis [27]. The gap heat transfer coefficient (h_{gap}) is a function of many variables, including burnup and linear heat generation rate[28] [29].

Since h_{gap} is a function of burnup, this parameter will vary from one assembly to the next and even locally within a fuel assembly. Variations in burnup and h_{gap} are found in power reators because of the non-uniform neutron flux and fuel management schemes. The gap heat transfer coefficient is also temperature dependent [27] and may vary in the course of a transient analysis.

The effect of changes in h_{gap} are examined in this section.

5.4.1 Fuel Temperature Sensitivity to h_{gap}

5.4.1.1 Steady State

An equivalent heat transfer coefficient may be used to describe the effects of the h_{gap}, clad conductivity and the clad-coolant heat transfer coefficient. In terms of the electric circuit analogy, presented in Fig. 5.2, this corresponds to using an equivalent thermal resistance in place of the respec-

tive individual thermal resistances.

In cylindrical coordinates, the equivalent heat transfer coefficient is [24]

$$R_{eq} = \frac{1}{U_{eq}} = \frac{D_o/D_I}{h_{gap}} + \frac{D_o}{2k_c} \ln\left[\frac{D_o}{D_I}\right] + \frac{1}{h_c} \tag{5.19}$$

The difference between steady state fuel surface temperature and the bulk coolant temperature, in terms of this equivalent resistance is

$$\Delta T = q'' R_{eg} \tag{5.20}$$

Typical PWR thermal data were substituted into Eq. 5.19 which was used with Eq. 5.20 to generate the curves presented in Fig. 5.19. These curves depict the effects of h_{gap} on the fuel surface - bulk coolant temperature difference, ΔT, for different surface heat fluxes.

An analytic expression for the sensitivity of ΔT to h_{gap} may be found. Substitution of Eq. 5.19 into Eq. 5.20 yields an expression for ΔT in terms of h_{gap}:

$$\Delta T = \{q'' \frac{a_1}{h_{gap}} + a_2\} \tag{5.21}$$

where

$$a_1 = [\frac{D_o}{D_I}]$$

$$a_2 = \frac{[h_c D_o \ln a_1 + 2k_c]}{2k_c h_c}$$

The sensitivity of ΔT to h_{gap} is found upon differentiation of Eq. 5.21 with respect to h_{gap}:

$$\frac{\delta \Delta T}{\delta h_{gap}} = \frac{-q'' a_1}{h^2_{gap}} \tag{5.22}$$

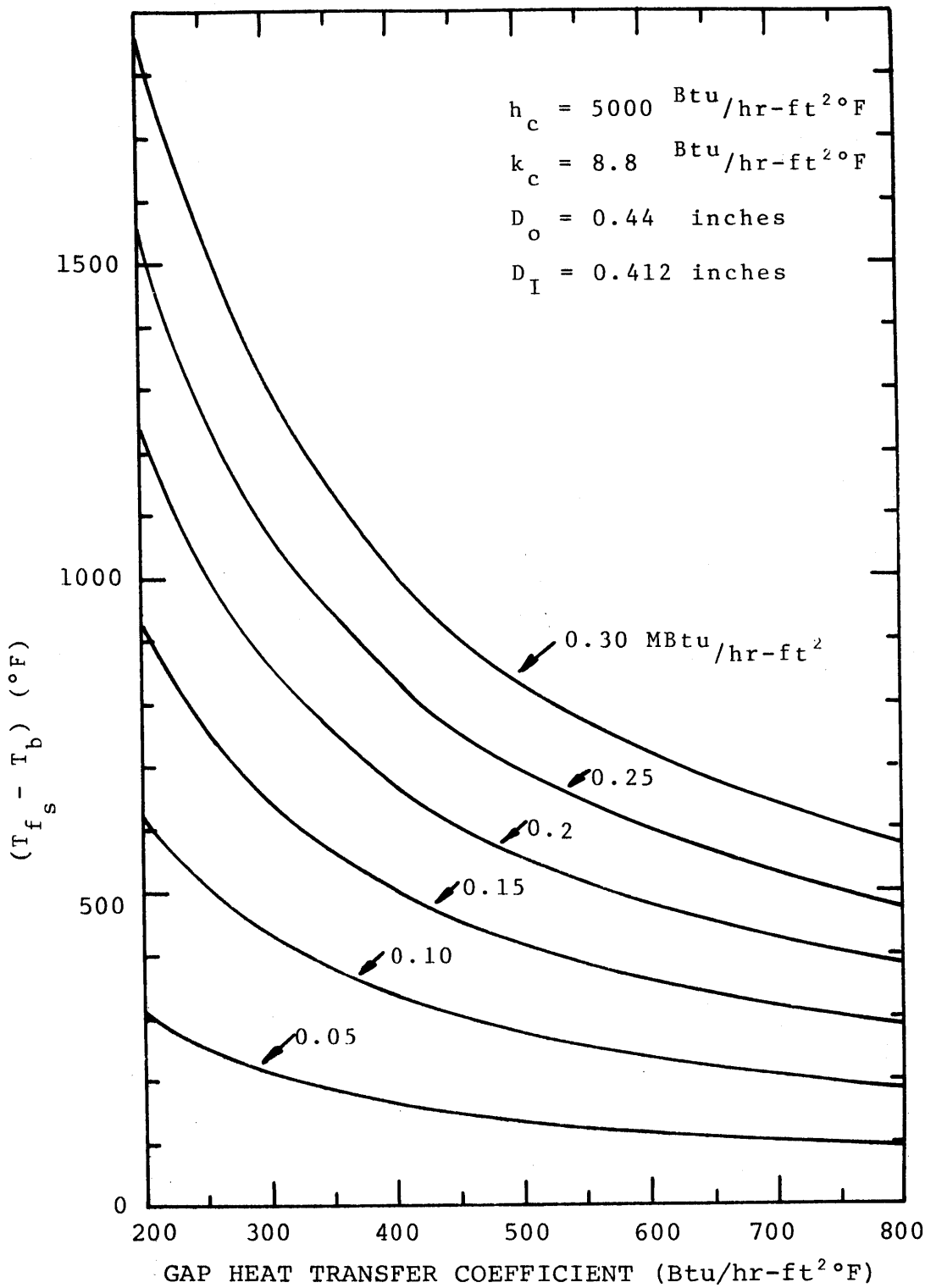

FIG. 5.19: FUEL SURFACE TEMPERATURE SENSITIVITY TO h_{gap}

Increasing sensitivity to h_{gap} is seen as the surface heat flux increases and as h_{gap} decreases. At a typical surface heat flux of 0.15 $^{MBtu}/hr\text{-}ft^2$ and a nominal h_{gap} of 600 $\frac{Btu}{hrft^2\,°F}$, changes of 100 $\frac{Btu}{hrft^2\,°F}$ in h_{gap} will result in ~50°F changes in fuel surface temperature if the coolant temperature remains constant.

In the steady state, the shape of the radial fuel temperature is determined by the volumetric heat generation rate and the fuel conductivity. The entire fuel temperature profile is shifted in magnitude based on the surface temperature of the fuel. Thus the average fuel temperature will exhibit the same sensitivity to h_{gap} as the surface temperature.

5.4.1.2 Transient

Although the derivation of Eq. 5.22 was based on steady state assumptions, the formula has been found to provide good estimates of the fuel temperature sensitivity to h_{gap} in power transients that are short in comparison with the fuel response time.

Both the magnitude of the fuel temperature and the time at which the maximum fuel temperature will be observed in a transient are dependent on h_{gap}. Time constants are used to characterize the responsiveness of the fuel temperature to changes in the coolant temperature or conversely, the time needed for the coolant to respond to changes in the fuel temperature. The time constant represents the time required for the average fuel or coolant temperature to change by $(1-{}^{1}/e)$

of the maximum value [30].

The time constants for the fuel and coolant are calculated from Eqs. 5.23 and 5.24 respectively:

$$\tau_f = \frac{\rho_f C_{p_f} R_f}{2U_{eq}} \tag{5.23}$$

$$\tau_w = \frac{\rho_w C_{p_w} A}{U_{eq} P_h} \tag{5.24}$$

Values of the time constants for typical PWR fuel and coolant parameters are plotted as a function of h_{gap} in Fig. 5.20.

The sensitivity of the time constants to h_{gap} may be determined by substituting for U_{eq} from Eq. 5.19 and differentiating Eqs. 5.23 and 5.24 with respect to h_{gap}. The resulting sensitivities are:

$$\frac{\delta \tau_f}{\delta h_{gap}} = - \frac{\rho_f C_{p_f} R_f (\frac{D_o}{D_I})}{2h_{gap}^2} \tag{5.25}$$

$$\frac{\delta \tau_w}{\delta h_{gap}} = - \frac{\rho_w C_{p_w} A \; [\frac{D_o}{D_I}]}{P_h \; h_{gap}^2} \tag{5.26}$$

Thus, the time constant sensitivity to h_{gap} is found to be significant at low values of h_{gap}. Coolant sensitivity is discussed further in the following section.

5.4.2 Coolant Parameter Sensitivity to the Gap Heat Transfer Coefficient

The gap heat transfer coefficient regulates the release of energy from the fuel to the coolant in a transient. An increase in the heat transfer coefficient results in an increased

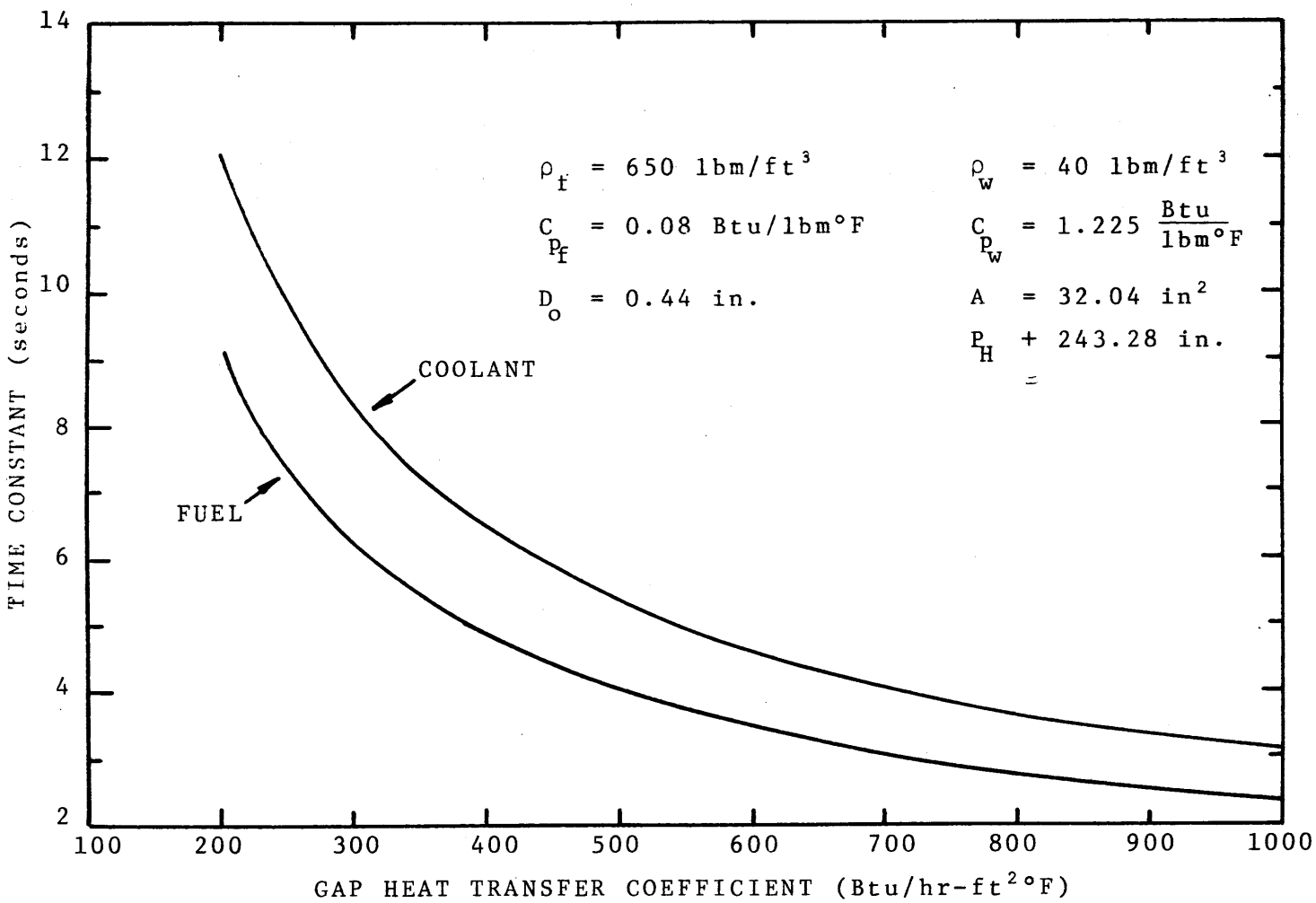

FIG. 5.20: FUEL AND COOLANT TIME CONSTANT SENSITIVITY TO h_{gap}

energy release rate or heat flux and hence decreased fuel and coolant time constants. Variations in the heat flux bring about variations in the vehavior of the coolant, as seen in Sec. 5.2.

5.4.2.1 Methodology

The gap heat transfer coefficient was varied while all other parameters were held constant in a series of COBRA analyses. The five channel, thirteen axial level model described in Sec. 4.1 was used. Two different transients were considered, the 3 second simulated rod ejection transient (power profile class 2A), and the 12 second power excursion transient (power profile class 4). The 3 second transient was shorter than predicted fuel and coolant response times; this allowed determination of the effects of h_{gap} on the magnitude of coolant parameters. On the other hand, the 12 second transient exceeded predicted response times, and the effects of h_{gap} on the coolant parameter history could be observed.

5.4.2.2 Results

It is clear from Eqs. 5.19 and 5.20 that increases in h_{gap} will bring about increases in the heat flux from the fuel if all other parameters are held constant. This increased heat flux raises the coolant enthaply significantly, as shown in Figs. 5.21 and 5.22.

Higher coolant enthalpies result in lower coolant densities: the effects of h_{gap} on the coolant density are shown in Figs. 5.23, 5.24 and 5.25. From these graphs it is apparent that the sensitivity of the coolant enthalpy to h_{gap} is amplified even further in the density sensitivity. This is especially noticeable when the coolant is a low-quality two phase

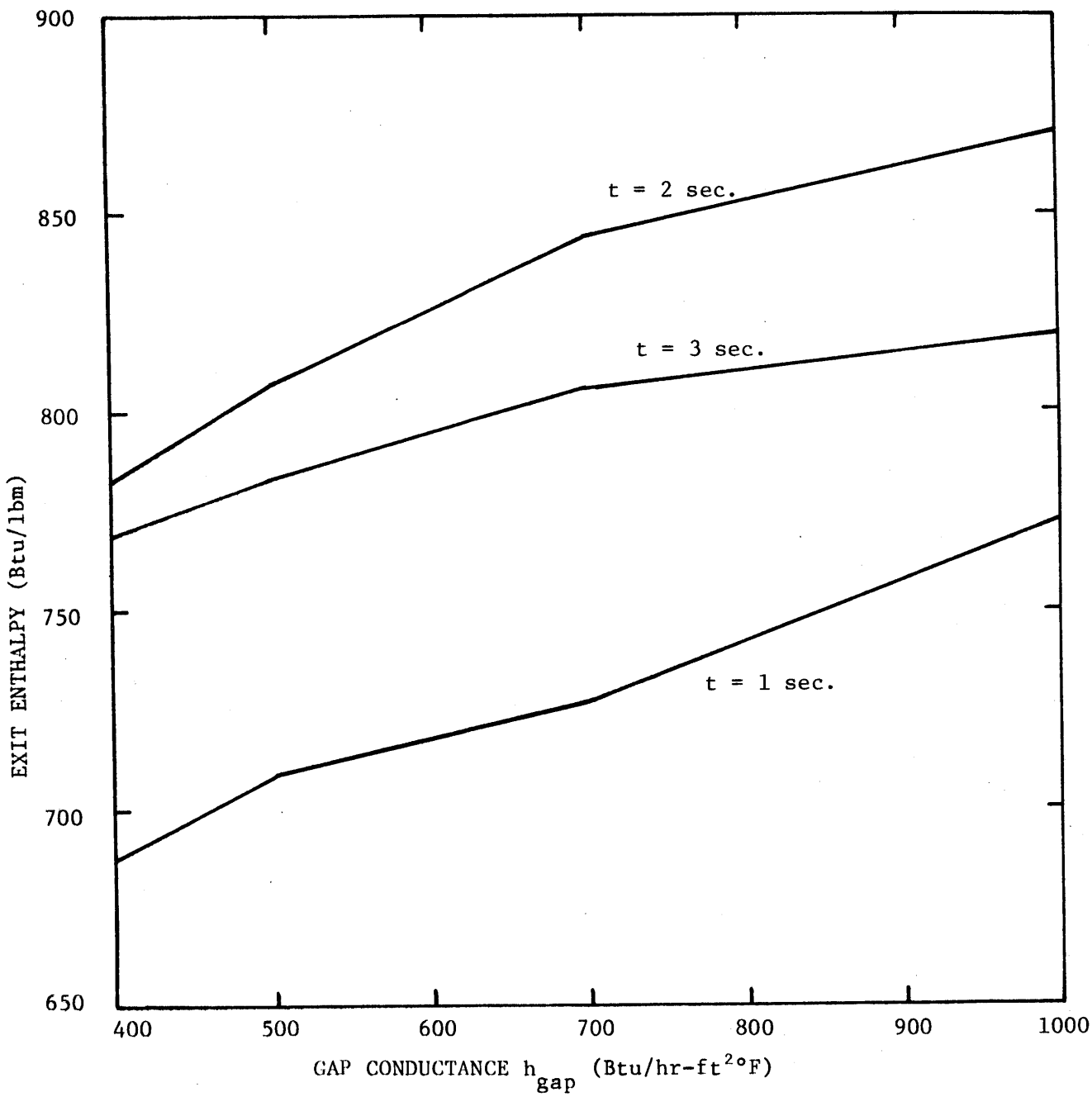

FIG. 5.21: EXIT ENTHALPY VS. GAP CONDUCTANCE (3.0 SEC. TRANSIENT)

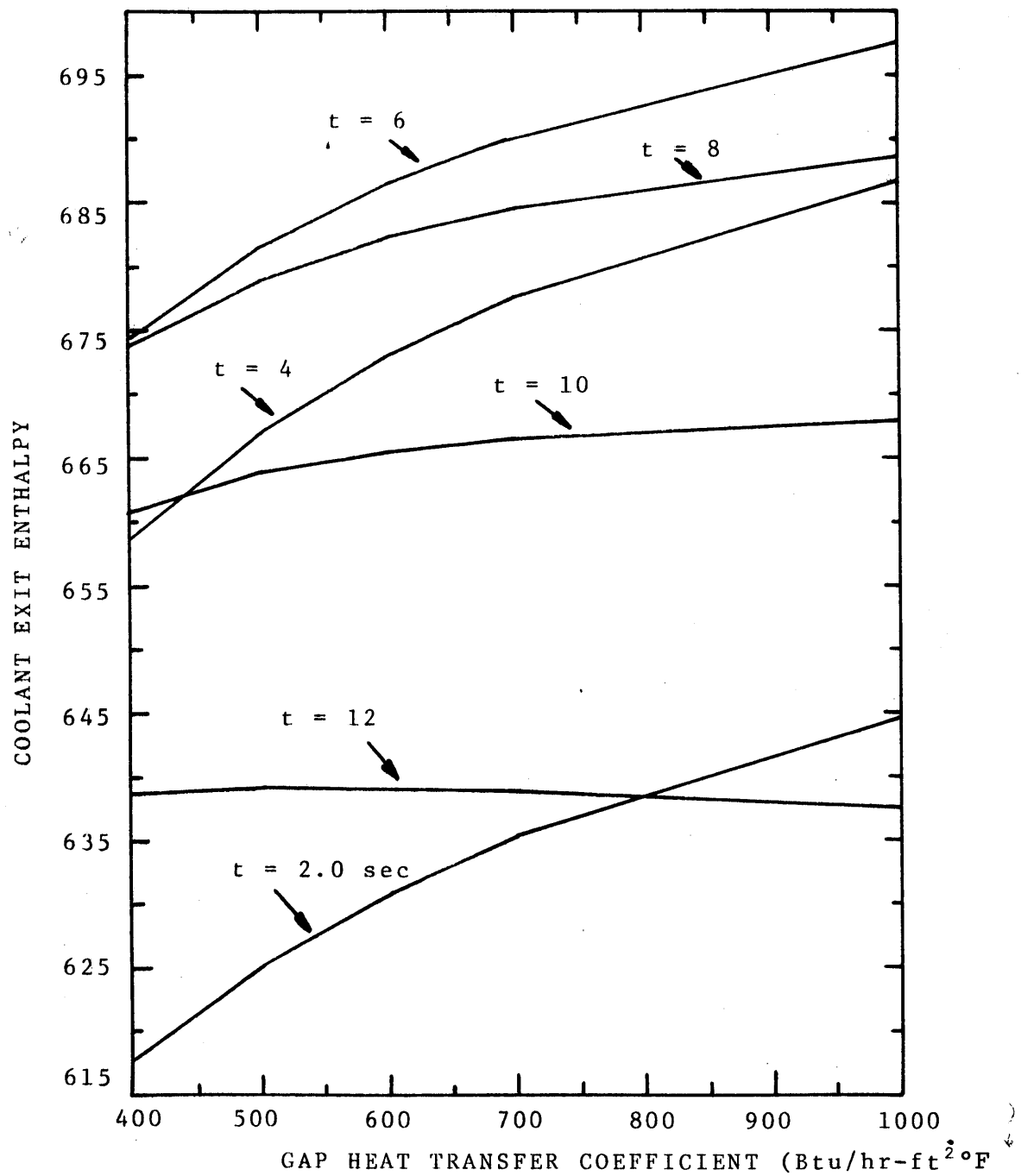

FIG. 5.22: COOLANT ENTHALPY SENSITIVITY TO h_{gap}

(Power Profile Class 4)

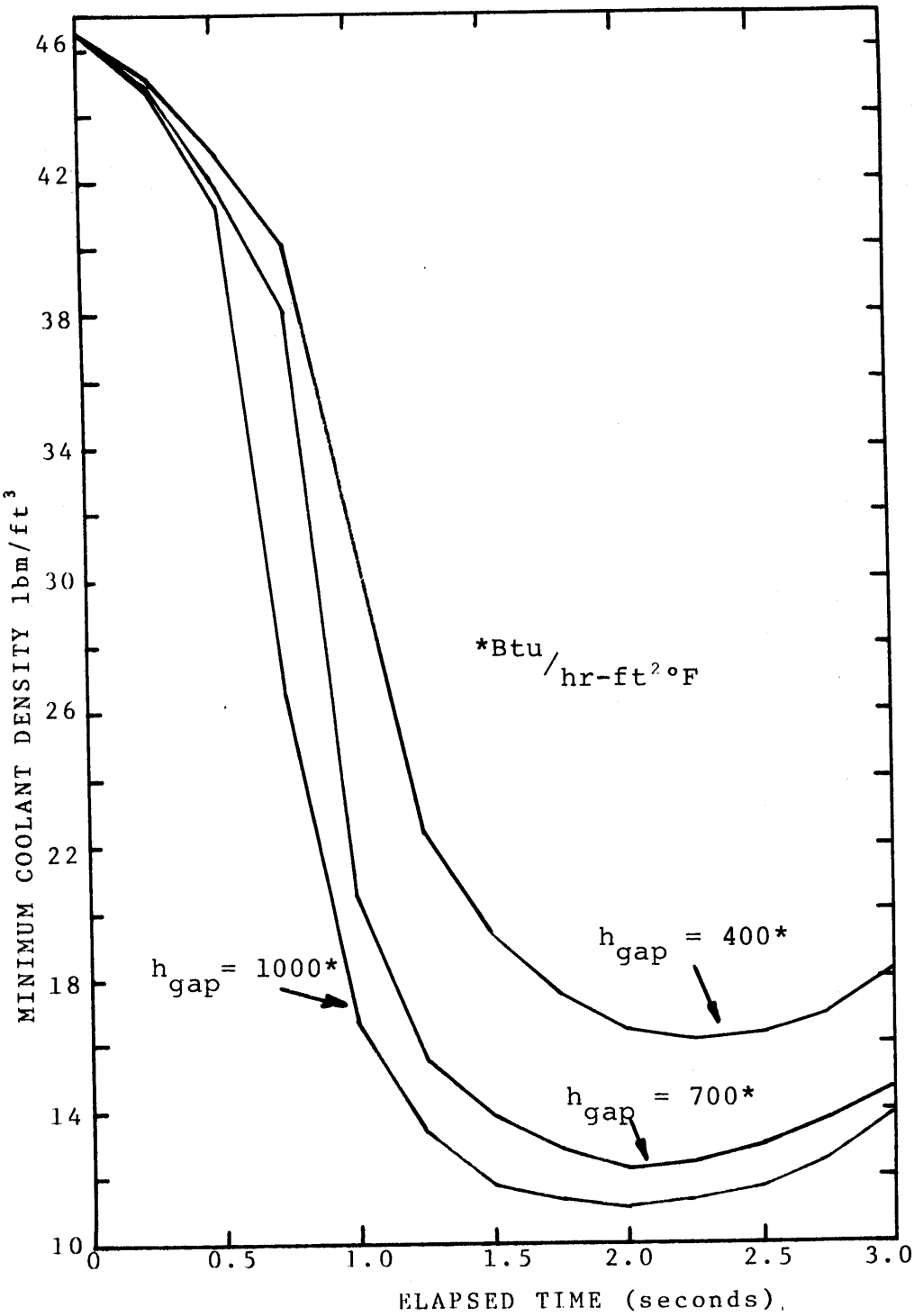

FIG. 5.23: COOLANT DENSITY SENSITIVITY TO h_{gap}

(Power Profile Class 2A)

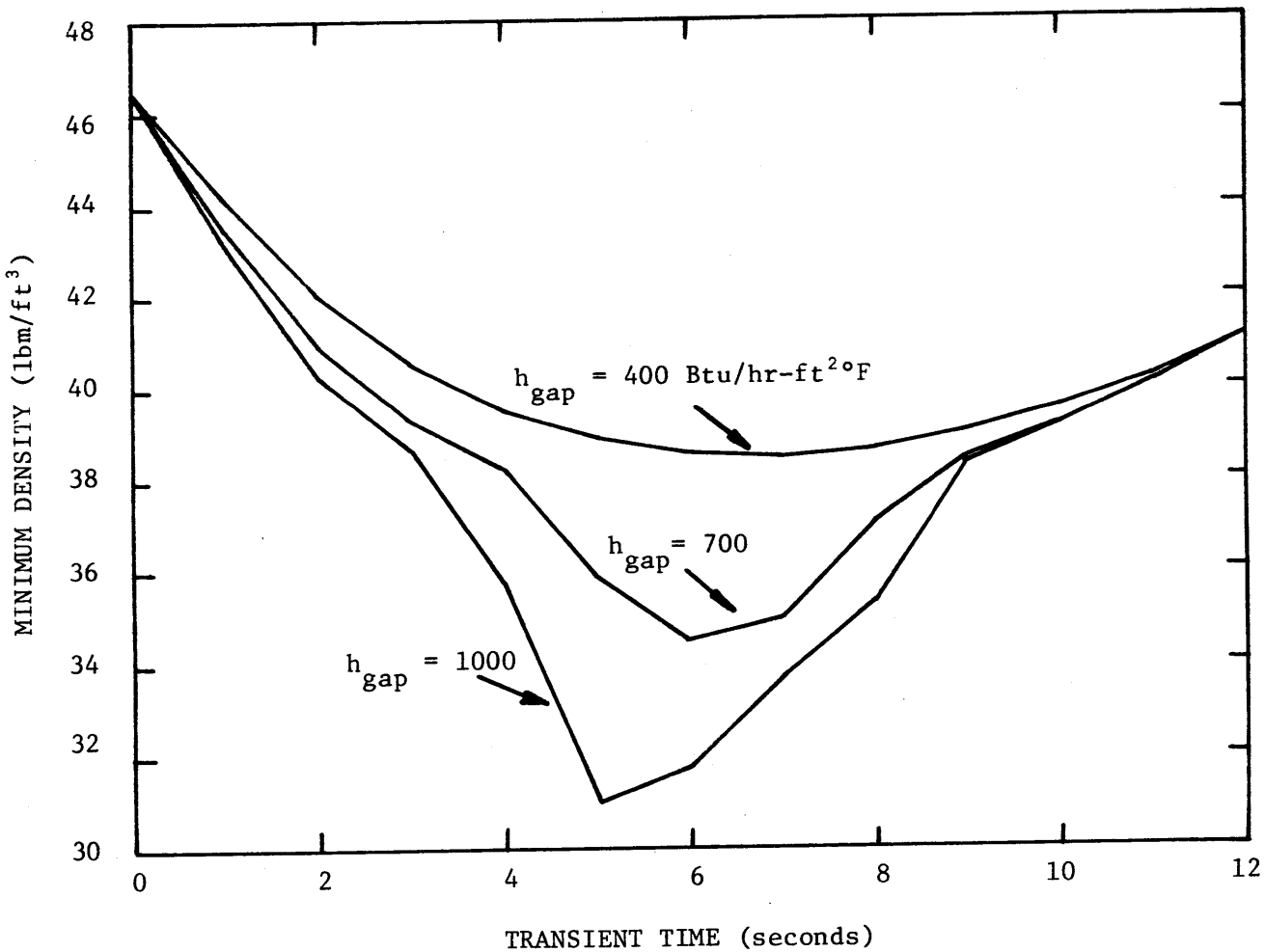

FIG. 5.24: COOLANT DENSITY SENSITIVITY TO GAP CONDUCTANCE (12 SECOND TRANSIENT)

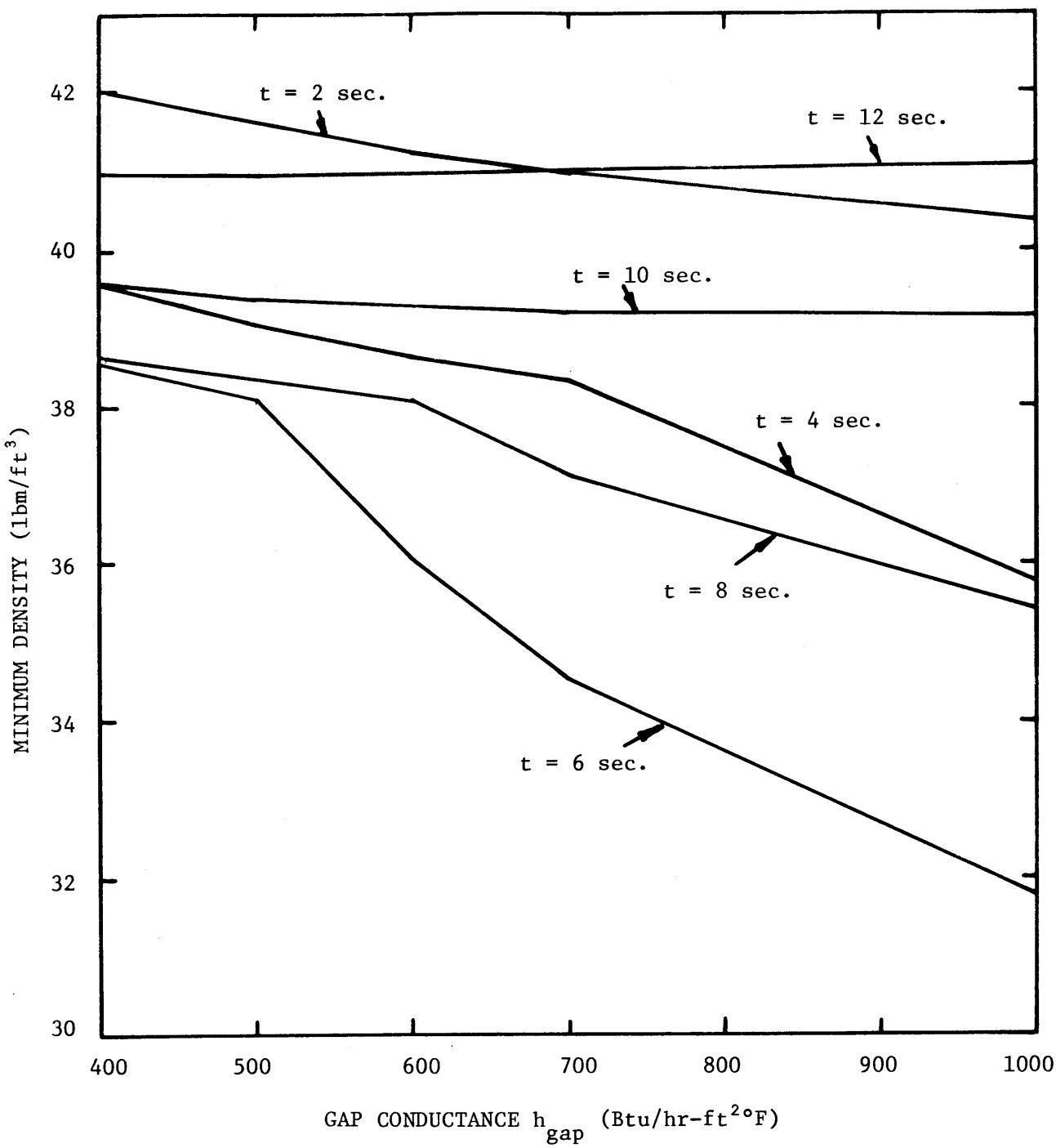

FIG. 5.25: COOLANT DENSITY SENSITIVITY TO GAP CONDUCTANCE (12 SEC TRANSIENT)

mixture just after the onset of nucleate boiling (i.e. at elapsed times of 1.0 and 3.5 seconds respectively, in the 3 and 12 second transients). At this stage of the hot sero power transient, coolant densities change by more than 100 percent when h_{gap} is changed from 400 $\frac{Btu}{hr\text{-}ft^2\,°F}$ to 1000 $\frac{Btu}{hr\text{-}ft^2\,°F}$, typical PWR values of h_{gap} [29]. Drastic shifts in the magnitude of the minimum coolant density history in the 3 second transient are caused by changes in h_{gap}.

Similar shifts in the magnitude of the coolant density history are seen in the 12 second transient. Because the length of this transient exceeded the fuel and coolant response times, the shape of the density history also is altered by changes in h_{gap}. As h_{gap} is decreased, heat transfer to the coolant is inhibited and the minimum value of the density is seen later in the transient.

Results of transient T-H analyses are very sensitive to the value of h_{gap}. This input parameter overshadows all other user-supplied values in its impact on the fuel conduction model. It is ludicrous to calculate a clad-coolant heat transfer coefficient at each axial level of every channel when a core-wide average value of h_{gap} is used. Modifications must be made to the code to allow, at the very least, different values of h_{gap} to be input for each T-H channel. Provisions should be made in later versions of MEKIN to calculate h_{gap} from correlations based on experimental data since h_{gap} is a function of temperature and will change in the course of a transient.

5.5 Limitations of the Fuel Conduction Model

5.5.1 Introduction

Actual irradiated, in-core fuel pins may differ significantly from the idealized model presented in Sec. 5.1 and used for transient temperature calculations in COBRA and MEKIN. The actual thermal properties of the fuel are not constant, but vary with temperature [31], as seen in Figs. 5.26 - 5.29. The volumetric heat generation rate may vary both radially and circumferentially in actual fuel pins; central voids have been found in irradiated fuel pins; finally, axial conduction takes place in actual fuel pins.

Each of these topics has already been at least partially investigated by other researchers. No attempt is made here to add to this previous work. Rather, this section serves to make the COBRA and MEKIN user aware of some of the shortcomings of the fuel conduction model.

5.5.2 Spatially Dependent Volumetric Heat Generation Rate

A constant heat generation rate (q''') is assumed throughout the fuel at an axial level of a T-H channel in the MEKIN fuel conduction model. In an actual fuel pin, neutronic effects are present, such as spatial self shielding and non-uniform accumulation of fission products and fissile isotopes. These effects impart radial and circumferential dependence to q''' (i.e. $q''' = q'''(r,\theta)$). A flux depression factor has been defined [23] to take into account the radial dependence.

Yamnikov et. al. [32] have found significant changes in

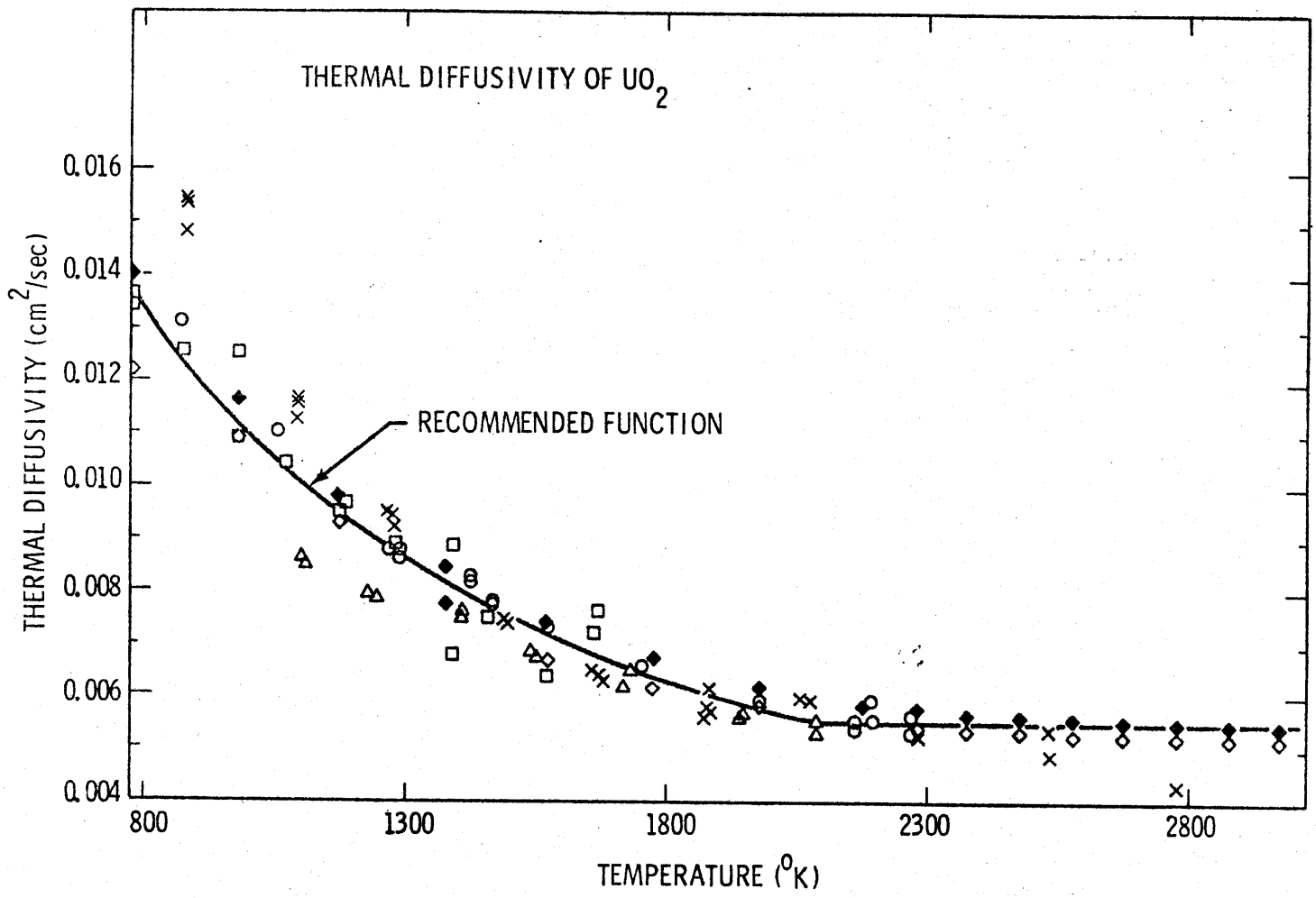

FIG. 5.26: TEMPERATURE DEPENDENCE OF UO_2 DIFFUSIVITY (from reference [31])

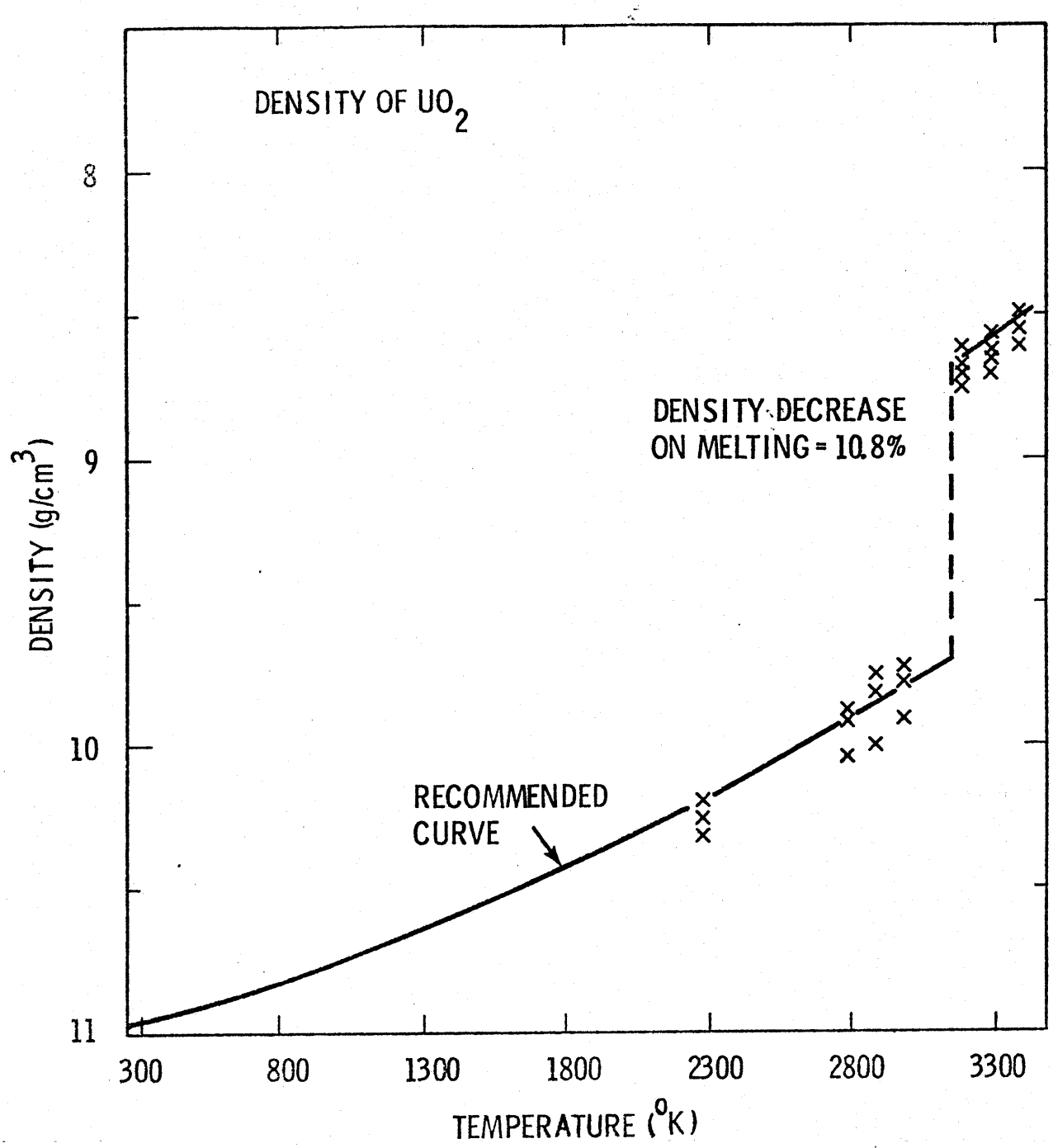

FIG. 5.27: TEMPERATURE DEPENDENCE OF UO_2 DENSITY
(from reference [31])

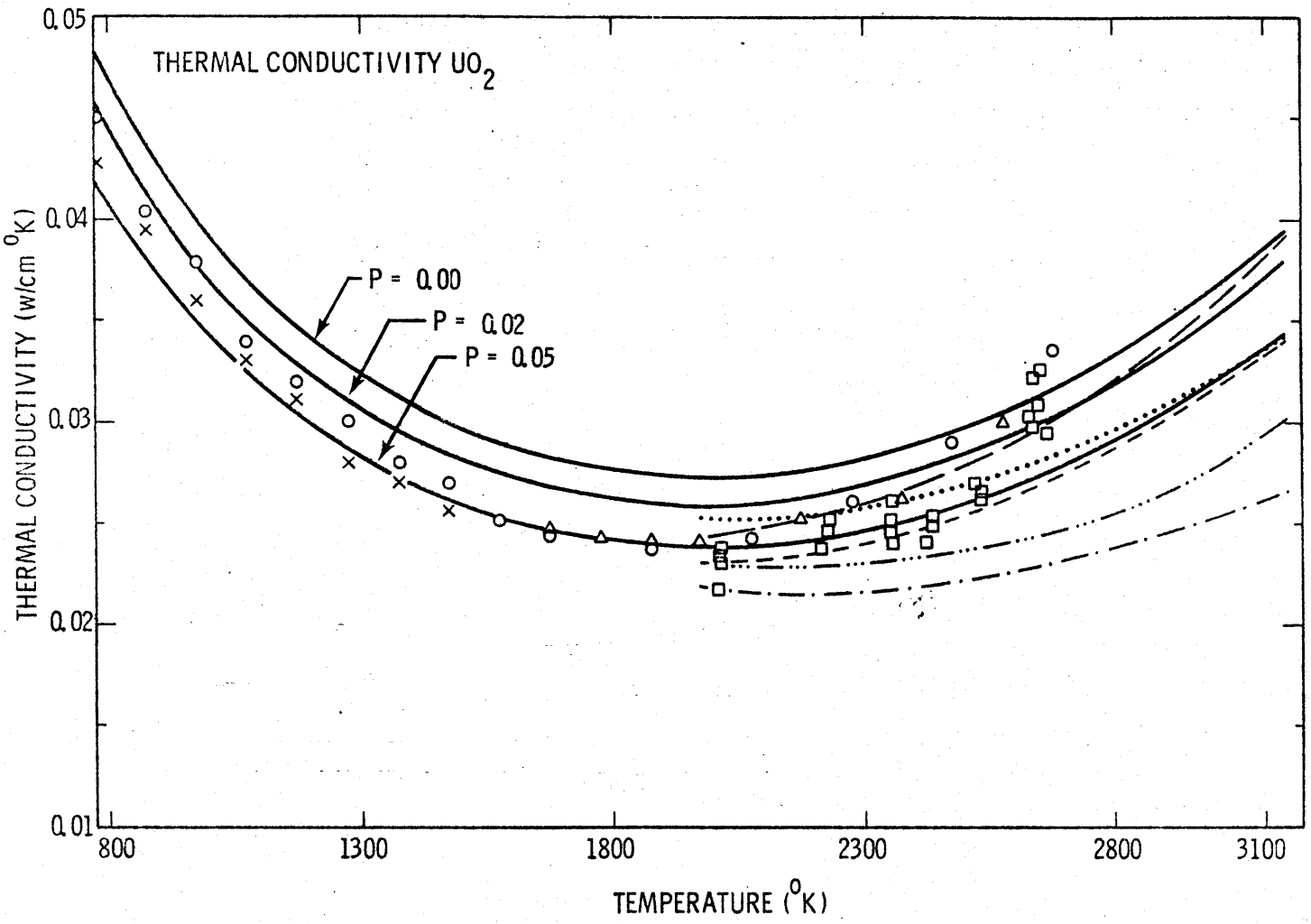

FIG. 5.28: TEMPERATURE DEPENDENCE OF UO_2 THERMAL CONDUCTIVITY (from reference [31])

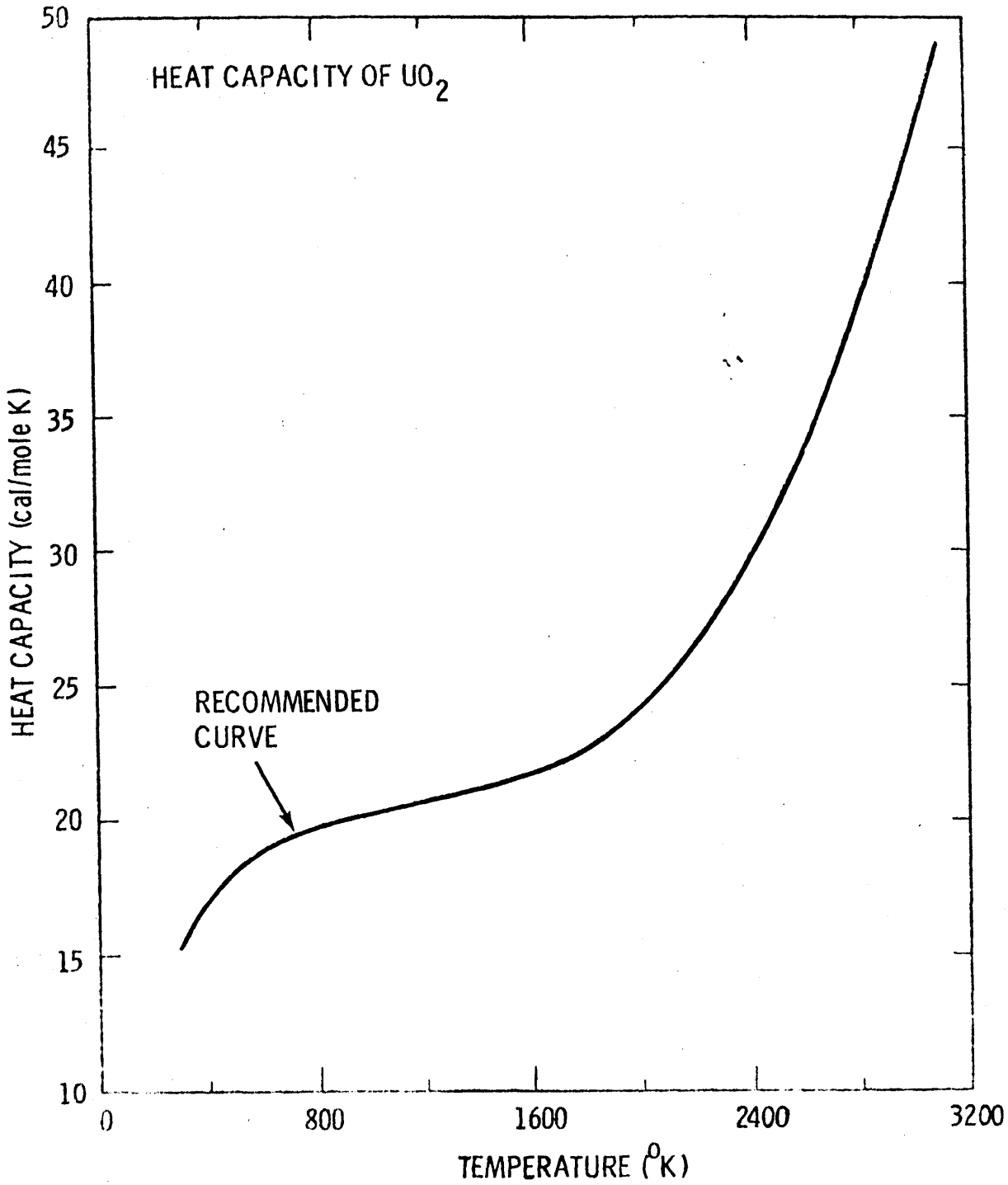

FIG. 5.29: TEMPERATURE DEPENDENCE OF UO_2 HEAT CAPACITY (from reference [31])

the fuel temperature profile when radial variation of q''' was taken into account. A 600°F difference in fuel centerline temperature was found between typical LWR beginning-of-life and end-of-life (30MW-day/kgU) temperature profiles. The difference was the result of changes in the radial dependence of q''' that had occurred with burnup. Circumferential variations in q''' had little effect on the fuel temperature profile. A method for calculation of steady-state temperature profiles with varying q''' has been developed by Andrews and Dixmier [33].

5.5.3 Axial Conduction Effects

Axial conduction is neglected in the MEKIN fuel model. Analyses were done by Fagan and Mingle [34] to determine the effect of axial conduction in fuel plates for a steady-state, natural circulation reactor. They found that neglecting axial conduction resulted in overestimates of 4.5 percent in the maximum surface heat flux and 4.8 percent in the maximum temperature rise.

When small axial steps are selected or large axial gradients are found in the power profile, axial conduction must be included for realistic representation of the fuel temperature distribution. The fuel temperature profiles calculated when axial conduction is taken into account will be less "jagged" than those found with a 1-D radial conduction model. This might possibly justify the use of a larger axial mesh, based on the arguments presented in Sec. 4.2.2.

A simple formula is derived in Appendix D to test the

validity of neglecting axial conduction in a T-H analysis. Thermal resistances are used to represent the fuel in this derivation. The approximate ratio of radial to axial heat fluxes that would exist for a calculated fuel temperature profile if axial conduction were taken into account may be estimated from

$$\frac{q''_r}{q''_z} \approx \left(\frac{\Delta z}{\Delta r}\right)^2 \left| \frac{(T_{i,j} - T_{i+1,j})\, r}{(T_{i,j} - T_{i,j+1})\, z} \right| \tag{5.27}$$

After a MEKIN or COBRA analysis has been made, it is suggested that the resulting temperature profile be tested with the formula given in Eq. 5.27. If the ratio of q''_r/q''_z is much greater than unity, neglecting axial conduction effects was a valid assumption. If the ratio is near unity, axial conduction must be taken into account and the MEKIN fuel model is inadequate.

In a typical MEKIN analysis the radial fuel mesh size is an order of magnitude less than the axial mesh size. The heat flux ratio depends on the square of the mesh size ratio in Eq. 5.27. This dominance of the mesh size ratio resulted in heat flux ratios of 500 in simulated rod ejection accident analyses. Axial conduction was clearly negligible in this case.

5.5.4 Temperature Dependent Thermal Properties

The transient heat conduction equation is

$$\nabla \cdot k\nabla T + q''' = \rho C_p \frac{\delta T}{\delta t} \tag{5.28}$$

Upon expansion of the divergence term, this becomes

$$\nabla^2 T + \frac{1}{k(T)} \frac{dk}{dT} [\nabla T \cdot \nabla T] + \frac{q'''}{k(T)} = \frac{1}{\alpha(T)} \frac{\delta T}{\delta t} \tag{5.29}$$

Hence, the temperature dependence of the thermal conductivity may be neglected if the term $\frac{1}{k}\frac{dk}{dT}\left[\frac{T_{i,j} - T_{i+1,j}}{\Delta r}\right]^2$ is negligible in calculations with the MEKIN fuel model.

Given the temperature dependence of UO_2 thermal conductivity, shown earlier in Fig. 5.26 and the radial temperature profiles seen in typical PWR transients (e.g. Fig. 5.6 and Fig. 5.16), it is clear that the temperature dependence will be significant in some cases. Rehbein and Carlson [35] modified the existing COBRA fuel conduction model to include variable thermal conductivity. Difference of 20% were found in the fuel centerline temperature predictions of the constant and variable conductivity models in transient analyses. Andrews and Dixmier [33] developed an analytic technique that took into account variable thermal conductivity in LWR fuel pin temperature calculations. A numerical solution scheme which also takes into account variable thermal conductivity has been developed by Chawla, et. al. [36]; this scheme uses collocation methods to reduce computations.

5.5.5 Remarks on Limitations

Local three dimensional effects are caused by axial pellet separation, small defects in the fuel pellets, circumferential variation in the fuel-clad gap width, and local increases in the clad thermal resistance. These effects were examined with a finite difference solution scheme by Olson and Bohman [37] and were found to have a minor effect on the average fuel temperature.

The current, idealized, one-dimensional fuel conduction model in MEKIN appears to be adequate to determine the average fuel temperatures for updating neutronic cross sections. This model would certainly be adequate if variable thermal conductivity were included. The model cannot, however, be used to determine detailed, accurate fuel temperature profiles for individual fuel pins. In such cases, more versatile, two or three dimensional models capable of taking into account local effects should be applied.

5.6 Summary of Results

The surface heat flux was the fuel parameter most sensitive to the radial mesh size used in the fuel. The mesh sensitivity was dependent on the transient that was analysed. In the hot full power transient, the fuel temperature profile is established from the onset of the transient and is merely shifted in magnitude during the transient. Five fuel nodes were found to be adequate for this transient.

In the hot zero power transient, the temperature is initially constant across the fuel; this flat profile eventually becomes parabolic in the coarse of the transient. The changes in both the shape and magnitude of the temperature profile during this transient strain the fuel conduction model. Fourteen fuel nodes were needed for accurate prediction of the heat flux in hot zero power transients. Suggested numbers of radial fuel mesh nodes are listed in Table 5.5.

The parabolic temperature averaging scheme currently used in MEKIN was found to be appropriate for most PWR transients. If

doubt arises as to the applicability of the parabolic scheme, use of a fine mesh (i.e. 10 fuel nodes) will provide accurate averages regardless of the temperature profile encountered.

The gap heat transfer coefficient was found to be an extremely important input parameter for the fuel conduction model. The magnitude of the fuel temperature and coolant density is sensitive to the value of h_{gap} in short transients. In longer transients, both the magnitude and shape of the temperature and density histories are affected by the value of h_{gap}.

The use of a single, core-average value of h_{gap} in each channel is the weakest part of the MEKIN fuel conduction model. The code must be modified to allow input of different values of h_{gap} for each T-H channel. These values would be determined prior to a MEKIN analysis from experiments or computer codes, such as GAPCON-THERMAL II [38]. Future versions of MEKIN should calculate the value of h_{gap} from correlations in an iterative scheme for transient analysis since the value of h_{gap} is temperature dependent and will vary throughout a transient.

The MEKIN fuel conduction model is idealized. Many effects that are present in actual fuel pins are neglected in this model. The model is thus inadequate for the accurate determination of temperature distributions in actual, individual fuel pins. However, this fuel conduction model is compatible with the MEKIN modeling scheme in which the behavior of the average fuel pin in an assembly is sought. It may be necessary to include the effect of temperature dependent thermal conductivity in the fuel conduction model for some transient analyses.

CHAPTER 6

SENSITIVITY TO THE COOLANT MODELS

6.1 Introduction

6.1.1 Models and Objectives

The COBRA III-C/MIT and MEKIN user has several options for modeling two phase coolant flow. In addition to the following alternatives that are included in the codes, the user may also elect to input a correlation of his own.

The user may choose from the Armand [40], Baroczy [41], or homogeneous flow pressure drop correlations; the modified Armand [42], Smith [43], or homogeneous flow (slip ratio = 1) slip ratio correlations; and may input a correlation for the turbulent mixing factor (β) in terms of the Reynold's number. Subcooled boiling may be taken into account using the Levy correlation [44]. If the user selects the default option, homogeneous pressure drop and slip ratio models are used throughout the analysis with a constant turbulent mixing factor ($\beta = 0.02$); subcooled boiling is neglected.

The impact of each of these models on the results of a simulated rod ejection transient analysis is discussed in this chapter. Appropriate models are suggested after the data bases of the repective correlations are examined.

6.1.2 Methodology

The five channel, thirteen axial level model described in section 4.1.2 was used throughout these studies with the

three second, simulated rod ejection power history (power profile class 2-A). COBRA III-C/MIT analyses were performed for this transient with different flow models. The results of the analyses were compared to determine the effect of the flow models. Since the fuel response time was greater than the duration of this transient, fuel temperature was insensitive to the choice of flow models throughout this study.

The original papers that presented the correlations used in MEKIN were examined to determine the data bases of the correlations. Those correlations with data bases closest to PWR operating and transient conditions were deemed "most appropriate" for use in a MEKIN analysis. A detailed comparison of these correlations has been made by Emami [8].

6.2 Two Phase Pressure Drop Correlation Sensitivity

The simulated rod ejection transient took place at full coolant flow, with a mass flux of 2.48×10^6 lbm/hr-ft^2. Little sensitivity to the pressure drop model was anticipated at such high mass flow rates. Selected parameters found with the homogeneous flow (i.e. two phase friction factor equal to $^{\rho}f/\rho$), Armand and Baroczy pressure drop correlations are presented in Table 6.1. Only a slight sensitivity is observed.

The coolant density, a neutronic feedback parameter, displays minimal sensitivity to the chosen pressure drop correlation (i.e. maximum differences less than 2%). Even the pressure drop across the channel and the exit mass flow rate are affected only marginally by changing the pressure drop correlation. More dramatic sensitivities may appear in reduced flow transients [9].

	1 sec.				2 sec.				3 sec.			
model	Δp	h_{exit}	ρ_{min}	$\dot{m}_{exit}$	Δp	h_{exit}	ρ_{min}	$\dot{m}_{exit}$	Δp	h_{exit}	ρ_{min}	$\dot{m}_{exit}$
homogeneous flow	16.10	724.76	22.15	148.63	19.12	825.6	13.28	136.65	15.56	796.76	15.47	127.18
Armand Pressure Drop	16.16	724.79	22.13	146.46	19.98	827.72	13.14	127.19	15.98	797.97	15.38	122.07
Baroczy Pressure Drop	16.03	724.8	22.19	150.75	18.35	823.67	13.38	139.38	15.16	795.54	15.56	129.56

Δp = pressure drop across core (lbf/in^2)

h_{exit} = exit enthalpy (Btu/lbm)

ρ_{min} = minimum density ($^{lbm}/ft^3$)

$\dot{m}_{exit}$ = exit mass flow rate (lbm/sec)

TABLE 6.1: SENSITIVITY TO THE CHOICE OF PRESSURE DROP CORRELATIONS

When applied to the test transient, the Armand correlation predicted slightly higher pressure drops and correspondingly lower mass flow rates than the homogeneous correlation. Lower mass flow rates resulted in higher exit enthalpy and lower coolant density. The Armand correlation underpredicted the homogeneous mass flow rate by a maximum of 7%; this resulted in a 1% underprediction of coolant density.

Pressure drops found with the Baroczy correlation fell below homogeneous results. This gave rise to higher mass flow rates (e.g. maximum difference of 2%) and, ultimately, higher coolant density (e.g. maximum difference of 0.7%). Parameters found with the Baroczy correlation were in better agreement with homogeneous results than those found with the Armand correlation.

The Armand correlation is based on data from air-water flow experiments in horizontal pipes [40] which hardly simulated PWR conditions. The data base for the Baroczy correlation covers a range of liquid-vapor combinations [41] which include 590, 944 and 2000 psi steam in vertical test sections. Good agreement was found when this correlation was compared with data from independent steam experiments in horizontal test sections [41].

The data base of the Baroczy correlation is clearly superior to that of the Armand correlation in simulating LWR conditions. However both sets of data were obtained with flow through tubes rather than in rod bundles. After a careful examination of available pressure drop correlations, Idsinga [45] concluded that the homogeneous and Baroczy pressure drop correlations were best suited for use in reactor T-H analyses.

6.3 Turbulent Mixing Factor Sensitivity

The turbulent mixing factor, β, weights the effect of interchannel momentum and energy transport by turbulent mixing. The turbulent mixing, $w'_{i,j}$ between two adjacent channels i and j is defined [46] as

$$w'_{i,j} = \frac{1}{2}\beta S_{i,j}(G_i + G_j) \tag{6.1}$$

An increase in β will increase turbulent mixing and enhance its effects on momentum and energy transport between channels.

A series of COBRA III-C/MIT analyses were performed in which all other parameters were held constant while four values of β, namely 0.005, 0.01. 0.02 and 0.04, were used. These values spanned the range of β that was observed in experiments [47]. This range of values for β was computed with COBRA I when the experiments were intially performed. The lateral momentum equation used in COBRA III-C/MIT is more complicated than the equation used in COBRA I. Hence, the values of β that would be calculated if COBRA III-C/MIT were used with the experimental data [47], may differ from those found using COBRA I. In this study, the major concern was the sensitivity of the T-H results to β. Since accurate determination of β was not necessary for such a study, the range of values found with COBRA I was used.

A correlation for β in terms of the Reynold's number was also used:

$$\beta = 0.0038 \quad D_h \quad Re^{-0.1} \tag{6.2}$$

This correlation was proposed by Rowe [48] for use in subchannel analyses with single phase coolant flow, and also was intended for use with COBRA I. The effect of β on the predicted coolant

density in the rod ejection transient may be seen in Figs. 6.1 - 6.4. Only slight sensitivity was found with single phase coolant flow. However, 20 percent differences in the coolant density were observed at the onset of nucleate boiling and for all two phase flow regimes when analyses with $\beta = 0.005$ and $\beta = 0.04$ were compared. In general, the predicted density was greater for larger values of β.

The correlation proposed by Rowe predicts values of less than 0.005. However, this corelation was based on single phase flow subchannel experiments and Rowe warned that it should not be used in analyses with large channels. The correlation was included in this series of tests so that trends in the results of constant β analyses could be compared with those of an analysis in which β was dependent on the Reynold's number. No major differences in the observed trends were found.

The turbulent mixing parameter has been found to vary with the mass flow rate and equilibrium quality in two phase flow regimes [48] [49]. Typical variations are presented in Figs. 6.5 and 6.6. In low quality two phase flow, β increases greatly with small increases in quality.

A marked sensitivity to β was noted in the two phase flow regimes. Hence MEKIN should be modified to calculate β accurately in the two phase flow regimes based on the coolant quality and massflow rate. Experiments should be performed to determine an appropriate correlation for β to be used in analyses with large channels.

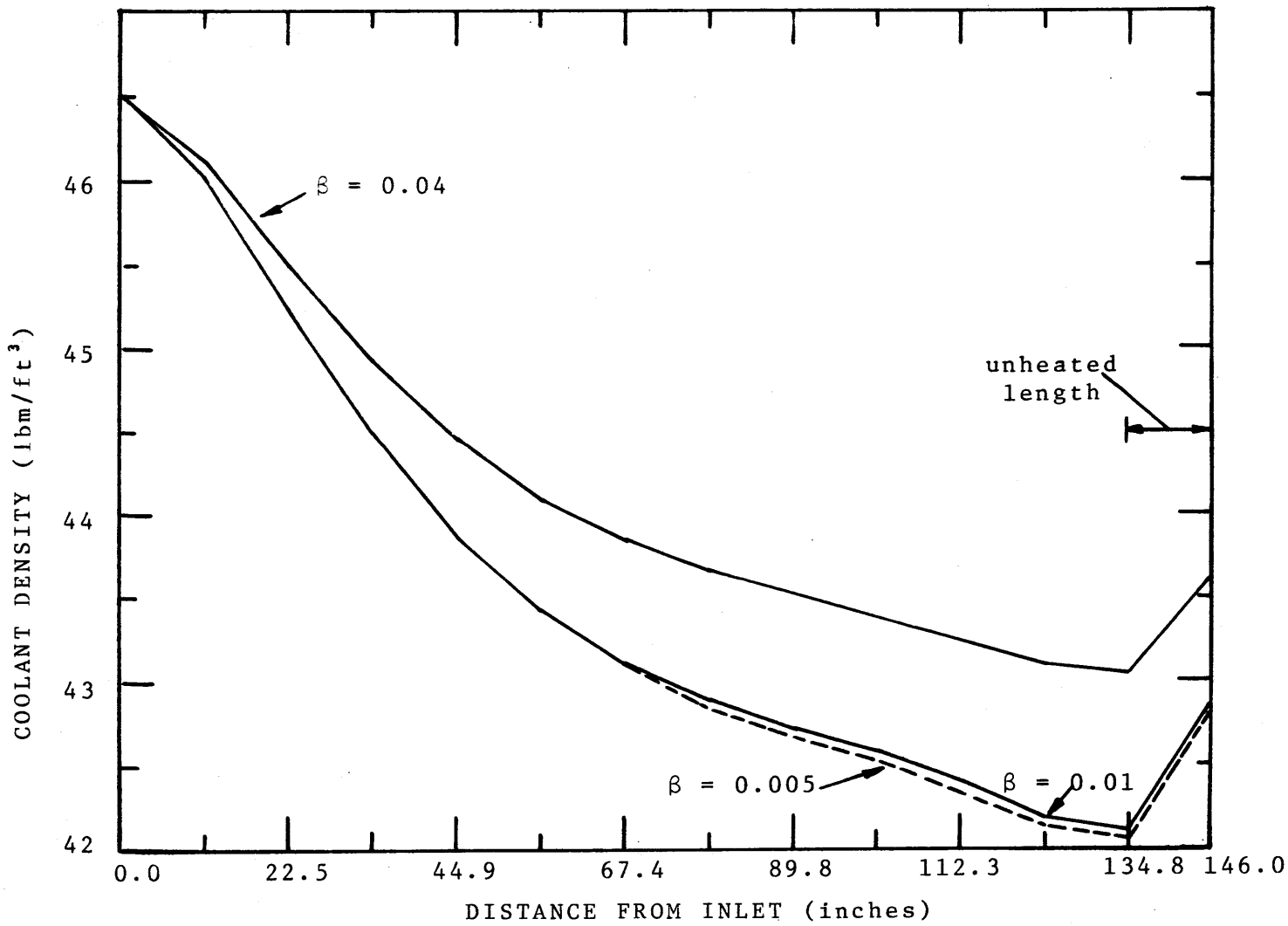

FIG. 6.1: SINGLE PHASE COOLANT SENSITIVITY TO β
(t = 0.5 seconds)

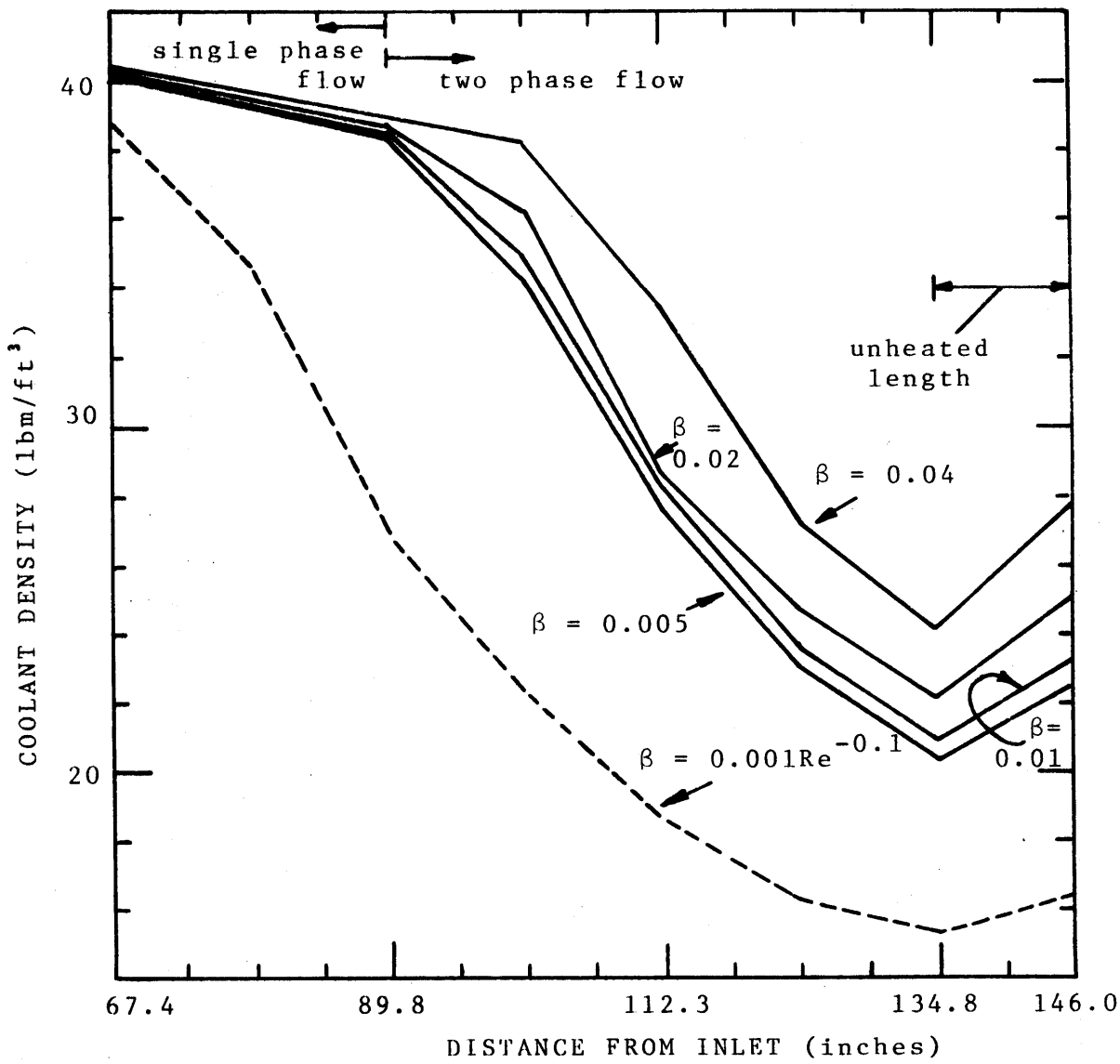

FIG. 6.2: COOLANT DENSITY SENSITIVITY TO β
(t = 1 second, just after onset of nucleate boiling)

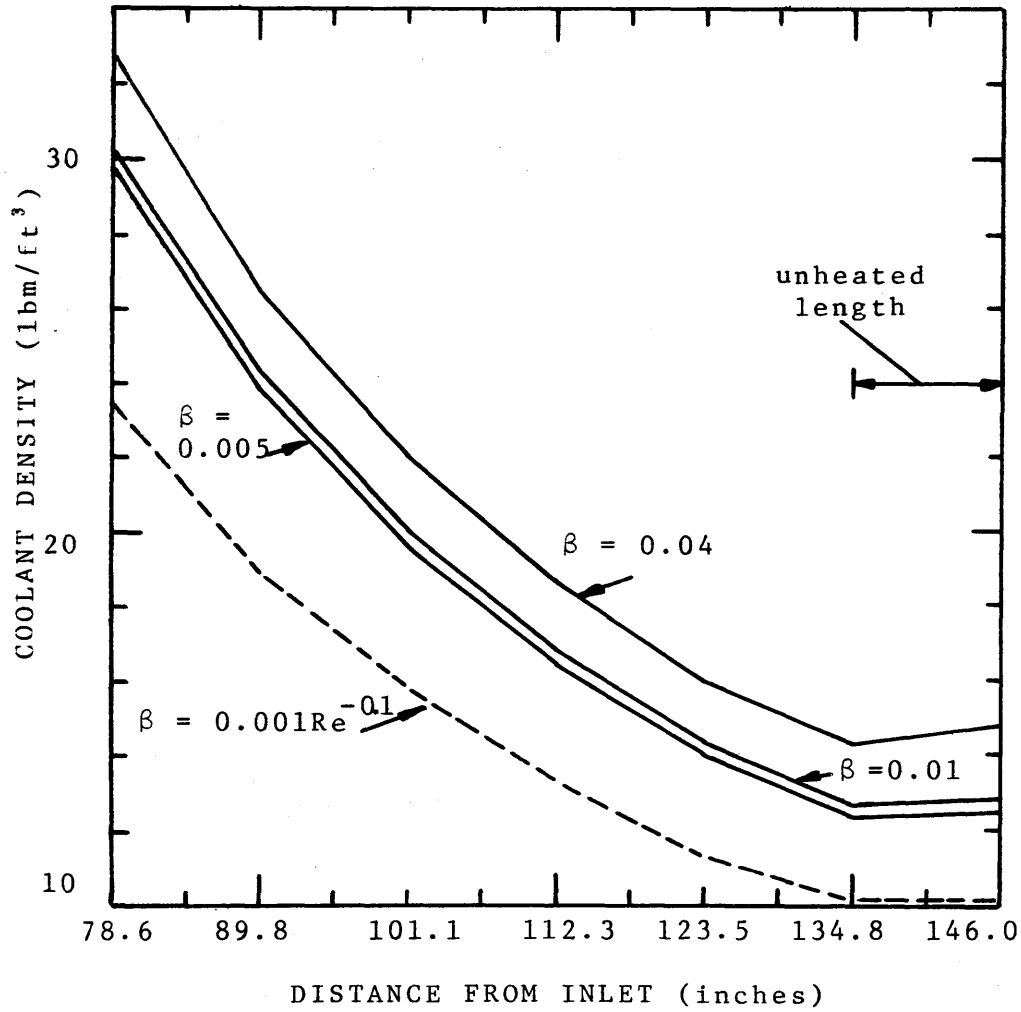

FIG. 6.3: TWO PHASE COOLANT DENSITY SENSITIVITY TO β

(t = 2 seconds, boiling well established)

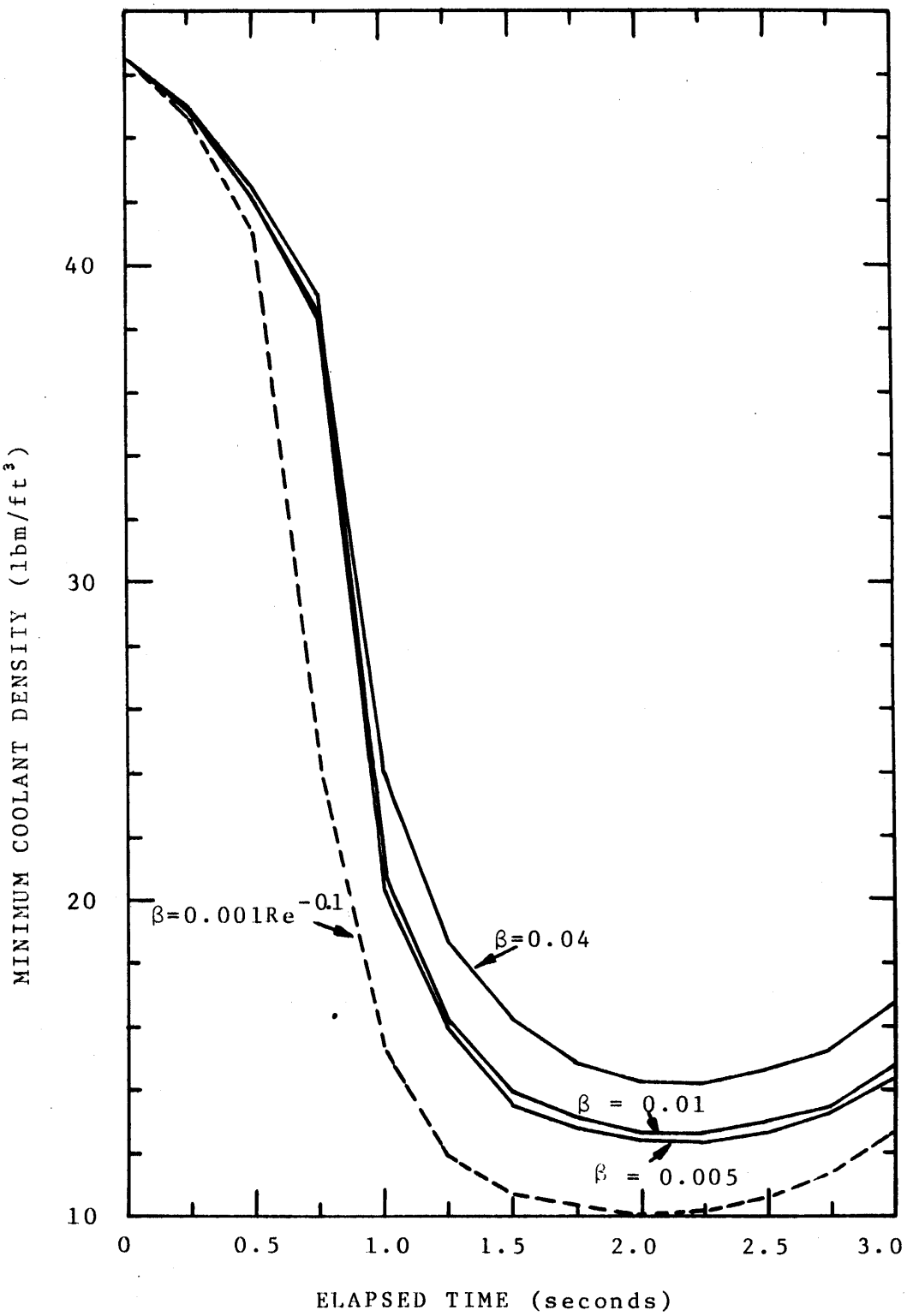

FIG. 6.4: SENSITIVITY OF MINIMUM COOLANT DENSITY HISTORY TO β

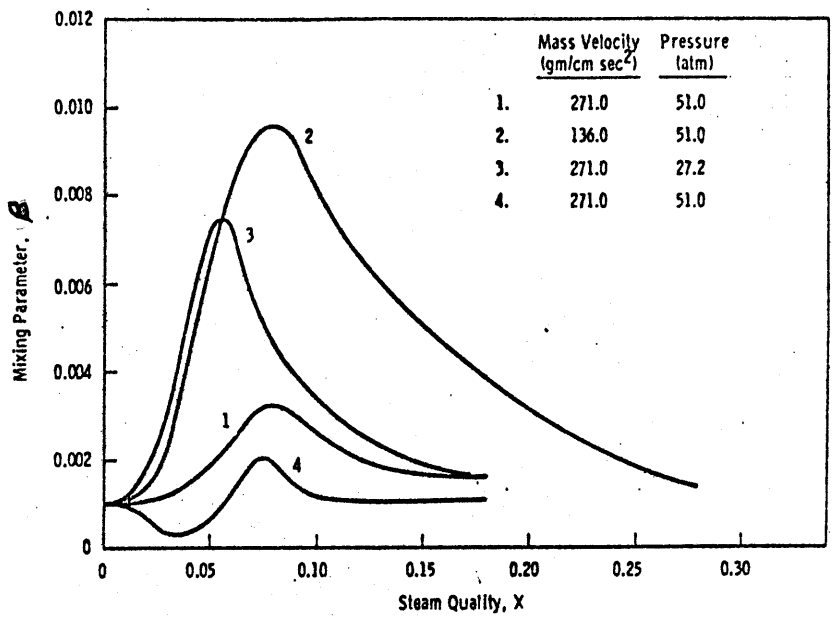

FIG. 6.5: DEPENDENCE OF β ON COOLANT QUALITY AND MASS FLOW RATES (from reference [48])

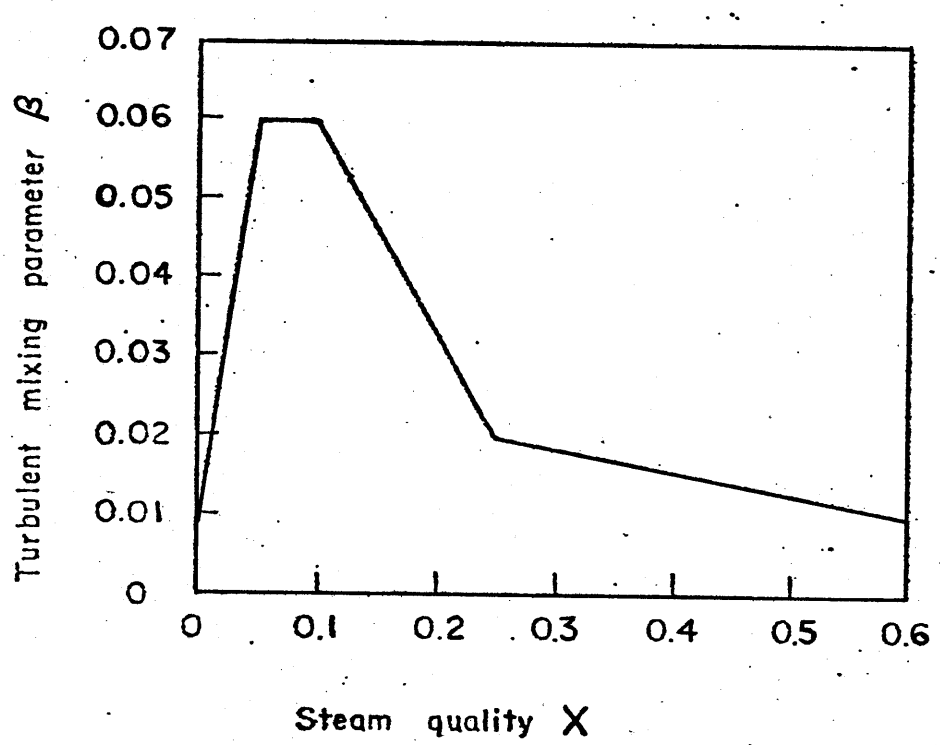

FIG. 6.6: DEPENDENCE OF β ON COOLANT QUALITY (from reference [49])

6.4 Slip Ratio and Subcooled Void Correlation Sensitivity

Different analyses were made using the homogeneous (slip ratio equal to 1), Smith and modified Armand slip ratio correlations. In addition, two analyses were performed in which the Levy subcooled void correlation was used with the modified Armand and homogeneous flow slip correlations. The void fraction and coolant density found in these analyses are presented in Figs 6.7 - 6.10.

Results of analyses that used the modified Armand and Smith slip ratio correlations were in excellent agreement. Homogeneous slip ratio results differed from those found with the other correlations. Densities predicted with the homogeneous slip ratio model were generally lower than those found with the modified Armand and Smith correlations. Hence, void fractions predicted with the homogeneous slip ratio were generally greater than those calculated using the other slip ratio correlations. The minimum density predicted with the homogeneous slip ratio model was ∿20% lower than those found with the modified Armand and Smith correlations.

Void fraction and density curves retained essentially the same shape but were shifted in magnitude when the Levy subcooled void model was used. The shift was caused by void formation in the coolant before the coolant became a saturated liquid. Higher void fraction and lower coolant density were found when the Levy subcooled void correlation was used. In addition, two phase flow extended throughout most of the hot channel. Use of the Levy correlation decreased the minimum coolant density by ∿25% and increased the maximum void fraction by ∿15%.

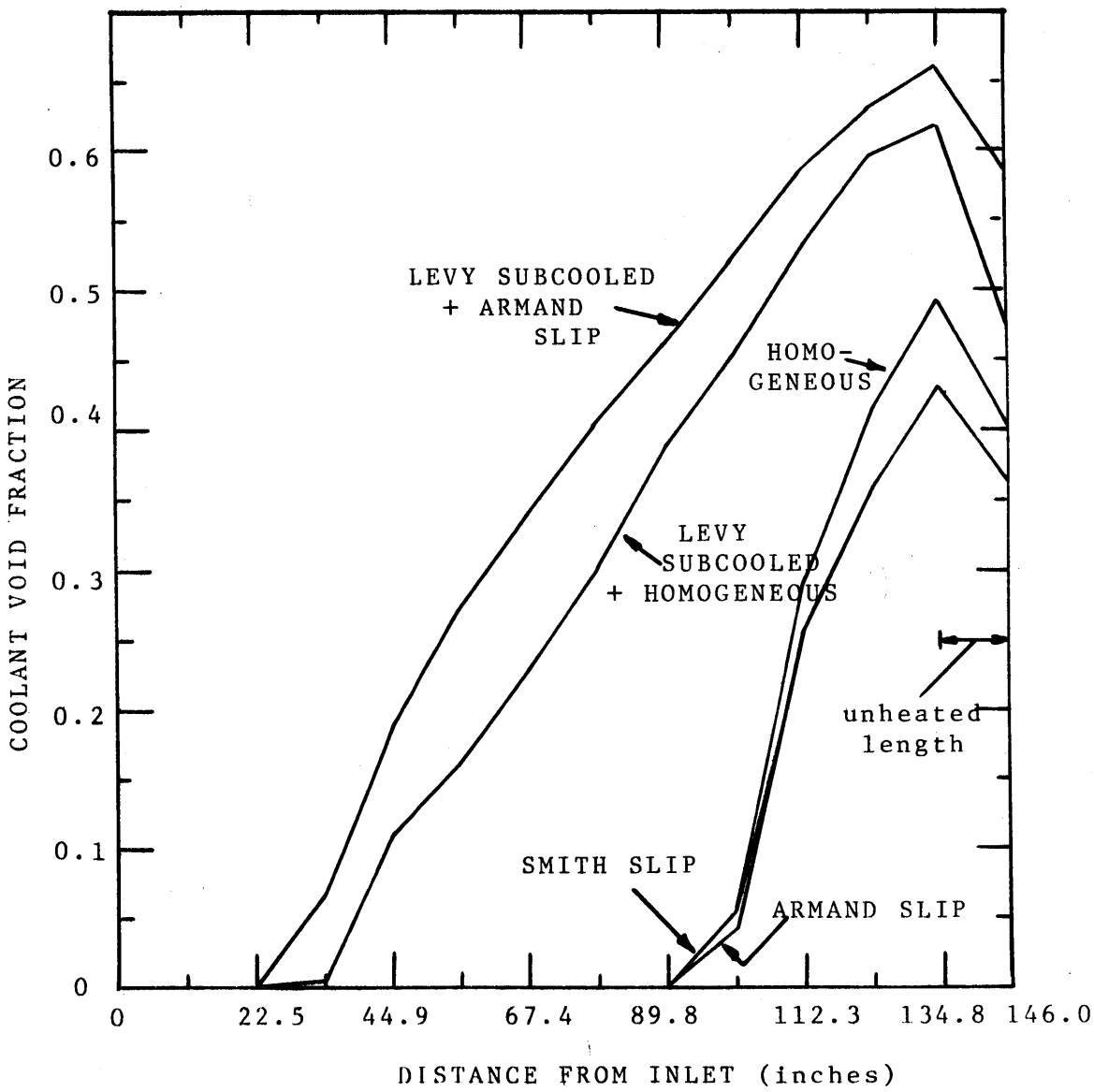

FIG. 6.7: VOID FRACTION SENSITIVITY TO SLIP RATIO AND SUBCOOLED VOID CORRELATIONS

(t = 1 second, just after onset of nucleate boiling)

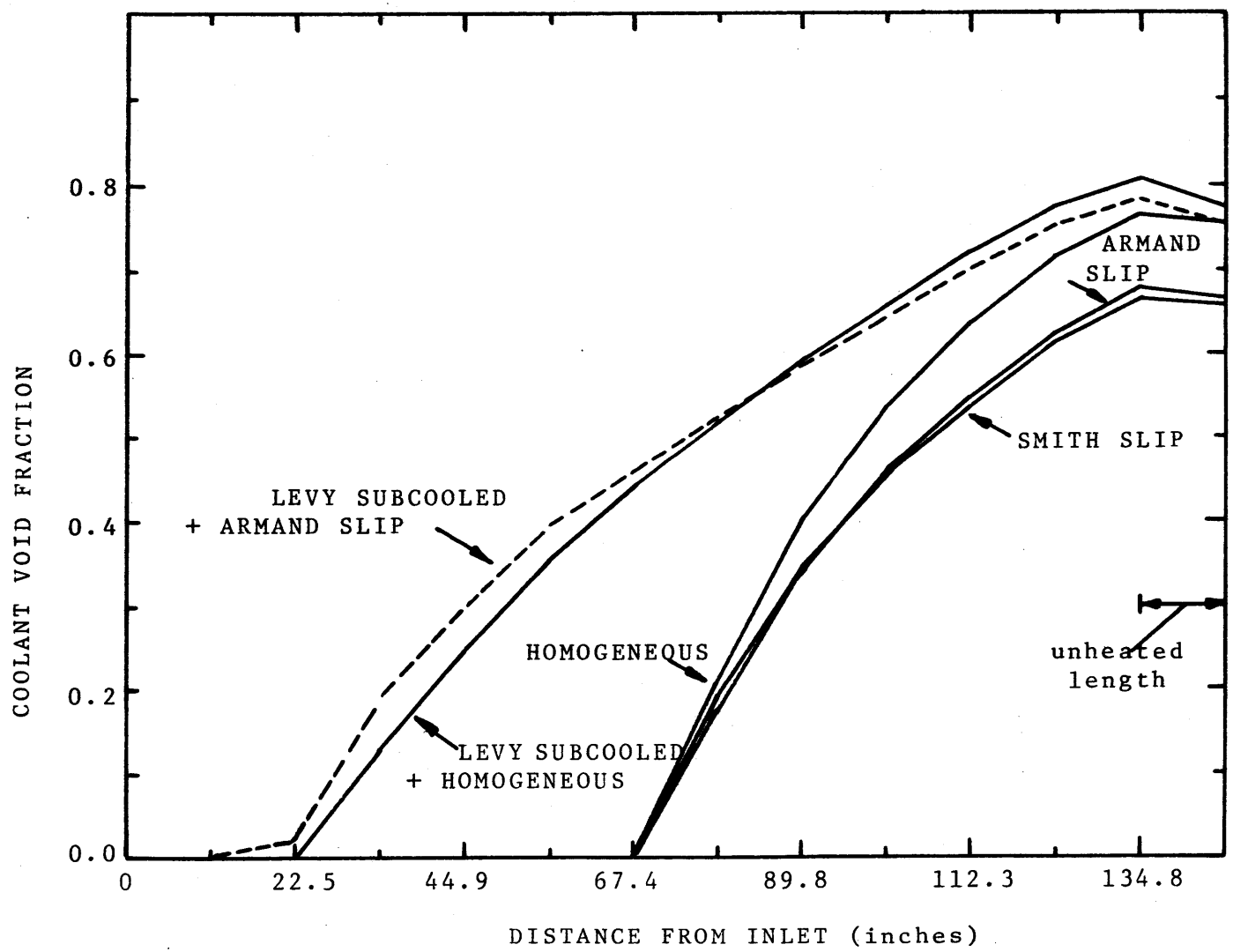

FIG. 6.8: VOID FRACTION SENSITIVITY TO SLIP RATIO AND SUBCOOLED VOID CORRELATIONS

(t = 2 seconds, boiling well established)

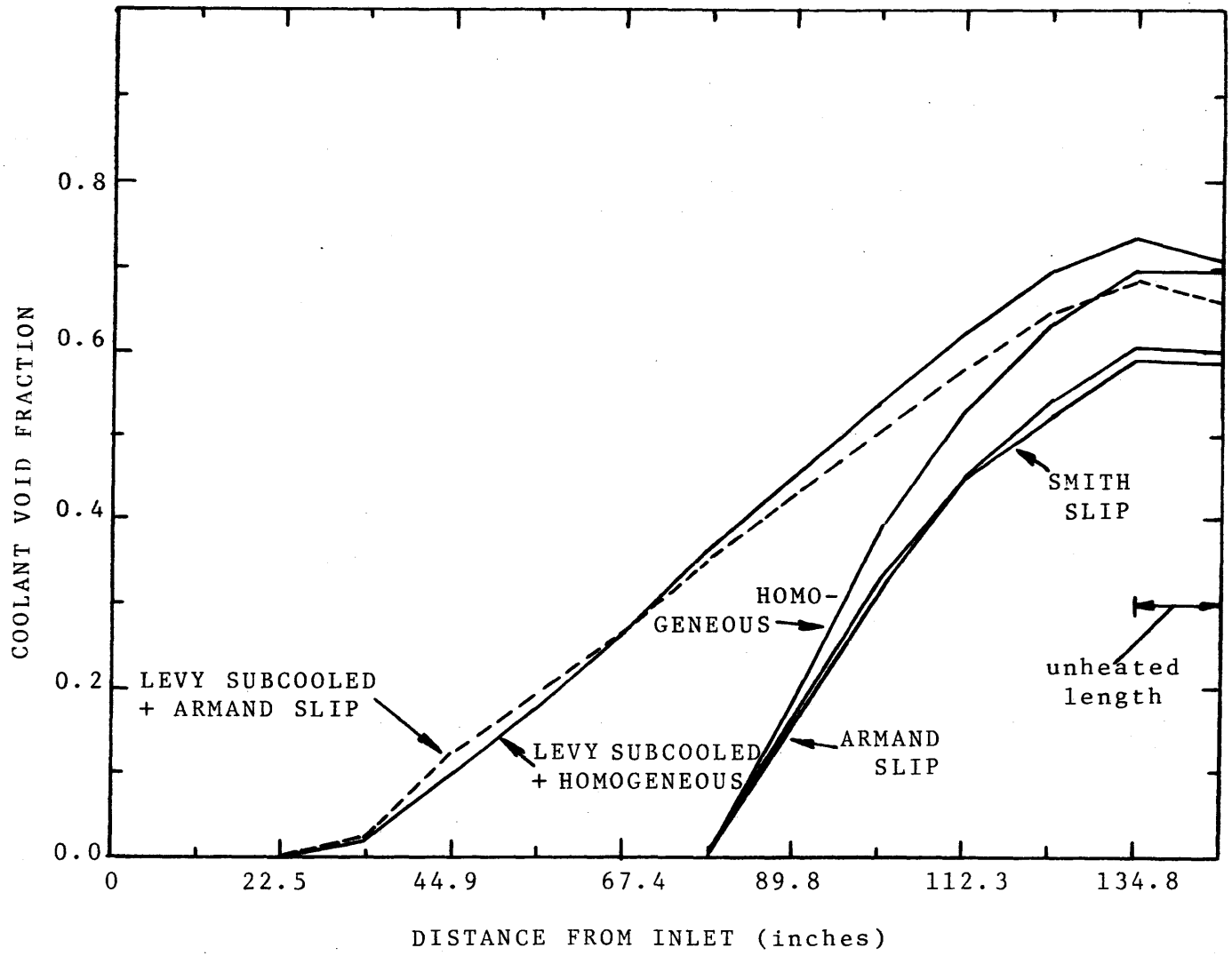

FIG. 6.9: VOID FRACTION SENSITIVITY TO SLIP RATIO AND SUBCOOLED VOID CORRELATIONS

(t = 3 seconds, zero power generation)

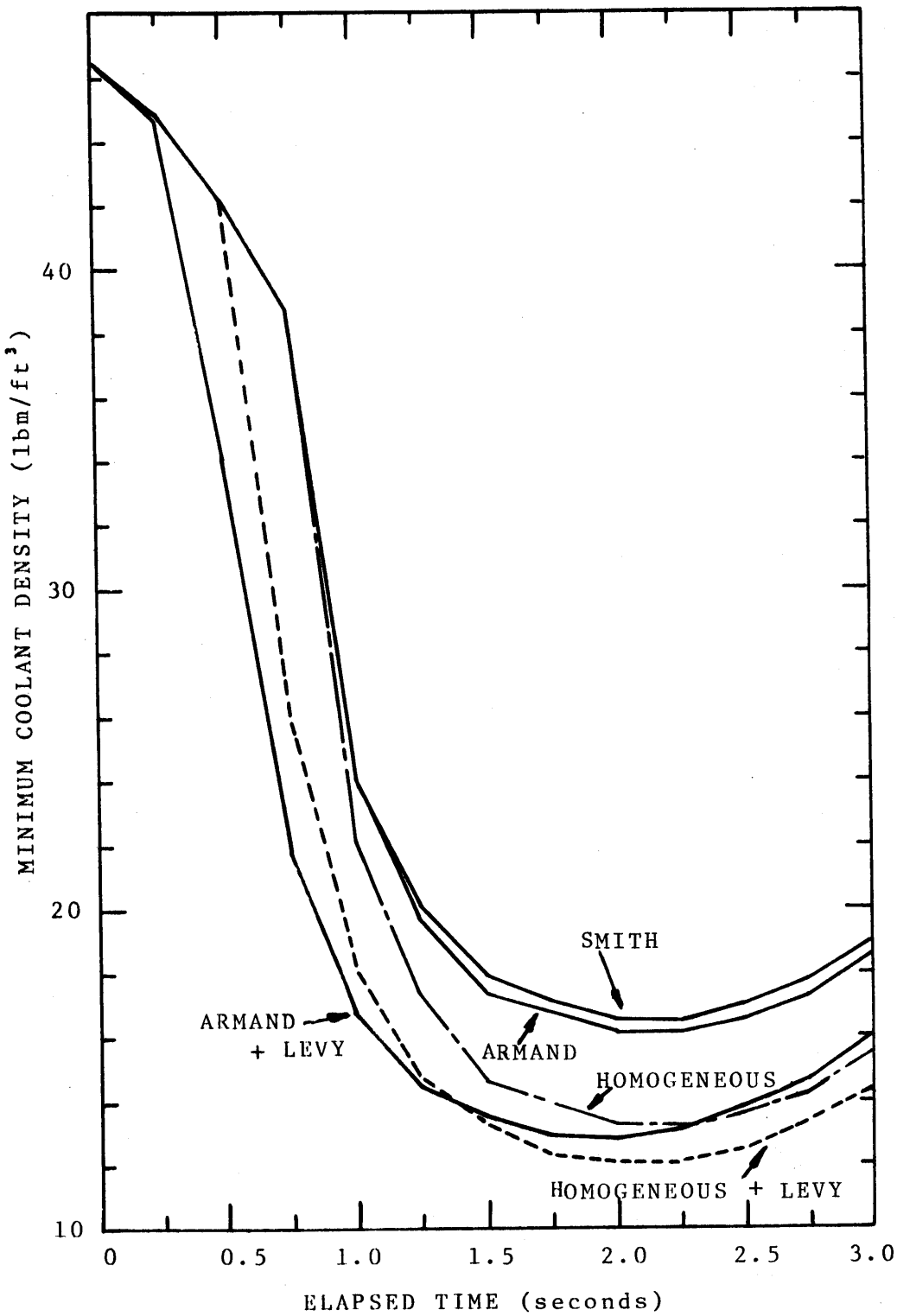

FIG. 6.10: COOLANT DENSITY SENSITIVITY TO SLIP RATIO AND SUBCOOLED VOID CORRELATIONS

The coolant density and void fraction were found to be quite sensitive to the modeling of the slip ratio. Subcooled void formation also caused significant changes in these parameters when it was taken into account.

Unfortunately, no clear-cut guidelines may be established for the choice of slip ratio and subcooled void models. All correlations included in MEKIN are based on experiments with flow in channels (e.g. pipes and ducts) rather than in rod bundles. Because so many physical phenomena are coupled in two phase flow, it is possible for a correlation to provide good results in certain cases even though it neglects several physical effects. For example, Cheung et. al. [50] found that through a fortuitous canceling of errors, the homogeneous flow model predicted void fractions that were in excellent agreement with their experimental data. This data originated from a simulated loss of coolant transient experiment at high flow rates.

The Smith slip ratio correlation is based on a range of data that approximates LWR operating conditions [43] and is thus recommended over the homogeneous slip ratio model. Similarly, predictions from the Levy subcooled void correlation compare well with a range of experimental data at various pressures [44]. Independent comparisons of Levy's model with experimental data [51] showed that the model predicted steam quality very well at the onset of boiling. Unfortunately, the model predicted higher void fractions than were observed when the equilibrium quality was positive.

Independent correlations for subcooled boiling such as

the Bergles-Rohsenow correlation [52] indicate that a very slight wall superheat (e.g. 5-10°F) is sufficient to cause subcooled boiling at typical PWR operating conditions. It is therefore suggested that the Levy subcooled void correlation be used in transient analyses with MEKIN, since the clad temperature will be great enough to cause subcooled boiling.

6.5 Summary

The fuel temperature was found to be insensitive to the choice of coolant flow models in power transients shorter than the fuel response time. At the high mass flow rates encountered under PWR operating conditions and in power transients, coolant parameters are relatively insensitive to the two phase pressure drop correlation that is chosen. Of the available MEKIN options, the Baroczy pressure drop correlation data base best approximates PWR conditions. The Baroczy correlation should therefore be used in MEKIN analyses unless a superior correlation is input by the user.

Single phase flow coolant density was found to be relatively insensitive to the turbulent mixing factor, β. However differences in predicted density of $\sim$20% were found in two phase flow when constant values of β were used which bounded the experimentally observed range. Since other researchers have found that β is a function of the coolant quality and mass flow rate in two phase flow, the current MEKIN representation of β appears to be inadequate. The code should be modified to use either a correlation or a tabular look-up for β, based on the coolant

quality and mass flow rate.

Most measurements of β to date have been made in subchannel experiments. Since a typical MEKIN channel encompasses an entire fuel assembly, additional experimental measurements of β should be made in larger test sections.

Coolant density was found to be quite sensitive to the slip ratio and void fraction modeling in the power transient studied. Of the available options, the Smith slip ratio and Levy subcooled void correlations are most apprpriate for PWR analysis.

Because of the marked sensitivity to the slip ratio and void fraction correlations that was observed, a literature survey should be made. Such a survey would map appripriate slip ratio and subcooled void correlations to specific "ranges of applicability" in LWR transient analyses. Modifications should then be made to MEKIN to switch to the appropriate correlations in the course of a transient analysis.

The MEKIN user must exercise caution in the selection of β, and the modeling of the slip ratio and subcooled void behavior. The sensitivity of the coolant density is great enough to yield inaccurate results if the models are arbitrarily selected. Ultimately, the sensitivity of the coupled MEKIN solution to these models must be investigated. It is possible that neutronic feedback effects will make the overall solution less sensitive to the choice of flow

CHAPTER 7

LIMITATIONS OF THE MEKIN T-H SOLUTION SCHEME

7.1 Introduction and Objectives

Many simplifying assumptions were made to arrive at the current MEKIN T-H solution scheme. Some of the assumptions have been carried over from earlier codes and have limited applicability in MEKIN analyses. For example, many of the T-H models employed by the code were orginally intended for use in subchannel analysis. Yet each fuel assembly is modeled as a single T-H channel in a typical MEKIN analysis. The use of large channels in T-H analyses has been shown thus far to provide accurate prediction of hot channel parameters only if the hot assembly is divided into several small channels [5] [9].

The limitations of the T-H solution scheme are discussed in this chapter. The objectives of this discussion are similar to those mentioned in Sec. 5.5 for the fuel conduction model. No attempt is made to modify any questionable assumptions. The purpose of this chapter is to inform the MEKIN user of some of the T-H assumptions and to describe the implications of these assumptions. With this information, the user will be better prepared to decide whether a MEKIN analysis is appropriate.

Two sets of assumptions were made to arrive at the MEKIN T-H solution scheme. The first set was used to simplify the set of coupled nonlinear differential equtions that describe T-H behavior (e.g. the Navier-Stokes equations). The limitations that result from these assumptions will be referred to

as "physical limitations."

The second set of assumptions was made to facilitate the numerical solution of the simplified governing equations. These numerical approximations have been examined by others [15] and will not be discussed here. However, some of the limitations that arise because of these approximations will be examined. These will be referred to as "calculational limitations."

7.2 Physical Limitations of the MEKIN T-H Solution Scheme

7.2.1 Applicability of the Momentum Integral Equations

The set of momentum integral equations [53] that are assumed in the T-H solution scheme were derived for use in subchannel analysis. A rigorous mathematical derivation was presented [18] [39] in which subchannel average parameters were defined as

$$\rho_{i,j} \equiv \frac{1}{A_i \Delta z} \iint \rho dA_i dz_j \tag{7.1}$$

$$v_{i,j} \equiv \frac{1}{A_i} \iint v_{i,j} dA_i \tag{7.2}$$

$$\dot{m}_{i,j} \quad \frac{1}{A_i} \iint \rho v_j dA_i \tag{7.3}$$

These average quantities do not, in general, satisfy the conservation equations, since mass conservation is expressed as

$$\frac{1}{A_i \Delta z} \iint \rho dA_i dz_j \iint v_j dA_i \neq \iint \rho v_j dA_i \tag{7.4}$$

and momentum conservation is

$$\frac{1}{A_i} \iint \rho v_j dA_i \iint {}_j dA_i \neq \iint \rho v_j^2 dA_i \tag{7.5}$$

The left and right hand sides of Eqs. 7.4 and 7.5 would be equal and the conservation requirements would be satisfied if coolant density and velocity were independent of location in each T-H "box". This is the principal assumption of the slug flow model. Although it is rarely stated in the COBRA and MEKIN literature, the T-H solution scheme is based on a slug flow model of the coolant. Even the most thorough derivation of the COBRA equations to date [54] fails to mention that the equations are based on the slug flow model.

In the slug flow model, coolant parameters are assumed to be constant across a channel at any radial plane. Discontinuities in coolant parameters are found at the channel boundaries. Because of the turbulent flow and strong mixing that occur under most LWR operating conditions, the slug flow model is an excellent approximation in subchannel analysis.

However, the accuracy of this assumption decreases as the number of fuel pins in the channel is increased. A large single channel, composed of nine subchannels is presented in Fig. 7.1. In a single subchannel no radial obstructions are present. Turbulent mixing results in almost uniform coolant parameters across the subchannel, except in the boundary layers immediately adjacent to the fuel pins. But turbulent mixing and diversion crossflow between subchannels are impeded when a large channel contains many fuel pins and subchannels. In this case, the

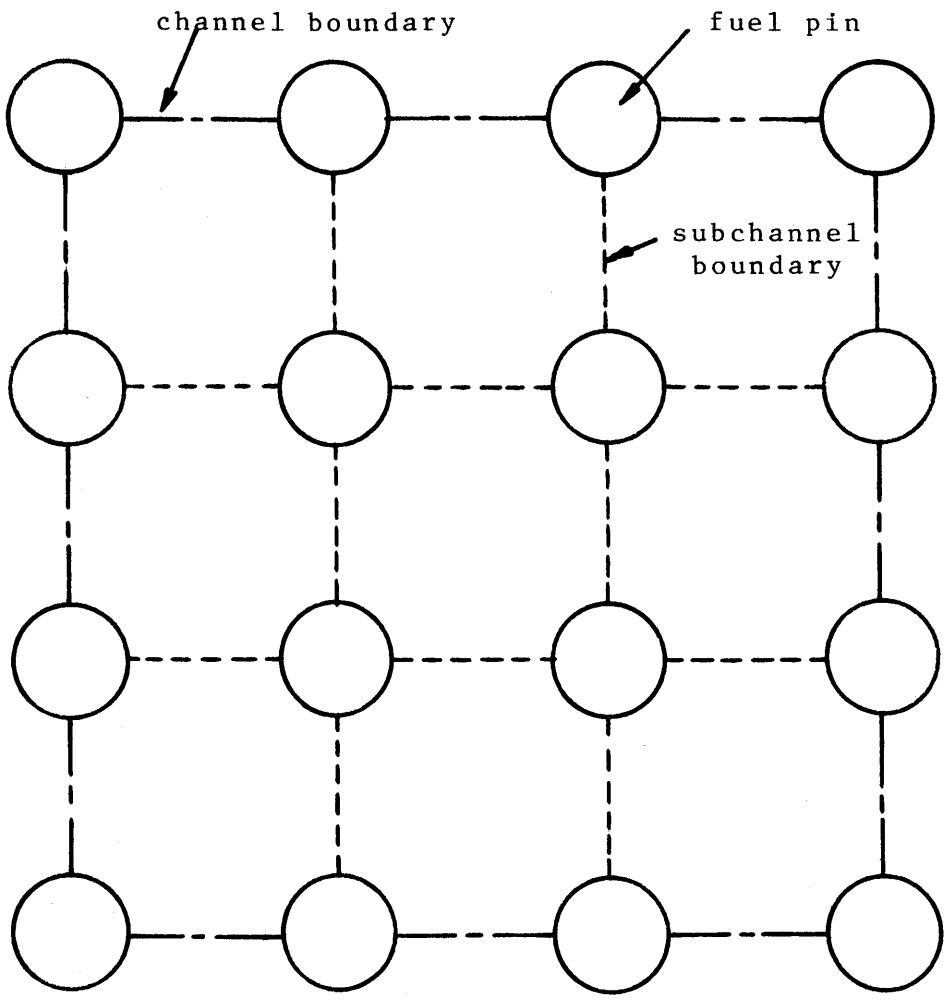

FIG. 7.1: CHANNEL COMPOSED OF NINE SUBCHANNELS

assumption of uniform properties across the large channel is not valid. The breakdown of this assumption gives rise to the differences between local and assembly average behavior that were presented in Chapter 3.

7.2.2 Limitations in Extreme Power Transients

All correlations and models that are used to describe the coolant flow are based on steady state experiments and assume thermodynamic equilibrium. Many flow transients may be modeled with a series of quasi-steady analyses. The assumption of thermodynamic equilibrium and the use of steady-state correlations are certainly appropriate in these analyses.

However, in extreme power transients, large amounts of energy may be deposited in the coolant over a short time by instantaneous neutron and γ heating. This brings about large enthalpy and density changes over a short period of time. It is possible that the assumption of thermodynamic equilibrium will break down in extreme transients of this nature.

Incompressible flow was also assumed where the governing T-H equations were simplified. If large "pockets" of vapor form quickly in extreme power transients, compressible effects may become important [53].

Local flow reversals may also develop when large vapor pockets form quickly in extreme power transients, especially at reduced flow rates [10]. Analyses with more advanced codes, such as COBRA IV, may be needed in these cases.

7.2.3 Limitations of the Coolant Model

A homogeneous model is used to describe two-phase coolant behavior in MEKIN. This model assumes that the liquid and vapor phases are well mixed and uniformly distributed throughout one another. The model is refined somewhat by using slip ratio correlations which allow the vapor and liquid phases to move at different speeds.

The homogeneous flow model is most appropriate at low qualities, when vapor bubbles are dispersed throughout the liquid, and at very high qualities when liquid droplets are suspended in the vapor. The homogeneous flow model is least applicable in the annular flow regimes [18] that may be encoutnered in BWR analyses. In the annular flow regime, the fuel pins are covered by a liquid film while the remainder of the channel is filled with vapor and some entrained liquid. Annular flow regimes are typically encountered at void fractions above 0,85.

7.3 Calculational Limitations of the MEKIN T-H Scheme

7.3.1 Clad-Coolant Heat Transfer Correlation

The Thom correlation [22] is used to compute the heat transfer coefficient between the cladding and coolant, based on the clad heat flux and coolant parameters. The correlation used data from experiments that simulate PWR operating conditions. However, only single phase flow and subcooled boiling were observed in these experiments. No net steam generation was detected and equilibrium quality never exceeded zero in these ex-

periments.

The data base of the Thom correlation suggests that the correlation is appropriate for use in steady state or transient PWR analyses with subcooled or zero equilibrium quality coolant. The correlation is extended far beyond the data base when it is used in BWR analyses or in transient PWR analyses with non-zero equilibrium quality. An additional correlation, such as that proposed by Chen [55], should be included in the code for use in these latter cases.

7.3.2 Deficiencies of the Axial Iteration Scheme

The axial iteration scheme was described in Sec. 4.1.1. Masterson [15] found unsettling, but not fatal, results when a fine axial mesh (i.e. Δz = 1 inch) was used in a COBRA III-C analysis. Unphysical oscillations in the crossflow between two adjacent channels were found when several axial iterations were performed (i.e. a "tight" T-H C.C. was selected) and a fine axial mesh was used.

Masterson also found that the effects of a flow blockage propagated progressively farther upstream of the blockage as the number of axial iterations was increased. That is, with each successive iteration, the crossflow distribution farther upstream of the blockage was changed.

However, as explained in Sec. 4.5.5, slight changes in the crossflow and axial mass flow have little effect on other coolant parmeters. Hence, Masterson noted that the crossflow oscillations had only a minor effect on the other coolant para-

meters. The oscillatory behavior remains unsettling, since a numerical method should converge to one result as a finer mesh is used and more iterations are performed.

Numerical instabilities were found in COBRA III-C analyses when the code was used to model a 90 percent flow blockage [56]. These instabilities were eliminated by clever modifications to the model. However, the instabilities could not be eliminated when the flow blockage was adjacent to a spacer in the channel.

7.3.3 Pressure Drop Instability at Small Time Steps

A very small T-H time step (e.g. 10^{-3} sec) may be needed in a coupled MEKIN analysis of an extreme power transient [16]. In such a transient, very high power generation rates rapidly increase the fuel temperature. Hence the average fuel temperature must be updated often if neutronic feedback effects are to be modeled accurately. When small time steps were used in both COBRA III-C/MIT and MEKIN analyses, the coolant solution scheme broke down and predicted unphysical mass flow rates and pressure drops.

Although no change in coolant density was observed over such a small time step, mass flow rates changed appreciably, violating mass conservation. Very large negative pressure drops across the core (e.g. -10,000 psia) were also predicted when very small time steps were used.

This problem was noticed in several different analyses. It first became apparent in a coupled MEKIN analysis of an

extreme rod ejection transient. Similar behavior was also observed when COBRA III-C/MIT was used to analyze a simulated version of the transient. The unphysical behavior was also predicted when a small time step, transient COBRA III-C/MIT analysis was performed on an unperturbed model. In this last case, all transient forcing functions were set to zero, hence the reactor was unperturbed, and the coolant should have remained at steady state conditions. As expected, coolant enthalpy and density remained unchanged. howver, axial mass flow and core pressure drop predictions were unphysical. Decreasing the time step size and tightening the T-H C.C. aggravated this problem.

Use of very small time steps in T-H analyses amplifies the small differences in coolant density that are found from one time step to the next. This amplification comes about when the term $\frac{\rho-\bar{\rho}}{\Delta t}\ \frac{\Delta x}{\Delta t}$ is used to compute the pressure drop (overscore "—" denotes value at previous time step). The unphysical behavior was eliminated when the density difference was set to zero for arbitrarily small density differences (i.e. $[\rho-\bar{\rho}] < 0.001$ lbm/ft^3).

The reason for this instability is not understood. Round-off errors in the computation of coolant enthalpy or in the determination of the density from that enthalpy may result in small errors in density differences. These errors would be amplified at small time steps. If this is the case, use of "double precision" operations to compute these values may eliminate the instability.

If the instability at small time steps cannot be eliminated, a bypass option might be included in the T-H scheme. Since small time steps are needed primarily to update the fuel temperature, an option could be included in the code to separate fuel temperature and coolant calculations. With such an option, fuel temperatures would be calculated with small time steps but coolant properties would be updated only after an appreciable amount of energy is transferred to the coolant. Such an option also would greatly reduce the calculations needed in a coupled analysis.

7.4 Experimental Verification of the T-H Solution Scheme

The ultimate test of an solution scheme lies in how well predicted results correspond to experimental data. Unfortunately no comparisons have yet been made between the MEKIN T-H solution scheme (i.e. COBRA III-C/MIT) and transient experimental data. However, some comparisons of other solution schemes in the COBRA family have been performed.

Liu [9] presented a survey of steady state comparisons that were made using COBRA I and COBRA II. He concluded that the codes agreed well with experimental data only when the coolant equilibrium quality was less than 0.02. Good agreement was also found between a steady-state COBRA III-C analysis and experimental data [57]. The results of transient analyses with extended versions of COBRA IV have been compared to experimental results [58]. However, the explicit solution technique used in COBRA IV differes greatly from that of COBRA III-C/MIT. Even if COBRA IV results were found to agree very well with experimental

data, no conclusions could be drawn about the validity of the COBRA III-C/MIT, since the solution techniques in the two codes are so different.

Experimental verification of the MEKIN T-H scheme is essential. Comparisons between results found with this scheme and those obtained from more advanced (e.g. COBRA IV) analyses will verify the solution scheme to some extent. However, MEKIN should not be accepted as a benchmark code until some experimental verification has been made.

7.5 Summary

The MEKIN user must exercise caution when applying this code in a transient analysis. The T-H solution scheme is best suited for subchannel analysis of mild PWR transients. A slug flow model was tacitly assumed to arrive at the governing equations used in this scheme. When many fuel pins are lumped into a single T-H channel, the slug flow model breaks down, giving rise to the differences between local and channel average behavior that were discussed in Chapter 3.

Thermodynamic equilibrium and incompressible flow were assumed in order to simplify the T-H solution scheme. These assumptions may break down in extreme power transients if rapid void formation takes place. Local flow reversals might also be found in these transients. Analysis of flow reversal transients is beyond the ability of the MEKIN T-H scheme.

The homogeneous flow model and Thom heat transfer correlation applied in the MEKIN T-H schme are best suited

for low quality coolant flow, as is typically encountered in mild PWR transients. These models are not suitable for BWR or extreme PWR transient analyses.

A numerical method should converge as the mesh and time step size are decreased. However, oscillations in the crossflow solution were observed in COBRA III-C analyses with a fine axial mesh and "tight" T-H C.C. Unphysical core pressure drops and axial mass flow rates were predicted when very small time steps were used in COBRA III-C/MIT and MEKIN analyses.

Since many assumptions and approximations were made to arrive at the MEKIN T-H solution scheme, predictions from the code should be compared with experimental data. Little work has been done in this area, but the comparisons must be made before MEKIN can be used with confidence as a benchmark code.

CHAPTER 8

CONCLUSIONS AND RECOMMENDATIONS

8.1 Conclusions

Sensitivities that were observed in neutronic feedback parameters for the simulated hot zero power rod ejection transient are presented and crudely ranked in Table 8.1. Coolant density and average fuel temperature, the neutronic feedback parameters, were found to be most sensitive to three T-H input options. These were:

i) the value of the gap heat transfer coefficient (h_{gap}) used in the fuel conduction model;

ii) the number of T-H channels used in the hot assembly;

iii) the use of a subcooled boiling correlation.

Both neutronic feedback parameters were found to be insensitive to the T-H convergence criterion (T-H C.C.), the number of radial fuel nodes used in a hot full power transient, the two-phase pressure drop correlation, and the value of the turbulent mixing parameter in single phase flow. Average fuel temperature was also found to be insensitive to the radial size of the model, the value of the two-phase turbulent mixing parameter, and the slip ratio and subcooled boiling correlations.

Formulas were presented which describe the response of the predicted fuel temperatures to changes in axial mesh and time step size. Axial mesh and time step sensitivity resulted primarily from an energy deposition error. Since most of the energy gener-

user selected option	discussed in section	coolant density	avg. fuel temperature
radial lumping scheme:			
steady state:			
average results	3.2.2.1	I	I
local results	3.2.2.2	***	***
transient:			
average results	3.3.4.1	**	I
local results	3.3.4.2	**	**
radial size of model	3.4.3	**	I
axial mesh size	4.2	*	F
time step size	4.3	**	F
T-H C.C.	4.5	I	I
nodes in radial fuel mesh:			
hot zero power transient	5.2.2	**	*
hot full power transient	5.2.3	I	I
h_{gap}	5.4	***	***
two phase pressure drop	6.2	I	I
turbulent mixing:	6.3		
single phase		I	I
two phase		**	I
slip ratio	6.4	**	I
subcooled boiling	6.4	***	I

F - formula presented to predict effects

I - insensitive (< 2% difference in results)

* - sensitive (2 - 10% difference in results)

** - very sensitive (10-20% difference in results)

*** - extremely sensitive (> 20% difference in results)

TABLE 8.1: Summary of Observed Sensitivities in the Simulated Rod Ejection Transient

ated is initially deposited in the fuel, axial mesh and time step sizes that minimize fuel temperature error will also minimize coolant density error.

Transient volumetric flow weighted average coolant densities supplied by the T-H solution scheme differ significantly from the area weighted average densities that should be used in neutronic feedback calculations. A method was proposed which uses "feedback correction coefficients" to adjust the coolant density supplied by the T-H solution scheme for use in updating neutronic cross sections.

Average fuel temperatures calculated with the parabolic averaging scheme used in MEKIN agreed well with analytic results for artificial fuel temperature profiles. The parabolic averaging scheme will provide acceptable results in all LWR transients if appropriate fuel mesh sizes are selected.

8.2 Recommended Modifications to the Current Version of MEKIN

Since neutronic feedback parameters were found to be insensitive to the T-H, C.C., loose values (e.g. 0.05) should be chosen in power transients. This will reduce the computation time significantly without altering the results of a coupled analysis. The code could be modified to accept the desired number of axial T-H iterations as input instead of using the T-H C.C. to limit the number of axial iterations. One axial iteration is sufficient with single phase coolant flow; two iterations should be used in two-phase flow.

Neutronic feedback parameters were found to be extremely sensitive to the choice of h_{gap}. At present, only a single

core average value of h_{gap} is used in MEKIN. The code should be modified to accept different values of h_{gap} for each T-H channel. These values could be obtained from experiments, or through the use of computer codes such as GAPCON-THERMAL II.

In fast power transients, fuel temperatures change rapidly with time, but coolant parameters respond much more slowly. An option should be included in the T-H portion of MEKIN to decouple fuel temperature and coolant parameter calculations. Such an option would allow the user to request fuel temperature calculations at every T-H time step (Δt) while requiring that sluggish coolant parameters be calculated only after every N time steps ($N\Delta t$, $N \geq 1$). Such an option would reduce the required computations in fast power excursion transients.

8.3 Recommended Features for a New Version of MEKIN

Variable radial mesh size in T-H calculations is essential if MEKIN is to produce accurate, economical results in transient analyses. If the radial mesh size could be varied, inactive, uninteresting regions of the core could be modeled with large T-H channels while many small channels were used in the hot assembly and in areas with large power gradients.

Energy deposition error is primarily responsible for the T-H time step sensitivity observed in MEKIN. The error arises because MEKIN assumes that the power remains constant over each T-H time step. This error would be reduced substantially if a simple ramp change in power was assumed over each time step.

The strong sensitivity to h_{gap} indicates that this parameter should be modeled more accurately in a future version of

MEKIN. A correlation for h_{gap} in terms of burnup and gap temperature should be included in the code. The user would specify the burnup of the fuel in each assembly at the beginning of a transient analysis. The code would then calculate values of h_{gap} at each axial level of every T-H channel based on the user input fuel burnup and the transient gap temperature. Iterations between the fuel conduction model and the h_{gap} correlation would be needed in such a scheme.

If the modeling of h_{gap} is improved, an alternative clad-coolant heat transfer correlation should also be included in the code. The Thom correlation that is currently in use is excellent for subcooled boiling analyses with no net steam generation; however, its data base does not extend into positive equilibrium quality flow regimes. The Chen correlation should be added to the code for use in analyses with positive equilibrium coolant quality (e.g. extreme PWR transients and all BWR analyses).

The two-phase coolant density is quite sensitive to β, the turbulent mixing parameter. This parameter is a function of the coolant quality and mass flow rate. A future version of MEKIN should calculate β based on the coolant quality and mass flow rate either with a correlation or by tabular "look up." The option to calculate β with a correlation in terms of the Reynold's number is inadequate in two-phase flow regimes.

8.4 Recommendations for Future Study

This sensitivity study was concerned primarily with a simulated rod ejection transient. An attempt should be made to extend the results of this study to other classes of transients (e.g.,

slower power excursion transients).

Coolant density is extremely sensitive to the slip ratio and subcooled void correlations that are used in an analysis. A literature survey and comparison of various slip ratio and subcooled void correlations should be undertaken. In this study, predictions from several correlations would be compared to experimental data. Ideally, these experiments would be typical of LWR operating and transient conditions. This work would be used to establish the range of applicability for available correlations. Appropriate correlations for use in various transient analyses would then be suggested.

Measurements of the turbulent mixing parameter have been made in subchannel experiments using COBRA I and COBRA II. Experiments should be done to determine appropriate values of β for use in MEKIN analyses. These experiments would be carried out in a "mock-up" of several fuel assemblies. Values of β would then be determined using the MEKIN T-H solution scheme or COBRA III-C/MIT. In these calculations, the value of β would be adjusted until the results of the analysis agreed well with experimental data.

Many assumptions and approximations were made to arrive at the MEKIN T-H solution scheme. As a result, this scheme has a limited range of applicability. Analyses for a range of transients should be performed using the MEKIN T-H solution scheme or COBRA III-C/MIT and less approximate codes, such as COBRA IV. The results of these analyses would be compared to determine the classes of transients that can be analyzed

adequately with the MEKIN T-H solution scheme.

The ultimate test of any analysis is how well the results of the analysis correspond to reality. An effort should be made to compare the results of MEKIN analyses with experimental data to determine the accuracy of the code. Such a comparison must be made before MEKIN is accepted as a benchmark code.

The sensitivities discussed in this thesis were determined using COBRA III-C/MIT, the MEKIN T-H solution scheme. The sensitivity of the overall, coupled neutronic/T-H analysis to various input parameters has not yet been examined because of economic constraints. The effects of T-H sensitivities in coupled analyses must be established to determine which sensitivities are most important in the overall MEKIN solution.

REFERENCES

1. Webster's New World Dictionary, Second College Edition, Collins & World Publishing Co., Cleveland-New York

2. D.A.Dahlgren, "Proposed Core Meltdown Sensitivity Study Method", Sandia Laboratory (internal document)

3. R.N.Gupta, "Maine Yankee Core Analysis Model Using CHIC-KIN", Yankee Atomic Electric Company, September 1976 (internal document)

4. D.H.Risher, "The Control Rod Ejection Transient in a Pressurized Water Reactor", Westinghouse Nuclear Energy Systems

5. P.Moreno, "Thermal/Hydraulic Analysis Method for PWR's", Nucl. Eng. Thesis, Department of Nuclear Engineering, MIT, 1976

6. C.Chiu, "Two Dimensional Transport Coefficients for PWR Thermal Analysis", S.M.Thesis, Department of Nuclear Engineering, MIT, 1976

7. A.E.Ladieu, "A Thermal Hydraulic Model Using COBRA III-C", Yankee Atomic Electric Company, YAEC-1099, June 1976

8. F.Emami, S.M. Thesis, Department of Nuclear Engineering, MIT, 1977

9. Y.J.Liu, "Thermal/Hydraulic Analysis for PWR's by a One Pass Method", Nucl. Eng. Thesis, Department of Nuclear Engineering, MIT, 1977

10. J.U.G.Valente, "Multi-Dimensional Modeling of the Rod Drop Accident", Nucl. Eng. Thesis, Department of Nuclear Engineering, MIT, 1976

11. T.Gozani, H.Kirch, E.Lim, "Dynamic Analysis of Scrammed Power Reactors, Interim Internal Report", Science Applications, Inc, May 1976, SAI/SR-147-PA

12. R.W.Bowring, J.W.Stewart, R.A.Shober, R.N.Sims, "MEKIN: MIT-EPRI Nuclear Reactor Core Kinetics Code, Computer Code Manual", September 1975, EPRI Research Project 227

13. R.N.Sims, "A Coarse Mesh Nodal Diffusion Method Based on Response Matrix Considerations", Sc.D. Thesis, Department of Nuclear Engineering, MIT, 1977

14. R.A.Shober, "Non-Linear Methods for Solving the Diffusion Equation", Ph.D. Thesis, Department of Nuclear Engineering, MIT, 1976

15. R.E.Masterson, "Improved Multidimensional Numerical Methodds for the Steady State and Transient Thermal-Hydraulic Analysis of Fuel Pin Bundles and Nuclear Reactor Cores", Sc.D. Thesis, Department of Nuclear Engineering, MIT, 1977

16. A.Cook, Ph.D. Thesis, Department of Nuclear Engineering, MIT, 1978

17. P.Moreno, C.Chiu, R.Bowring, E.Kahn. J.Liu, N.Todreas, "Methods for Steady State Thermal/Hydraulic Analysis of Pressurized Water Reactor Cores", MIT Energy Lab Report No. MIT-EL 76-006, Revision 1, July 1977.

18. D.Rowe, "COBRA III-C: A Digital Computer Program for Steady State and Transient Thermal-Hydraulic Analysis of Rod Bundle Nuclear Fuel Elements", BNWL-I695, March 1973

19. R.Bowring, P.Moreno, COBRA III-C/MIT Computer Code Manual, (to be issued as an EPRI report)

20. W.L.Kirchner, "Investigation of Thermal Hydraulic Radial Node Averaging Scheme", MEKIN: MIT-EPRI Nuclear Reactor Core Kinetics Code Program Development Notes, Vol.2.1, pp. 1-22

21. W.L.Kirchner, "Investigation of a Modified Thermal Hydraulic Radial Node Averaging Scheme", MEKIN: MIT-EPRI Nuclear Reactor Core Kinetics Code Program Development Notes, Vol.2.1, pp. 23-29

22. R.G.Quirk, "Mixed Flow Averages for BWR Power and Flow Transients", MEKIN: MIT-EPRI Nuclear Reactor Core Kinetics Code Program Development Notes, Vol.2.2, pp. 817-837.

23. L.S.Tong, J.Weisman, "Thermal Analysis of Pressurized Water Reactors", American Nuclear Society, 1970

24. V.S.Arpaci, "Conduction Heat Transfer", Addison-Wesley Publishing Co., Reading, Mass.

25. J.R.S.Thom, W.M.Walker, T.A.Fallon, G.F.S.Reising, "Boiling in Sub-Cooled Water During Flow Up Heated Tubes or Annuli", Proc. Instn. Mech. Engrs. 1965-66, paper 6

26. R.W.Bowring, "Information Transferred between Neutronics and Thermal-Hydraulics in MEKIN", MEKIN: MIT-EPRI Nuclear Reactor Core Kinetics Code Program Development Notes, Vol. 2.2, pp. 641-647

27. T.G.Taxelius(ed.), "Quarterly Technical Report SPERT Project January-March, 1967", Phillips Petroleum Company, Idaho Falls, Idaho, Atomic Energy Division, IDO-17260, February 1968. Contract AT(10-1)-205

28. "MATPRO-Version 9 A Handbook of Material Properties for Use in the Analysis of Light Water Reactor Fuel Rod Behavior", EG&G Idaho, Inc., December 1976, TREE-NUREG-1005, p.320

29. S.P.Shultz, "The Utilization of Fuel Integrity Prediction in Light Water Reactor Fuel Management", Sc.D. Thesis, Department of Nuclear Engineering, MIT, 1977

30. M.M.El-Wakil, "Nuclear Heat Transport", International Textbook Company, Scranton, 1971

31. "Properties for LMFBR Safety Analysis", Argonne National Laboratory, ANL-CEN-RSD-76-1, Supplement 1

32. S.Yamnikov, L.L.Malanchenko, V.I.Solyanyi, "The Effect of Changes in the Non-Uniformity of Energy Evolution in the Fuel of Thermal Reactors on the Temperature Distribution in the Fuel Elements", Translated from Atomnaya Energiya, 36, No. 4, 269-272(1974)

33. D.A.Andrews, M.Dixmier, "Calculation of Temperature Distributions in Fuel Rods with Varying Conductivity and Asymmetric Flux Distribution", Nucl. Sci. Eng., 36, 259-267(1969)

34. J.R.Fagan, J.O.Mingle, "The Effect of Axial Heat Conduction in Fuel Plates on Maximum Heat Flow Rates and Temperatures", Nucl. Sci. Eng. 18, 443-447(1964)

35. D.A.Rehbien, R.W.Carlson, "The Effect of Variable Thermal Conductivity in Thermal-Hydraulic Calculations", Nuclear Technology 31, 348(1976)

36. T.C.Chawla, G.Leaf. W.L.Chen, M.A.Grolmes, "The Application of the Collocation Method Using Hermite Splines to Non-Linear One-Dimensional Heat Conduction Problems", ASME Journal of Heat Transfer, 76-HT-B

37. C.A.Olson, L.H.Boman, "Three Dimensional Thermal Effects in PWR Fuel Rods", ASME 75 WA/HT-78

38. C.E.Beyer, C.R.Hann. D.D.Lanning, F.E.Panisko, L.J.Parchen, "GAPCON-THERMAL-2: A Computer Program for Calculating the Thermal Behavior of an Oxide Fuel Rod", BNWL-1898(NRC 1 and 3), November 1975

39. P.Buettiker, D.S.Rowe, Discussion: "A Mathematical Model for Transient Subchannel Analysis of Rod Bundle Nuclear Fuel Elements", ASME Journal of Heat Transfer, November 1974, pp. 565-566

40. A.A. Armand, "The Resistance During the Movement of a Two-Phase System in Horizontal Pipes", Translated by V. Beak, AERE Trans. 828, Invesiya Vsesojuznogo Teplotekhnicheskoga Instituta (1), pp. 16-23(1946)

41. C.J.Baroczy, "A Systematic Correlation for Two-Phase Pressure Drop", Chemical Engineering Progress Symposium Series, No. 64, Vol. 62, Heat Transfer - Los Angeles

42. W.A.Massena, "Steam-Water Pressure Drop and Critical Discharge Flow-A Digital Computer Program", HW-65706, Hanford Atomic Products Operation, Richland, Washington, June 1960

43. S.L.Smith, "Void Fractions in Two-Phase Flow: A Correlation Based upon an Equal Velocity Head Model", Proc. Instn. Mech. Engrs. 1969-70, Vol. 184, Pt.1, No. 36, pp. 647-657

44. S.Levy, "Forced Convection Subcooled Boiling-Prediction of Vapor Volumetric Fractions", Journal of Heat and Mass Transfer, Vol. 10, pp. 951-965

45. W.Idsinga, N.Todreas, R.W.Bowring, "An Assessment of Two-Phase Pressure Drop Correlations for Steam-Water Systems", MEKIN: MIT-EPRI Nuclear Reactor Core Kinetics Code Program Development Notes, Vol. 2.2, pp. 924-973

46. J.Weisman, R.W.Bowring, "Methods for Detailed Thermal and Hydraulic Analysis of Water-Cooled Reactors", Nucl. Sci. Eng. 57, 255-276(1975)

47. R.T.Lahey, B.S.Shiralkar, D.W.Radcliffe, "Two-Phase Flow and Heat Transfer in Multirod Geometrics: Subchannel and Pressure Drop Measurements in a Nine Rod Bundle for Diabatic and Adiabatic Conditions", GEAP-13049, AEC Research and Development Program, March 1970

48. D.S.Rowe, "A Thermal Hydraulic Subchannel Analysis for Rod Bundle Nuclear Fuel Elements", Paper No. FC 7.11, 4th International Heat Transfer Conference, Versailles, France (1970)

49. Doi, Uchikawa, Kiguchi, Tokida, "Three Dimensional Nuclear Thermal Hydraulic Analysis of BWR Fuel Bundles", Atomic Energy Research Laboratories, Hitachi, Ltd., Japan

50. Y.L.Cheung, J.F.Pearson, P.Griffith, "Modeling Two-Phase Flow in Flow Transients" Submitted through AIChE HT&EC Division for 1977 National Heat Transfer Conference

51. R.Martin, "Measurement of the Local Void Fraction at High Pressure in a Heating Channel", Nucl. Sci. Eng. 48, 125-138 (1972)

52. A.E. Bergles, W.M.Rohsenow, "The Determination of Forced Convection Surface Boiling Heat Transfer", Paper 63-HT-22. Paper presented at 6th National Heat Transfer Conference of ASME-AIChE held in Boston (11-14 August 1963)

53. J.E.Meyer, "Hydrodynamic Models for the Treatment of Reactor Thermal Transients", Nucl. Sci. Eng. 19, 269-277(1961)

54. C.W.Stewart, C.L.Wheeler, et.al., "COBRA IV: The Model and the Method", BNWL-2214, July 1977

55. J.C.Chen, "A Correlation for Boiling Heat Transfer to Saturated Fluids in Convective Flow", ASME preprint 63-HT-34, Paper presented at 6th National Heat Transfer Conference, Boston (11-14 August 1963)

56. J.M.Creer, D.S.Rowe, J.M.Bates, A.M.Sutey, "Effects of Sleeve Blockages on Axial Velocity and Intensity of Turbulence in an Unheated 7x7 Rod Bundle", BNWL-1965, January 1976

57. G.Ulrych, H.Kemner, "Exercise of the European Two-Phase Flow Group Meeting, 1976; Survey on the Experimental and Computed REsults", Erlangen, 16 March 1977

58. C.W.Stewart, C.A.McMonagle, et.al., "Core Thermal Model: COBRA IV Development and Applications", BNWL-2212, January 1977

APPENDIX A: INPUT DATA USED THROUGHOUT SENSITIVITY STUDY

APPENDIX A

INPUT DATA USED THROUGHOUT SENSITIVITY STUDY

The data used in the majority of the T-H analyses performed in this sensitivity are presented in this appendix. Much of this data describes the Cycle III core of the Maine Yankee PWR.

Operating Conditions

system pressure:	2100 psia
uniform inlet mass velocity:	2.48×10^6 lbm/hr-ft^2
uniform inlet temperature:	541 °F

Assembly Dimensions

flow area:	0.22472 ft^2
wetted perimeter:	21.733 ft
heated perimeter:	20.275 ft
effective gap width:	1.82 inches
fuel clad O.D.:	0.44 inches
channel length:	146.0 inches
channel orientation:	0.0 degrees

Fuel Thermal Parameters

		fuel	clad
thermal conductivity	(Btu/hr-ft-°F)	1.40	8.80
specific heat	(Btu/lbm°F)	0.080	0.078
density	(lbm/ft^3)	650.0	410.0

fuel diameter: 0.3765 inches

clad thickness: 0.0280 inches

nominal heat transfer coefficient: 600 Btu/hr-ft^2°F

Spacer Data

normalized axial location (z/L)	spacer type
0.0	1
0.007	2
0.096	2
0.234	2
0.372	2
0.510	2
0.648	2
0.786	2
0.924	2
1.000	3

spacer drag coefficient	spacer type
0.645	1
0.461	2
0.554	3

T-H Models

The MEKIN default T-H models were used throughout most of this study.

model	value or correlation used
turbulent mixing parameter	0.02
single phase friction factor	$0.184\ Re^{-0.2}$
two phase friction factor	homogeneous model
void fraction	homogeneous model
slip ratio	homogeneous model (i.e. slip ratio = 1)
crossflow resistance coefficient	0.5
turbulent momentum factor	0.0
transverse momentum factor	0.5

APPENDIX B: POWER HISTORIES USED IN THE SENSITIVITY STUDY

APPENDIX B
POWER HISTORIES USED IN THE SENSITIVTIY STUDIES

The data that was used to generate the artificial power histories is presented in this appendix and the computer program that was used to generate these powers is discussed. The prompt jump power history that was obtained from a "neutronics-only" MEKIN analysis is also presented in this appendix. This power history was used in axial mesh and time step sensitivity studies.

B.1 Data Used to Generate Power Histories

Two sets of steady state assembly average and local radial peaking factors were determined from neutronic analyses using the PDQ computer code. These analyses were performed by the staff of the Yankee Atomic Electric Company for the Cycle III core of the Maine Yankee PWR. The first set of radial peaking factors were determined with the maximum worth control rod gang fully inserted; these peaking factors are presented in Figs. B.1 and B.2. The second set of radial peaking factors were determined with the highest worth control rod gang fully withdrawn; these peaking factors are presented in Figs. B.3 and B.4. The axial power profile found with similar calculations is shown in Fig. B.5. Axial peaking factors that were found from this profile for use with the 13 axial level model shown earlier in Fig. 4.2 are presented in Table B.1.

1.3269		1.1903							
1.4657		1.1942	1.4829	1.5232	1.2354				
0.6385		1.1209	1.2078	1.4841	1.7839	1.2185			
0.6385		0.4106	0.8189	1.2584	1.4330	1.3244	1.2524		
0.5015		0.4643	0.4589	0.9424	1.2660	1.4741	1.8745	1.3189	
0.3914		0.4580	0.5559	0.7641	0.9633	1.3233	1.5994	1.6679	
0.2105		0.3908	0.5425	0.5636	0.4780	0.8870	1.3527	1.6975	
0.2481		0.3332	0.3948	0.4707	0.4894	0.4521	1.3256	1.4465	1.4375
0.1646		0.2491	0.2138	0.4049	0.4644	0.5362	0.7997	1.8559	1.6197

CONTROL ROD EJECTED FROM THIS ASSEMBLY

FIG. B.1: ASSEMBLY AVERAGE RADIAL PEAKING FACTORS
(maximum worth control gang fully inserted)

1.014	1.083	1.132	1.176	1.222	1.264	1.302	1.341	1.380	1.415	1.449	1.493	1.554	1.634
1.081	1.092	1.088	1.120	1.189	1.248	1.288	1.321	1.347	1.348	1.336	1.378	1.487	1.609
1.126	1.085	0.	0.	1.151	1.228	1.265	1.294	1.312	1.280	0.	0.	1.411	1.582
1.168	1.115	0.	0.	1.176	1.228	1.240	1.266	1.303	1.290	0.	0.	1.393	1.564
1.211	1.180	1.146	1.174	0.	1.215	1.183	1.205	1.283	0.	1.311	1.325	1.429	1.554
1.249	1.236	1.220	1.222	1.212	1.126	1.028	1.044	1.180	1.304	1.347	1.382	1.453	1.543
1.285	1.274	1.264	1.232	1.177	1.026	0.	0.	1.064	1.248	1.333	1.389	1.454	1.531
1.320	1.304	1.279	1.254	1.196	1.039	0.	0.	1.068	1.250	1.333	1.386	1.448	1.523
1.356	1.326	1.295	1.289	1.271	1.171	1.059	1.066	1.194	1.312	1.346	1.373	1.436	1.518
1.388	1.324	1.260	1.273	0.	1.292	1.239	1.245	1.309	0.	1.309	1.309	1.401	1.512
1.419	1.311	0.	0.	1.274	1.332	1.321	1.324	1.340	1.306	0.	0.	1.356	1.507
1.459	1.349	0.	0.	1.305	1.364	1.374	1.374	1.364	1.304	0.	0.	1.367	1.514
1.516	1.453	1.381	1.367	1.405	1.431	1.435	1.432	1.423	1.391	1.345	1.364	1.446	1.539
1.591	1.570	1.545	1.531	1.525	1.517	1.508	1.503	1.501	1.499	1.497	1.507	1.535	1.579

PIN PEAKING FACTORS

1.067	1.039	1.129	1.177	1.230	1.276	1.313	1.347	1.372	1.387	1.414	1.478	1.571	
1.096	.816	.552	.865	1.204	1.257	1.292	1.318	1.321	.991	.679	1.069	1.522	
1.123	.550	0.	.582	1.196	1.240	1.266	1.294	1.296	.642	0.	.701	1.487	
1.168	.850	.580	.587	.905	1.216	1.223	1.264	.969	.650	.659	1.037	1.485	
1.219	1.195	1.190	.902	.888	1.138	1.115	1.178	.942	.990	1.341	1.397	1.495	
1.261	1.246	1.232	1.211	1.135	.795	.518	.822	1.199	1.308	1.363	1.420	1.495	
1.296	1.278	1.255	1.215	1.109	.516	0.	.533	1.158	1.291	1.360	1.419	1.489	
1.326	1.301	1.279	1.252	1.159	.817	.531	.832	1.206	1.310	1.360	1.411	1.481	
1.349	1.301	1.279	.956	.933	1.190	1.152	1.203	.954	.992	1.334	1.380	1.466	
1.360	.974	.633	.642	.979	1.296	1.282	1.304	.989	.654	.655	1.016	1.444	
1.384	.665	0.	.650	1.324	1.348	1.346	1.351	1.328	.652	0.	.681	1.436	
1.444	1.046	.587	1.019	1.376	1.401	1.404	1.398	1.370	1.011	.678	1.044	1.466	
1.532	1.487	1.456	1.457	1.469	1.473	1.470	1.465	1.454	1.434	1.429	1.463	1.525	

COOLANT SUBCHANNEL PEAKING FACTORS

FIG. B.2: LOCAL RADIAL PEAKING FACTORS IN EJECTING FUEL ASSEMBLY
(maximum worth control rod gang fully inserted)

2.2773		2.1803							
2.4991		2.3403	3.4955	4.2520	3.8715				
1.1184		2.3357	3.0415	4.3798	6.0827	4.8610			
0.8350		0.8702	2.1856	3.8959	5.2425	6.7344	4.8669		
0.7144		0.9374	1.2065	2.8698	4.2805	5.2493	6.0985	3.8861	
0.6162		0.8913	1.3265	2.1077	2.8731	3.9069	4.4002	4.2779	
0.3105		0.7121	1.1551	1.3270	1.2089	2.1962	3.0684	3.5353	
0.3082		0.5152	0.7122	0.8918	0.9386	0.8705	2.3792	2.3914	2.2131
0.1714		0.3804	0.3107	0.6168	0.7150	0.8239	1.565	2.5655	2.3114

CONTROL ROD EJECTED FROM THIS ASSEMBLY

FIG. B.3: ASSEMBLY AVERAGE RADIAL PEAKING FACTORS
(maximum worth control rod gang fully withdrawn)

4.677	5.187	5.592	5.803	5.834	5.836	5.893	6.012	6.198	6.444	6.670	6.735	6.666	6.650
5.186	5.752	6.319	6.502	6.289	6.098	6.079	6.186	6.421	6.832	7.261	7.305	7.015	6.834
5.591	6.319	0.000	0.000	6.823	6.374	6.261	6.357	6.665	7.306	0.000	0.000	7.389	6.991
5.802	6.501	0.000	0.000	7.142	6.663	6.487	6.572	6.928	7.576	0.000	0.000	7.403	6.992
5.832	6.287	6.822	7.141	0.000	6.879	6.790	6.861	7.109	0.000	7.623	7.412	7.035	6.829
5.834	6.096	6.373	6.662	6.879	7.084	7.365	7.417	7.251	7.159	7.030	6.833	6.689	6.648
5.889	6.077	6.259	6.485	6.789	7.365	0.000	0.000	7.470	6.970	6.738	6.592	6.524	6.535
6.008	6.183	6.354	6.570	6.860	7.416	0.000	0.000	7.480	6.973	6.731	6.576	6.500	6.504
6.193	6.417	6.662	6.925	7.106	7.249	7.468	7.480	7.285	7.167	7.008	6.783	6.616	6.554
6.439	6.827	7.301	7.572	0.000	7.156	6.968	6.972	7.166	0.000	7.573	7.317	6.911	6.673
6.664	7.255	0.000	0.000	7.619	7.027	6.736	6.729	7.007	7.573	0.000	0.000	7.228	6.779
6.728	7.299	0.000	0.000	7.407	6.830	6.589	6.573	6.781	7.316	0.000	0.000	7.188	6.740
6.659	7.008	7.383	7.397	7.030	6.685	6.521	6.497	6.614	6.909	7.227	7.188	6.834	6.580
6.643	6.827	6.985	6.985	6.824	6.643	6.531	6.501	6.551	6.671	6.777	6.739	6.579	6.463

PIN PEAKING FACTORS

5.201	5.713	6.054	6.107	6.014	5.977	6.042	6.204	6.474	6.802	6.993	6.930	6.791	
5.712	4.598	3.205	4.904	6.396	6.203	6.221	6.407	6.806	5.350	3.642	5.427	7.057	
6.053	3.205	0.000	3.491	6.751	6.446	6.419	6.631	7.119	3.720	0.000	3.698	7.194	
6.106	4.903	3.491	3.571	5.171	6.705	6.677	6.868	5.403	3.800	3.759	5.462	7.065	
6.012	6.395	6.749	5.170	5.210	7.030	7.108	7.159	5.380	5.453	7.225	6.992	6.800	
5.974	6.201	6.445	6.704	7.029	5.453	3.695	5.534	7.212	6.974	6.798	6.659	6.599	
6.039	6.218	6.417	6.676	7.107	3.695	0.000	3.738	7.223	6.853	6.659	6.548	6.516	
6.200	6.404	6.628	6.865	7.158	5.533	3.737	5.561	7.226	6.970	6.774	6.619	6.544	
6.469	6.802	7.115	5.401	5.378	7.210	7.222	7.226	5.405	5.437	7.170	6.907	6.688	
6.797	5.346	3.718	3.798	5.451	6.972	6.851	6.968	5.436	3.786	3.723	5.364	6.898	
6.987	3.639	0.000	3.757	7.221	6.795	6.657	6.773	7.169	3.722	0.000	3.604	6.984	
6.924	5.423	3.695	5.459	6.988	6.656	6.545	6.617	6.905	5.363	3.604	5.302	6.835	
6.784	7.051	7.187	7.059	6.795	6.595	6.512	6.541	6.686	6.896	6.983	6.835	6.614	

COOLANT SUBCHANNEL PEAKING FACTORS

FIG. B.4: LOCAL RADIAL PEAKING FACTORS IN EJECTING FUEL ASSEMBLY
(maximum worth control rod gang fully withdrawn)

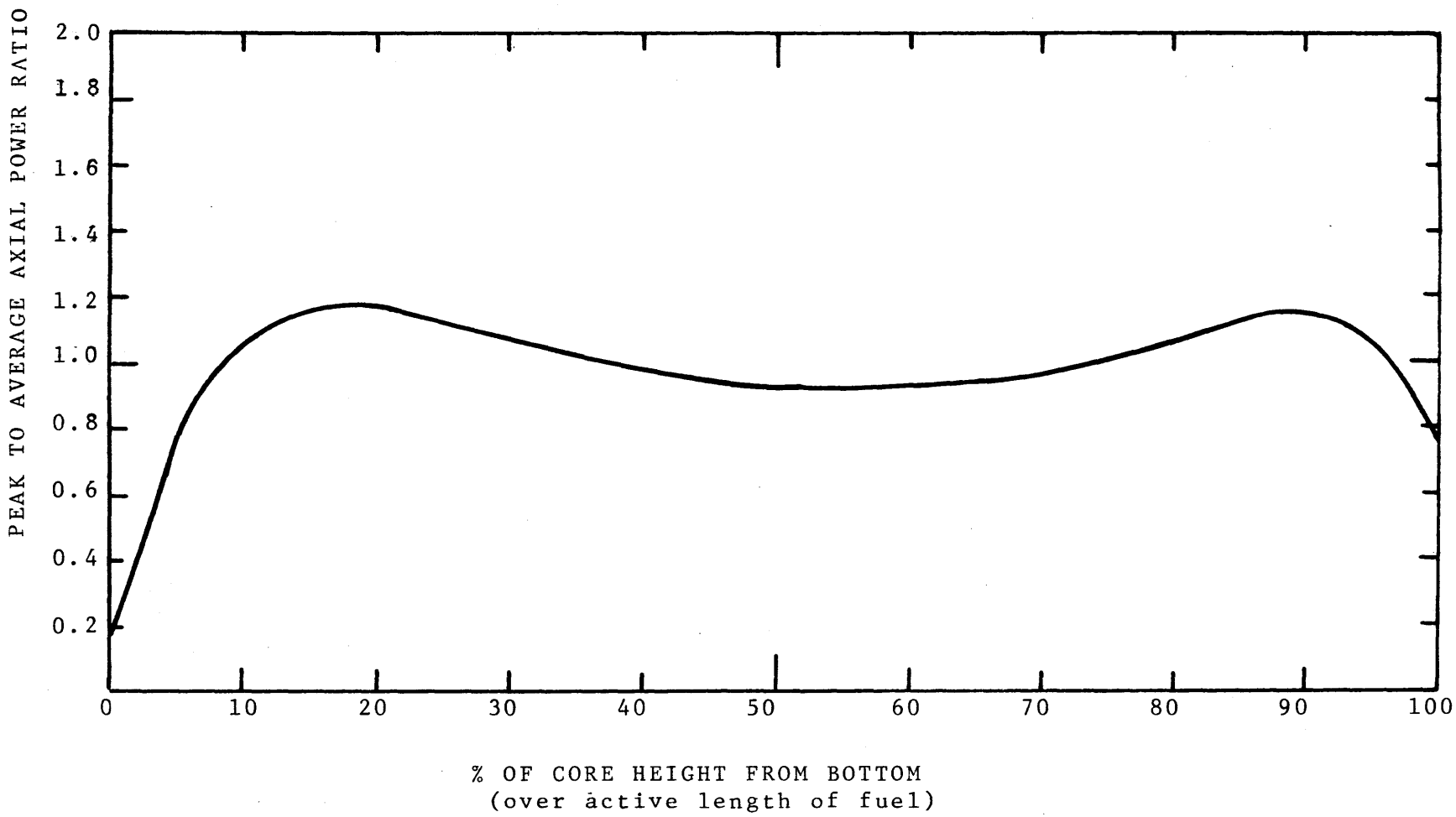

FIG. B.5: AXIAL POWER PROFILE USED TO GENERATE POWER PROFILE CLASSES 2,3,AND4

axial level	peaking factor
1	0.66
2	1.08
3	1.16
4	1.08
5	1.00
6	0.94
7	0.93
8	0.935
9	0.965
10	1.06
11	1.14
12	1.01
13	0.00

TABLE B.1: AXIAL POWER PEAKING FACTORS

B.2 Methods Used to Generate Power Histories

The power generation rate for each axial level of every T-H channel was calculated as the product of the steady state power generation rate and a transient scaling factor. The transient scaling factors were found from graphs of total reactor power vs. time, as shown in Fig. 2.3 and Fig. 5.3. The steady state power generation rate was equal to the product of the axial and radial peaking factors and a power scaling factor. This power scaling factor was equal to the average steady state power generation rate for one axial level of a T-H channel. Radial peaking factors found with the maximum worth control rod gang fully inseted were used to compute the intitial power generation rates. Power generation rates for the remainder of the simulated transients were calculated using the radial peaking factors with the control rod gang fully withdrawn. This was reasonable since the postulated rod ejection time was 0.05 seconds.

This procedure was incorporated into a small computer program. Power generation rates computed by the program were written on magnetic tape in COBRA III-C/MIT input format. Card input was then concatenated with the power history file and used in a COBRA III-C/MIT analysis. Since the power generation rate for each axial level of every assembly was input at every time step, this input scheme significantly reduced card input.

B.3 Prompt Jump Power History

A MEKIN "neutronics only" analysis for the 2 channel, 3 axial level model shown in Fig. 4.2 was performed for the prompt

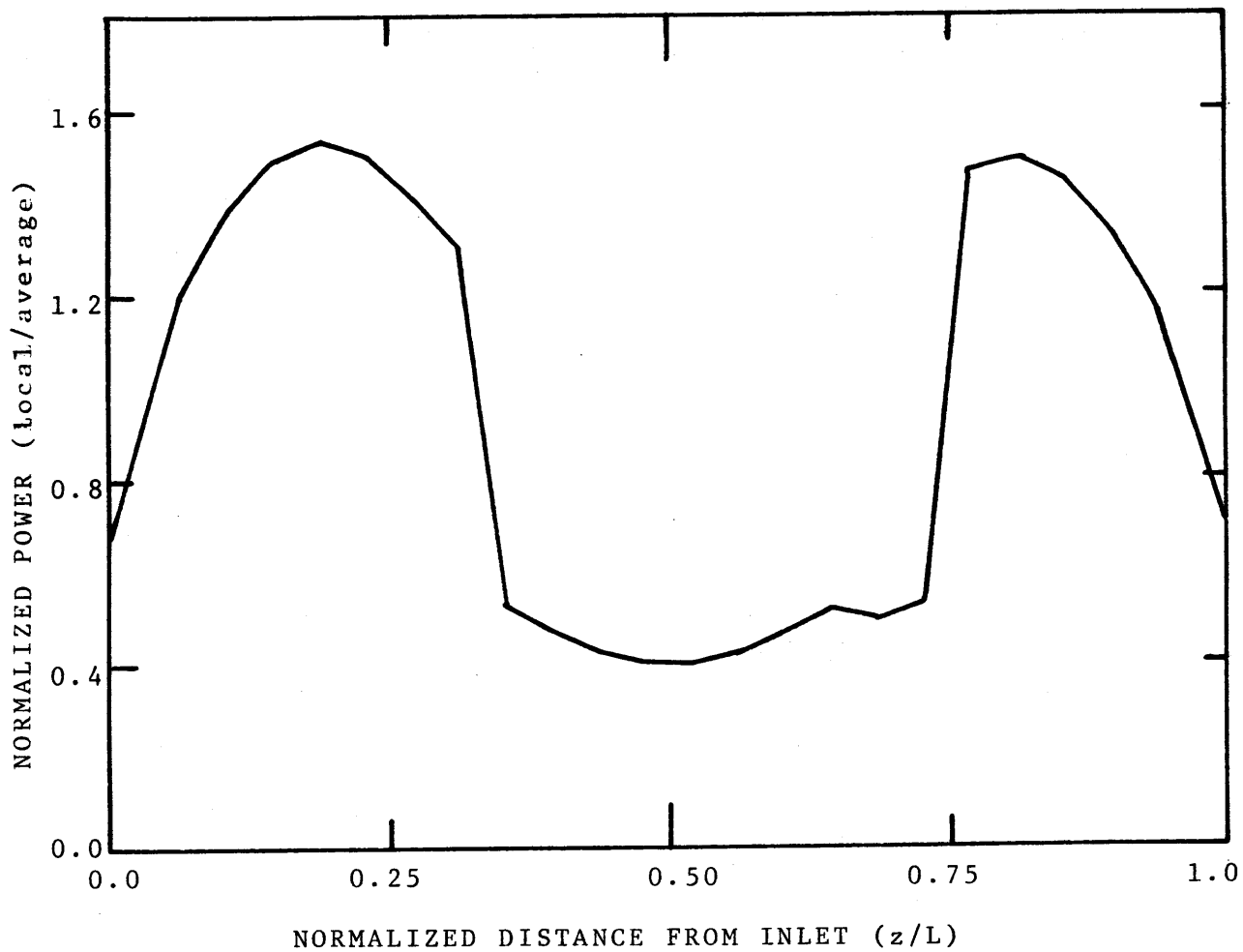

FIG. B.6: AXIAL POWER PROFILE FOR PROMPT JUMP TRANSIENTS
(power profile class 5)

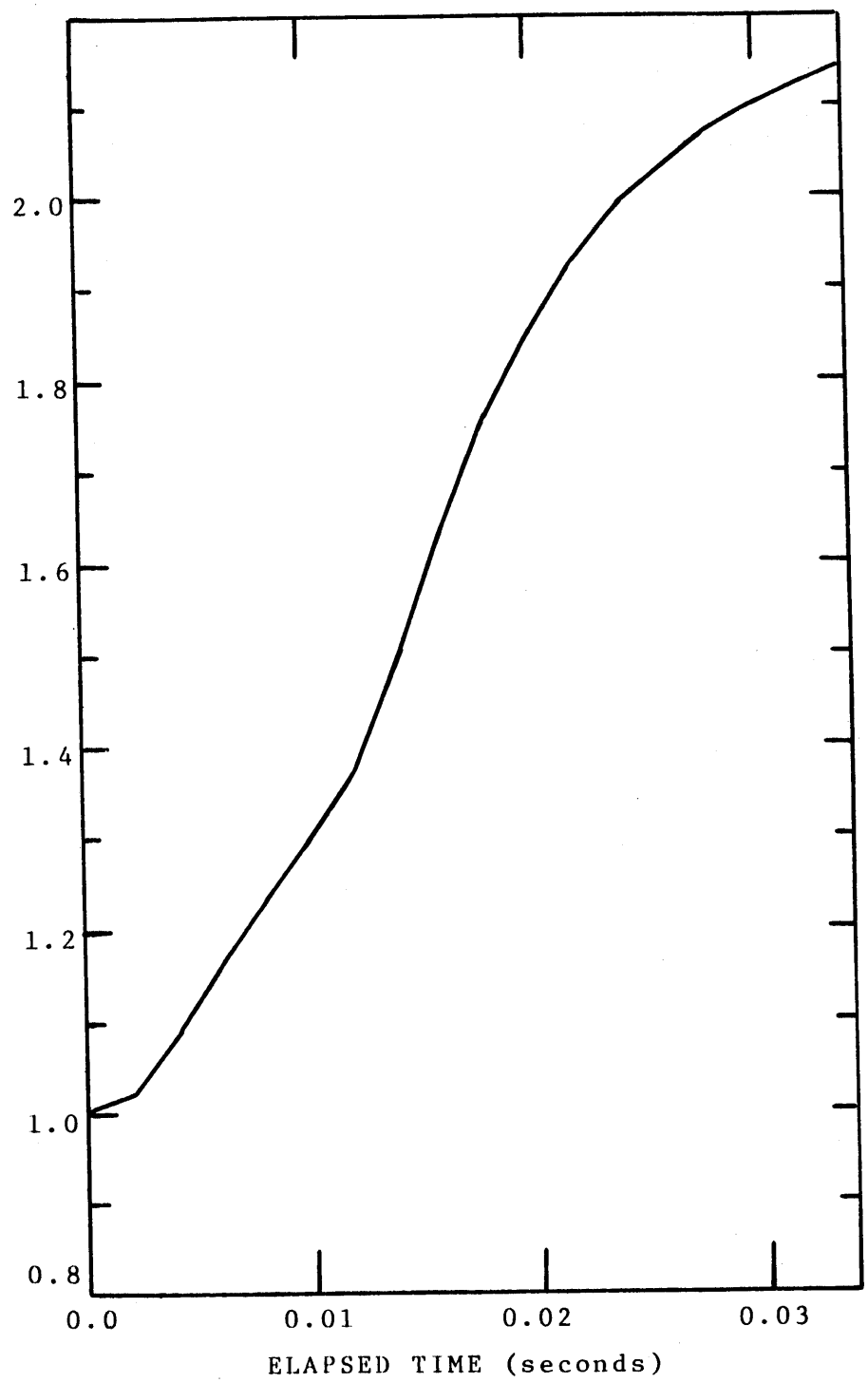

FIG. B.7: PROMPT JUMP POWER HISTORY
(power profile class 5)

jump phase of a rod ejection transient. Thermal-hydraulic feedback was not included in this analysis. The axial power profile and power history for this transient are presented in Figs. B.6 and B.7.

This problem was designed specifically for use in axial mesh and time step sensitivity studies. Neutronic cross-sections were adjusted to produce the "jagged" axial profile shown in Fig. B.6. Sensitivity of the T-H solution scheme to axial mesh size was readily apparent when this axial power profile was used.

APPENDIX C: FUEL TEMPERATURE ERRORS RESULTING FROM LARGE AXIAL MESHES AND TIME STEPS

APPENDIX C

FUEL TEMPERATURE ERRORS RESULTING FROM LARGE AXIAL MESHES AND TIME STEPS

Formulas are derived in this appendix that may be used to estimate the centerline temperature error that will be found with a coarse axial mesh and the average fuel temperature error that arises when large time steps are used. These formulas were presented in Chapter 4. Examples from COBRA analyses are included to demonstrate the use and the validity of these formulas.

C.1 Fuel Centerline Temperature Error with Coarse Axial Mesh

In a COBRA analysis, the axial power profile, a continuous function, is represented by a series of steps, as shown in Fig. C.1. The average heat generation rate over the axial level from j to (j + 1) is defined as

$$q'''_j = \frac{\int_{j\Delta z}^{(j+1)\Delta z} q'''(z)\,dz}{\int_{j\Delta z}^{(j+1)\Delta z} dz} \tag{C.1}$$

The average heat generation rate over a region of size $2\Delta z$ is given by

$$q'''_{2\,zj} = \frac{\int_{j\Delta z}^{(j+2)\Delta z} q'''(z)\,dz}{\int_{j\Delta z}^{(j+2)\Delta z} dz}$$

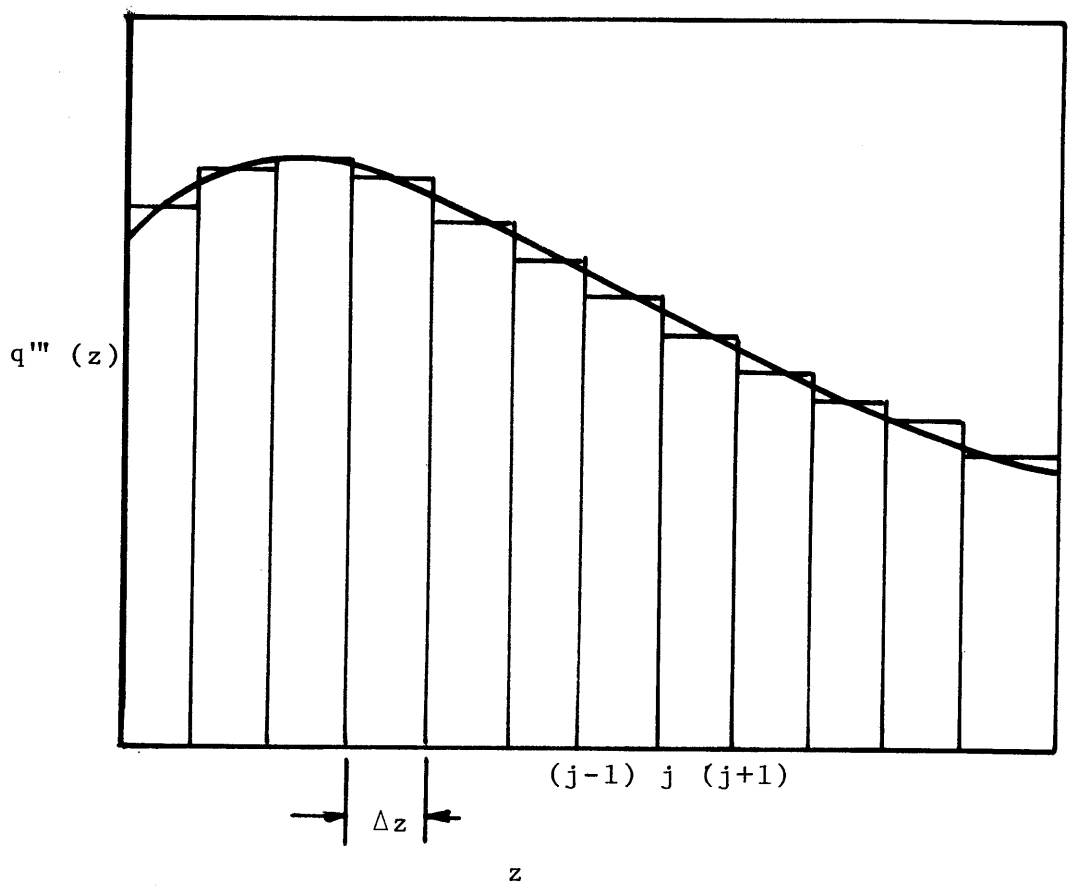

FIG. C.1: COBRA STEP APPROXIMATION TO AXIAL POWER PROFILE

The integral of Eq. C.2 may be broken into two parts so that the definition in Eq. C.1 may be applied:

$$q'''_{2\Delta z_j} = \frac{q'''_j + q'''_{j+1}}{2} \tag{C.3}$$

In a similar fashion, the average power generated over an axial level of size $n\Delta z$ is given by

$$q'''_{n\Delta z_j} = \frac{1}{n}\sum_{k=1}^{n} q'''_{n(j-1)+k-1} \tag{C.4}$$

In the steady state, the difference between the fuel centerline and bulk coolant temperature is related to the heat generation rate by the following equation, if there is no gap between fuel and clad (i.e. $h_{gap} \rightarrow \infty$):

$$(T_{\mathfrak{C}} - T_f) = \frac{q''' R^2}{4k_f} + \frac{q''' R^2}{2}\left[\frac{1}{k_c}\ln\left[\frac{R+c}{R}\right] + \frac{1}{h(R+c)}\right] \tag{C.5}$$

This may be rewritten as

$$(T_{\mathfrak{C}} - T_f) = q''' \frac{R^2}{4k_f} + \frac{R^2}{2}\left[\frac{1}{k_c}\ln\left[\frac{R+c}{R}\right] + \frac{1}{h(R+c)}\right] \tag{C.6}$$

The ratio of the temperature difference found with a coarse axial mesh to that found with a fine axial mesh is given by

$$\frac{(T_{\mathfrak{C}} - T_f)_{n\Delta z}}{(T_{\mathfrak{C}} - T_f)_{n\Delta z}} = \frac{q'''_{n\Delta z}}{q'''} \tag{C.7}$$

After substituting for $q'''_{n\Delta z}$ from Eq. (C.4) and rearranging terms, the temperature ratio is expressed as

$$\frac{(T_{\mathfrak{C}} - T_f)_{n\Delta z}}{(T_{\mathfrak{C}} - T_f)^*} = \frac{1}{n}\left\{1 + \sum_{j+1}^{n} \frac{q_j}{q_j^*}\right\}_{\substack{j=1 \\ j\neq 1^*}} \tag{C.8}$$

The subscript j denotes the fine mesh sublevel of the coarse

mesh level of size $n\Delta z$. The index j^* indicates the sublevel of interest for which the temperature difference $(T_{\mathfrak{C}} - T_f)^*$ is to be found. Little error is introduced in most cases if the same value of T_f is used in the numerator and denominator of Eq. C.8. Use of this formula is demonstrated in examples at the end of this appendix.

Although this formula was derived based on steady state assumptions, it has been found to yield excellent results in fast transients if the axial power profile is not time dependent.

The above equation may be written in analytic form as

$$\frac{(T_{\mathfrak{C}} - T_f)_{n\Delta z}}{T^*_{\mathfrak{C}} - T_f} = \frac{\int_{z_1}^{z_2} q'''(z)\,dz}{\frac{z_2 - z_1}{z_4 - z_3}\int_{z_3}^{z_4} q'''(z)\,dz} \tag{C.9}$$

Where the coarse mesh axial level extends from z_1 to z_2 and the fine mesh interval lies within z_1 and z_2 from z_3 to z_4.

If the functional dependence of the axial power shape is known, the error in the centerline temperature may be determined analytically for any axial mesh size. For example, a "chopped cosine" shape which is symmetric about the reactor midplane will be assumed. The reactor midplane will be designated as $z = 0$. If H_e is the extrapolation height, the "chopped cosine" power shape is given by

$$q'''(z) = q'''_c \cos\left[\frac{\pi z}{H_e}\right] \tag{C.10}$$

After substitution of this expression into Eq. C.9 and inte-

gration, the ratio of the temperatures is found to be

$$\frac{(T_{\mathfrak{C}}-T_f)_{n\Delta z}}{(T^*_{\mathfrak{C}} - T_f)} = \frac{z_4-z_3}{z_2-z_1}\left\{\frac{\sin\left[\frac{\pi(z_2-\frac{H_e}{2})}{H_e}\right] - \sin\left[\frac{\pi(z_1-\frac{H_e}{2})}{H_e}\right]}{\sin\left[\frac{\pi(z_4-\frac{H_e}{2})}{H_e}\right] - \sin\left[\frac{\pi(z_3-\frac{H_e}{2})}{H_e}\right]}\right\} \quad (C.11)$$

C.2 Average Fuel Temperature Error with Large Time Steps

As explained in Chapter 4, time step sensitivity in the T-H solution scheme results primarily from an energy deposition error. This error is qualitatively illustrated in Fig. 4.15. In this section, a formula will be derived for quantitative determination of the energy deposition error for large time steps. This energy deposition error will then be translated into an approximate error in average fuel temperature. Illustrative examples of the use of this formula are included at the end of this appendix.

To determine the energy deposition error, it is assumed that a small time step, Δt and a large time step $N\Delta t$ are to be compared. Here N is an integer and $N \geq 1$. Since COBRA assumes that the power is constant over a time step, the larger the value of N, the greater the energy deposition error. Over a single time step, the volumetric energy error between the two time steps is

$$\Delta q_j = \sum_{n=1}^{N-1} n\Delta t \; [q'''_{j-N+n+1} - q'''_{j-N+n}] \quad (C.12)$$

where j is an integer that multiplies the time step and in-

dicates the time of interest in the transient, that is

$$j = \frac{t}{\Delta t} \tag{C.13}$$

The total volumetric energy deposition error after a time $M\Delta t$ that is incurred through the use of a large time step of size $N\Delta t$ is then

$$\Delta Q = \sum_{k=1}^{M/N} \sum_{n=1}^{N-1} n\Delta t \; [q'''_{N(k-1)+n+1} - q'''_{N(k-1)+n}] \tag{C.14}$$

where M/N is an integer.

With the total volumetric energy deposition error known, an estimate of the resulting error in average fuel temperature may be determined. To arrive at this estimate, the fuel pin is assumed to transfer heat to the coolant at a rate that is independent of the time step size. In fact, the energy deposition error alters the fuel temperature profile and the heat flux to the coolant. This is neglected in the following derivation.

A brief digression is in order at this point to examine the validity of the above assumption. If the fuel surface temperature is increased by 50°F at typical PWR conditions and all coolant parameters are unchanged, the surface heat flux will increase by $\sim 10^4$ Btu/hr-ft or ~3 kW/ft . A 1 foot "unit height" of a typical PWR assembly will now be considered. The heat transfer surface area in this section of the assembly is ~0.1 ft . The error in neglecting changes in the surface heat flux is then $\sim 10^3$ Btu/hr or ~300 W .

The energy needed to raise the average fuel temperature

by 50°F is ~350 ^{Btu}/ass'y-ft or ~100^{W-hr}/ass'y-ft. Hence to produce a 50°F temperature rise in the fuel in a 10 second transient an energy deposition error of ~35 kW is needed. When this error is compared with the heat flux error of 300W that is caused by the 50 °F change in temperature, the latter error is seen to be inconsequential and may be neglected. Thus the following formula is limited to relatively short (i.e. less than 10 seconds) transients with temperature errors less than ~100°F. Longer transients with higher temperature errors will cause the surface heat flux changes to become important.

Now that bounds have been established on the validity of the basic assumption, the derivation will be continued. If the fuel energy deposition error is known, the change in average fuel temperature may be found from a heat balance, assuming that all energy depositied as a result of the error is stored in the fuel. If this is the case,

$$V_f \rho_f C_{p_f} \Delta T_{av} = \Delta Q \tag{C.15}$$

or,

$$\Delta T_{av} = \frac{\Delta Q}{\rho_f C_{p_f} V_f} \tag{C.16}$$

The temperature error incurred over a single large time step $N\Delta t$ may be found by substitution of Eq. C.12 into Eq. C.16:

$$\Delta T_{av_j} = \frac{\Delta t}{\rho_f C_{p_f}} \sum_{n=1}^{N-1} n[q'''_{i+j+1-N} - q'''_{i+j-N}] \tag{C.17}$$

Finally, the total temperature error that results from the energy deposition error at a time $M\Delta t$ after the start of the transient is found by substitution of Eq. C.14 into C.16:

$$\Delta T_{av}(M\Delta t) = \frac{\Delta t}{\rho_f C_{p_f}} \sum_{k=1}^{M/N} \sum_{n=1}^{N-1} n[q'''_{N(k-1)+n+1} - q'''_{N(k-1)+n}] \quad (C.18)$$

Examples will now be presented to demonstrate the use of these formulas.

C.3 Examples

Example 1: Axial Level Size

Powers are compiled in Table C.1 for an existing COBRA run. The error in fuel ℄ temperatures resulting from representing eight axial levels by a single level will be found. Since the highest power occurs at the 5th level, choose this as the reference "*" value to determine maximum-deviation.

Substitution into Eq. C.8 yields:

$$\frac{[T_{℄}-T_f]_{8\Delta z}}{T^*_{℄}-T_f} = \frac{1}{8}\left\{1+\frac{1}{1.75770}\,[0.99017+1.36589+1.58107+1.70879+1.72934+1.63181+1.50793]\right\}$$

$$\frac{[T_{℄}-T_f]_{8\Delta z}}{T^*_{℄}-T_f} = 0.87278 \qquad \underline{\text{PREDICTED}}$$

This result is now compared with the temperature difference ratio that was actually found:

$$T_{℄_{8\Delta z}} = 4058.3°F$$

$$T^*_{℄} = 4576.0°F$$

$$T_f \simeq 545.75°F$$

$$\frac{[T_{℄}-T_f]_{8\Delta z}}{T^*_{℄}-T_f} = \frac{4058.3 - 545.75}{4576.0 - 545.75} = 0.8715 \quad \underline{\text{OBSERVED}}$$

Example 2: Axial Level Size

Using the power data in Table C.2 estimate the error in c temperature that results when 4 axial levels are lumped into one. Since highest power occurs at the second of these levels, maximum deviation may be found by using this as the reference value:

Substitution into Eq. C.8 yields:

$$\frac{[T_{\mathfrak{C}}-T_f]_{4\Delta l}}{T^*_{\mathfrak{C}}-T_f} = \frac{1}{4}\left\{1 + \frac{1}{1.09797}\,[4.02013+3.91244+3.23045]\right\}$$

$$\frac{[T_{\mathfrak{C}}-T_f]_{4\Delta z}}{T^*_{\mathfrak{C}}-T_f} = 0.931 \quad \underline{\text{PREDICTED}}$$

The result is compared with the actual temperature difference ratio found in the analysis:

$$T_{\mathfrak{C}_{4\Delta z}} = 4190.8°F$$

$$T^*_{\mathfrak{C}} = 4457.0°F$$

$$T_f \simeq 643°F$$

$$\frac{[T_{\mathfrak{C}}-T_f]_{4\Delta z}}{T^*_{\mathfrak{C}}-T_f} = \frac{4190.8 - 643}{4457.0 - 643} = 0.930 \quad \underline{\text{OBSERVED}}$$

Example 3: Axial Level Size

Using the same data as in Example 2, a different reference value will be chosen to determine whether the formula will also provide good results in this case. Arbitrarily choose the first power as the reference power.

Substitution into Eq. C.8 yields:

$$\frac{(T_{\mathfrak{C}}-T_f)_{4\Delta z}}{T^*_{\mathfrak{C}} - T_f} = \frac{1}{4}\ 1 + \frac{1}{4.02013}[4.09797+3.91244+3.23045]$$

$$\frac{(T_{\mathfrak{C}}-T_f)_{4\Delta z}}{T_{\mathfrak{C}}-T_f} = 0.9490 \qquad \underline{\text{PREDICTED}}$$

Once again, comparison with the actual results shows good agreement:

$$T_{\mathfrak{C}_{4\Delta z}} = 4190.8°F$$

$$T^*_{\mathfrak{C}} = 4388.3°F$$

$$T_f \simeq 643°F$$

$$\frac{[T_{\mathfrak{C}}-T_f]_{4\Delta z}}{T^*_{\mathfrak{C}} - T_f} = \frac{4190.8-643}{4388.3-643} = 0.9473 \quad \underline{\text{OBSERVED}}$$

NOTE: It should be clear from the formula and examples that the absolute power generation rates need not be known and substituted into Eq. C.8 to obtain accurate results. Since ratios of power generation rates are used, any multiplicative constant may be used with the rates, hence fluxes may be used or even region powers, so long as the regions are all of equal size.

	Level	Power Generation
	1	0.99017
	2	1.36589
	3	1.58107
	4	1.70879
reference level	5	1.75777
	6	1.72934
	7	1.63181
	8	1.50793

TABLE C.1: Power Generation Rates for Example 1

	Level	Power Generation
example 1 reference	1	4.02013
example 2 reference	2	4.09797
	3	3.91244
	4	3.23045

TABLE C.2: Power Generation Rates for Examples 2 and 3

Example 4: Time Step Size (Power Increases with Time)

Find total average fuel temperature error at 0.03 sec. with power in Table C.3.

$\Delta t = 0.002$ sec $\qquad N\Delta t = 0.01$ sec.

$\rho_f = 650\ ^{lbm}/ft^3 \qquad C_{p_f} = 0.08\ ^{Btu}/lbm°F$

176 fuel pins in assembly

$\Delta z = 11.39$ inches

i) convert power generated per axial level of assembly to volumetric heat generation rate

$$q''' = P\ \frac{MW}{region} \times \frac{3.412 \times 10^6\ Btu/hr}{MW} \times \frac{1\ region}{\pi\left[\frac{D}{2}\right]^2 L\ [176]}$$

$$q''' = \frac{P \times 3.412 \times 10^6}{\pi\left[\frac{.3765}{24}\right]^2 \left[\frac{11.39}{12}\right] 176}$$

$$q''' = 2.64178 \times 10^7\ \frac{Btu/hr\text{-}ft^3}{MW/region} P$$

ii) substitute into Eq. C.18

$$\Delta T_{av} = \frac{\Delta t}{\rho_f C_{p_f}} [2.64178 \times 10^7] \sum_{k=1}^{3} \sum_{n=1}^{4} n \left[P_{5(k-1)+n+1} - P_{5(k-1)+n}\right]$$

expanding

$$\Delta T_{av} = 0.282239 \Big\{(1)[P_2-P_1]+(2)[P_3+P_2]+(3)[P_4-P_3]+(4)[P_5-P_4]+$$
$$+(1)[P_7-P_6]+(2)[P_8-P_7]+(3)[P_9-P_8]+(4)[P_{10}-P_9]+$$
$$+(1)[P_{12}-P_{11}]+(2)[P_{13}-P_{12}]+(3)[P_{14}-P_{13}]+(4)[P_{15}-P_{14}]\Big\}$$

substitutuing from Table C.3 and adding

$$\Delta T_{av} = 0.282239 \left\{2.0887 + 2.6827 + 0.7982\right\}$$

$$\Delta T_{av} = 1.572°F$$

n	P_n (MW/region)
1	2.208725
2	2.290638
3	2.426620
4	2.577471
5	2.709466
6	2.921873
7	3.224825
8	3.582548
9	3.849261
10	4.06003
11	4.224398
12	4.353068
13	4.453857
14	4.551266
15	4.595195

TABLE C.3: Powers for Use in Example 4

<u>Example 5:</u> Time Step Size (Power Decreases with Time)

Find average fuel temperature error at 0.5 seconds into transient with powers in Table C.4.

$\Delta t = 0.05$ sec. $\qquad N\Delta t = 0.10$ sec.

$\rho_f = 650\ ^{lbm}/ft^3$ $\qquad C_{p_f} = 0.08\ ^{Btu}/lbm°F$

172 fuel pins in assembly $\qquad \Delta z = 11.23$ inches

fuel diameter = 0.3765 in.

i) convert power generated per region into volumetric heat generation rate (similar to part (i) of example 4)

$$q''' = P \frac{3.412 \times 10^6}{\pi \left[\frac{.3765}{24}\right]^2 \left[\frac{11.23}{12}\right] 172}$$

$$q''' = 2.74173 \times 10^7 \frac{Btu/hr\text{-}ft^3}{MW/region} P$$

ii) substitute into Eq. C.18:

$$\Delta T_{av} = \frac{\Delta t}{\rho_f C_{p_f}} [2.74173 \times 10^7] \sum_{k=1}^{5} [P_{2k} - P_{2k-1}]$$

$$\Delta T_{av} = 7.323\ [P_2 - P_1] + [P_4 - P_3] + [P_6 - P_5] + [P_8 - P_7] + [P_{10} - P_9]$$

$$\Delta T_{av} = -13.56°F$$

(minus sign indicates average fuel temperature is lower with larger time step)

n	P_n (MW/region)
1	22.62419
2	22.25394
3	21.88365
4	21.51340
5	21.14313
6	20.77286
7	20.40259
8	20.03232
9	19.66206
10	19.29179

TABLE C.4: Powers for Use in Example 5

APPENDIX D: LIMITING CRITERION FOR NEGLECTING AXIAL CONDUCTION IN FUEL PINS

APPENDIX D

LIMITING CRITERION

FOR NEGLECTING AXIAL CONDUCTION IN FUEL PINS

A "rule of thumb" criterion is derived in this appendix to test the validity of neglecting axial conduction in the MEKIN and COBRA fuel pin conduction models. The criterion is derived from thermal resistances.

A section of the fuel pin between the radial fuel nodes i and i+1 and axial nodes j and j+1 is presented in Fig. D.1 Also included in the figure is the equivalent resistance network that may be used to describe this section of the fuel.

The equivalent thermal resistance between two points in the radial plane of the fuel is given by

$$R_r = \frac{\ln\left(\frac{r_1}{r_2}\right)}{2\pi kL} \tag{D.1}$$

With the geometry shown in Fig. D.1, the thermal resistance R_{r_i} between the radial fuel nodes (i) and (i+1) is

$$R_{r_i} = \frac{\ln\left(\frac{i}{i-1}\right)}{2\pi k\Delta z} \tag{D.2}$$

Similarly, the equivalent thermal resistance between two points in the axial plane of the fuel is given by

$$R_z = \frac{L}{kA} \tag{D.3}$$

For the geometry shown in Fig. D.1, the equivalent thermal resistance between the axial modes j and (j+1) at the ith radial plane is

$$R_{z_i} = \frac{\Delta z}{k\Delta r^2(2i-1)} \tag{D.4}$$

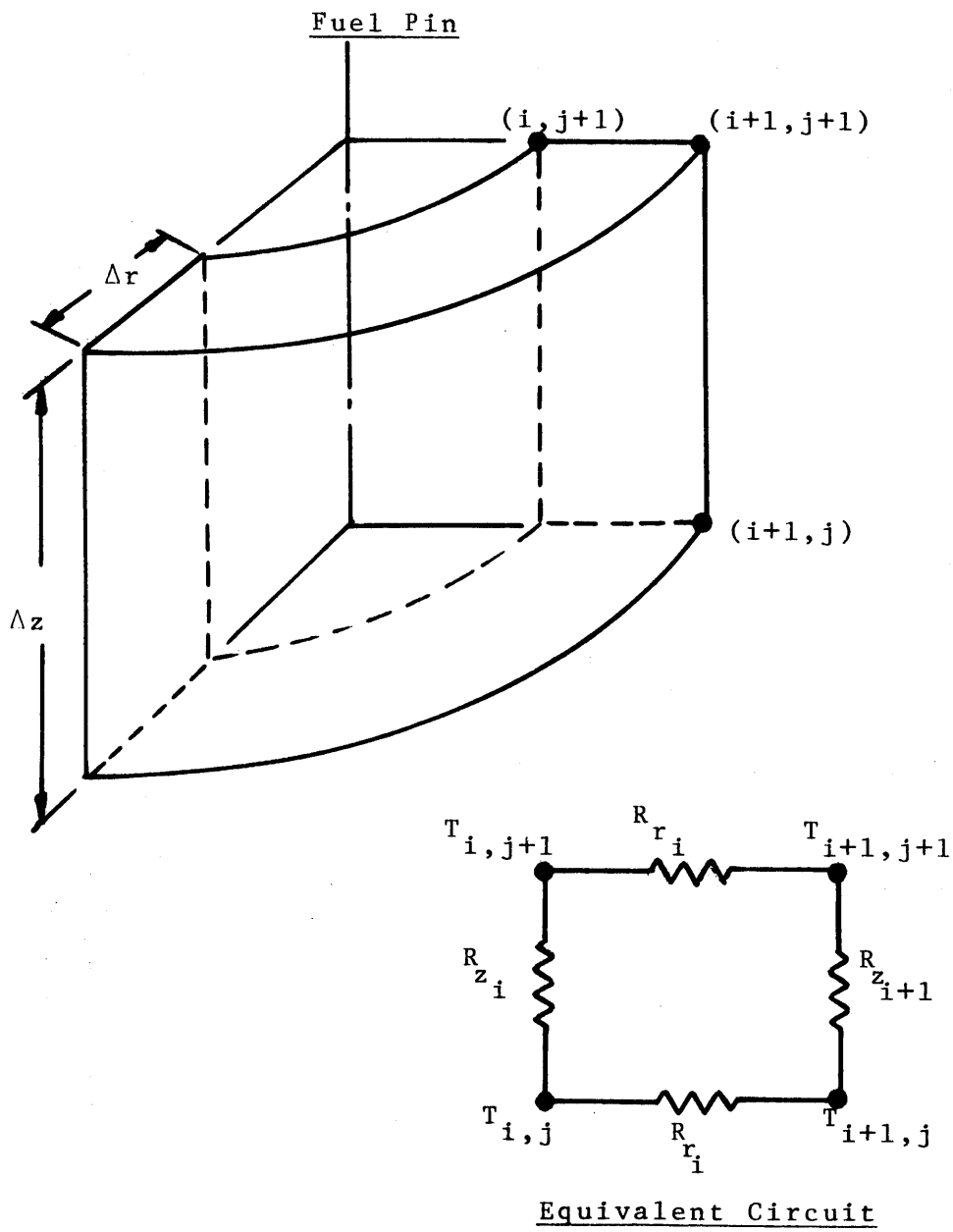

FIG. D.1: EQUIVALENT THERMAL RESISTANCES BETWEEN AXIAL AND RADIAL FUEL NODES

The heat flux between two points is determined from the temperature difference and thermal resistance between the two points by the relation.

$$q''' = \frac{\Delta T}{R} \tag{D.5}$$

The axial heat flux between nodes j and (j+1) is thus

$$q''_z = \frac{\pi k \Delta r^2 [T_{i,j} - T_{i,j+1}][2i-1]}{\Delta z} \tag{D.6}$$

Similarly, the radial heat flux between the nodes i and (i+1) is

$$q''_r = \frac{2\pi k \Delta z [T_{i,j} - T_{i+1,j}]}{\ln\left(\frac{i}{i-1}\right)} \tag{D.7}$$

The ratio of the radial to axial heat flux is found upon division of Eq. D.7 by Eq. D.6:

$$\frac{q''_r}{q''_z} = 2\left[\frac{\Delta z}{\Delta r}\right]^2 \left[\frac{T_{i,j} - T_{i+1,j}}{T_{i,j} - T_{i,j+1}}\right] \left[\frac{1}{(2i-1)\ln\left[\frac{i}{i-1}\right]}\right] \tag{D.8}$$

This may be further simplified, since

$$\frac{1}{(2i-1)\ln\left[\frac{i}{i-1}\right]} \simeq \frac{1}{2} \tag{D.9}$$

With this slight approximation, the ratio of radial to axial heat flux may be estimated from

$$\frac{q''_r}{q''_z} \simeq \left[\frac{\Delta z}{\Delta r}\right]^2 \left|\frac{T_{i,j} - T_{i+1,j}}{T_{i,j} - T_{i,j+1}}\right| \tag{D.10}$$

The absolute value of the temperature difference ratio was taken because only the magnitude of the ratio is of interest and not its "sign." In typical COBRA analyses that have been done using an axial mesh size $\Delta z \simeq 1$ ft. and 5 nodes in the radial fuel mesh, the heat flux ratio of Eq. D.10 is

found to be ~500, indicating that axial conduction is indeed negligible.